

FACILITY FORM 502

N65-30776

(ACCESSION NUMBER)

301

(PAGES)

C-64160

(NASA CR OR TMX OR AD NUMBER)

(THRU)

(CODE)

(CATEGORY)

ANNUAL REPORT

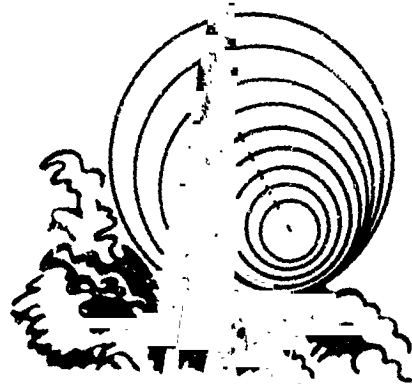
FOR

RESEARCH AND DEVELOPMENT
IN THE FIELD OF PHYSICAL DETERMINATION
OF MASS PROPERTIES

TO

GEORGE C. MARSHALL SPACE FLIGHT CENTER
NATIONAL AERONAUTICS AND SPACE ADMINISTRATION
HUNTSVILLE, ALABAMA

CONTRACT NUMBER
NAS8-11314



SPACO, INC.
HUNTSVILLE, ALABAMA

ANNUAL REPORT

FOR

**RESEARCH AND DEVELOPMENT
IN THE FIELD OF PHYSICAL DETERMINATION
OF MASS PROPERTIES**

TO

**GEORGE C. MARSHALL SPACE FLIGHT CENTER
NATIONAL AERONAUTICS AND SPACE ADMINISTRATION
HUNTSVILLE, ALABAMA**

**CONTRACT NUMBER
NAS8-11314**

June, 1965

BY

**SPACO, INC.
HUNTSVILLE, ALABAMA**

FOREWORD

This report presents a summary of all activity performed by SPACO, INC. under Contract NAS8-11314, covering the time period of June 12, 1964 to June 12, 1965. This work has established the present state of the art for mass properties measurement in the areas of moment and product of inertia, center of gravity, and principal axes.

The importance of accurate mass properties measurements to the performance of the Saturn V vehicle has long been recognized by the Propulsion and Vehicle Engineering Laboratory, as evidenced by earlier work in the field. SPACO, INC., in performance of the scope of work of this contract, has extended the original NASA developments to a new level of accuracy and automation.

TABLE OF CONTENTS

Chapter	Title	Page
I	INTRODUCTION	1
1.1	BACKGROUND	1
	1.1.1. Previous Work in the Field of Mass Metrology	2
	1.1.1.1 Moment of Inertia	2
	1.1.1.2 Product of Inertia	2
	1.1.1.3 Principal Axis	2
	1.1.1.4 Mass Properties of Liquids	2
	1.1.1.5 Center of Gravity	3
1.2	OBJECTIVES	3
	1.2.1 Moment of Inertia	3
	1.2.2 Product of Inertia	3
	1.2.3 Principal Axis	4
	1.2.4 Mass Properties of Liquids	4
	1.2.5 Center of Gravity	4
1.3	SUMMARY OF ACCOMPLISHMENTS AND RECOMMENDATIONS	5
	1.3.1 Accomplishments	5
	1.3.1.1 Moment of Inertia	5
	1.3.1.1.1 Mathematical Basis	5
	1.3.1.1.2 Automated Systems	5
	1.3.1.2 Product of Inertia	6
	1.3.1.3 Principal Axis	6
	1.3.1.4 Mass Properties of Liquids	6
	1.3.1.5 Center of Gravity	6
	1.3.1.6 General Laboratory Improvements	6
	1.3.2 Recommendations	7
	1.3.2.1 Moment of Inertia	7
	1.3.2.2 Product of Inertia	7
	1.3.2.3 Principal Axis	7
	1.3.2.4 Mass Properties of Liquids	8
	1.3.2.5 Center of Gravity	8
	1.3.2.6 General Laboratory Improvements	8

TABLE OF CONTENTS (Continued)

Chapter	Title	Page
II	TECHNICAL DISCUSSION	9
	2.1 INTRODUCTION	9
	2.2 MOMENT OF INERTIA PROGRAM	9
	2.2.1 Math Basis	9
	2.2.2 Experimental Apparatus	19
	2.2.2.1 Air Bearing Table	19
	2.2.2.2 Torsion Rod	19
	2.2.2.3 Photocell Timing Device and Associated Equipment	25
	2.2.2.4 Displacement Measuring Equipment	26
	2.2.3 Testing Program	26
	2.2.3.1 Rod Calibration Program	26
	2.2.3.2 Moment of Inertia Determination Program	28
	2.2.3.3 Table Load and Air Pressure Tests Program	28
	2.2.3.4 Aerodynamic Drag Test Program	41
	2.2.3.5 Temperature Test Program	47
	2.2.3.6 Error Analysis	60
	2.2.3.7 Conclusions	75
	2.2.4 Automated Systems Development	75
	2.2.4.1 MIA Prototype Development	75
	2.2.4.1.1 Technical Discussion	75
	2.2.4.1.2 Procedure	76
	2.2.4.1.2.1 Photocell Transducer Method	76
	2.2.4.1.2.2 Capacitance Transducer Method	76
	2.2.4.1.2.2.1 The Prototype Capacitor	76
	2.2.4.1.2.2.2 Cylindrical Capacitor	76
	2.2.4.1.2.3 Revised System	76
	2.2.4.1.3 Test Results	79
	2.2.4.1.4 Conclusions	75
	2.2.4.1.5 Recommendations	85
	2.2.4.2 MIB Prototype Development	85
	2.2.4.2.1 Problem Definition	85
	2.2.4.2.2 Problem Solution	87
	2.2.4.2.2.1 Computer Solution	89
	2.2.4.2.2.2 Computer Scaling	89
	2.2.4.2.2.3 Accuracy Considerations	94
	2.2.4.2.3 Testing and Analysis	94

TABLE OF CONTENTS (Continued)

Chapter	Title	Page
	2.2.4.2.3.1 Laboratory Equipment Arrangement	94
	2.2.4.2.3.2 Time Errors	1
	2.2.4.2.3.3 Moment of Inertia Errors	10
	2.2.4.2.4 Conclusions	10
2.3	PRODUCTS OF INERTIA	102
	2.3.1 Basis for System Design	102
	2.3.2 Methods of System Solution	104
	2.3.3 System Design	105
	2.3.3.1 Electrical Concepts and Design	108
	2.3.3.2 Mechanical Concepts and Design	108
	2.3.4 System Evaluation	110
	2.3.4.1 Results	110
	2.3.4.2 Analysis of Results	110
2.4	PRINCIPAL AXES	110
	2.4.1 Math Basis	110
2.5	MASS PROPERTIES OF LIQUIDS	121
	2.5.1 Technical Discussion of the Problem	121
	2.5.1.1 Background	121
	2.5.1.2 Requirements	121
	2.5.1.3 Solution	122
	2.5.2 Procedure	122
	2.5.2.1 Equipment	122
	2.5.2.2 Test Program	125
	2.5.2.2.1 Center of Gravity and Moment of Inertia of Empty Tank	125
	2.5.2.2.2 Rod Calibration	125
	2.5.2.2.3 Moment of Inertia of Liquid Systems	130
	2.5.2.2.3.1 Objective	130
	2.5.2.2.3.2 Equipment and Equipment Function	130
	2.5.2.3 Test Procedure	130
	2.5.2.4 Results Analysis	131
	2.5.3 Test Results	133
	2.5.3.1 Experimental	133
	2.5.3.2 Theoretical	137

TABLE OF CONTENTS (Continued)

Chapter	Title	Page
	2.5.4 Conclusions	150
	2.5.5 Recommendations	154
2.6	CENTER OF GRAVITY	154
	2.6.1 Background	154
	2.6.2 System Description	156
	2.6.2.1 Optical System	156
	2.6.2.2 Moment Detection (Bytrex) System For Location of Center of Gravity	158
	2.6.2.2.1 Test Object Support Surface	161
	2.6.2.2.2 Support and Leveling Stand	161
	2.6.2.2.3 Overload Protection Support	161
	2.6.2.2.4 Moment Detector Unit	163
	2.6.2.2.5 Instrumentation and Power Supply Unit	163
	2.6.2.2.6 System Accuracy	163
	2.6.2.3 Air Bearing Table for Location of Center of Gravity	170
	2.6.2.3.1 Equipment Description	172
	2.6.2.3.1.1 Test Object Support Surface	172
	2.6.2.3.1.2 Spherical-Segment Air Bearing	172
	2.6.2.3.1.3 Stabilizing Air Cylinders	172
	2.6.2.3.1.4 Air Cylinder Control Valve	173
	2.6.2.3.1.5 Support and Leveling Stand	173
	2.6.2.3.1.6 Test Object Positioner	173
	2.6.2.4 Operation	173
	2.6.2.5 Evaluation	173
	2.6.2.6 Recommendations	175
2.7	FACILITIES AND EQUIPMENT	176
	2.7.1 Description of Laboratory	176
	2.7.2 General Laboratory Improvements	178
	2.7.2.1 Photocell Timing Device	178
	2.7.2.2 Capacitive Motion Transducer	178
	2.7.2.3 Analog Computer	179
	2.7.2.4 General Laboratory Improvements	179
APPENDIX A	Moment of Inertia	181
APPENDIX A1	Torsional Pendulum System	183

TABLE OF CONTENTS (Continued)

Chapter	Title	Page
APPENDIX A2	Torsion Rod Calibration Test Procedure	191
APPENDIX A3	Moment of Inertia Test Procedure	193
APPENDIX A4	Table Load and Air Bearing Pressure Test Procedure	195
APPENDIX A5	Air Drag Test Procedure	197
APPENDIX A6	Temperature Effect Test Procedure	199
APPENDIX A7	MIA Schematic Diagrams	201
APPENDIX A8	MIA Test Procedure	209
APPENDIX B	Mass Properties of Liquids	211
APPENDIX C	Center of Gravity	221
APPENDIX C1	Optical Equipment Test Procedure I & II	223
APPENDIX C2	Mirror Alignment System Test Procedure II	227
APPENDIX C3	Bytrex System Preliminary Test IV	229
APPENDIX C4	Preliminary Test of Bytrex System Using The Optical Equipment for Measurements	233
APPENDIX C5	Spherical Air Bearing Table Test Procedure	235
APPENDIX D	Nonlinear Twin-T Network Capacitive Transducer Employing Printed Circuit Board Capacitors	237
APPENDIX D1	Capacitive Transducer Calculations	261
APPENDIX E	Electronic Concepts and Theory Employed In Basic Analog Computation	265

LIST OF ILLUSTRATIONS

Figure	Title	Page
1	Compound Pendulum	10
2	Linear Spring System	10
3	Variable Center of Gravity Pendulum	11
4	Filar Pendulum	11
5	Torsional Pendulum	12
6	Plot of Maximum Displacements vs Total Time Rod No. 120 Dumbbell-C Suspended Test	15
7	Logarithmic Plot of Maximum Displacements vs Total Time	16
8	Plot of Period vs Maximum Displacements	17
9	Plot of Period vs Total Time	18
10	Curve Fitting Program	20
11	24 Inch Air Bearing Table	21
12	24 Inch Air Bearing Table and Stand	22
13	Torsional Pendulum Test Apparatus	27
14	Plot of Maximum Displacements vs Total Time Rod No. 120 Dumbbell-D Suspended Test	29
15	Logarithmic Plot of Maximum Displacements vs Total Time	30
16	Plot of Period vs Total Time	31
17	Plot of Period vs Maximum Displacements	32

18	Air Shield	37
19	Weight Mounting Procedure	38
20	Natural Log Displacement vs Time	39
21	Damping Constant vs Load	42
22	Drag Plate Configurations	43
23	Cylindrical Weights	44
24	Table Configuration for Test	45
25	No Drag Plate Period vs Time	48
26	No Drag Plate Natural Log Displacement vs Time	49
27	Drag Plate A Period vs Time	50
28	Drag Plate A Natural Log Displacement vs Time	51
29	Drag Plate Period vs Time	52
30	Drag Plate B Natural Log Displacement vs Time	53
31	Drag Plate C Period vs Time	54
32	Drag Plate C Natural Log Displacement vs Time	55
33	Dumbbell Configuration	64
34	Equation Solving Computer Program	65
35	Equation Solution Using Parameters From Table 11	66
36	Plot of DM_T and DL vs DI	71
37	Plot of dI and dT vs dK	72
38	Plot of dK and dT vs % Error of Total I	73
39	Capacitance Transducer	77
40	MIA Revised Prototype System Block Diagram	78

41	Test No. 8 - Initial Amplitude 0.005 Radian	80
42	Test No. 7A - Initial Amplitude 0.13 Radians	81
43	Test No. 1 - Initial Amplitude 0.05 Radian	82
44	Timing Analysis	83
45	24 Inch Air Bearing Table and Associated Equipment	86
46	Waveform Chart	88
47	Interface Equipment and Analog Computer Functional Diagram	90
48	Prototype MIB	91
49	Complete Analog System	92
50	MIB Schematic	93
51	Test Equipment Arrangement	95
52	Coordinate System for Product of Inertia Solution	103
53	Product of Inertia Table and Acquisition of Variables	106
54	Electrical Design of Analog Product of Inertia Machine	109
55	Classical Three - Dimensional Rotor	111
56	Arbitrarily Shaped Object	114
57	Rectangular Solid	118
58	Computer Program for Determining Principal Axis	120
59	Mass Properties of Liquids (Test System)	123
60	Oscillating Tank System	124
61	Set Up for Static Testing of Torsion Rods	126
62	Plot of Period vs Maximum Displacement	132

63	Conversion From a Hemispherical Bottom Tank to an Equivalent Flat Bottom Cylindrical Tank	136
64	Plot of Moment of Inertia vs Aspect Ratio	144
65	Plot of Ratio of I_{Liquid} to I_{Solid} vs Aspect Ratio for Various Angular Velocities	145
66	Rotational Motion of a Partially Filled Tank About the Liquids Center of Gravity	147
67	Plot of the Ratio of I_{Liquid} to I_{Solid} vs Aspect Ratio for Experimental Results at $\omega = 4.3$ Radians Per Second and Theoretical Results	152
68	Plot of Moment of Inertia vs Aspect Ratio	153
69	Center of Gravity Location System Using a Spherical Segment Air Bearing and Optical Telescope	157
70	Moment Detection System for Center of Gravity Determination	162
71	Indicated Moment vs Actual Moment 25 in. -lb Detector	165
72	Indicated Moment vs Actual Moment 250 in. -lb Detector	166
73	Spherical Air Bearing Table for Center of Gravity Determination	171
74	Center of Gravity Test Fixture	177

LIST OF TABLES

Table	Title	Page
1	Moment of Inertia Test Standards	24
2	Results of Four Dumbbell Standards	25
3	Rod Constant Determination	33
4	Repeatability Test Results	34
5	Moment of Inertia Determination Test Results	35
6	Damping Constant C at 71°C for Various Loads And Pressures	40
6A	Aerodynamic Drag Test Results	46
7	Temperature Effect Test Results	56
8	Rod #120 Air Bearing Table (25 PSI) - 60 in. - lb-sec^2 Dumbbell (April 21, 1965)	57
9	Rod #120 Air Bearing Table (25 PSI) - 60 in. - lb-sec^2 Dumbbell (April 19-20, 1965)	58
10	Rod #120 Air Bearing Table (25 PSI) - 60 in. - lb-sec^2 (April 22, 1965)	59
11	Dumbbell Dimensions	64
12	Partial Derivatives of I	67
13	Total Differentials of I for Various Tolerances	68
14	Effect of dI and dT on dK in Suspended Pendulum Rod Calibration Test	69
15	Effect of dI of Standard and dK on dT	74
16	Timing Analysis of MIA Revised System	84

17	Prototype MIB Moment of Inertia Determination Capability Final Test No. 1	96
18	Prototype MIB Moment of Inertia Determination Capability Final Test No. 2	97
19	Prototype MIB Moment of Inertia Determination Capability Final Test No. 3	98
20	Prototype MIB Moment of Inertia Determination Capability Final Test No. 4	99
21	Prototype MIB Moment of Inertia Determination Capability Final Test No. 5	100
22	Product of Inertia Machine Test Result Summary	112
23	Experimental Values of Torsion Rod Constants	127
24	Theoretical Values of Torsion Rod Constants	128
25	Comparison of Theoretical and Experimental Values of Torsion Rod Constants	129
26	Result of Mass Properties of Liquids Test Program	134
26A	Results of Theoretical Calculations	151
27	Accuracy Test Results Using the Brunson Line Scope (No. 1172)	159
28	Comparison of the New Alignment System Against Original Method	160
29	Tests Using the 25 in. -lb Moment Detection Unit	167
30	Tests Using the 250 in. -lb Moment Detection Unit	168
31	Bytrex Test	169
32	Evaluation of Spherical Segment Air Bearing Table Test Results	174

1 INTRODUCTION

1.1 BACKGROUND

Weight and balance criteria have proven to be vital factors in the successful performance and operation of space flight vehicles. Location of excess weight becomes geometrically a more serious problem in the upper stages of space flight vehicles. Weight and balance estimates must be made and continuously checked during design, construction, and assembly of vehicles.

Since weight and balance are of prime importance, accurate and dependable data must be maintained on the center of gravity of each component. Data, related to center of gravity, is required to assure proper distribution of weight for efficient vehicular flight performance. Variances between estimated and actual weights, balances, and/or centers of gravity are assured of resulting in vehicles deviating from the calculated course. Unpredicted forces due to erroneous center of gravity estimates can be of sufficient magnitude to cause mission failure.

In addition to static weight, balance, and center of gravity data, other parameters must be known to engineer the requirements of space flight vehicles. For components having relative motion with respect to the vehicle it is vitally important to know their moment of inertia, product of inertia and principal axes. (Items having relative motion to the vehicle include: valves, controls, actuators, gimbals, rotors, pistons, pumps, et cetera.) Data related to components of this type must be extremely precise because of high speeds and critical environments in which they operate. The inertial effects of liquids (i.e. fuel, lox) as compared with solids of the same density must also be known. Movement of these components during vehicle acceleration produces secondary forces such as gyroscopic couples and coriolis effects, which affects the stability and response of vehicular flight. Consequently, careful studies and analyses are required on dynamic components to assure no harmful interactions or harmonics develop to cause resonance and/or excessive vibrations.

Taking into consideration the importance of the above mentioned critical factors, studies and design of reliable measuring devices has been undertaken in the following areas:

- A. Moment of Inertia
- B. Product of Inertia
- C. Principal Axis
- D. Mass Properties of Liquids
- E. Center of Gravity

1.1.1 Previous Work in the Field of Mass Metrology: Until the time that SPACO, INC. began a study in five areas of Mass Metrology, moment of inertia, product of inertia, principal axis, mass properties of liquids, and center of gravity, the amount of test, studies, and development had been limited.

1.1.1.1 Moment of Inertia: One outstanding piece of work was found in NASA TN-1114, which had been widely accepted as a significant contribution to the store of knowledge on "additional mass efforts". Developments under the present contract are extending this work by improved techniques and processes for measurement of true moment of inertia. A year ago, the best accuracy attainable was to the nearest 0.1 in-lb-sec^2 . Under the present efforts of the Mass Metrology Laboratory at SPACO precision measurements to the nearest 0.01 in-lb-sec^2 on components is obtainable, a full order of magnitude better.

1.1.1.2 Product of Inertia: A survey of available literature shows that diminutive amounts of work has been performed in the past to determine experimentally, to an appreciable degree of accuracy, the product of inertia of a mass about a pre-determined axis.

1.1.1.3 Principal Axis: In the study of principal axis determination there also appeared a shortage of up-to-date information available on measurement systems.

1.1.1.4 Mass Properties of Liquids: In the past, considerable effort has been made by many people in the theoretical and experimental study of liquids. Studies have included, viscosity, pressure, flow, baffles, vibration, acceleration, and many other aspects too numerous to mention. The work of the Mass Metrology Laboratory, at SPACO, INC., has been to utilize a cylindrical tank, oscillating about the yaw-pitch axis using various liquid levels and various frequencies in the range of 0.25 to 2 cps and to compare the experimentally determined values of moment of inertia with theoretical values assuming a solid of the same density.

1.1.1.5 Center of Gravity: One of the more popular methods of center of gravity location utilizes a strain gage transducer which measures the static unbalance moment created about the center of the transducer. This value, divided by the object weight, yields the distance to the cg. However, this system is hampered by the lack of a method of determining these measurements accurately with respect to a reference point on the object. This method at best can yield cg location to the nearest hundredth of an inch. The Mass Metrology Laboratory has pursued and developed a method of measurement utilizing a precision telescope and tooling bar which will allow the measurement of objects to the nearest thousandth of an inch. Advantages of the system are that there is no physical contact with the object, therefore any type reference point can be used. Another development of the Laboratory is the use of a spherical-segment air bearing table for more precise and more rapid location of center of gravity.

1.2 OBJECTIVES

NASA contract NAS8-11314 detailed five areas where literature searches, studies, test, and development of methods were to be made. The following is a brief description of the objectives in each of the five areas.

1.2.1 Moment of Inertia: The initial investigation was to conduct a series of tests and experiments orientated toward the ultimate goal of developing a completely automatic system for measuring mass moments of inertia. This automated system was to operate in conjunction with a government furnished 46 inch air bearing device.

The immediate task was to calibrate the device using a series of test specimens with accurately known moments of inertia. After calibration, efforts were to be directed at developing the automatic system.

Transducers were to be selected to accept signals, generated by moving parts of the system. The output of these transducers would be amplified and routed to an analog computer. The computer was to be programmed to solve the differential equations of motion associated with a swinging damped pendulum. Test results from the computer were to be processed through a digital converter and printed out on paper. Viscous and aerodynamic damping, temperature, were to be taken into consideration.

1.2.2 Product of Inertia: A device for measuring product of inertia of masses about any axis was to be designed, developed, and tested. Moments were to be measured by sensing loads on a tiltable, rotating table, using

either electrical transducers or differential air gages. The design specified that resultant moment signals could be read off directly or fed into a computer together with inputs concerning table angular velocity to yield product of inertia in suitable units. The table calibration was to be accomplished by using masses of known or previously calculated products of inertia and comparing to readouts from the table and its instrumentation. Adjustments were to be provided to account for initial errors or null readings.

1.2.3 Principal Axis: These test were to be performed using a government-furnished three-degree freedom pendulum. This test required a motion sensing device with necessary computer. A series of test were to be performed to develop a means of determining the principal axis of a body. These test were to be performed utilizing the spherical air bearing that was used in conjunction with the center of gravity test. The method used in this effort utilized a mass, with a known principal axis, placed on the air bearing with the center of gravity of the mass located near the radius of the air bearings. This set up is on the principle that oscillating motion induced about an arbitrary axis (not principal axis) will also produce motion about another axis. Studies were to be performed to design a means of sensing this motion and converting this data into the principal axis location.

1.2.4 Mass Properties of Liquids: These test were to be performed using a government-furnished pendulum and container. Mathematical equations and parameters were to be developed from test results for application to launch vehicles and space vehicles. An extensive series of tests were to be made to determine the percentage of fluid which acts as a solid in measuring mass moments of inertia liquids. A cylindrical tank closed on one end by a spherical bulkhead was to be oscillated in an upright position between two rigid support pillars which contain the bearing assembly, with horizontal torsion rods fastened to each side of the container through the bearings.

Test were to be performed with different levels of liquid with ten or twelve different frequencies for each level. Different frequencies were to be generated by sizing the torsion rods. At the conclusion of these tests a series of baffling configurations were to be placed in the tank and test repeated. Data from these tests were to be used in an effort to correlate the measured results with theoretical values.

1.2.5 Center of Gravity: A government furnished three degree freedom air bearing balance was used in locating centers of gravity on irregular shaped objects. This government furnished air bearing device was a prototype design utilizing a 10 inch diameter spherical polished steel segment floating on air. This device was capable of yielding favorable accuracy. To operate the device the test specimen to be measured was

placed on the air bearing device, and leveled at static equilibrium. A plumb bob, which had previously been set to the exact center of the system was lowered to locate the center of gravity of the test specimen.

Efforts were to be made to refine design of the "Center of Gravity Locator" whereby the sensitivity of the system could be changed by moving a system of weights in respect to the center of gravity of the system. In addition the plumb bob arrangement was to be replaced by a vernier thus, improving accuracy in readout. Comprehensive tests were to consist of measuring the centers of gravity on a series of various shaped configurations with different weights and centers of gravity.

1.3 SUMMARY OF ACCOMPLISHMENTS AND RECOMMENDATIONS

1.3.1 Accomplishments

1.3.1.1 Moment of Inertia

1.3.1.1.1 Mathematical Basis

(1) The "Period Decay Rate" concept has been developed to a practical technique which enables moments of inertia to be determined experimentally to an accuracy of $\pm 0.1\%$.

(2) A detailed analysis of analytical curve fitting techniques was made for use in conjunction with the above concept.

(3) Specific procedures have been established for the experiments performed in the laboratory.

(4) The effects of dead weight, air bearing pressure, and external air drag on the damping constant of the system have been determined experimentally.

(5) The effect of environmental temperature on the accuracy of the moment of inertia measurement system has been determined experimentally.

(6) The effects of errors in moment of inertia standards and test parameters on system accuracy have been determined analytically.

1.3.1.1.2 Automated Systems

(1) A prototype system for measurement of moment of inertia using a capacitive transducer for motion detection was designed, fabricated, and tested.

(2) A prototype system was developed for measurement of moment of inertia using an analog computer for real time calculation of the result.

1.3.1.2 Product of Inertia

A prototype machine for measurement of products of inertia was designed, fabricated, and tested. The prototype utilizes an instrumented rotating tilt table and an analog computer to solve for the desired results.

1.3.1.3 Principal Axis

A computer program for calculating the location of principal axis from measured moment and products of inertia was tested and proven.

1.3.1.4 Mass Properties of Liquids

(1) A test program to experimentally determine the moment of inertia of a partially filled liquid tank oscillating about its yaw-jitch axis was performed.

(2) Progress was made on the derivation of a mathematical expression for the moment of inertia of the above system, although the solution obtained thus far is a poor approximation of the experimental results.

1.3.1.5 Center of Gravity

(1) A precision optical system for center of gravity location was procured, modified and tested.

(2) The government furnished moment detection center of gravity location system was improved and evaluated.

(3) The spherical segment air bearing system was refined to a significantly greater accuracy capability than was originally possible.

1.3.1.6 General Laboratory Improvements

(1) A capacitive transducer motion measurement system was designed, fabricated and evaluated.

(2) Numerous improvements to the laboratory capabilities were made by the design and construction of equipment and accessories.

1.3.2 Recommendations

As a result of the experience accumulated in this contract effort, the need for additional research in specific areas has become apparent. These needs are outlined below according to the major areas of development.

1.3.2.1 Moment of Inertia

(1) Improvements are needed in measurement techniques, in the areas of oscillation period time, amplitude measurement, and dimensional and mass measurement of standards.

(2) A study should be performed of the potential system errors created by the torsion rod restoring force. This should include a survey of torsion rod materials, and development of rod calibration instrumentation.

(3) The effect of all other significant variables on the performance of the torsional pendulum system should be determined experimentally.

(4) A mathematical model of the system should be developed in terms of the parameters developed experimentally.

(5) A small commercial electronic digital calculator should be adapted to the solution of the developed model, and incorporated into a high accuracy integrated automatic measurement system.

1.3.2.2 Product of Inertia

(1) The basic system developed under this contract for measurement of products of inertia should be further tested to determine the nature and origin of all errors.

(2) The system should be converted to a digital computation capability, to improve the potential system accuracy. The same basic techniques could be used, differing only in the nature of the electrical variables and the type of computer.

1.3.2.3 Principal Axis

Experiments should be made to determine the relative performance of two methods of principal axis location. These two methods are 1. calculation from moment & products of inertia or 2, location of a null point on the product of inertia test machine.

1.3.2.4 Mass Properties of Liquids

(1) Further testing with the government furnished tank system is required to determine empirically the parameters which affect the fluid moment of inertia. For this effort, additional instrumentation for the tank system will be required to measure these parameters.

(2) Development of the mathematical model of the system should be continued along the same approach, with additional emphasis on development of a technique to transfer axes of the fluid inertia.

1.3.2.5 Center of Gravity

(1) Further tests of the new spherical segment air bearing cg location system are needed to determine the causes of present errors.

(2) An improved leveling system for use with the spherical air bearing table is needed. The present air cylinder system is inadequate.

(3) An improved counterweight system for the air bearing table should be designed.

(4) The need exists for a new method of marking cg points on objects after they are located optically. Projection of a mark on to a photosensitized area of the object is one possibility.

(5) The construction of a spherical air bearing table and optical telescope as an integrated system on one base is recommended.

(6) Improvements to the moment detection cg locator to increase its accuracy and convenience should be undertaken.

(7) A feasibility study of more advanced and automated techniques of C.G. location is needed to advance the state of the art of up to a level comparable to the moment and product of inertia machines.

1.3.2.6 General Laboratory Improvements

A study of load measurement techniques should be made to determine the best approach to establishment of a precision load measurement capability in the Mass Metrology Laboratory.

II TECHNICAL DISCUSSION

2.1 INTRODUCTION

The research and development work performed during the year was divided into six major area of effort, with the overall responsibility for each area assigned to an engineer. Each of these major areas was subdivided into several projects which were assigned to individual engineers according to the type of work involved. All previously published weekly and monthly progress reports were organized according to this arrangement. The discussions following are in the same format, making possible reference back to individual progress reports when more information is required. The numerous minor tasks performed during the year which had no technical significance are not included in this report.

2.2 MOMENT OF INERTIA PROGRAM

2.2.1 Math Basis: The two methods of determining moments of inertia are: static and dynamic. The static method is accomplished by using standard moment of inertia formulae and known dimensions and weights of a specimen. The dynamic method basically consists of oscillating the specimen about a given point and measuring its period of oscillation. This period of oscillation is then used in the proper formula, depending on the system, to calculate the moment of inertia. Both methods have their advantages and disadvantages. The controlling factors which determine the method to be used are the size and shape of the specimen, and the accuracy desired. For a regular shaped homogeneous specimen with known dimensions the static determination would be the superior method. For specimens of irregular shape and non-uniform density the static method would be time consuming, if not entirely inadequate, thus, the dynamic method would be best. There are several types of dynamic methods, some of which are; compound pendulum, linear spring system, variable center of gravity pendulum, filar pendulum, and torsional systems. An illustration of each method and the formula for determining the moment of inertia is shown in Figures 1 through 5. Each of these dynamic methods has its advantages and disadvantages which are mainly determined by the specimen to be measured. Since our main interest is in determining moments of inertia rapidly and accurately the most feasible approach was to use a torsional system which had a frictionless rotatable table top. This type of top makes for ease in mounting specimens to be measured. The ideal instrument for this program is the torsional pendulum air bearing table which has been designed, fabricated and furnished by NASA. After the method of determining moments of inertia had been decided upon, a complete investigation of the system both theoretically and experimentally had to be performed so that maximum accuracy could be obtained.

$$I = \frac{WLT^2}{4\pi^2}$$

W = WEIGHT

L = DISTANCE C G BELOW PIVOT POINT

T = PERIOD

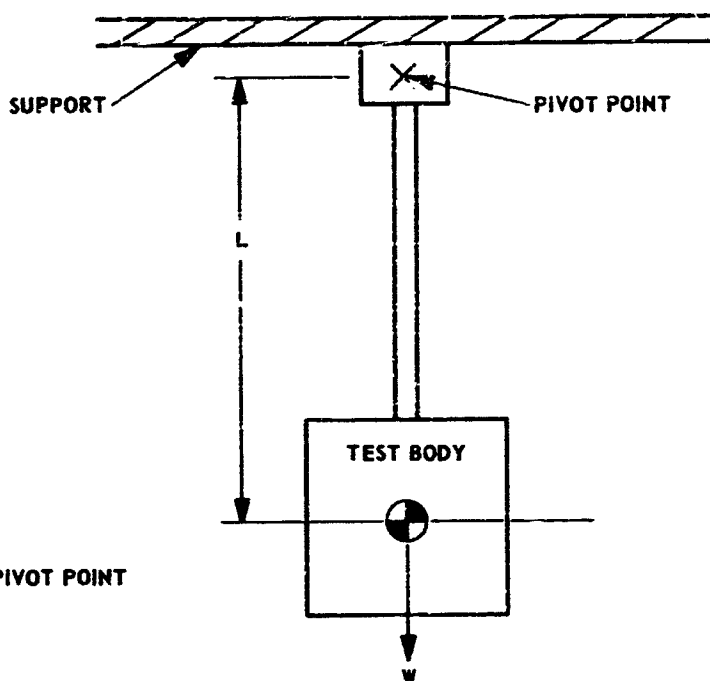
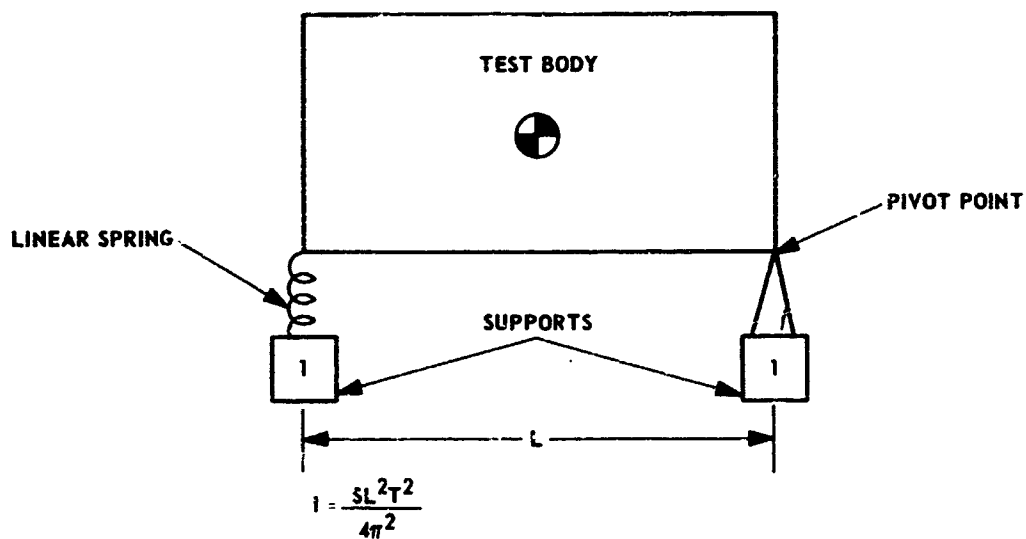


FIGURE 1 COMPOUND PENDULUM



S = SPRING CONSTANT

L = DISTANCE FROM SPRING TO PIVOT POINT

T = PERIOD

FIGURE 2 LINEAR SPRING SYSTEM

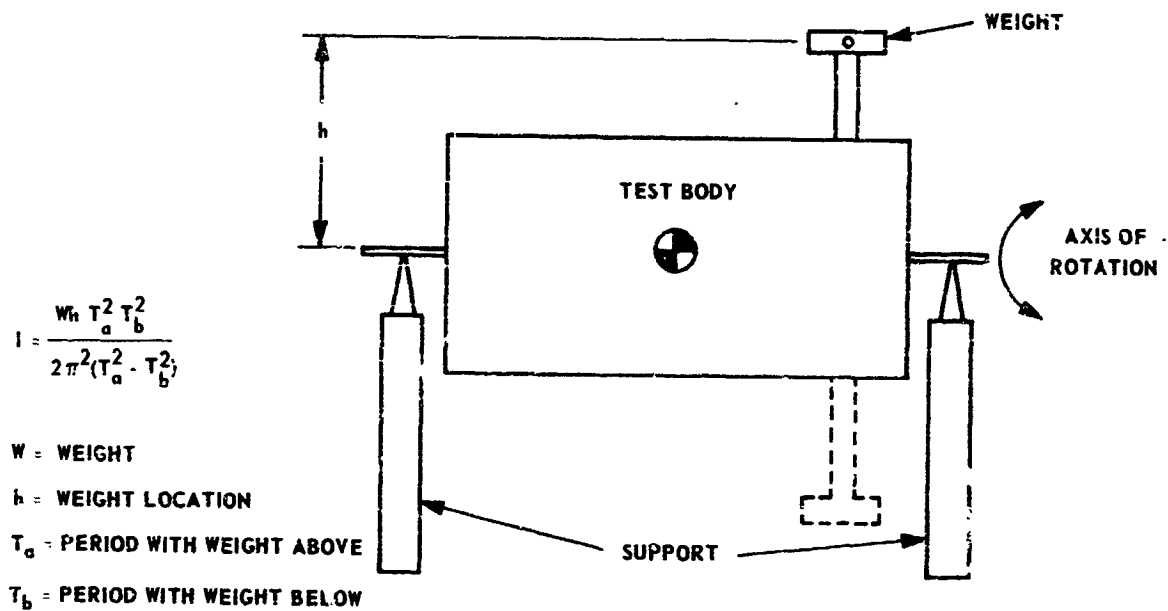


FIGURE 3 VARIABLE CENTER OF GRAVITY PENDULUM

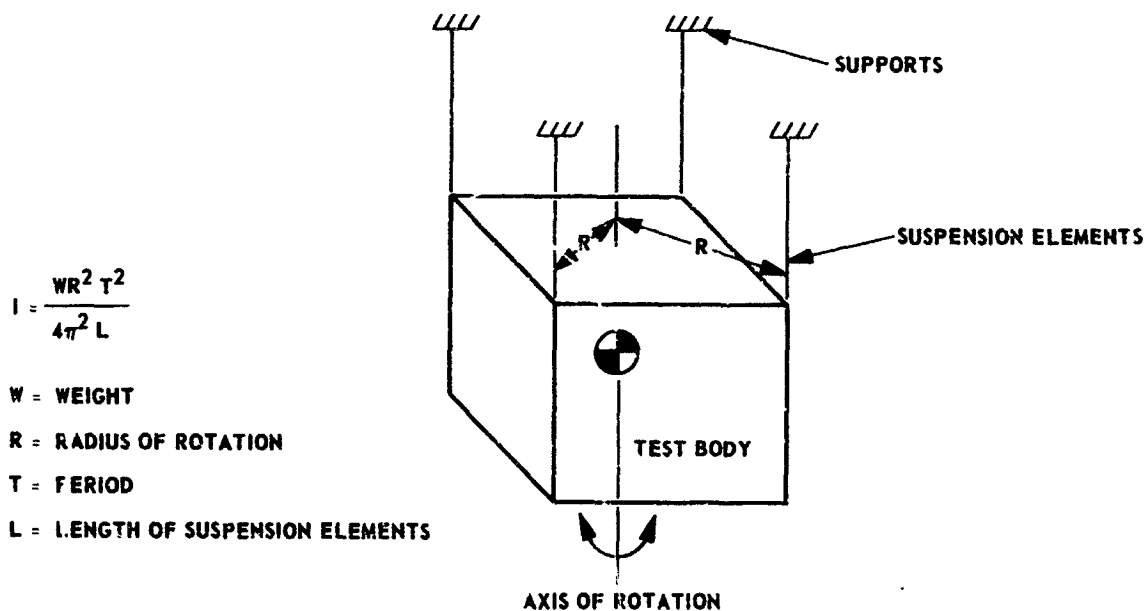


FIGURE 4 FILAR PENDULUM

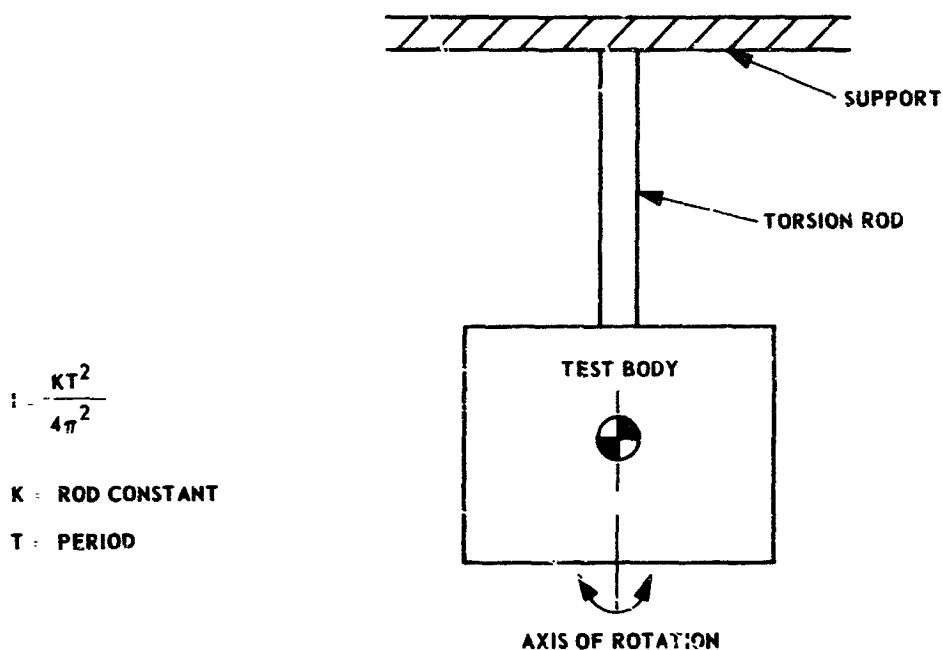


FIGURE 5 TORSIONAL PENDULUM

The theoretical approach in determining the moment of inertia by period measurement is based on the classical harmonic oscillator. Since the main concern is that of a torsional pendulum, the equations used to demonstrate a harmonic oscillator will be those of the torsional pendulum. The equation of motion of a torsional pendulum with no dissipational losses is

$$I \ddot{\theta} + K \theta = 0. \quad (1)$$

A standard solution of this equation yields

$$\omega = \sqrt{\frac{K}{I}} \quad (2\pi \text{ times the natural frequency}), \quad (2)$$

or
$$I = \frac{KT^2}{4\pi^2} \quad (\text{the true moment of inertia}) \quad (3)$$

as shown in Appendix A1.

The equation of motion of the above system with viscous damping proportional to the velocity is written below:

$$I \ddot{\theta} + C \dot{\theta} + K \theta = 0 \quad (4)$$

A solution to this equation is

$$\theta = A e^{\frac{-Ct}{2I}} \sin (qt + \phi) \quad (5)$$

where

$$q = \sqrt{\frac{K}{I} - \frac{C^2}{4I^2}} \quad (6)$$

as shown in Appendix A1.

Equation 6 gives the frequency of oscillation of the damped oscillating system. In this equation the damping constant C is related to the frequency q in such a manner that as C decreases, q approaches ω , shown in equation 2.

Equation 5 describes completely the damped oscillating system. However, if only maximum amplitudes are of concern, these may be obtained by setting $\sin (qt + \phi)$ equal to unity. The envelope of maximum amplitudes is then given by

$$\theta = A e^{\frac{-Ct}{2I}} \quad (7)$$

Equation 8 is then obtained by taking the natural logarithm of Equation 7

$$\ln \theta = \ln A - \frac{Ct}{2I} \quad (8)$$

If y is set equal to $\ln \theta$ and $\ln A$ is denoted by a constant b , Equation 8 has the form

$$y = mx + b = -\frac{Ct}{2I} + b, \quad (9)$$

representing a straight line with slope equal to

$$-\frac{C}{2I}.$$

For a given moment of inertia I , the slope of the line will be proportional to C . Previous reports have shown that the additional mass effect has a direct relationship with the decay amplitude. As the amplitude decays, the time rate at which it decays decreases; therefore, the damping decreases as the amplitude decreases. This effect is shown by typical experimental data from the torsional pendulum system presented in Figure 6. The plot of number of cycles in Figure 6 is effectively the total time in seconds. A semi-log plot of the same data is shown in Figure 7. This curve shows that as the amplitude decreases, the slope of the curve decreases. Analysis of Equation 9 indicates that if I remains constant, a decrease in the slope will produce a decrease in the decay constant. As seen in Figure 7, the decay constant varies during the initial time interval and then approaches a fixed value. This fixed value is in the order of magnitude of 10^{-3} , and the quantity

$$\frac{C^2}{4I^2}$$

is in the order of magnitude of 10^{-6} . Since the value of

$$\frac{K}{I}$$

is in the order of magnitude of 2 to 25, it can be seen from Equation 6 that the quantity q does not differ significantly from the quantity ω . Accordingly, the limiting value of the decay constant was taken to be zero. This analysis indicates that the true period for moment of inertia determination is obtained when the amplitude decreases to zero.

The method of experimentally determining the period as the amplitude decreases to zero is illustrated in Figure 8. The data used here is the same as that used in Figures 6 and 7 with different parameters. Experimental difficulties occur at small amplitudes, and this is attributed to the fact that at small amplitudes (approximately 0.001 of a radian) the energies caused by air currents and building vibrations are comparable to those of the oscillating torsional system. Figure 9 shows 10-period averages plotted versus total time. To obtain the period at zero amplitude, an extrapolation must be performed from the minimum displacement recorded to zero. This extrapolation is shown in Figure 8 and this is the correct period to use in determining the moment of inertia in the equation

$$I = \frac{KT^2}{4\pi^2} \quad (10)$$

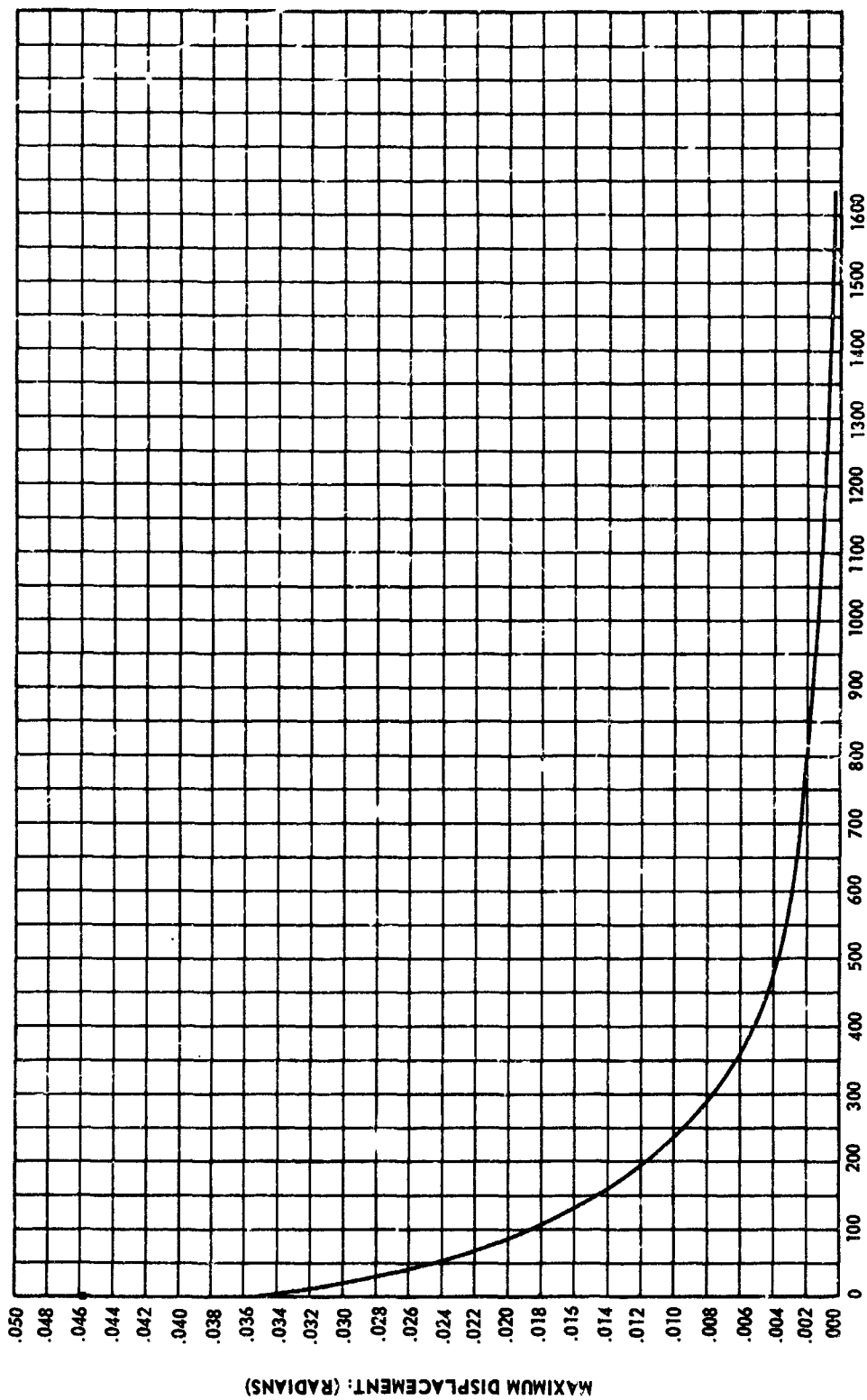
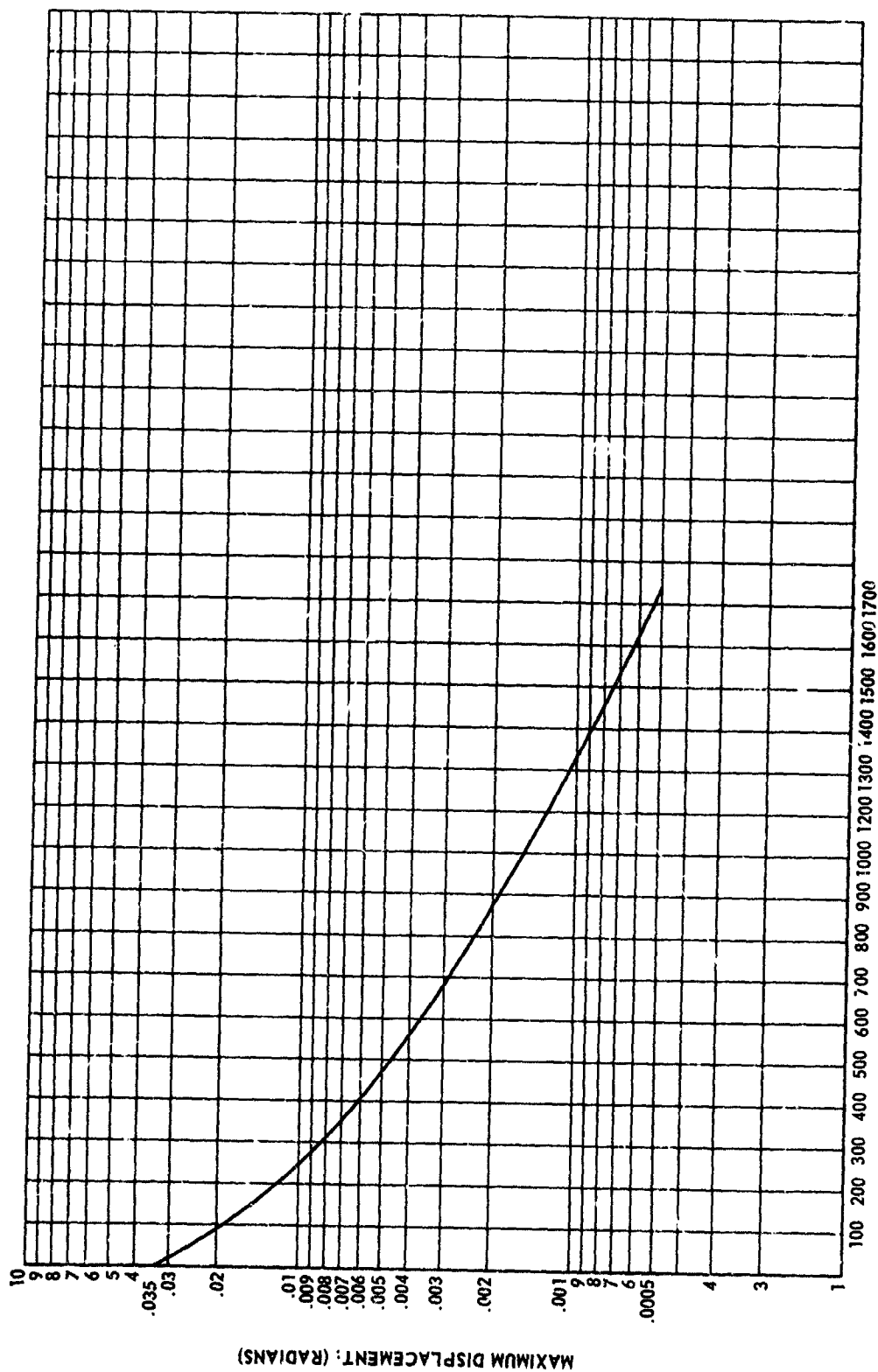


FIGURE 6 PLOT OF MAXIMUM DISPLACEMENTS VS TOTAL TIME
ROD NO. 120 DUMBBELL-C SUSPENDED TEST



TOTAL TIME: (PERIOD IN SECONDS X NUMBER OF CYCLES)
 FIGURE 7 LOGARITHMIC PLOT OF MAXIMUM DISPLACEMENTS
 VS TOTAL TIME

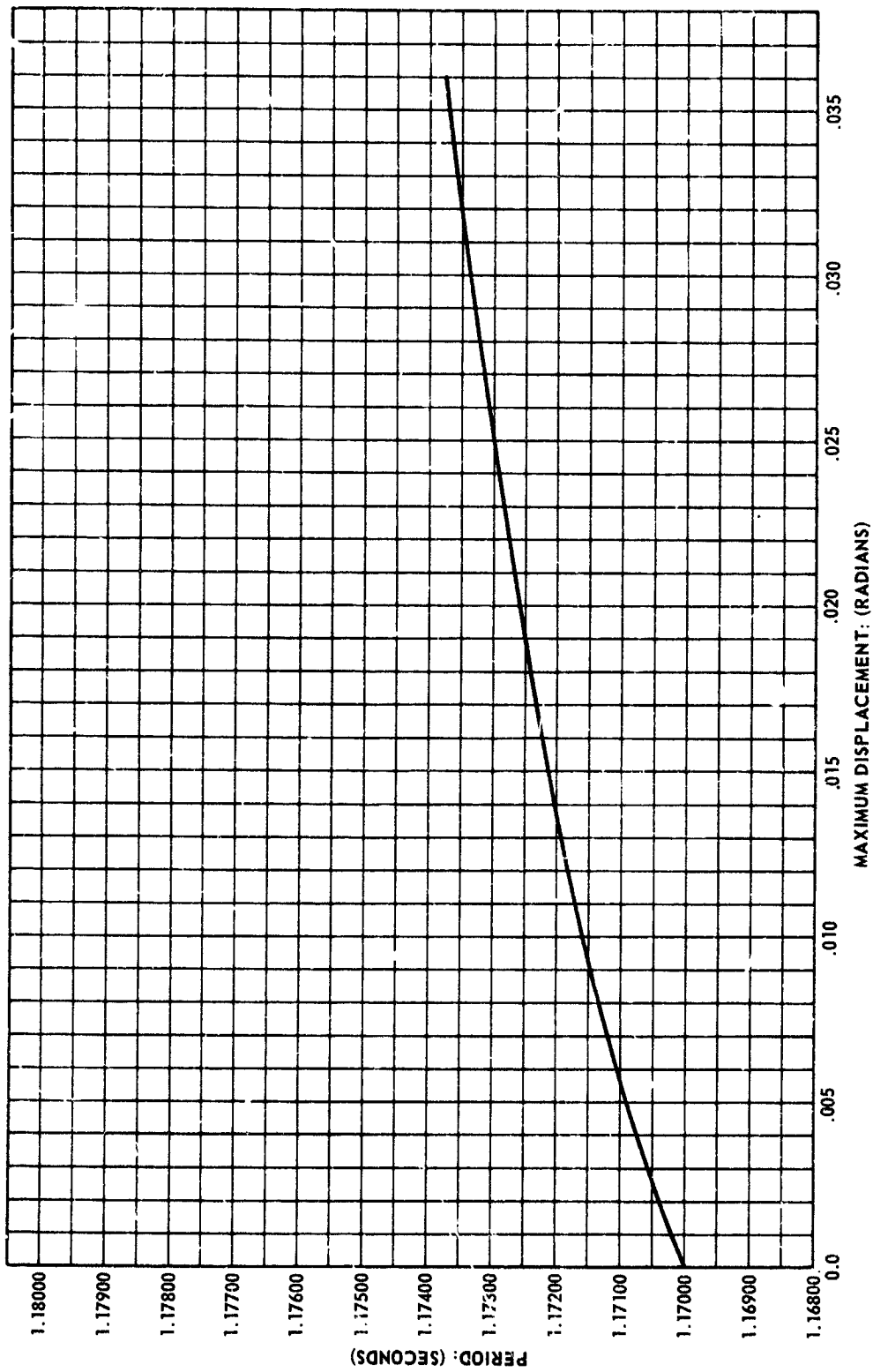


FIGURE 8 PLOT OF PERIOD VS MAXIMUM DISPLACEMENTS

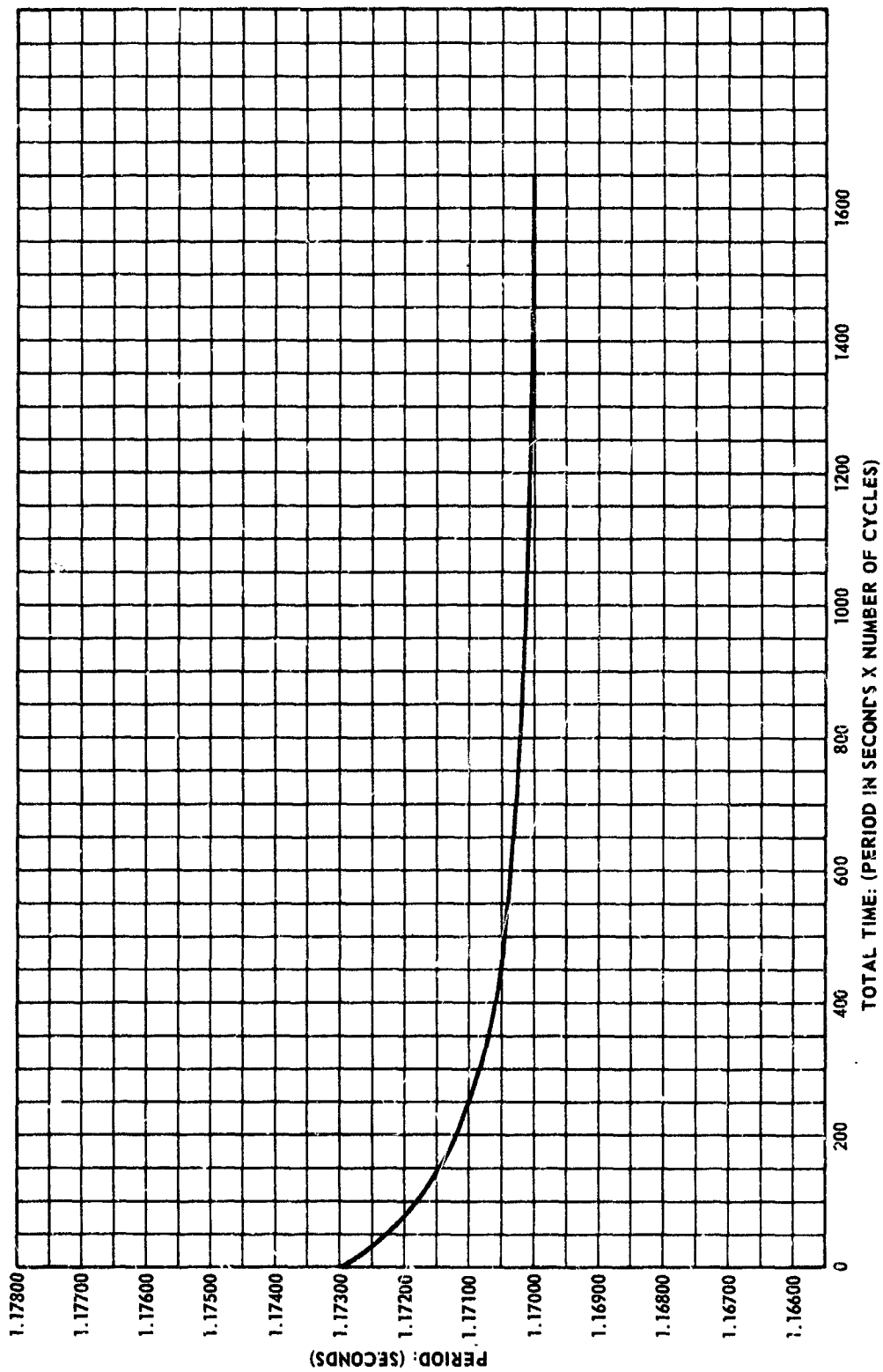


FIGURE 9 PLOT OF PERIOD VS TOTAL TIME

To improve the results of the period decay method, curve fitting techniques for analyzing the period decay of an oscillating system were investigated. A computer program for curve fitting by polynomials has been obtained and is shown in Figure 10. This program has been used on some curves to check its accuracy.

2.2.2 Experimental Apparatus: The experimental apparatus used in the moment of inertia determination program consists of the following: (See Figure 11)

1. Air bearing table
2. Torsion rod
3. Photo-cell timing device and associated equipment
4. Displacement measuring equipment

2.2.2.1 Air Bearing Table: The prime instrument which makes possible rapid determination of moment of inertia is the air bearing table, Figure 12. The turntable is supported by air bearings and represents a spring damped torsional pendulum which oscillates about a fixed position of equilibrium. It is supported vertically by a 24-inch diameter thrust air bearing and stabilized horizontally by a modified AB-9 air bearing.

The thrust air bearing surface area is approximately 250 square inches and consists of 120 feeder air holes arranged in two rows. The AB-9 radial air bearing under the center of the table has a special inner cylinder which has a radial air gap of 0.0020 to 0.0030 of an inch to prevent metal contact when the turntable is tilted.

Air is fed through an air filter to the air bearing by way of small holes drilled in special inserts. The turntable is normally operated at pressures of 25 pounds per square inch or less for safety reasons. Actual pressures used may be programmed with load so that a constant air gap and constant viscous damping can be maintained. Concentric grooves on the top of the table aid in centering the test specimen directly over the axis of the table.

2.2.2.2 Torsion Rod: The torsion rod material and design was obtained from previous work performed by the Measuring Methods Unit at MSFC/NASA. The circular shaped rod was used so that only pure rotational stresses would act as torque was applied to the rod. The material used in making

```

ENTER SOURCE PROGRAM, PUSH START
08300 DIMENSION X(100),Y(100),A(10,10),SUMX(21),SUMY(11)
08301 1 READ 200,N,TOL,LAST
08302 DO 40 I=1,N
08303 20 READ 201,X(I),Y(I)
08400 40 CONTINUE
08401 SUMX(1)=0
08516 SUMX(2)=0
08517 SUMX(3)=0
08518 SUMY(1)=0
08519 SUMY(2)=0
08612 DO 90 I=1,N
08613 SUMX(2)=SUMX(2)+X(I)
08614 SUMX(3)=SUMX(3)+X(I)*X(I)
08700 SUMY(1)=SUMY(1)+Y(I)
08701 SUMY(2)=SUMY(2)+Y(I)*Y(I)
08972 NORD=1
08973 1 IF(SENSE SWITCH 4)92,93
09016 2 ACCEPT 222,TOL,LAST
09052 93 L=NORD+1
09053 KX=L+1
09124 DO 101 I=1,L
09125 DO 100 J=1,L
09140 IK=J+1
09141 100 A(I,KK)=SUMX(IK)
09142 101 A(I,KK)=SUMY(IK)
09484 DO 110 I=1,L
09485 A(I,1)=1
09486 KKK=I+1
09502 DO 110 J=KKK,KK
09503 110 A(KK,J)=0
09504 C=1./A(I,1)
09505 DO 120 J=KKK,KK
09506 DO 120 J=KKK,KK
09507 120 A(I,J)=A(I,J)-A(I,J)*A(I,1)*C
09508 DO 140 I=1,L
09509 DO 140 J=KKK,KK
09510 140 A(I,J)=A(I,J)-A(I,1)*A(I,J)
09511 S2=0
09512 DO 160 J=1,N
09513 S1=0
09514 S1=S1-A(I,KK)
09515 DO 150 J=1,NORD
09516 150 S1=S1+A(I+1,KK)*X(J)**I
09517 160 S2=S2+(S1-Y(J))*(S1-Y(J))
09518 B=N-1
09519 S2=(S2/B)**.5
09520 IF(SENSE SWITCH 2)163,161
09521 161 IF(NORD-LAST)162,163,162
09522 162 IF((2-TOL)163,163,1
09523 163 PRINT 199
09524 PRINT 203, NORD,TOL,S2,K
09525 PRINT 198
09526 PRINT 197
09527 DO 164 I=1,L
09528 J=I-1
09529 164 PRINT 204,J,A(I,KK)
09530 PRINT 196
09531 PRINT 198
09532 PRINT 198
09533 IF(SENSE SWITCH 3)167,165
09534 165 IF(NORD-LAST)166,167,166
09535 166 IF((2-TOL)167,167,171
09536 167 PRINT 196
09537 DO 207 I=1,N
09538 S1=0
09539 S1=A(I,KK)
09540 DO 166 J=1,NORD
09541 166 S1=S1+A(J+1,KK)*X(I)**J
09542 S2=Y(I)-S1
09543 207 PRINT 205,X(I),Y(I),S1,S2
09544 IF(NORD-LAST)170,173,173
09545 170 IF((2-TOL)173,173,171
09546 171 NORD=NORD+1
09547 J=2*NORD
09548 SUMX(J)=0
09549 SUMX(J+1)=0
09550 SUMY(NORD+1)=0
09551 DO 172 I=1,N
09552 SUMX(J)=SUMX(J)+X(I)**(J-1)
09553 SUMX(J+1)=SUMX(J+1)+X(I)**J
09554 172 SUMY(NORD+1)=SUMY(NORD+1)+Y(I)*X(I)**NORD
09555 GO TO 91
09556 173 PAUSE
09557 IF(SENSE SWITCH 4)171,1
09558 200 FORMAT(13,F10.5,12)
09559 202 FORMAT(F10.5,12)
09560 201 FORMAT(2F10.5)
09561 199 FORMAT(52H ORDER TOL STD. ERR. NO. OF OBSERVATIONS)
09562 198 FORMAT(1H )
09563 203 FORMAT(14,2E14.8,EX,17)
09564 204 FORMAT(2HA(13,3H) = 614.8)
09565 197 FORMAT(15H COEFFICIENTS)
09566 205 FORMAT(4E16.8)
09567 196 FORMAT(7X,1HX,15X,1HX,8X,15H CALC. Y USING 17H Y - CALCULATED Y)
09568 STOP
09569 END

```

PROG SW1 ON FOR SYMBOL TABLE, PUSH START
 SW 1 OFF TO IGNORE SUBROUTINES, PUSH START
 PROCESSING COMPLETE

FIGURE 10 CURVE FITTING PROGRAM

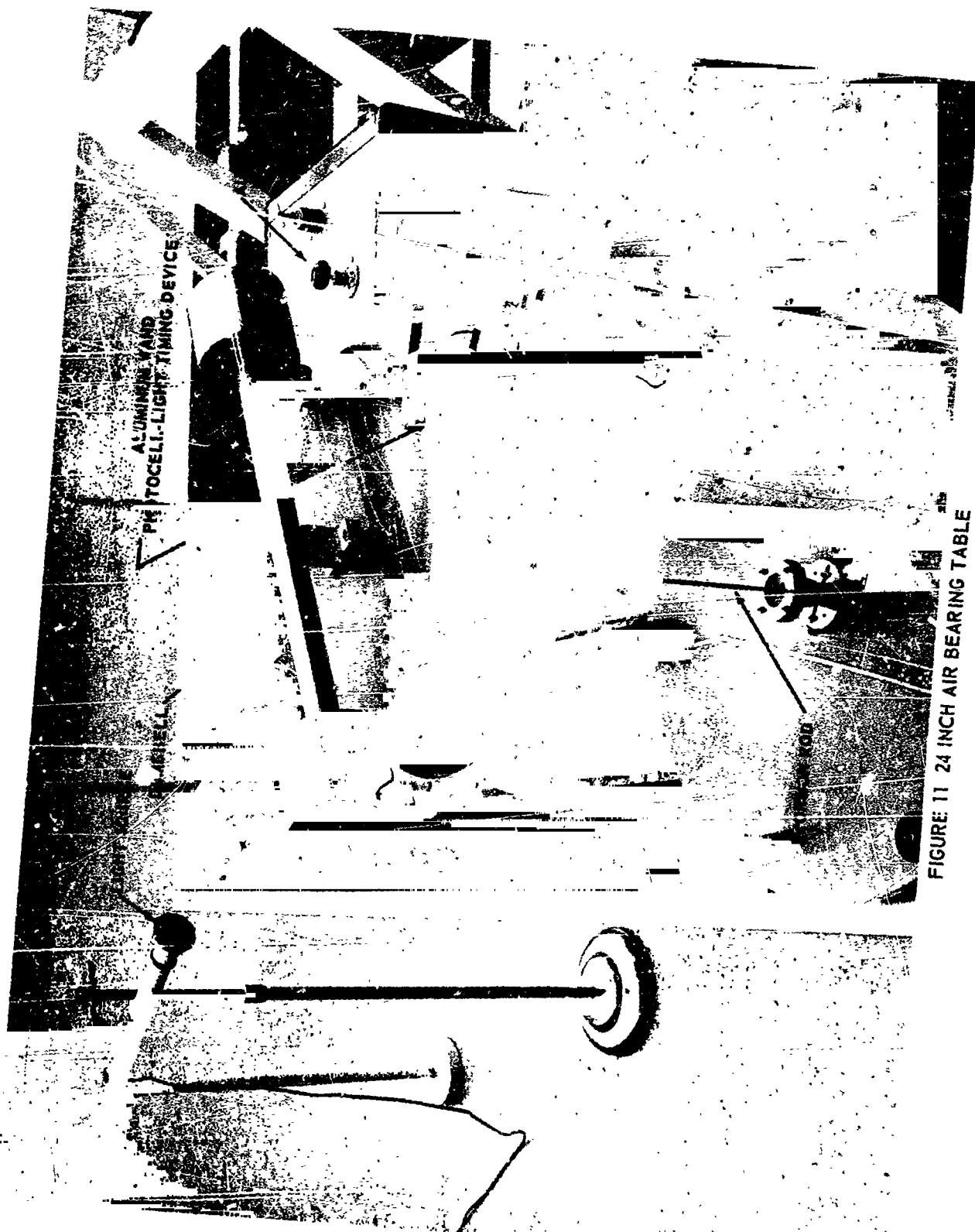


FIGURE 11 24 INCH AIR BEARING TABLE

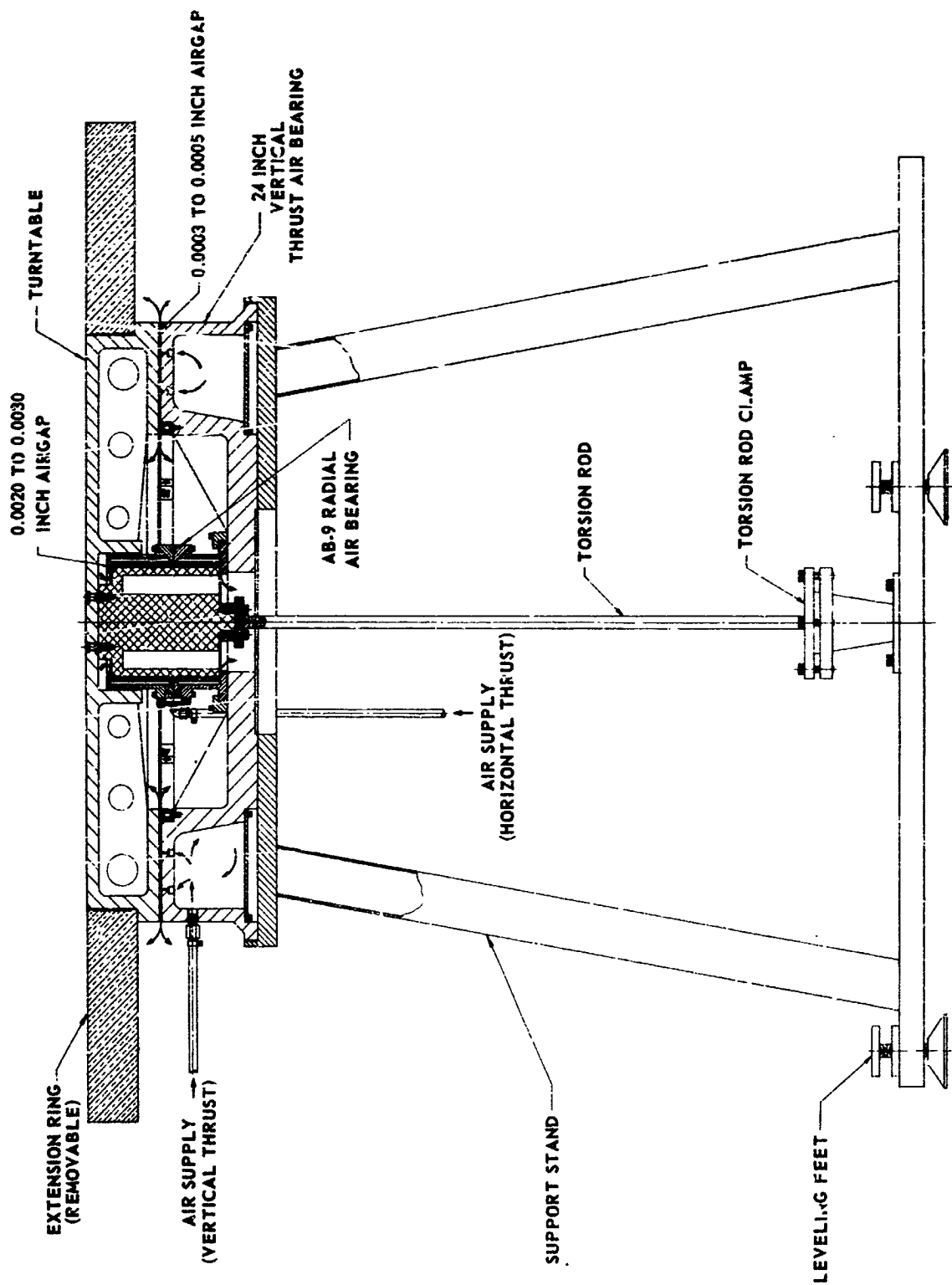


FIGURE 12 24 INCH AIR BEARING TABLE AND STAND

the rods was mild steel, B-1113. This material appeared to be very satisfactory since no hysteresis losses were noted. A research effort that might possibly find a better material or design for use as torsion rods should be conducted to improve the accuracy of the system.

The torsion rods were calibrated by using objects of known moment of inertia. These standards were five dumbbells. (See Table 1) Dumbbells A and C had previously been used by the Measuring Methods Unit at P&VE and were later refinished at SPACO, INC. to a tolerance of .001 of an inch. The other three dumbbells were fabricated at SPACO, INC. and were also finished to .001 of an inch.

All of the dumbbell standards were recalibrated by the Army Calibration Laboratory, using the new load cell procedure developed by the National Bureau of Standards. The procedure is capable of accuracies approaching that of a balance, and uses "off the shelf" components. The setup consists of a load cell, flexures, a hydraulic lift, weight standards, and digital instrumentation for monitoring the load cells. Basically the technique consists of comparing the unknown weight with two standards of approximately the same weight alternately, and statistically determining the difference. A typical procedure is outlined below.

1. Exercise the load cell with the load to be measured until stable readings occur, using the predetermined time cycle. (Exercising is loading and unloading the cell, a technique found to make the cell more stable.)

2. Three minutes after starting to release the weight (after stability is reached by exercising) take a zero reading. (While a zero reading is not used in the calculations, it is included in this procedure to monitor the stability of the instrument.)

3. Immediately (but gently) pick up standard weight and read after 2 minutes from start of pick up.

4. Release standard and read after 3 minutes from start of release.

5. Pick up unknown weight and read after 2 minutes from start of pick up.

6. Release unknown and read zero after 3 minutes from start of release.

7. Pick up unknown and a sensitivity weight that is a bit larger than the difference between the standard and the unknown, and read after 2 minutes from start of pick up.

Table 1 Moment of Inertia Test Standards

No.	Nominal Size in.-lb-sec ²	Weight (Pounds)	Mass $G = 385.68397 \text{ in./sec}^2$	Calculated Moment of Inertia (in.-lb-sec ²)
A	30	74.99	0.1944294	27.4996
B	60	112.91	0.2927420	60.9308
C	90	182.58	0.47339	91.38615
D	125	198.81	0.515474	124.1324
E	190	291.05	0.754633	188.1009

8. Release and read zero after 3 minutes from start of release.
9. Pick up standard and the same sensitivity weight and read after 2 minutes from start of pick up.
10. Release and read zero after 3 minutes from start of release.

This procedure is repeated many times to achieve the desired confidence level. It can be seen that the data produced can be used to determine accurately the difference between the unknown and standard weights. The results of this procedure used on four of the dumbbell standards is shown in Table 2. The new weights are believed to be reliable within ± 20 ppm. Calibration of the remaining standards is still being performed.

Table 2 Results of Four Dumbbell Standards

Dumbbell No.	Old Weight	New Weight
B	112.91	112.8745
C	182.58	182.821
D	198.81	198.750
E	291.05	290.966

These dumbbell moment of inertia standards were then used on the suspended torsional pendulum to calibrate the torsion rods. A static method of determining the rod constant was designed and used for the larger rods because an excessively short period time resulted from the dynamic system.

2.2.2.3 Photocell Timing Device and Associated Equipment: The photocell timing device for measuring periods has been greatly improved since testing began. The improvement basically consisted of converting the power supply from alternating current to direct current. Previously the alternating current had caused the light source to vary in intensity thereby causing the photocell to be triggered at random. This random effect caused the period measurements to be very scattered; therefore, individual period measurements were meaningless. To correct this unwanted error it was necessary to change the light source power to direct current so that a constant intensity could be obtained. The circuitry was modified to provide direct current from a storage battery to heat the filament of the light source. At the same time the power to the transistor amplifier was converted to direct

current to eliminate any transients which might produce erroneous output pulses. A rheostat was incorporated into the filament circuit of the light source to control the light source intensity.

2.2.2.4 Displacement Measuring Equipment: The displacement measuring equipment consists of a mirror, a light source and a calibrated scale. The mirror is located on the axis of rotation. The light source is reflected from the mirror onto the calibrated scale. The scale is designed to read angular displacements directly if the scale is located at 140". The displacement measurements are recorded manually by laboratory personnel. An automated method of measuring angular displacements using a capacitive transducer has been designed and is described in detail in paragraph 2.2.4.1.

2.2.3 Testing Program: Six different studies were performed to determine the performance of the moment of inertia measurement system. These test were:

1. Rod Calibration Program
2. Moment of Inertia Determination Program
3. Table Load and Air Pressure Tests
4. Aerodynamic Drag Tests
5. Temperature Tests
6. Error Analysis

2.2.3.1 Rod Calibration Program: The first series of tests was performed to determine the spring constants of the rods to be used in the air bearing table. The torsional pendulum apparatus was used with dumbbells of known moments of inertia. The dumbbells were suspended on the torsion rods from the overhead "I" beam. Figure 13 shows the test equipment. The photocell light timing device and the displacement measuring device are initially aligned for all systems to record zero when the dumbbell is in its static position.

The dumbbell was manually displaced to approximately 0.18 of a radian and released to start the oscillation. A Teflon bearing arrangement was used initially to steady the oscillations. When the dumbbell's maximum displacement decreased to 0.15 of a radian, the Teflon bearing was removed and the first period and the first maximum displacement measurements were recorded.

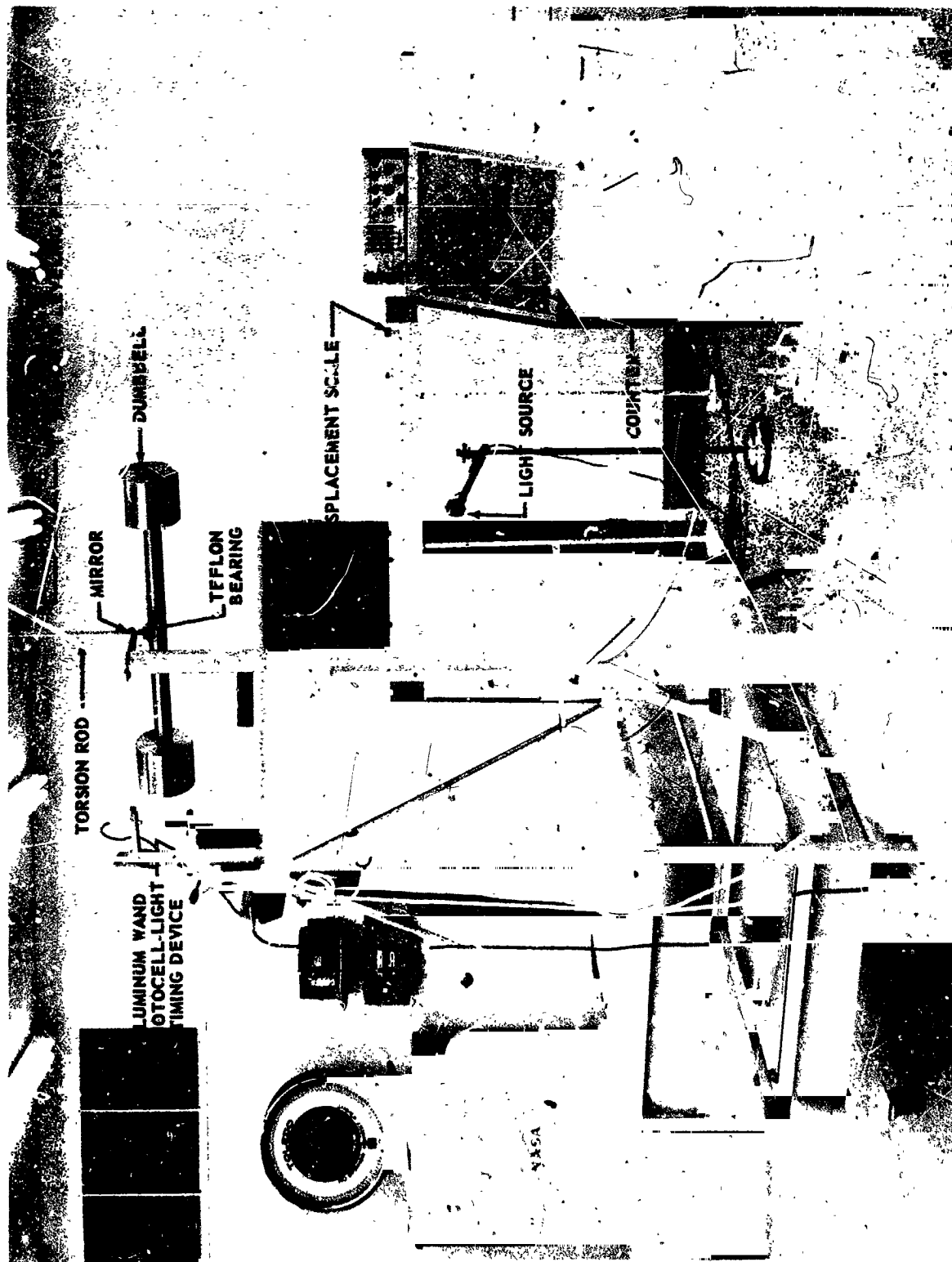


FIGURE 13 TORSIONAL PENDULUM TEST APPARATUS

In the first experiments the period was recorded every other cycle, and the displacements were recorded every 0.05 of a radian until the timing device stopped recording. This method proved to be very time consuming, especially in plotting data. Therefore, the counter was set to record 10-period averages, and displacements were recorded at intervals of 0.001 of a radian starting with 0.035 of a radian. Since 10-period averages tend to eliminate random errors, this data was used. The use of smaller increments also produces greater accuracy in the displacement measurements. Since small displacements are the main concern, no inconsistencies are introduced in measuring from 0.035 of a radian instead of 0.15 of a radian. Figures 14 through 17 show the results of a typical period decay test. Figure 17 shows that the period corresponding to zero amplitude is 1.35570 seconds. The correct value of the rod constant can now be calculated using the equation,

$$K = \frac{4\pi^2 I}{T^2} \quad (11)$$

where "I" is a known value. Table 3 shows the results of this series of tests using two different rods. Each test was repeated at least five times to obtain the average period. The exact procedure for this test is shown in Appendix A3.

2.2.3.2 Moment of Inertia Determination Program: The second series of tests were performed to determine moment of inertia by using the air bearing system. The previously calibrated rods were used in the air bearing table, and the periods were determined by the method of period decay. The basic equation,

$$I = \frac{KT^2}{4\pi^2} \quad (12)$$

was used to determine "I". Table 4 shows the repeatability of the system. Table 5 shows the results of this series of tests. The moments of inertia of the empty table with the dumbbell adapter was first determined. Later, various dumbbells were tested to determine their moments of inertia. The percentage error always remained less than 0.5 of one per cent, but even greater accuracy should result as techniques are improved. The test procedure for these tests is shown in Appendix A4.

2.2.3.3 Table Load and Air Bearing Pressure Tests Program: The performance characteristics of the air bearing table are affected by table load and air pressure going into the air bearings. To determine these effects a series of tests were conducted under various table loads and air pressures. In order to obtain the effect of table load and air pressure, other variables must remain constant. One of these variables is temperature, which was held constantly at 71°F. The other variable that greatly affects the results is aerodynamic drag. This was compensated for by building an

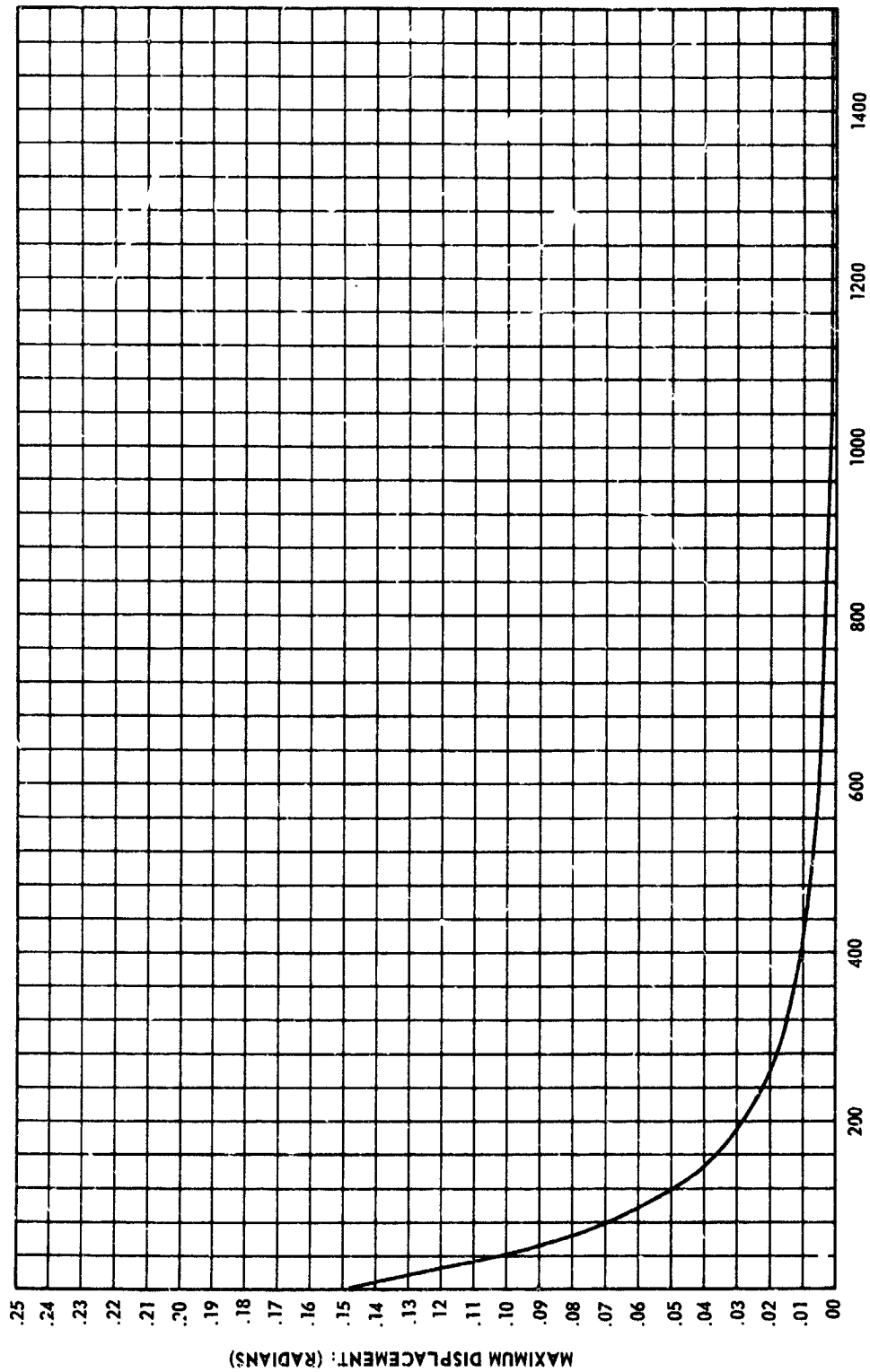


FIGURE 14 PLOT OF MAXIMUM DISPLACEMENTS VS TOTAL TIME
 (PERIOD IN SECONDS X NUMBER OF CYCLES)

ROD NO. 120 DUMBBELL-D SUSPENDED TEST

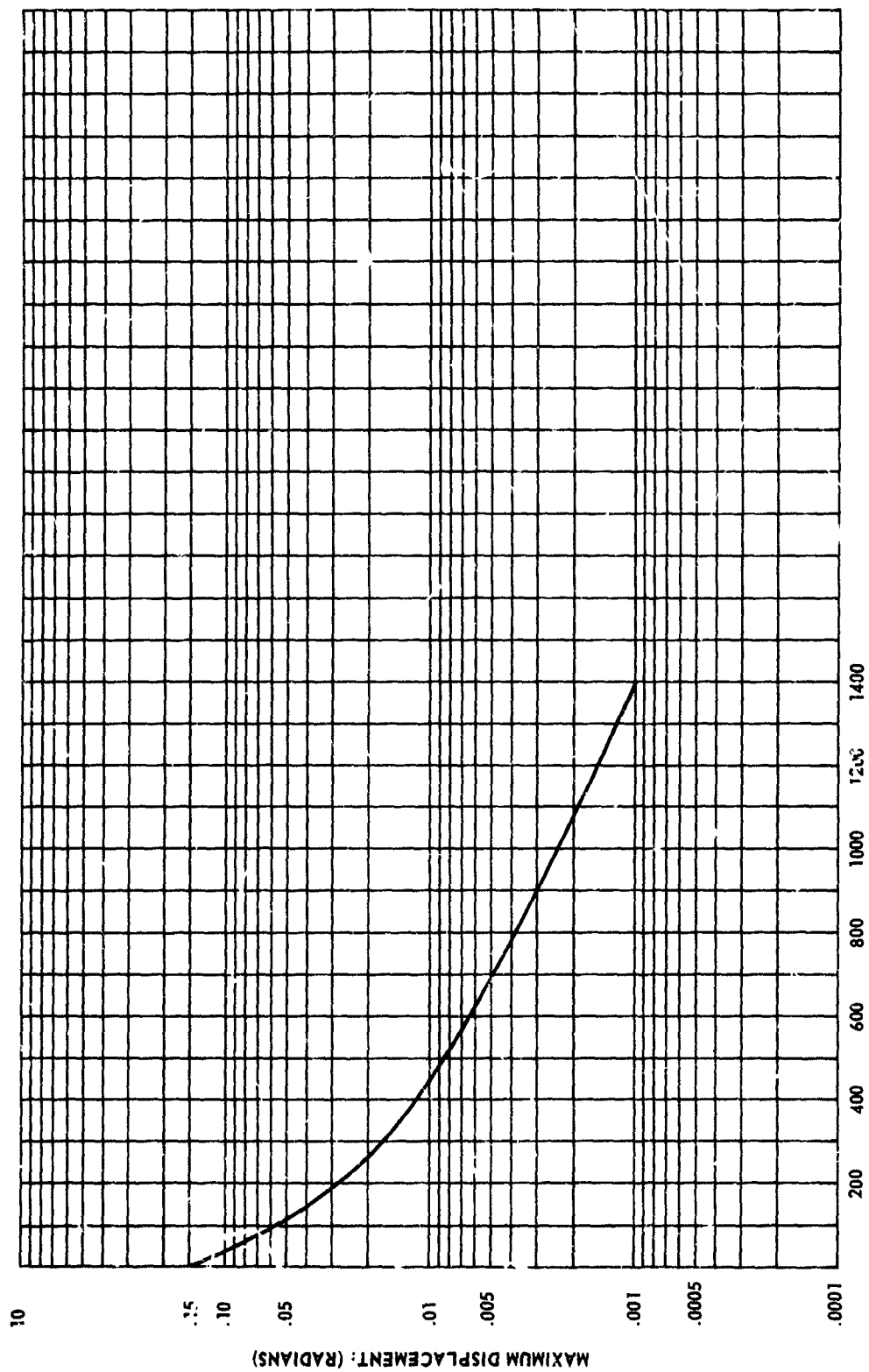
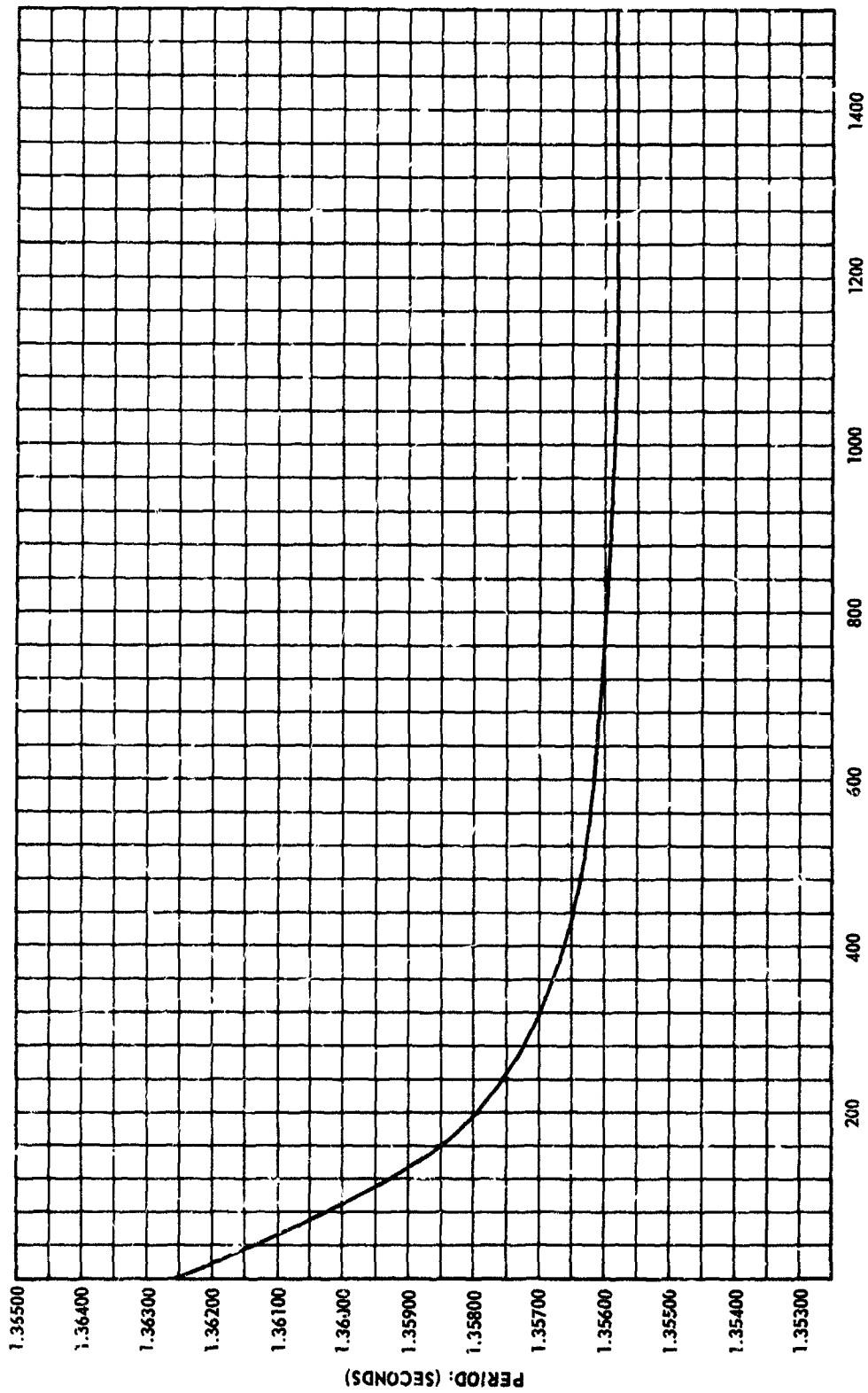


FIGURE 15 LOGARITHMIC PLOT OF MAXIMUM DISPLACEMENTS VS TOTAL TIME



TOTAL TIME: (PERIOD IN SECONDS X NUMBER OF CYCLES)

FIGURE 16 PLOT OF PERIOD VS TOTAL TIME

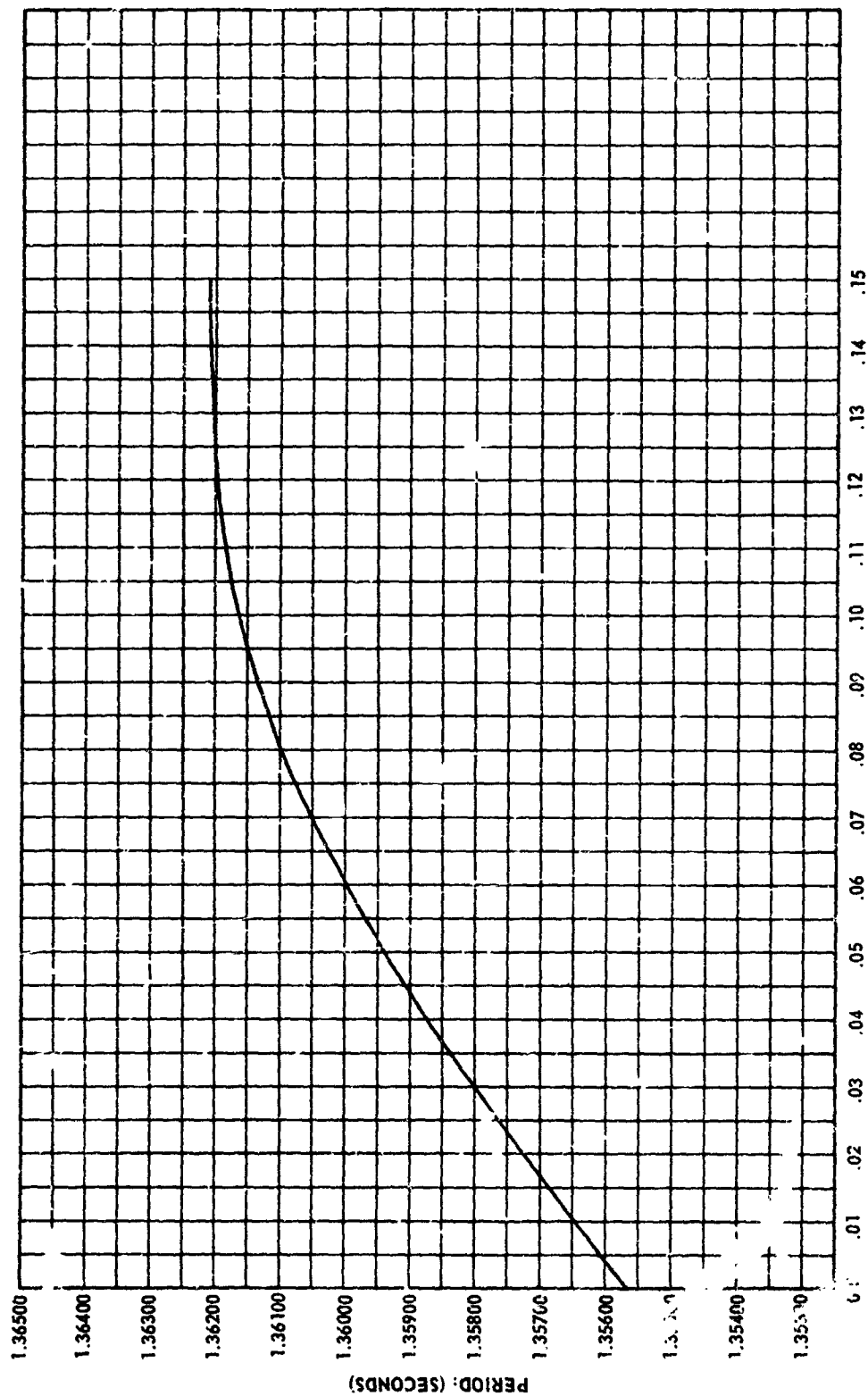


FIGURE 17 PLOT OF PERIOD VS MAXIMUM DISPLACEMENTS

Table 3. Rod Constant Determination

Rod Number 120 (0.5 inch diameter x 27.5 inches long)

Dumbbell	Average Period	Rod Constant - K
60.931 in. -lb-sec. ²	0.94963 sec.	2667.383 in. -lb/radian
124.132	1.35570	2666.350
188.101	1.66900	2665.858
	Average	2666.530

Rod Number 28 (0.25 inch diameter x 27.5 inches long)

Dumbbell	Average Period	Rod Constant - K
27.500 in. -lb-sec. ²	2.47825 sec.	176.765 in. -lb/radian
60.931	3.68700	176.950
124.132	5.26440	176.826
188.101	6.47700	177.012
	Average	176.888

Table 4. Repeatability Test Results

Rod Number 120 Air Bearing Table 60 in-lb-sec ² Dumbbell			
Test Number	Date	Temp.	Period
482	4-19-65	70	1.02633
483	4-19-65	70	1.02630
484	4-19-65	70	1.02628
485	4-19-65	70	1.02628
486	4-19-65	70	1.02632
487	4-19-65	70	1.02627
488	4-20-65	71	1.02622
489	4-20-65	70	1.02617
490	4-20-65	70	1.02628
491	4-20-65	71	1.02620
Average			1.02627
Standard Deviation			.00005

Table 5. Moment of Inertia Determination Test Results

Moment of Inertia of Dumbbell	Average Period	Calculated Moment of Inertia	Percentage Error
Rod Number 120			
No Load	0.38331 sec	9.924 in.-lb-sec ²	
60.931 in.-lb-sec ²	1.02627	61.057	0.2%
124.132	1.41212	124.765	0.5%
188.101	1.71655	189.098	0.5%
Rod Number 28			
No Load	1.48695	9.907	
27.500	2.89094	27.540	0.1%
60.931	3.97655	60.945	0.02%
124.132	5.46950	124.733	0.5%

air shield as shown in Figure 18 that would keep the drag constant as the load was changed. The loads used were cylindrical weights, weighing approximately 100 pounds each and were mounted on the table as shown in Figure 19. The shield was mounted over the weights so that the outside drag would be constant. The internal drag was assumed small and therefore was neglected.

The results of the tests are shown in Table 6. The damping constant C is used to depict the efficiency of the air bearing table. C is obtained from

$$I \ddot{\theta} + C \dot{\theta} + K \theta = 0. \quad (13)$$

Equation 13 has the solution

$$\theta = A e^{\frac{-Ct}{2I}} \sin (qt + \phi). \quad (14)$$

If maximum amplitudes are considered Equation 14 becomes

$$\theta = A e^{\frac{-Ct}{2I}} \quad (15)$$

or

$$\ln \theta = \ln A - \frac{Ct}{2I} \quad (16)$$

where the natural logarithm of Equation (15) was taken. If $\ln \theta$ is plotted against t the slope of the curve will be

$$\frac{-C}{2I}.$$

Now if the slope of the curve is multiplied by $2I$ the quantity C can be obtained. I is obtained by calculating the moments of inertia of the specimen on the table top. Figure 20 shows a typical plot of test data. Instead of plotting t , the total time, the number of cycles are plotted. The time t is then obtained by multiplying the number of cycles by the average period. Since the period is relatively constant this method is justifiable. The slopes of the curves were all taken from 0.002 to 0.001 radians since at this amplitude the system is most efficient. As an example in Figure 20 the slope of the curve is 0.00329, $2I$ is 88.978 and C is 0.293. This quantity C represents the efficiency of the system.

The results of the tests as depicted in Table 6 show in general that as the load increases the damping increases and as the pressure increases the damping decreases. For large loads with insufficient air pressure as

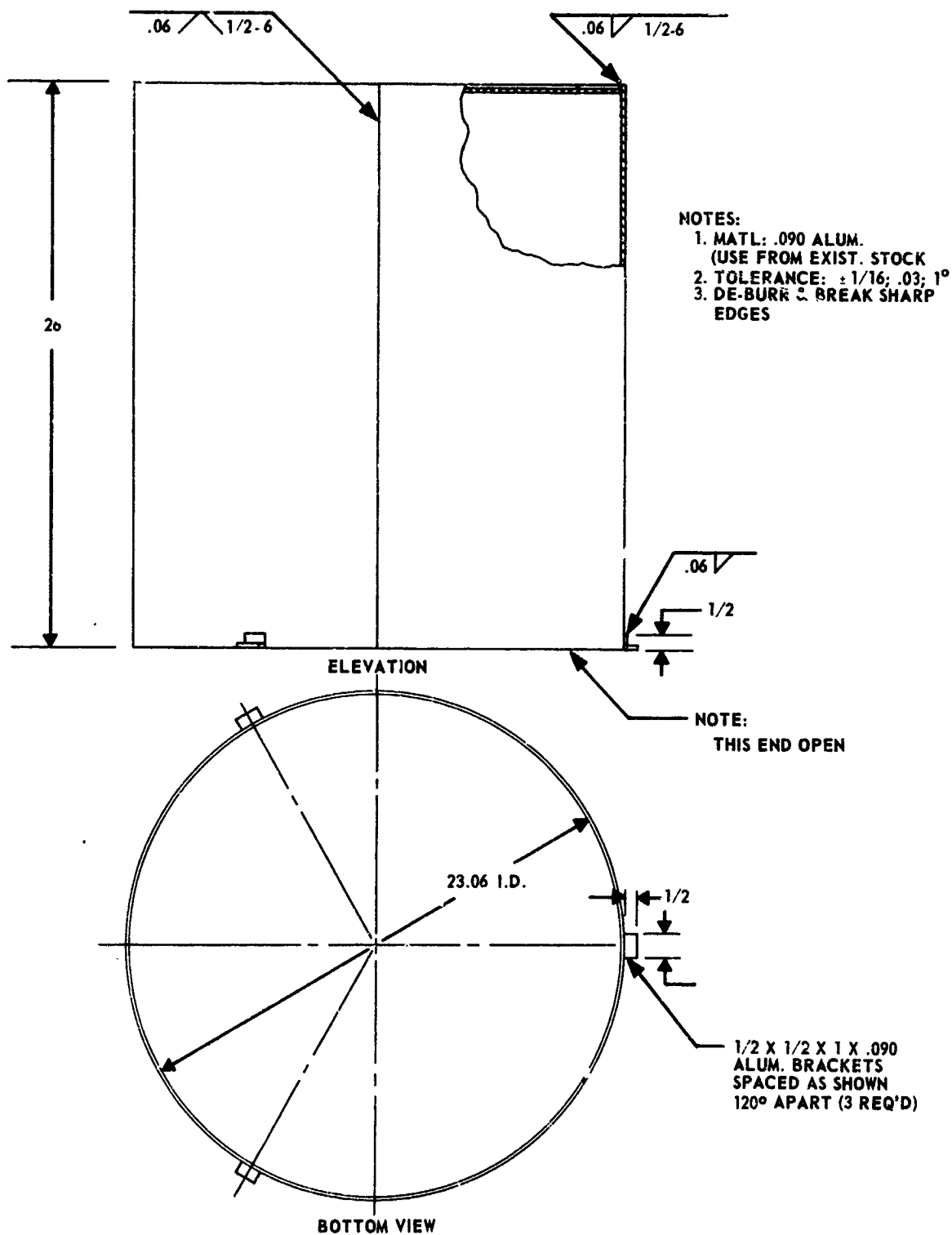


FIGURE 18 AIR SHIELD

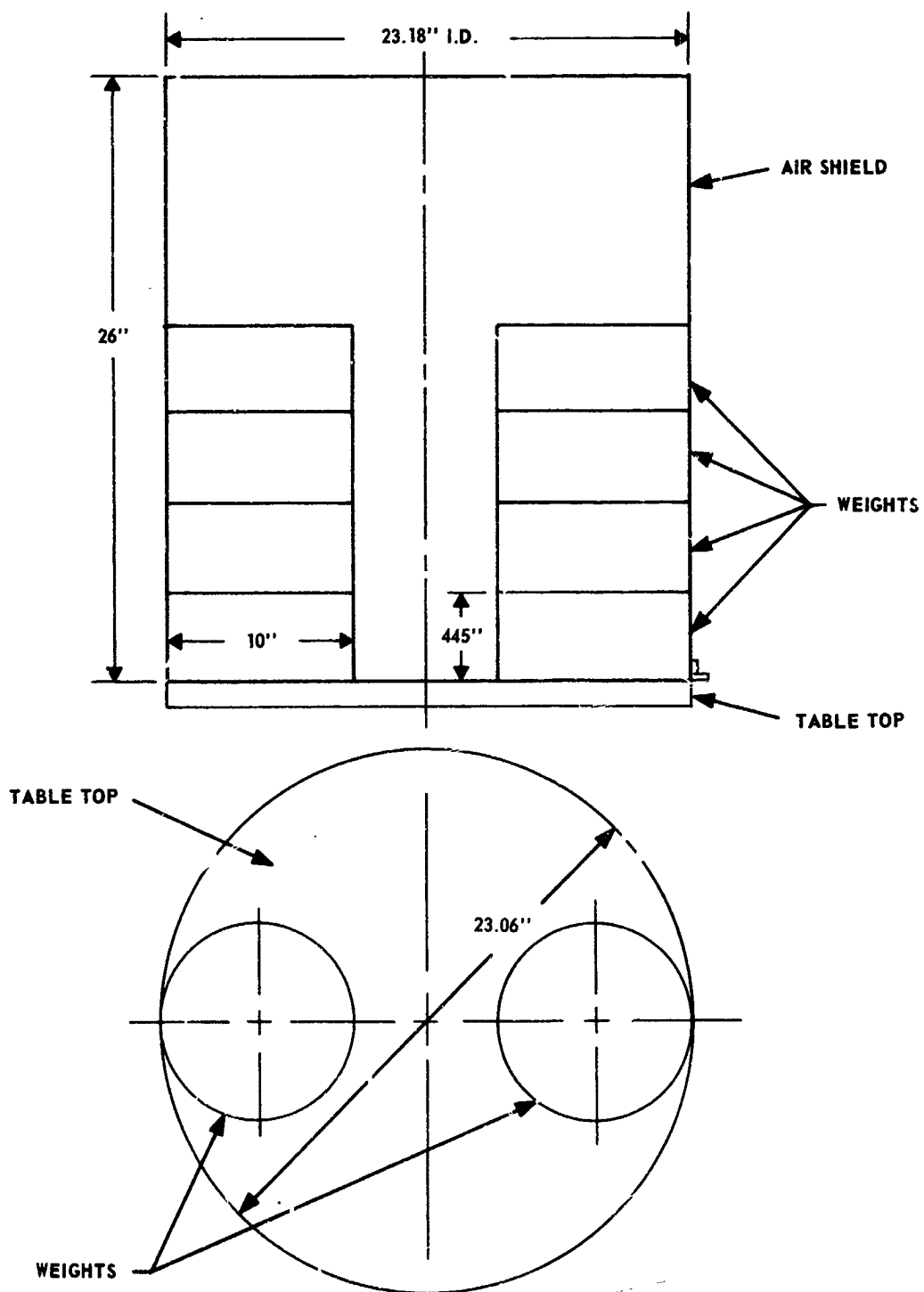


FIGURE 19 WEIGHT MOUNTING PROCEDURE

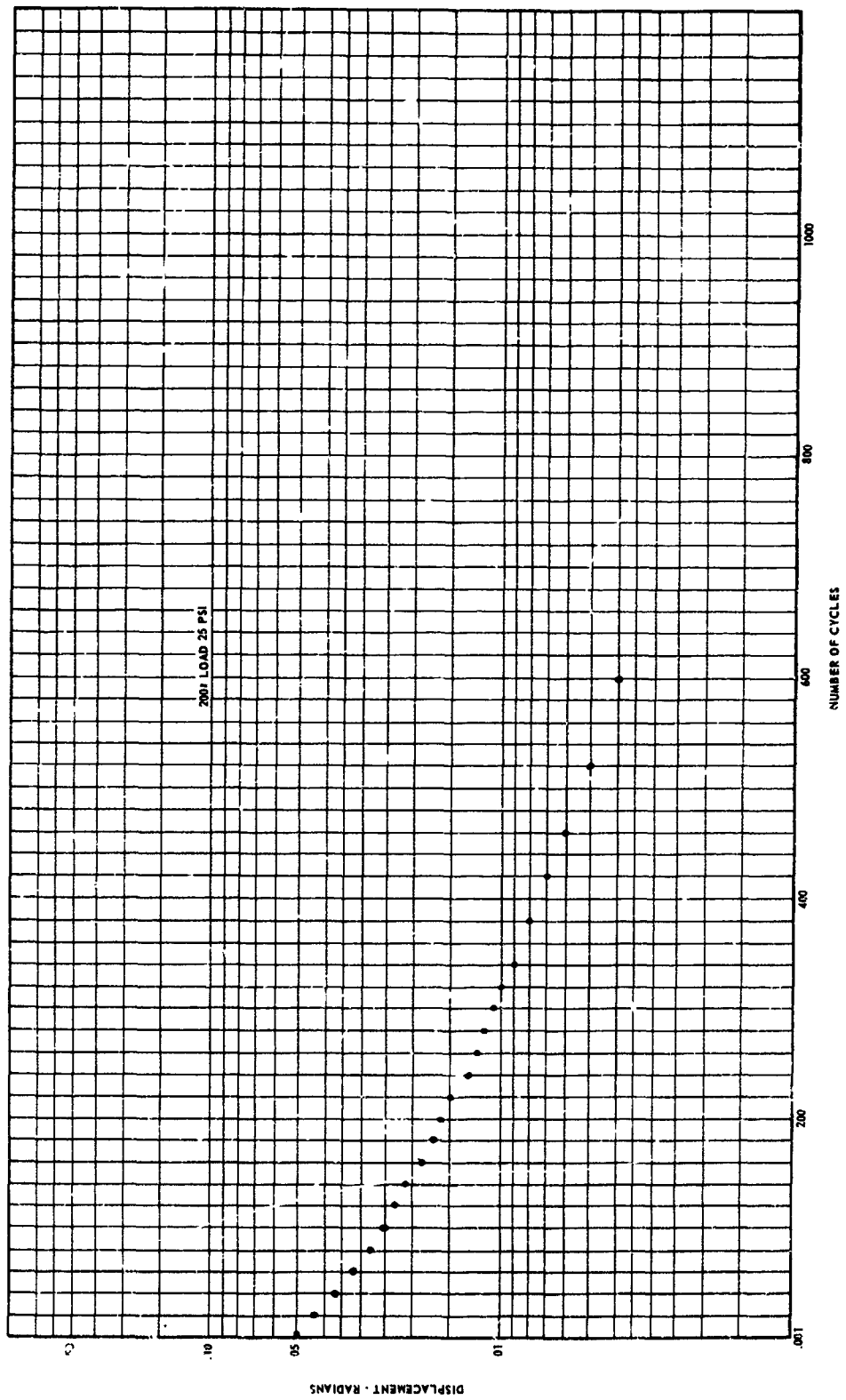


FIGURE 20 NATURAL LOG DISPLACEMENT VS TIME

Table 6. Damping Constant C at 71°F For Various Loads and Pressures

	10 PSI	20 PSI	25 PSI	30 PSI	40 PSI
No Load	0.246	0.197	0.197	0.208	0.191
200 #	0.426	0.367	0.319	0.270	-
400 #	0.463	0.445	0.435	0.371	-
600 #	-	0.490	0.508	0.409	0.474
800 #	-	2.702	0.672	0.641	0.588
1000 #	-	-	-	0.653	0.650

shown for 800# at 20 PSI the damping is very large. This is caused by the table dragging on the safety stops. From these test results it is obvious that the air pressure applied to the table must be programmed depending on the load. Figure 21 shows a plot of damping versus load for five different air pressures. The damping constant is relatively low in all cases except where the table top drags on the safety stops. This small damping does not; however, affect the moment of inertia determination since it is corrected for in the period decay method. The test procedure for these tests is included as Appendix A5.

2.2.3.4 Aerodynamic Drag Test Program: Aerodynamic drag is known to have a predominant effect on measuring moments of inertia. Therefore, a series of experiments was performed to investigate this effect. The test program consisted of twelve different tests using four drag configurations and three different moment of inertia values. The drag plate configurations are shown in Figure 22 along with their pertinent characteristics. The moment of inertia of each plate is calculated about its vertical axis, the axis of rotation. The objects used to change the moment of inertia of the table are cylindrical weights as shown in Figure 23. The characteristics of the weights are described in Figure 23. The moment of inertia I_{aa} is the value that will be used for each weight placed on the table since the center of gravity of each weight will be located 6.5 inches from the axis of rotation. Figure 24 shows how the table is configured during a test, with weights and drag plate. All tests are performed in the same manner except for changes in drag plates and weights. The test procedure used for each test is shown in Appendix A6.

The complete results of the test program is tabulated in Table 6A. The calculated moment of inertias are obtained by adding the moments of inertia of each component on the table. The moment of inertia of the table top is 9.924 in-lb-sec² and the moment of inertia of the drag plates and weights have previously been described in Figures 22 and 23. The experimental moments of inertia are obtained by using

$$I = \frac{KT^2}{4\pi^2} \quad (17)$$

where $K = 2655.96$

The percentage difference is calculated to give a comparison of the two quantities. The percentage difference of the first three drag configurations are within the limits of experimental error. The percentage difference of the last three tests can be attributed to high drag losses and an unstable plate mounting. The damping constant is obtained from

$$I \ddot{\theta} + C \dot{\theta} + K \theta = 0. \quad (18)$$

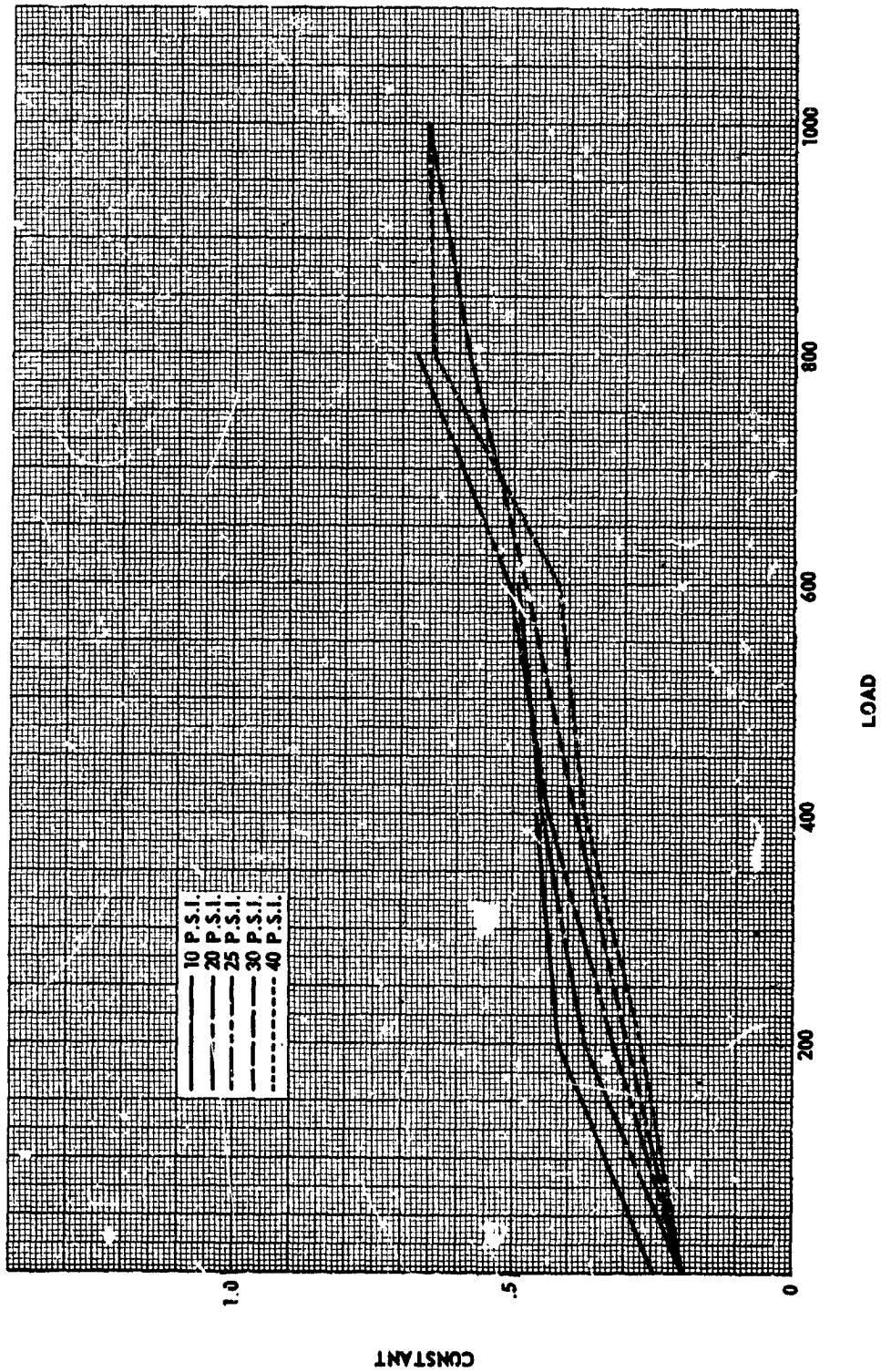


FIGURE 2: DAMPING CONSTANT VS LOAD

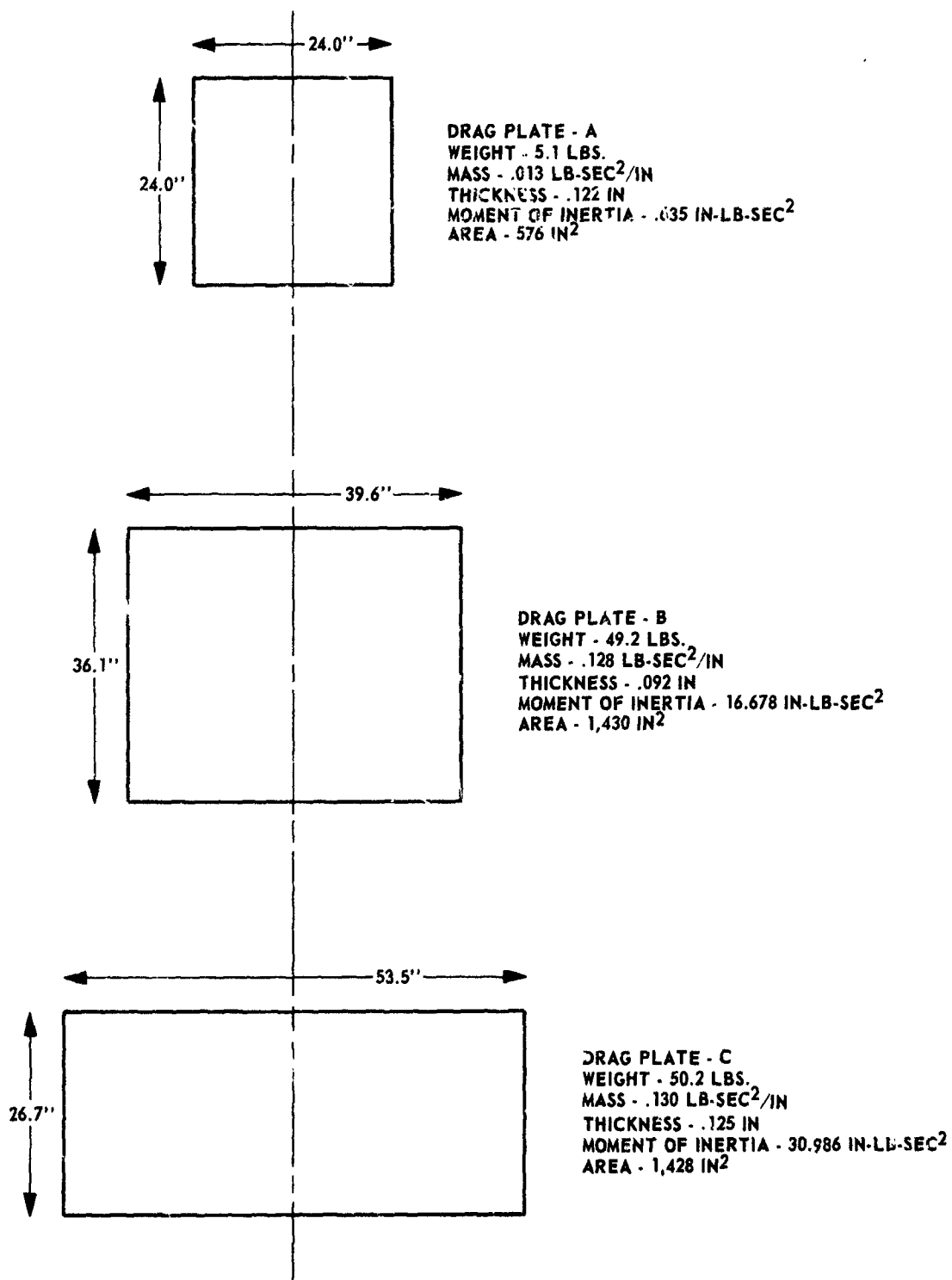
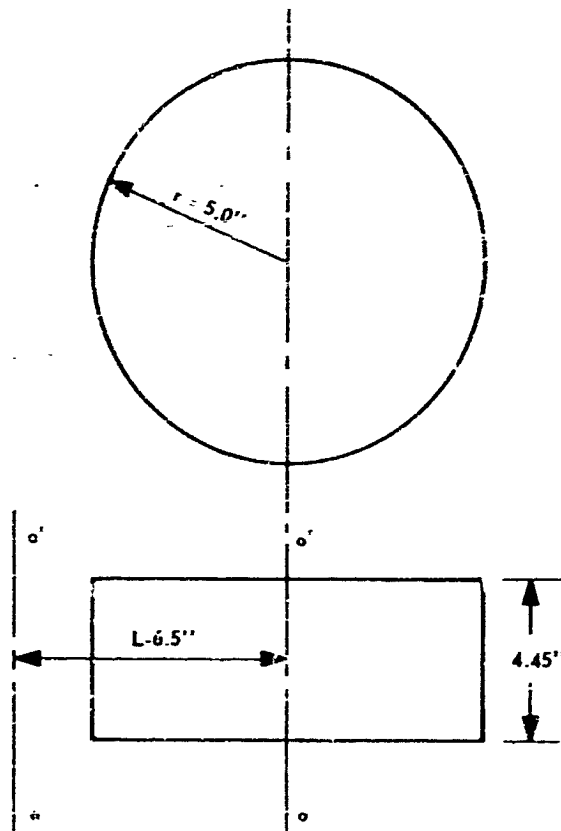


FIGURE 22 DRAG PLATE CONFIGURATIONS



WEIGHT - 99.0 LB.

MASS - .257 LB - SEC²/IN.

RADIUS - 5.0 IN.

$$I_{oo'} = \frac{Mr^2}{2} = 3.209 \text{ IN-LB-SEC}^2$$

$$I_{oo'} = I_{oo} + ML^2 = 14.087 \text{ IN-LB-SEC}^2$$

FIGURE 23 CYLINDRICAL WEIGHTS

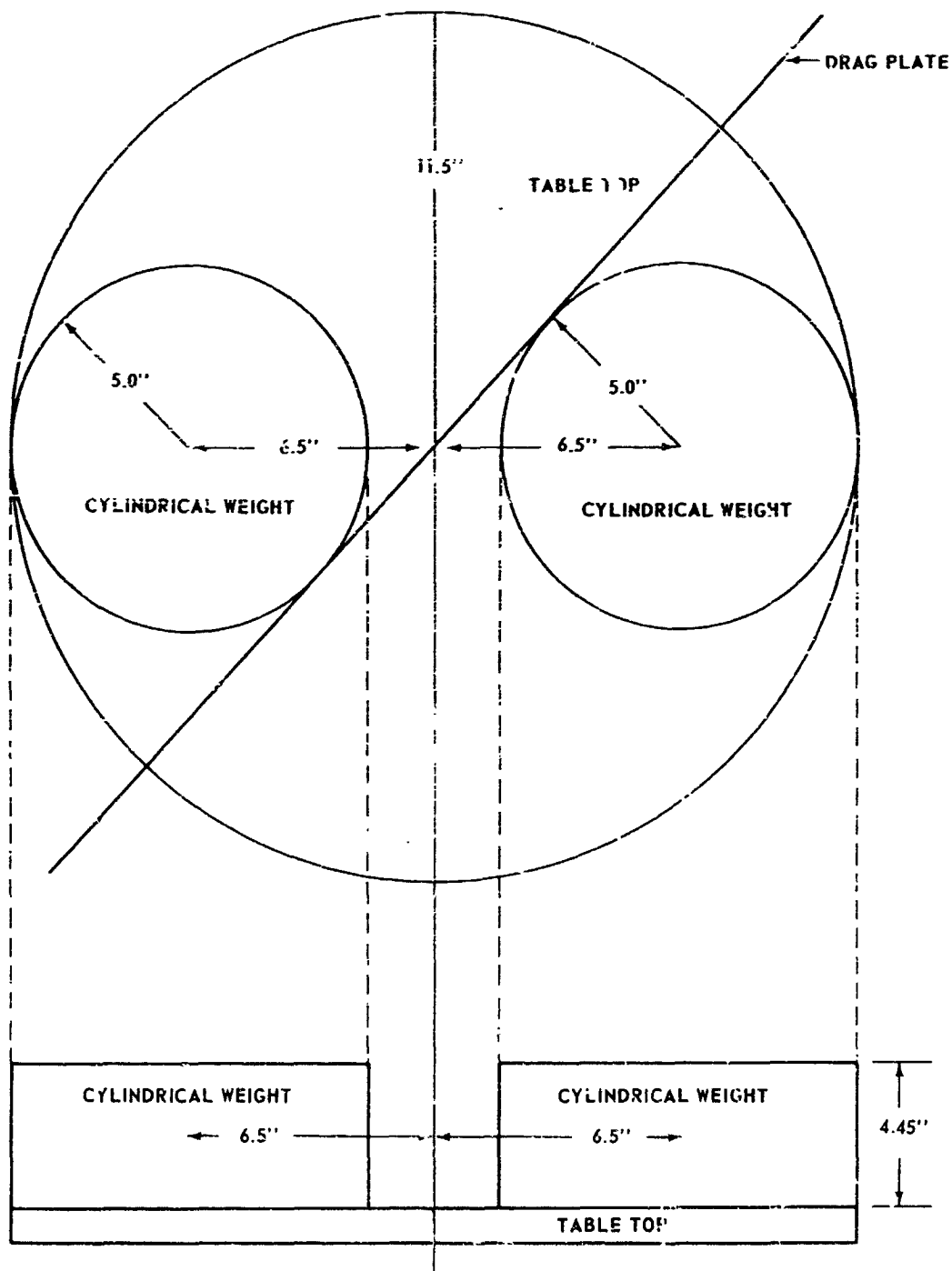


FIGURE 24 TABLE CONFIGURATION FOR TEST

Table 6A. Aerodynamic Drag Test Results

Air Bearing Table - 25 psi - Rod No. 120 - 71°C

Drag Plate	Weight	$I_{\text{calculated}}$	T (0.002 - 0.001 radian)	$I_{\text{experimental}}$	% Difference	$C_{\text{damping constant}}$
None	200 lb	38.10 in-lb-sec ²	0.75103 sec	37.95 in-lb-sec ²	0.4	0.25
	400	66.27	0.99115	66.09	0.3	0.42
	600	94.45	1.18244	94.06	0.4	0.60
"A"	200	38.73	0.75535	38.38	0.9	0.24
	400	66.91	0.99024	65.97	1.4	0.39
	600	95.08	1.18654	94.72	0.4	0.48
"B"	200	54.78	0.91434	56.24	2.6	0.44
	400	82.95	1.11466	83.58	0.8	0.64
	600	111.12	1.28562	111.19	0.06	0.89
"C"	200	69.08	1.05124	74.35	7.6	0.96
	400	97.26	1.22494	100.94	3.7	1.20
	600	125.43	1.37731	127.62	1.7	1.14

Equation 18 is the differential equation which describes the oscillating system at small amplitudes approximately .002 to .001 radians. The solution of Equation 18 yields

$$\beta = \sqrt{\frac{K}{I} - \frac{C^2}{4I^2}} \quad (19)$$

where β is the frequency of the damped oscillating system. The period of oscillation is

$$T = \frac{2\pi}{\beta} \quad (20)$$

Equation 19 can be rewritten as

$$I = \frac{K}{[\beta^2 + \alpha^2]} \quad (21)$$

where

$$\alpha = \frac{-C}{2I} \quad (22)$$

α is the slope of the curve of the natural logarithm of displacement plotted against time. The damping constant can now be obtained by dividing the slope of the curve by two times the calculated value of the moment of inertia.

Equation 21 shows the relationship between I , β and α . As β increases, or the period decreases, α must decrease at a proportional rate such that I remains constant. This effect has been verified experimentally and is shown in Figure 25 and 26. For precise moment of inertia determinations the damping must be considered in the calculations but for this quantitative analysis it will not be necessary. Figures 25 through 32 show the effect of different drag configurations on the period decay rate and the logarithmic slope.

Upon examining the decay constants for the various drag configurations it is obvious that as the size of the drag surface increases, especially away from the axis of rotation, the damping constant increases. This effect is not as obvious with drag plate A because the drag effect changes are of the same order of magnitude as the experimental errors.

The results of these tests clearly demonstrate the effect of aerodynamic drag on an oscillating system.

2.2.3.5 Temperature Test Program: The results of the tests to determine the effect of temperature change on moment of inertia determination are

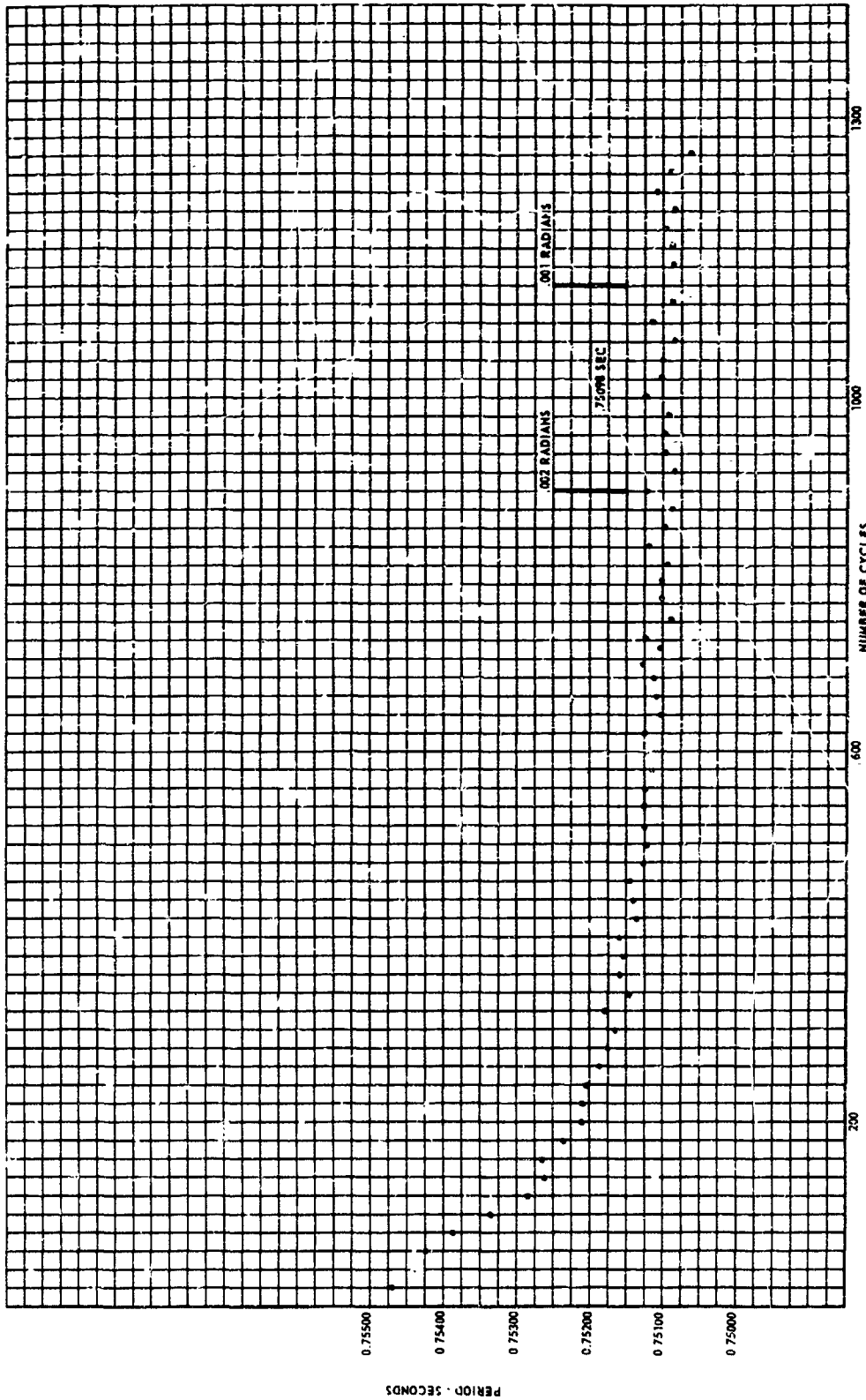


FIGURE 25 NO DRAG PLATE
PERIOD VS TIME

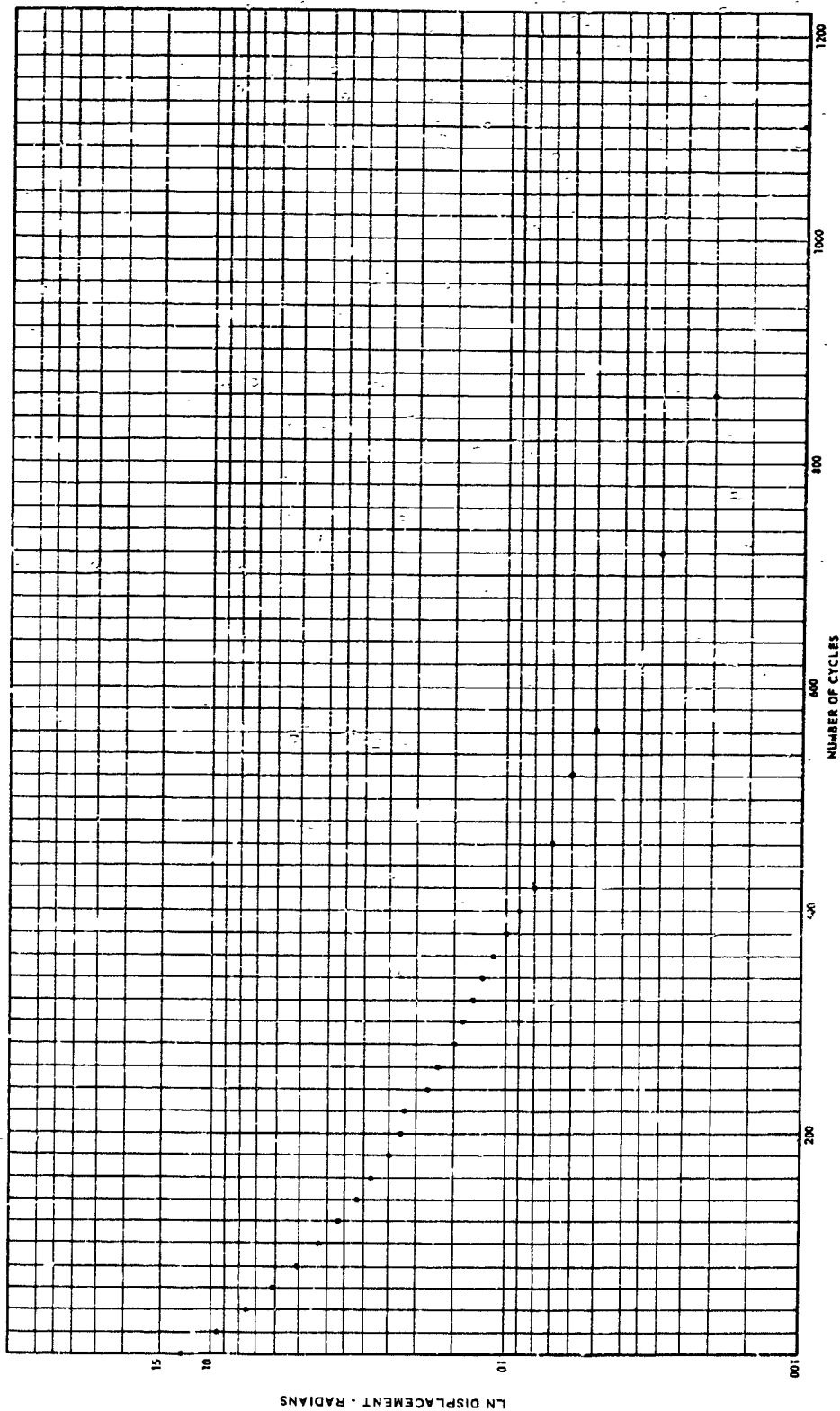


FIGURE 26 NO DRAG PLATE
NATURAL LOG DISPLACEMENT VS TIME

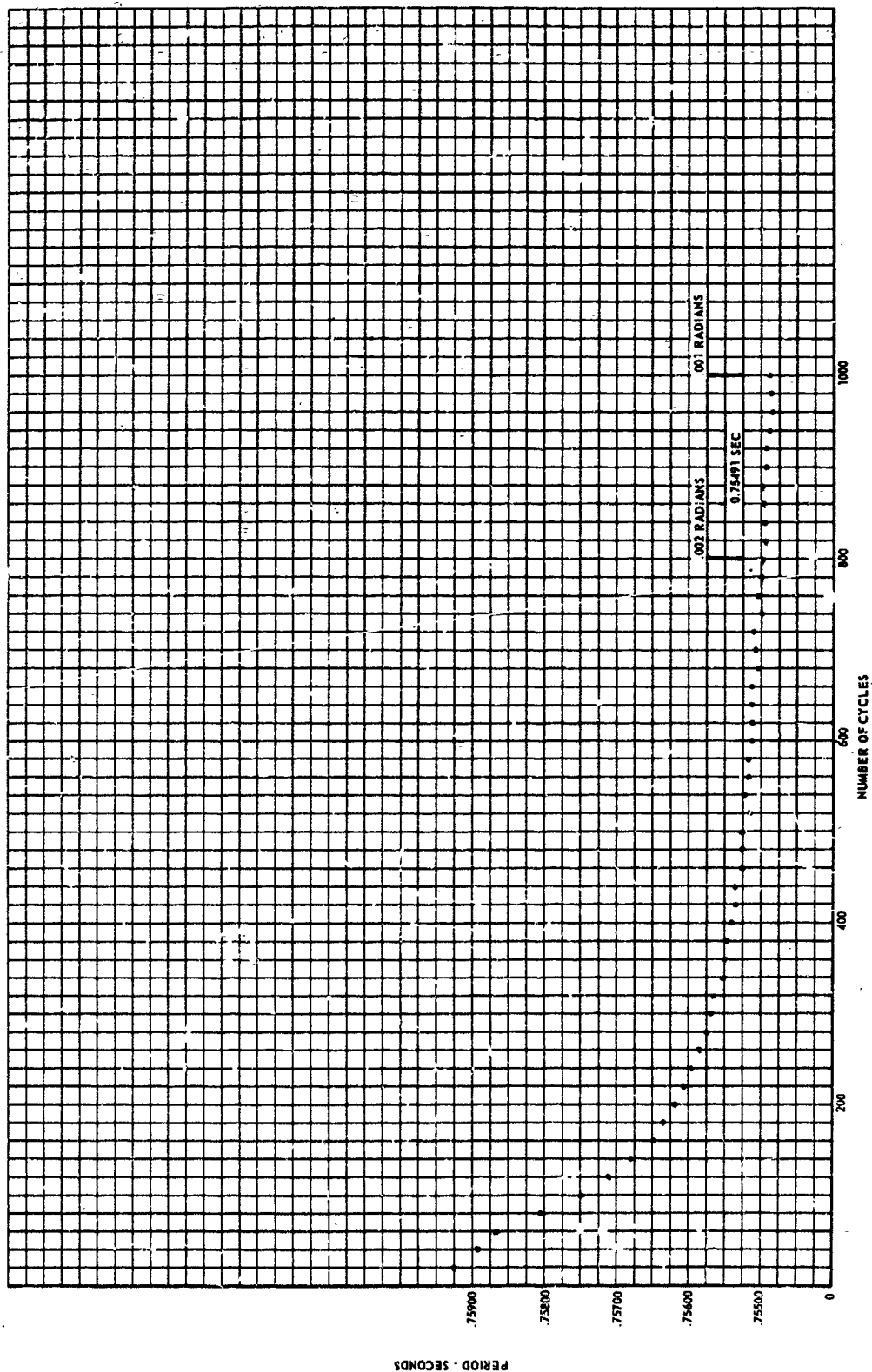


FIGURE 27 DRAG PLATE A
PERIOD VS TIME

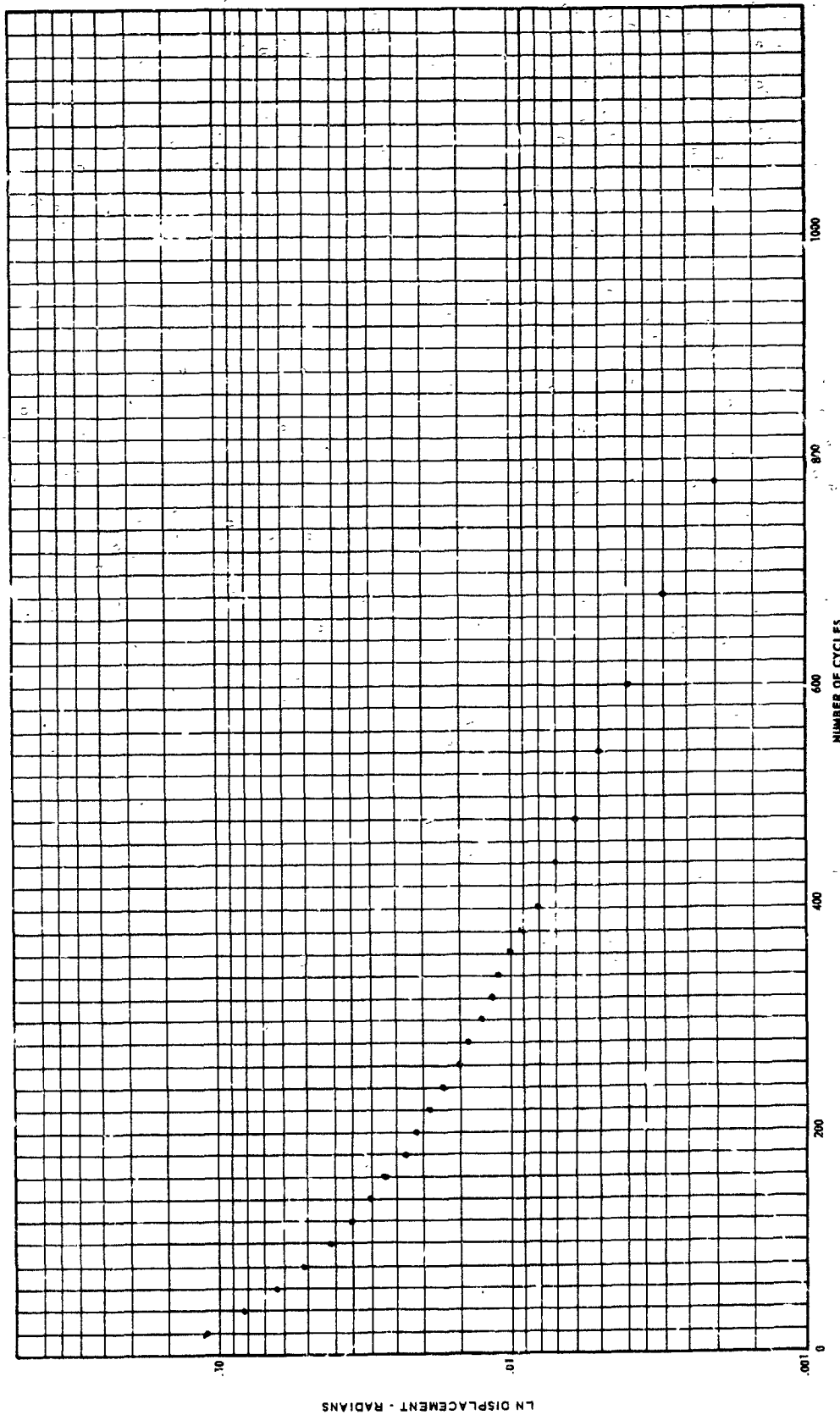


FIGURE 28 DRAG PLATE A
NATURAL LOG DISPLACEMENT VS TIME

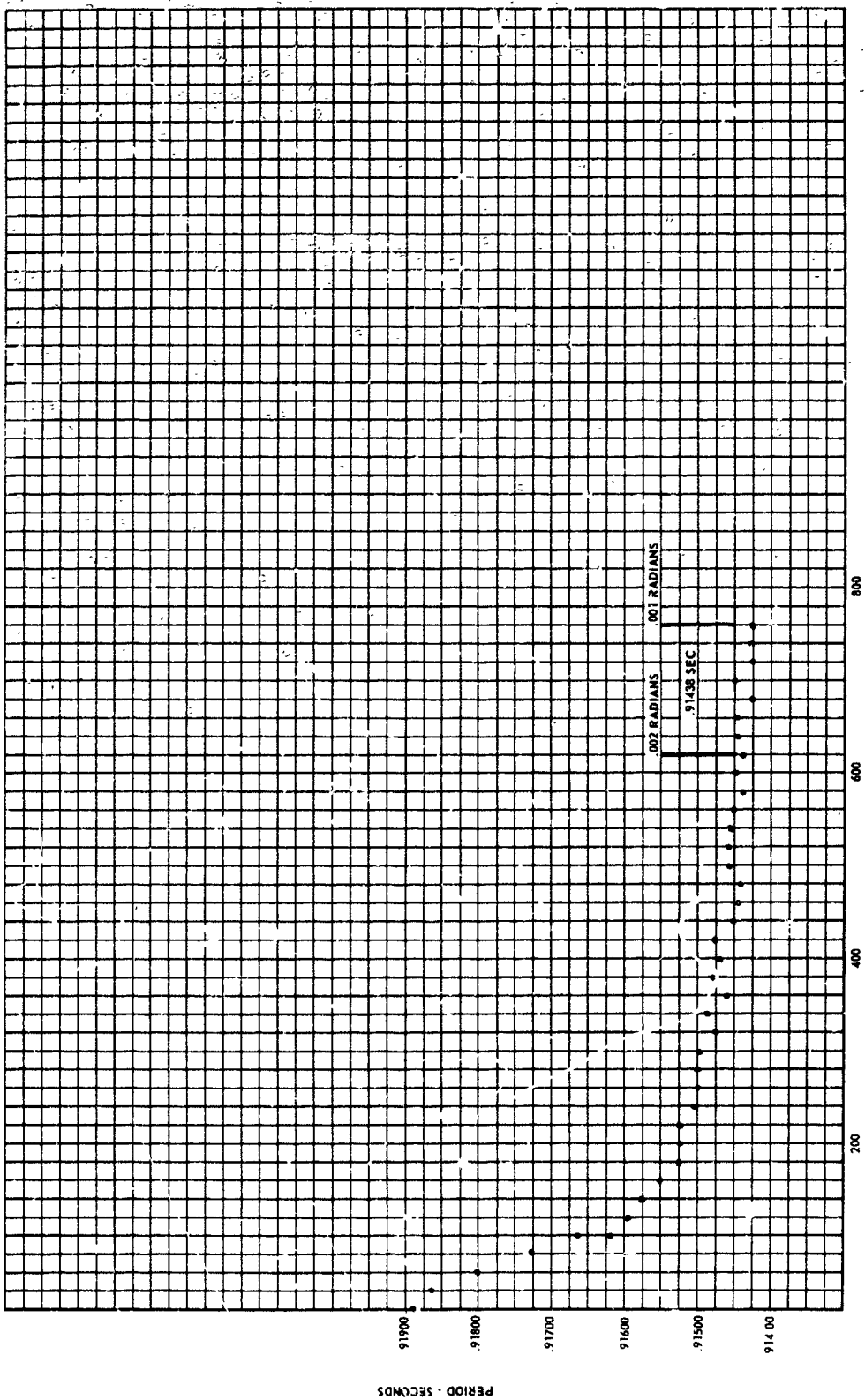


FIGURE 29 DRAG PLATE PERIOD VS TIME

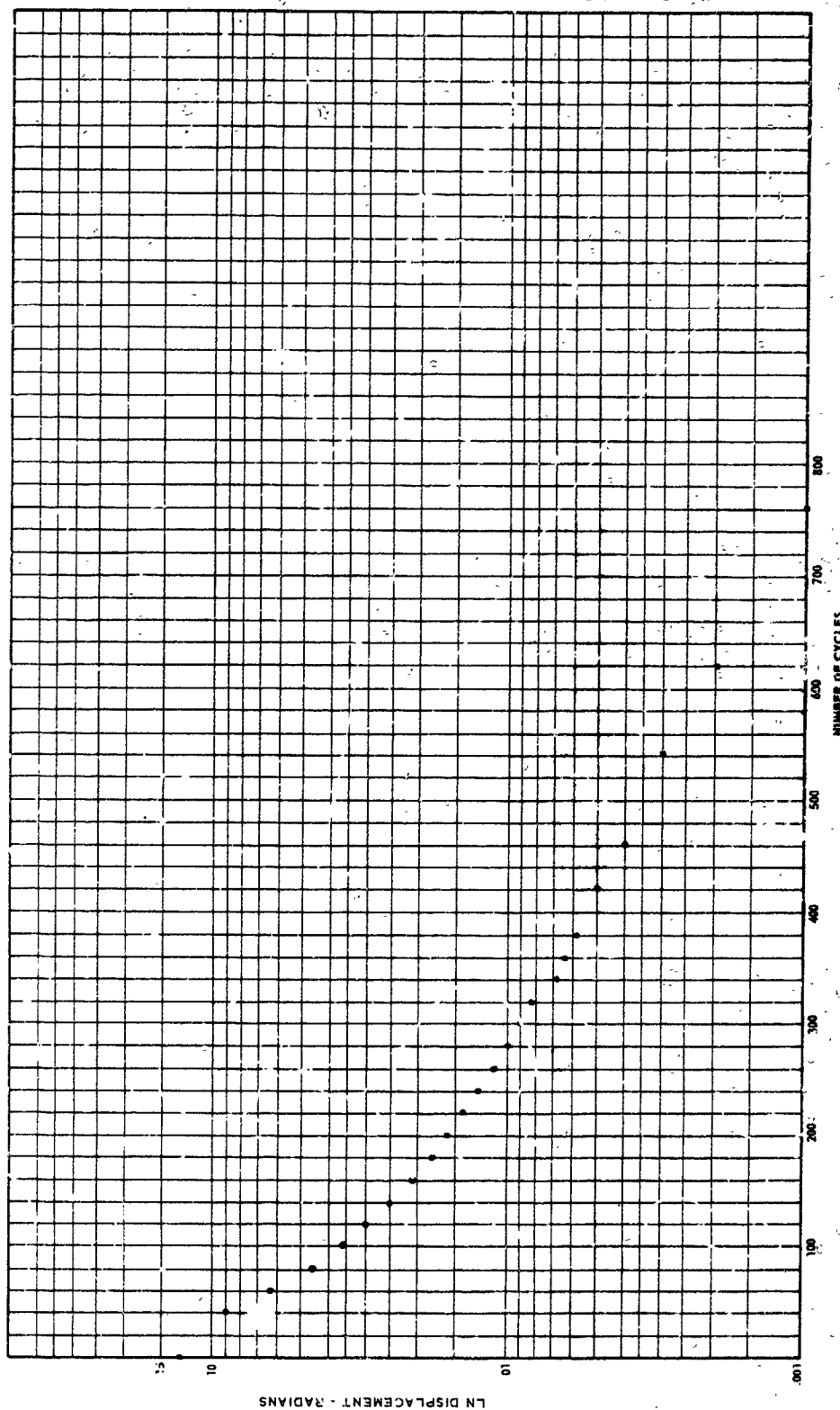


FIGURE 30 DRAG PLATE IB
NATURAL LOG DISPLACEMENT VS TIME

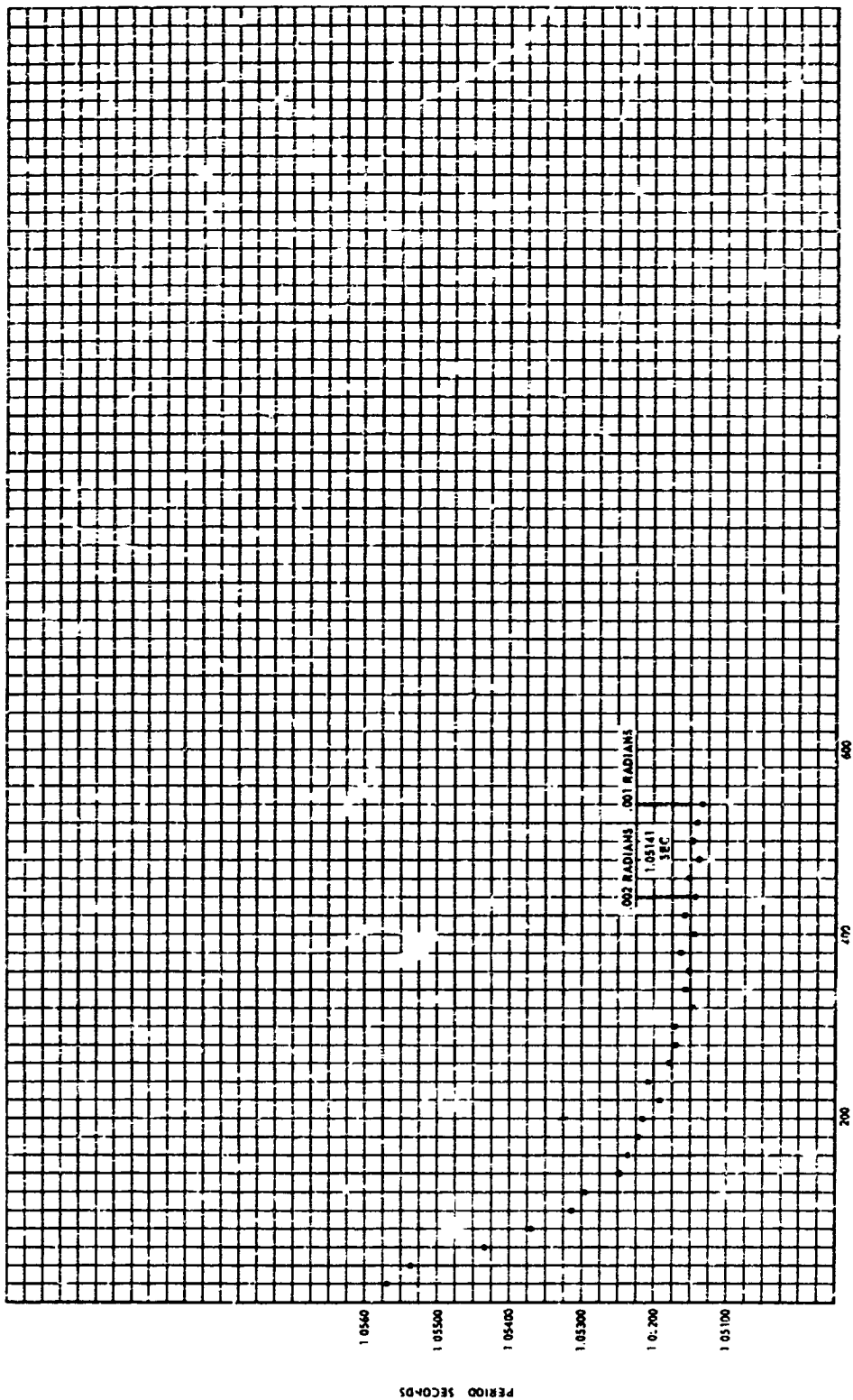


FIGURE 31 DRAG PLATE C
PERIOD VS TIME

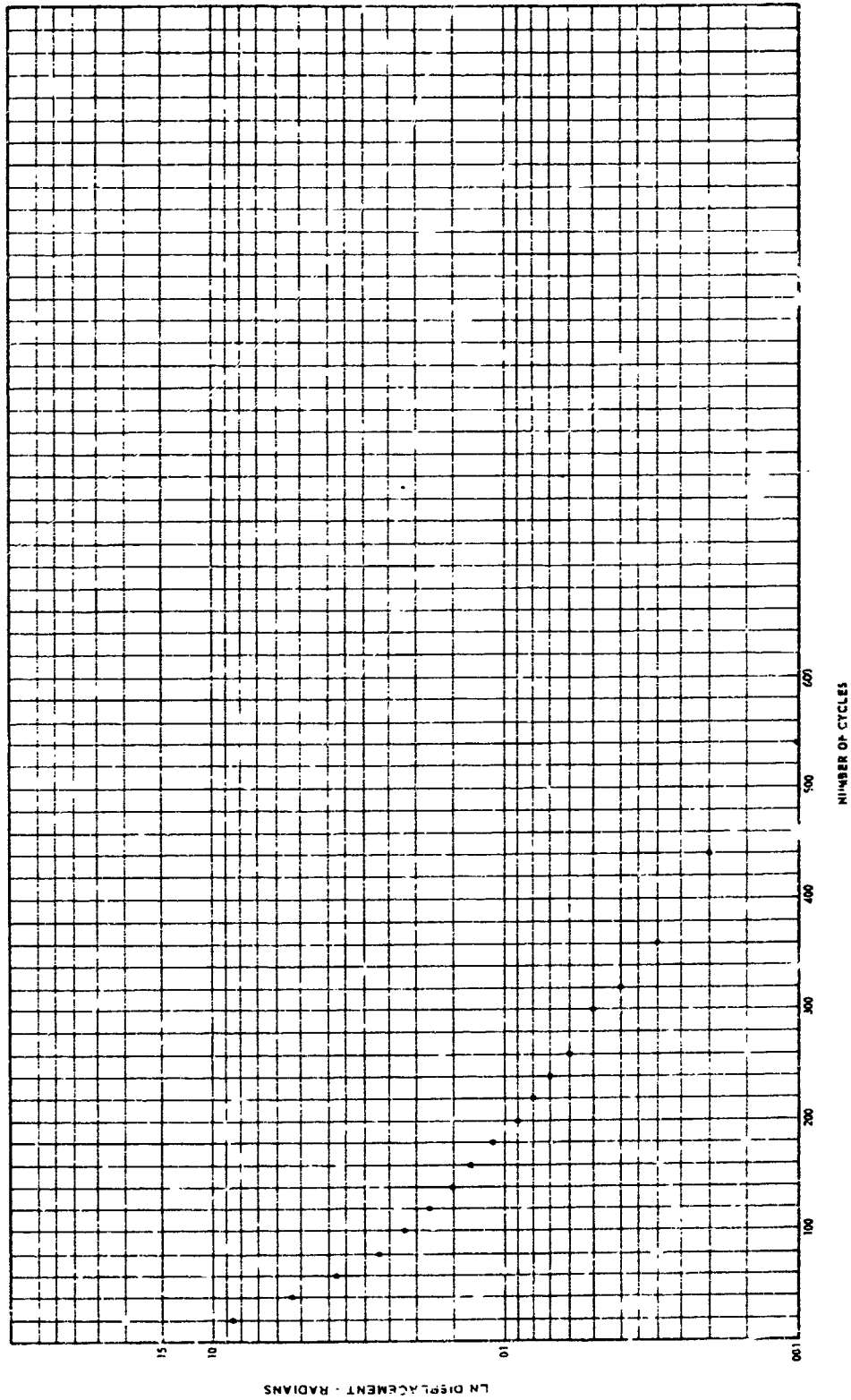


FIGURE 32 DRAG PLATE C
NATURAL LOG DISPLACEMENT VS TIME

shown in Tables 7 through 10. The procedure followed in performance of the tests is included as Appendix A6. The results of these tests definitely prove that that temperature changes affect the air bearing table. To understand these effects an investigation of each temperature dependent component must be undertaken. The components of the system which are most sensitive to temperature change are; torsion rod, test object, air bearing table, enviromental air and internal air within the table. These separate items will be discussed in greater detail.

The averages of the three tests are shown in Table 7.

Table 7 Temperature Effect Test Results

Temp.	Difference	Period	Difference	Moment of Inertia of Dumbbell B & Table Top	% Difference
67.1°F	3.1°F	1.02589 sec	0.00036 sec	70.8548 in.-lb.-sec ²	0.07
70.2	7.3	1.02625	0.00072	70.9046	0.14
77.5		1.02697		71.0041	

The temperature change seems to produce a linear relationship in period and moment of inertia change since the period difference and the percentage change in moment of inertia approximately doubles as the change in temperature doubles. These differences are small but they must be corrected to obtain high degrees of accuracy.

The temperature change can affect the test object in such a manner that as the temperature increases the object expands; therefore, its moment of inertia increases because its mass has moved further from the axis of rotation. The converse is also true for a decrease in temperature. This thermal effect on moment of inertia determination is very difficult to compensate for since many test objects are composed of different material. If the object is composed of different materials; therefore, different coefficients of expansion, it will be very difficult to project the moment of inertia at one temperature to another temperature. This would require that the moment of inertia of the test object be determined at the temperature or temperatures required by the customer.

Table 8 Rod #120 Air Bearing Table (25 PSI) - 60 in. -lb-sec² Dumbbell
(April 21, 1965)

Test No.	Temp	Cycles	Displacement Range	Average Period Between (0.002-0.001 radians)
492	67.1	1280	0.035 - 0.001	1.02588
493	67.1	1300	0.035 - 0.0005	1.02586
494	67.1	1320	0.035 - 0.001	1.02593
495	67.1	1320	0.035 - 0.0005	1.02575
496	67.1	1320	0.035 - 0.0005	1.02582
497	67.1	1360	0.035 - 0.0005	1.02592
498	67.0	1380	0.035 - 0.0005	1.02593
499	68.0	1320	0.035 - 0.0005	1.02596
500	67.8	1480	0.035 - 0.0005	1.02597
501	68.1	1400	0.035 - 0.0005	1.02587
502	68.0	1380	0.035 - 0.0005	1.02589
Average Temperature 67.1				Average 1.02589

Table 9 Rod #120 Air Peering Table (25 PSI) - 60 in. -lb-sec² Dumbbell
(April 19-20, 1965)

Test	Temp	Cycles	Displacement Range	Average Period
482	70	1320	0.035 - 0.0005	1.02633
483	70	1280	0.035 - 0.0005	1.02630
484	70	1320	0.035 - 0.0005	1.02628
485	70	1300	0.035 - 0.0005	1.02628
486	70	1280	0.035 - 0.0005	1.02632
487	70	1300	0.035 - 0.0005	1.02627
488	71	1340	0.035 - 0.0005	1.02622
489	70	1320	0.035 - 0.0005	1.02617
490	70	1300	0.035 - 0.0005	1.02628
491	71	1300	0.035 - 0.0005	1.02620
Average	70.2		Average	1.02625

Table 10 Rod #120 Air Bearing Table (25 PSI) - 60 in.-lb-sec² Dumbbell
(April 22, 1965)

Test No.	Temp	Cycles	Displacement Range	Average Period
503	76.5	1260	0.035 - 0.001	1.02699
504	77.1	1220	0.035 - 0.0005	1.02689
505	77.1	1260	0.035 - 0.0005	1.02693
506	77.5	1300	0.035 - 0.0005	1.02696
507	77.7	1260	0.035 - 0.0005	1.02707
508	77.9	1180	0.035 - 0.0005	1.02716
509	78.5	1340	0.035 - 0.001	1.02686
510	77.5	1420	0.035 - 0.0005	1.02690
Average	77.5		Average	1.02697

The rod constant is also affected by temperature change since the rod changes shape as temperature changes. The rod constant is calculated from

$$K = \frac{Gr^4}{2L} \quad (23)$$

where

G = Modulus of Rigidity

r = Rod Radius

L = Rod Length.

From this equation it is obvious that K would increase or decrease depending on how fast r^4 or L increased or decreased. Calculations have proved that K will decrease upon temperature rise since L is so much greater than r, even with r raised to the fourth power. Since K decreases the moment of inertia will appear to increase because the periods get larger. The converse is true for a temperature drop. The error can be over come by calibrating the rod and table at known temperatures.

The remaining items that might be affected by temperature change are the air bearing table, environmental air and the internal air in the air bearing. These items are affected very little by temperature change and any change they do have can be calibrated out at the same time the rod is being calibrated at various temperatures.

In conclusion, this test program has proved that temperature does definitely affect the determination of moments of inertia. The effect is relatively small and can be compensated for by calibrating the system at different temperatures.

2.2.3.6 Error Analysis: The error analysis presented here consists of determining the effect of different variables on the total moment of inertia of the object. This analysis is accomplished by taking the total derivative of the equation used in determining the moment of inertia and calculating

$$\frac{dI}{I} \times 100 = \% \text{ error} \quad (24)$$

to determine the percentage error of the total system. The equation used in determining moments of inertia is

$$I = \frac{KT^2}{4\pi^2} \quad (25)$$

The variables to consider are the rod constant K and the period of oscillation T. The rod constant determination depends upon

$$K = 4\pi^2 \frac{T^2}{I} \quad (26)$$

which is the same as Equation 25. In Equation 26 the period is determined experimentally, and the moment of inertia I is determined by mathematical calculations using measured dimensions from dumbbell standards. The period in Equation 25 is determined experimentally in the same manner as the period in Equation 26.

The first step in the error analysis is to determine the effect of mass and length tolerances on the moment of inertia of the dumbbell standards. The dumbbell configuration and dimensions are shown in Figure 33 and Table 11; and the moment of inertia calculation is as follows

M_t = Total Mass.

Assume $D_A = D_B = D$, $h_A = h_B = h$, $R_A = R_B = R$.

$$\rho = \frac{M_t}{2V + V_c} \text{ density;} \quad (27)$$

where

$$V = \frac{\pi D^2 h}{4} \quad (28)$$

and

$$V_c = \frac{\pi D_c^2 h_c}{4} \quad (29)$$

$$M_t = \rho V = M_t \left(\frac{D^2 h}{2D^2 h + D_c^2 h_c} \right) \quad (30)$$

and

$$M_c = M_t \left(\frac{D_c^2 h_c}{2D^2 h + D_c^2 h_c} \right) \quad (31)$$

$$I = M_t \left(\frac{D^2}{16} + \frac{h^2}{12} \right) \quad (32)$$

and

$$I_c = M_c \left(\frac{D_c^2}{16} + \frac{h_c^2}{12} \right) \quad (33)$$

$$I_{\text{total}} = I_A + M_A R_A^2 + I_B + M_B R_B^2 + I_c = 2I + 2M_t R^2 + I_c \quad (34)$$

$$I_{\text{total}} = \left(\frac{M_t}{2D^2h + D_c^2h_c} \right) \left(2D^2h \left[\frac{D^2}{16} + \frac{h^2}{12} \right] + R^2 + D_c^2h_c \left[\frac{D_c^2}{16} + \frac{h_c^2}{12} \right] \right) \quad (35)$$

Since

$$I_{\text{total}} = i(M_t, D, h, h_c, D_c, R) \quad (36)$$

the total derivative of I_{total} must be taken with respect to M_t , D , h , h_c , D_c and R .

Therefore, the total differential for moment of inertia of the dumb-bell where

$$I = f(M_t, D, h, h_c, D_c, R) \quad (37)$$

is

$$dI = \frac{\partial I}{\partial M_t} dM_t + \frac{\partial I}{\partial D} dD + \frac{\partial I}{\partial h} dh + \frac{\partial I}{\partial h_c} dh_c + \frac{\partial I}{\partial D_c} dD_c + \frac{\partial I}{\partial R} dR. \quad (38)$$

Using

$$I = M_t (2D^2h + D_c^2h_c)^{-1} \left(2D^2h \left[\frac{D^2}{16} + \frac{h^2}{12} + R^2 \right] + D_c^2h_c \left[\frac{D_c^2}{16} + \frac{h_c^2}{12} \right] \right) \quad (39)$$

the partial derivatives of I become:

$$\frac{\partial I}{\partial M_t} = (2D^2h + D_c^2h_c)^{-1} \left(2D^2h \left[\frac{D^2}{16} + \frac{h^2}{12} + R^2 \right] + D_c^2h_c \left[\frac{D_c^2}{16} + \frac{h_c^2}{12} \right] \right) \quad (40)$$

$$\frac{\partial I}{\partial D} = M_t (2D^2h + D_c^2h_c)^{-2} (4Dh) \left(2Dh \left[\frac{D^2}{16} + \frac{h^2}{12} + R^2 \right] + D_c^2h_c \left[\frac{D_c^2}{16} + \frac{h_c^2}{12} \right] \right)$$

$$+ M_t (2D^2h + D_c^2h_c)^{-1} \left(\frac{D^3h}{4} + \left[\frac{D^2}{16} + \frac{h^2}{12} + R^2 \right] 4Dh \right) \quad (41)$$

$$\frac{\partial I}{\partial h} = M_t (2D^2h + D_c^2h_c)^{-2} 2D^2 \left(2D^2h \left[\frac{D^2}{16} + \frac{h^2}{12} + R^2 \right] + D_c^2h_c \left[\frac{D_c^2}{16} + \frac{h_c^2}{12} \right] \right)$$

$$+ M_t (2D^2h + D_c^2h_c)^{-1} \left(\frac{D^2h^2}{3} + \left[\frac{D^2}{16} + \frac{h^2}{12} + R^2 \right] 2D^2 \right) \quad (42)$$

$$\frac{\partial I}{\partial h_c} = M_t (2D^2h + D_c^2h_c)^{-2} D_c^2 \left(2D^2h \left[\frac{D^2}{16} + \frac{h^2}{12} + R^2 \right] + D_c^2h_c \left[\frac{D_c^2}{16} + \frac{h_c^2}{12} \right] \right)$$

$$+ M_t (2D^2 h + D_c^2 h_c)^{-1} \frac{D_c^2 h_c^2}{6} + D_c^2 \left[\frac{D_c^2}{16} + \frac{h_c^2}{12} \right] \quad (43)$$

$$\begin{aligned} \frac{\partial I}{\partial D_c} = & M_t (2D^2 h + D_c^2 h_c)^{-2} 2D_c h_c \left(2D^2 h \left[\frac{D^2}{16} + \frac{h^2}{12} + R^2 \right] + D_c^2 h_c \left[\frac{D_c^2}{16} + \frac{h_c^2}{12} \right] \right) \\ & + M_t (2D^2 h + D_c^2 h_c)^{-1} \left(\frac{D_c^3 h_c}{8} + \left[\frac{D_c^2}{16} + \frac{h_c^2}{12} \right] 2D_c h_c \right) \end{aligned} \quad (44)$$

$$\frac{\partial I}{\partial R} = M_t (2D^2 h + D_c^2 h_c)^{-1} 4D^2 h R \quad (45)$$

The Computation Laboratory at NASA prepared a computer program and obtained solutions to these equations. Figure 34 shows the computer program, and Figure 35 shows the solution print out using data from Table 11. Table 12 shows the results of the partial derivatives in Equations 40 through 45 where the data in Table 11 has been used. Table 13 shows the change in moment of inertia dI for various tolerance of dM_t, dD, dh, dh_c, dD_c and dR. Data from five different dumbbells is shown.

The change in moments of inertia dI as shown in Table 13 was used to determine the change in rod constant dK. Equation 46 is used to evaluate dK. The total derivative of K where K = f(I, T), is

$$dK = \frac{\partial K}{\partial I} dI + \frac{\partial K}{\partial T} dT. \quad (46)$$

Partial derivatives of K are

$$\frac{\partial K}{\partial I} = \frac{4\pi^2}{T^3} \quad (47)$$

and

$$\frac{\partial K}{\partial T} = \frac{-8\pi^2 I}{T^4} \quad (48)$$

Now

$$dK = \frac{4\pi^2}{T^3} dI + \frac{3\pi^2 I}{T^4} dT. \quad (49)$$

The positive sign is used for maximum error. The sample values used are from data obtained from the suspended pendulum tests. Table 14 shows

Table 11 Dumbbell Dimensions

Dumbbell	A	B	C	D	E
D_A	5.938125	6.37595	6.6268125	10.0012	9.998166
D_B	5.938125	6.375325	6.6266875	10.001225	9.9973
D_C	0.981333	1.94658	1.94905263	1.9850	1.95384
h_A	4.500125	5.00015	8.4420	3.8749	5.9940
h_B	4.50025	5.000025	8.4420	3.875275	5.993625
h_C	19.502875	25.99995	20.05775	28.269575	26.005125
R_A	12.00168	15.49999	14.24961	16.07302	15.99774
R_B	12.00138	15.50005	14.25014	16.07302	16.00120
M_t	0.19442	0.29274	0.49117	0.51547	0.75463

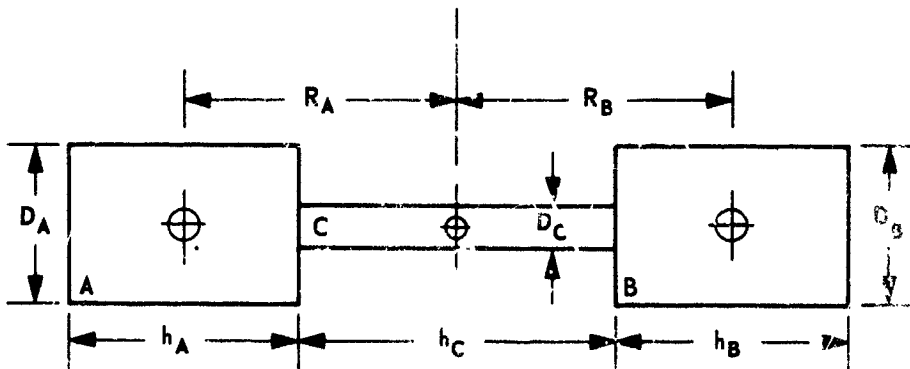


FIGURE 33 DUMBELL CONFIGURATION

```

DIMENSION DI(3),DEL(3)
J=0
DEL(1)=.001
DEL(2)=.01
DEL(3)=.1
READ 2,D,DC,H,HC,R,WT
FORMAT(6E10.6)
PAR1=2.*D*D*H+DC*DC*HC
PAR2=U*D/16.+H*H/12.+R*R
PAR3=DC*DC/16.+HC*HC/12.
DIWT=(2.*U*D*H*PAR2+DC*DC*HC*PAR3)/PAR1
DID1=((2.*D*H*PAR2+DC*DC*HC*PAR3)*WT*4.*D*H)/(PAR1*PAR1)
DID2=((D*DC*H/4.+PAR2*4.*D*H)*WT)/PAR1
DID=DID1+DID2
DIH1=((2.*D*D*H*PAR2+DC*DC*HC*PAR3)*2.*D*D*WT)/(PAR1*PAR1)
DIH2=((D*D*H*H/3.+PAR2*2.*D*D)*WT)/PAR1
DIH=DIH1+DIH2
DIHC1=((2.*U*D*H*PAR2+DC*DC*HC*PAR3)*DC*DC*WT)/(PAR1*PAR1)
DIHC2=((DC*DC*HC*HC/6.+DC*DC*PAR3)*W1)/PAR1
DIHC=DIHC1+DIHC2
DIUC1=((2.*U*D*H*PAR2+DC*DC*HC*PAR3)*2*DC*HC*WT)/(PAR1*PAR1)
DIUC2=((DC*DC*DC*HC/8.+PAR3*2.*DC*HC)*WT)/PAR1
DIDC=DIUC1+DIUC2
DIR=(4.*U*D*H*R*WT)/PAR1
DO 5 I=1,3
DI(I)=DEL(I)*(DIWT+DID+DIH+DIHC+DIDC+DIR)
PRINT 10,DIWT,DID,DIH,DIHC,DIDC,DIR
PRINT 20,(DEL(I),DI(I),I=1,3)
PRINT 30,D,DC,H,HC,R,WT
FORMAT (1X,3H D=E20.10,3H DC=E20.10,3H H=E20.10/1X,3H HC=E20.10,3H R
I=E20.10,3H WT=E20.10)
FORMAT (1H0,1X,7H DIWT= E20.10,6H DID= E20.10,6H DIH= E20.10/2X,7H
DIHC= E20.10,7H DIUC= E20.10,6H DIR= E20.10)
FORMAT(1X,6H DEL= E20.10,5H DI= E20.10)
J=J+1
IF(J-5)1,3,3
STOP
END

```

FIGURE 34 EQUATION SOLVING COMPUTER PROGRAM

Table 1² Partial Derivatives of I

Dumbbell	A	B	C	D	E
$\frac{\partial I}{\partial M_t}$	0.36672	0.53967	0.50598	0.62445	0.64615
$\frac{\partial I}{\partial D}$	10.84618	21.38828	33.14892	27.37601	41.85511
$\frac{\partial I}{\partial h}$	11.94154	21.54538	22.09400	59.22627	60.50154
$\frac{\partial I}{\partial h_c}$	0.13178	0.82883	0.67539	1.01005	0.92912
$\frac{\partial I}{\partial D_c}$	3.83598	15.54467	10.76278	20.09395	18.08619
$\frac{\partial I}{\partial R}$	4.40619	7.30479	12.69358	14.48849	22.29767

Table 13 Total Differentials of I for Various Tolerances

		dI	dM _i	dD	dh	dh _c	dD _c	dR	% Error
Danabell:	A	0.3482	0.10	0.01	0.01	0.01	0.01	0.01	1.26
	B	0.7201	"	"	"	"	"	"	1.18
	C	0.9476	"	"	"	"	"	"	1.02
	D	1.2844	"	"	"	"	"	"	1.03
	E	1.5013	"	"	"	"	"	"	0.79
	A	0.0348	0.10	0.001	0.001	0.001	0.001	0.001	0.25
	B	0.1032	"	"	"	"	"	"	0.17
	C	0.1403	"	"	"	"	"	"	0.15
	D	0.1846	"	"	"	"	"	"	0.14
	E	0.2082	"	"	"	"	"	"	0.11
	A	0.0348	0.010	0.001	0.001	0.001	0.001	0.001	0.13
	B	0.0720	"	"	"	"	"	"	0.12
	C	0.0948	"	"	"	"	"	"	0.10
	D	0.1284	"	"	"	"	"	"	0.10
	E	0.1501	"	"	"	"	"	"	0.08
	A	0.0315	0.001	0.001	0.001	0.001	0.001	0.001	0.11
	B	0.0672	"	"	"	"	"	"	0.11
	C	0.0902	"	"	"	"	"	"	0.10
	D	0.1228	"	"	"	"	"	"	0.10
	E	0.1443	"	"	"	"	"	"	0.08
	A	0.00346	0.001	0.0001	0.0001	0.0001	0.0001	0.0001	0.012
	B	0.00720	"	"	"	"	"	"	0.011
	C	0.00948	"	"	"	"	"	"	0.010
	D	0.01284	"	"	"	"	"	"	0.010
	E	0.01502	"	"	"	"	"	"	0.007
	A	0.00315	0.0001	0.0001	0.0001	0.0001	0.0001	0.0001	0.011
	B	0.00672	"	"	"	"	"	"	0.011
	C	0.00902	"	"	"	"	"	"	0.009
	D	0.01228	"	"	"	"	"	"	0.009
	E	0.01443	"	"	"	"	"	"	0.007

Table 4 Effect of dI and dT on dK in Suspended Pendulum
Rod Calibration Test.

Suspended Pendulum Test Dumbbell C Rod #120

$$I = 60.9308$$

$$T = 0.94968$$

$$\frac{\partial K}{\partial I} = \frac{4\pi^2}{T^2} = 43.7728$$

$$\frac{\partial K}{\partial T} = \frac{8\pi^2 I}{T^3} = 5616.854$$

$$dK = (43.7728) dI + (5616.854) dT$$

dK	dI	dT
49.3896	1.0	0.001
27.5033	0.5	0.001
9.9941	0.1	0.001
4.8156	0.1	0.0001
2.7501	0.05	0.0001
2.2447	0.05	0.00001 (10 ⁻⁵)
0.9994	0.01	0.0001 (10 ⁻⁴)
0.4938	0.01	0.00001 (10 ⁻⁵)
0.2750	0.005	0.00001 (10 ⁻⁵)
0.2245	0.005	0.000001 (10 ⁻⁶)
0.0494	0.001	0.000001 (10 ⁻⁶)

the results of these calculations.

Using the values of the change in rod constant dK and the change in period dT , the total change in the moment of inertia dI can be determined. Using Equation 25 the total derivative of I where $I = f(K, T)$ is

$$dI = \frac{\partial I}{\partial K} dK + \frac{\partial I}{\partial T} dT. \quad (50)$$

Partial derivatives of I are

$$\frac{\partial I}{\partial K} = \frac{T^2}{4\pi^2} \quad (51)$$

and

$$\frac{\partial I}{\partial T} = \frac{KT}{2\pi^2} \quad (52)$$

Now

$$dI = \frac{T^2}{4\pi^2} dK + \frac{KT}{2\pi^2} dT. \quad (53)$$

Sample values used are from data obtained from the suspended pendulum tests. Table 15 shows the results of these calculations.

The results of this error analysis shows how specific variables affect the final accuracy of the moment of inertia determination. Figure 36 graphically shows the results of Table 13. The effect of dM_t and dL , the change in length measurements, upon the dumbbell moment of inertia change dI for five dumbbells is shown. The solid curves show that for $dL = 0.001$ the increase in accuracy of the mass measurement dM_t does not significantly increase the accuracy of the moment of inertia dI . However, the increase in accuracy of the moment of inertia dI is significantly improved by increasing the accuracy of dI .

Figure 37 graphically shows the results of Table 14. The values $dT = 0.0001$ and $dI = 0.1$ are typical of the values that are obtained presently. From these curves it is noted that an increase in the accuracy of the dumbbell standards dI would increase the rod constant accuracy dK more than an increase in period accuracy dT .

The results of Table 15 is shown graphically in Figure 38. Again the effect of the rod constant accuracy dK is much more important than period accuracy dT . The present accuracies in moment of inertia determination are approximately 0.05% as shown in Figure 38. This figure is

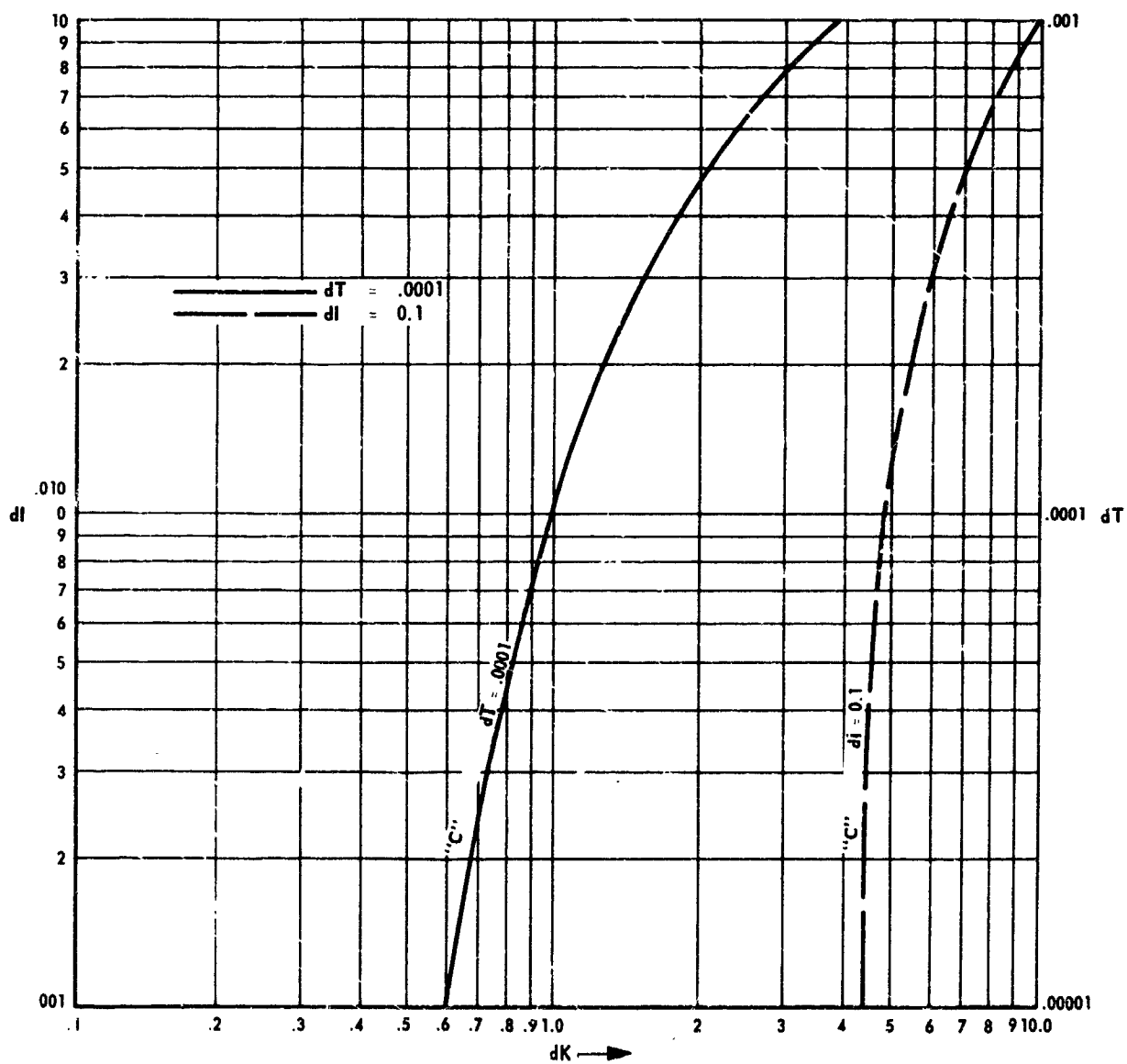


FIGURE 37 PLOT OF dI AND dT VS dK

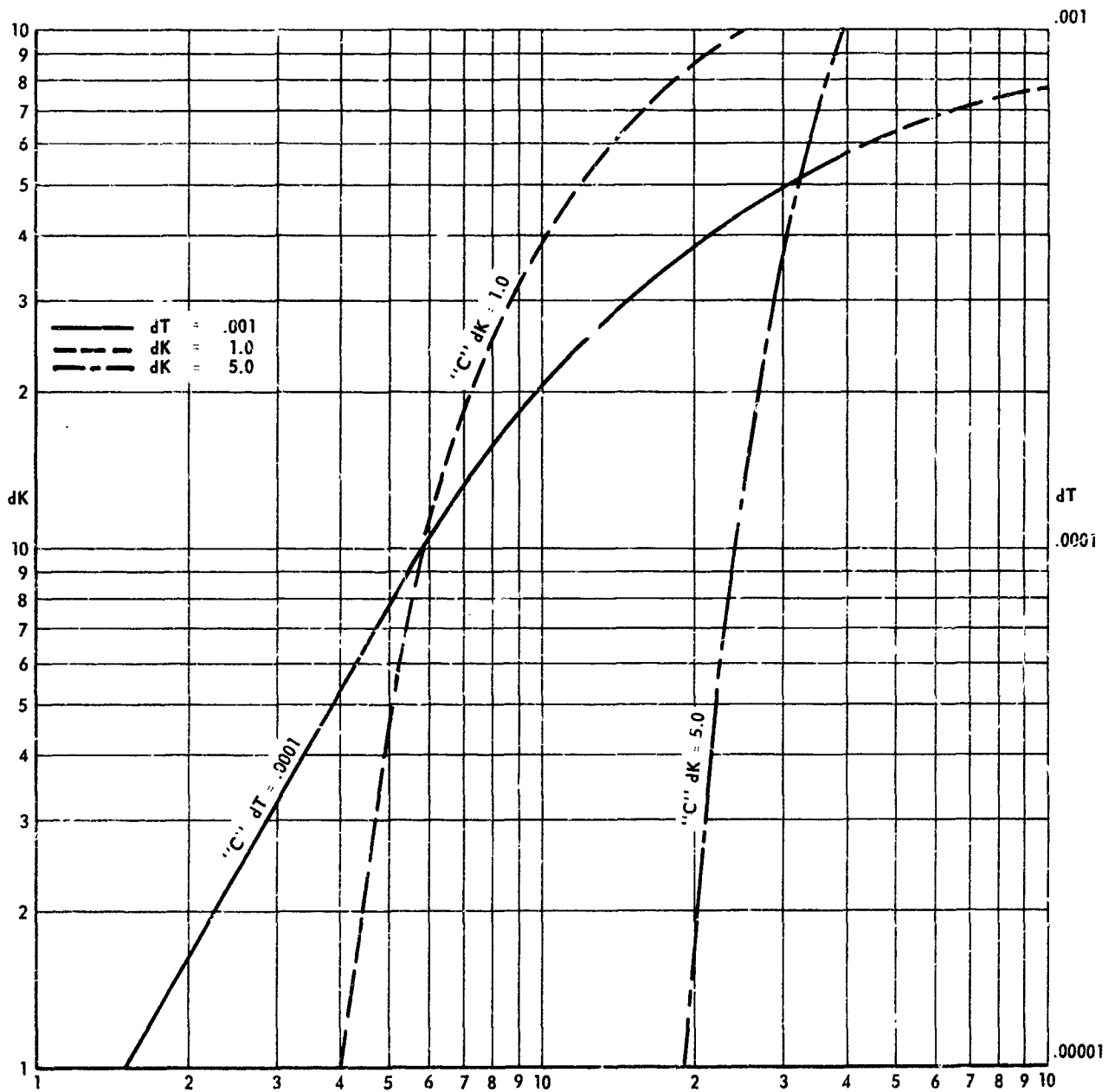


FIGURE 38 PLOT OF dK AND dT VS % ERROR OF TOTAL I

Table 15 Effect of dI of Standard and dK on dT

Suspended Pendulum Test Dumbbell C Rod #120

$$T = 0.94968$$

$$K = 2667.383$$

$$\frac{\partial T}{\partial K} = \frac{T^2}{4\pi^2} = 0.02284$$

$$\frac{\partial I}{\partial T} = \frac{KT}{2\pi^2} = 128.332$$

$$dI = (.02284) dK + (128.332) dT$$

dI	dK	dT	%Error
1.270?	50	0.001	2.08%
0.3567	10.0	0.001	0.58
0.1784	5.0	0.0005	0.29
0.1270	5.0	0.0001	0.21
0.0585	2.0	0.0001	0.096
0.0357	1.0	0.0001 (10 ⁻⁴)	0.058
0.0127	0.5	0.00001 (10 ⁻⁵)	0.020
0.0115	0.5	0.000001 (10 ⁻⁶)	0.018
0.0024	0.1	0.000001 (10 ⁻⁶)	0.003
0.0013	0.05	0.000001 (10 ⁻⁶)	0.002

obtained from a dK of 1.0 and a dT of 0.0001. To obtain an accuracy of 0.01% the present accuracy of dK and dI must be increased by an order of magnitude; but, dK is still the prime factor.

2.2.3.7 Conclusions: The experimental test program has proven that the torsional pendulum air bearing table is a very accurate and efficient method for determining moments of inertia. The error analysis has shown what accuracies in moment of inertia determination can be obtained for certain accuracies in period and rod constant value. Presently the period measurement appears to be sufficient but an increase in the accuracy of the rod constant value by a factor of ten will increase the overall moment of inertia accuracy to approximately 0.01 of one per cent. With these capabilities in the basic system other variables can be easily calculated out or compensated for. Some of these variables were investigated, such as temperature, aerodynamic drag and table load. The moment of inertia of an object will have to be given at a known constant temperature because the moment of inertia of an object is temperature dependent. This is true because an object will change shape depending on the thermal coefficients of the material in the object. The thermal effect on the table can be corrected at different temperatures. The aerodynamic drag will be compensated for by using the period decay rate of an oscillating system to determine the true moment of inertia. The effects of various loads on the table has been investigated experimentally so that the optimum air pressure can be applied to the table to provide the best table performance. Since all variables can be compensated for, the accuracy of determining moments of inertia on the air bearing table can be increased to 0.01 of one per cent without much difficulty.

2.2.4 Automated Systems Development

2.2.4.1 MIA Prototype Development

2.2.4.1.1 Technical Discussion: Various methods of accurately determining the moments of inertia of physical bodies have been investigated. The decaying oscillation method employing a gas bearing supported torsional pendulum appears to hold the most promise at present. In use, the pendulum is given an initial angular displacement and allowed to oscillate down to zero amplitude. The idea is to measure (or mathematically determine) the period of oscillation as the amplitude approaches zero. Knowing the period and the torsion rod constant, the moment of inertia can be determined from:

$$I = \frac{KT^2}{4\pi^2} \quad (54)$$

2.2.4.1.2 Procedure

2.2.4.1.2.1 Photocell Transducer Method: In order to measure the oscillation periods without affecting the oscillating system, two methods of detecting the oscillations have been investigated in the laboratory. One method involves the use of a photocell to detect the motion of a small wand attached to the oscillating mass. This method has proved quite successful, to a point, and is presently being used as a reference.

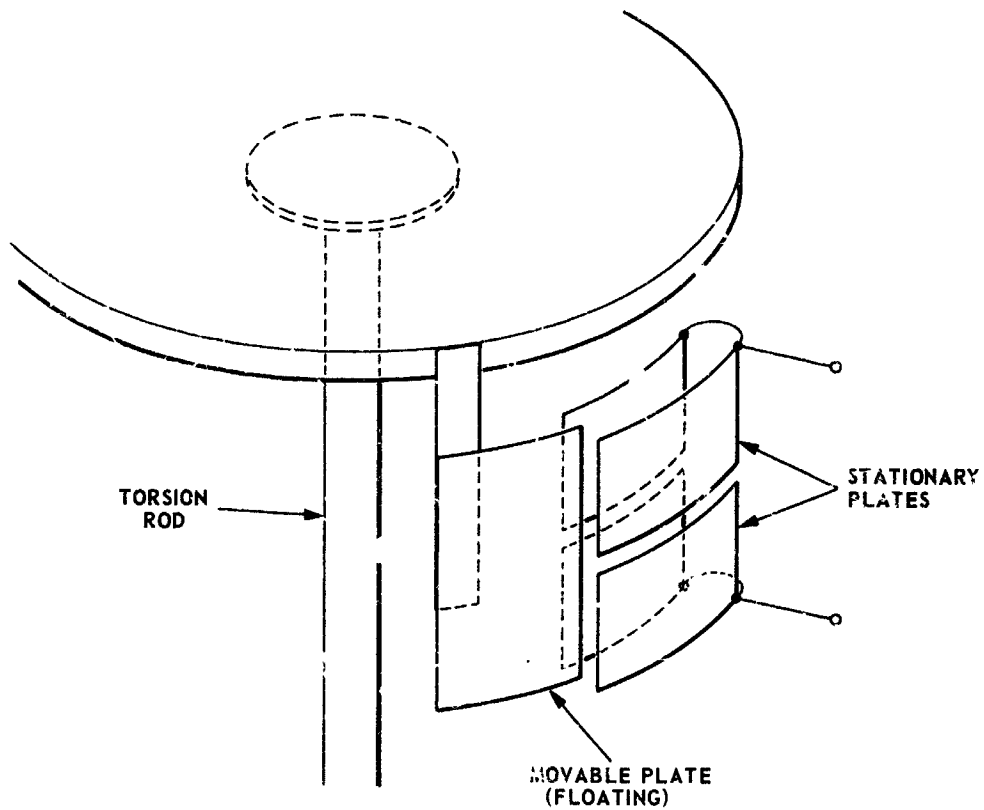
2.2.4.1.2.2 Capacitance Transducer Method: The oscillation detecting method using capacitance transducers has also been investigated in detail. This is the method with which we are most concerned. In the MIA prototype, one plate of a capacitor is attached to the oscillating system. Motion causes the capacitance of the capacitive transducer to vary. The capacitor is connected as part of an oscillator tank circuit. Motion produced in the capacitive transducer results in frequency modulation in the oscillator tank circuit.

2.2.4.1.2.2.1 The Prototype Capacitor: In the original system, the capacitor's movable plates were mounted on one end of a plexiglass arm. The other end was attached to the free end of the torsion rod. The fixed plates, along with the other oscillator components, were mounted in a metal box having an opening to allow the capacitor's plates to mesh.

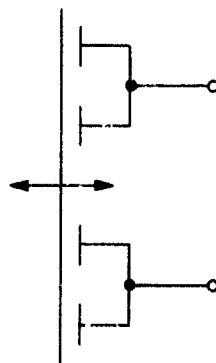
This arrangement was subject to vibrations and was not well shielded. It required disassembly each time the torsion rod was changed. To improve on this arrangement, a cylindrical capacitor was built.

2.2.4.1.2.2.2 Cylindrical Capacitor: The transducer, with which this report is primarily concerned, consists of aluminum plates which are cylindrical segments mounted co-axially with the torsion rod as shown in Figure 39. The movable plate, which is electrically floating, is mounted to the torsion rod's upper support. This arrangement makes it unnecessary to remove part of the capacitor when torsion rods are interchanged. The other oscillator components have been removed from the capacitor housing and relocated on the chassis with the other circuitry. A padding capacitor is located on the capacitor housing to provide a means for adjusting the oscillator's center frequency. Although the shielding is much better than with the prototype capacitor, some detuning is noticed while adjusting the padding.

2.2.4.1.2.3 Revised System: A block diagram of the revised prototype system is shown in Figure 40. The capacitance transducer is in the tank circuit of the 4.5 megacycle L-C oscillator so that the pendulum's oscillations cause frequency modulation of the oscillator's output voltage.



A. MECHANICAL CONFIGURATION



B. ELECTRICAL EQUIVALENT

FIGURE 39 CAPACITANCE TRANSDUCER

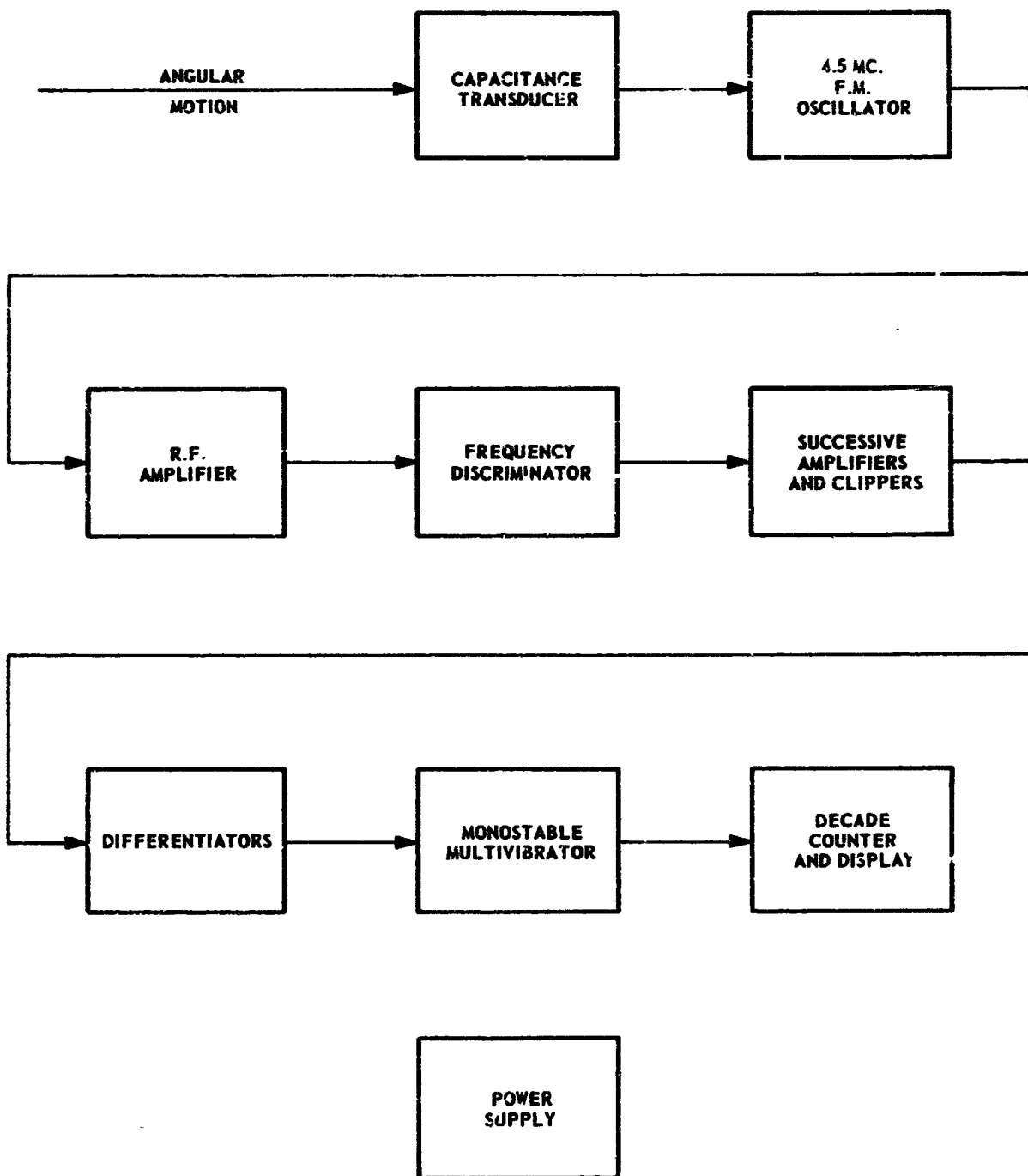


FIGURE 40 MIA REVISED PROTOTYPE SYSTEM BLOCK DIAGRAM

The 4.5 megacycle center frequency was chosen on the basis of resolution and component availability. The output from the oscillator is amplified and fed to a frequency discriminator. The output waveform from the discriminator is a replica of pendulum motion. This output is repetitively amplified and clipped to raise the rise time after which it is differentiated to produce alternating positive and negative pulses. These pulses represent the zero crossing points of the oscillations. The positive pulses are attenuated, leaving one negative pulse per oscillation. These negative pulses are scaled down by a factor of two by the monostable multivibrator to provide a square wave gating voltage for the decade counter. The duration of the gating voltage is equal to the period of oscillation of the pendulum. The gating voltage occurs every other cycle, thereby allowing time for the counter to be read. Electrical schematics of the system are located in Appendix A8.

To compare the accuracy of the revised system to the photocell method, eight tests were run. The tests were randomized to minimize setup variables.

Three torsion rods were used and mass was added to the table to make the periods approximately 1, 2, & 3 seconds for each rod. (The 3 second test was inadvertently omitted for the 1/4 in. dia. rod) A trial run for each test gave the approximate starting amplitude necessary to produce 200 cycles before the readout became erratic. The test data is given in Table 16, and the test procedure is contained in Appendix A9.

2.2.4.1.3 Test Results: Test data reveals that at low amplitudes the period measurement can be relied on only to three significant figures without averaging. This is due to noise which is experienced at these low amplitudes. This is caused by the inability of electronic equipment to accurately determine zero crossover of low amplitude sine waves.

The scatter pattern in some of the tests suggests some periodic disturbance. Plots of tests No. 1, 7A, & 8 are included for reference. (See Figures 41, 42, and 43) The plot of test No. 7A, a repeat of test No. 7 run at a larger amplitude, shows this periodic disturbance. Plot of test No. 1 also indicates periodic disturbances even though the test was at a lower amplitude. Although test No. 8, typical of the low amplitude tests, clearly shows a large disturbance, it doesn't appear to be periodic. The periodic effect can possibly be attributed to 60 and 120 cycle hum components, although this could not be definitely determined. These components can be observed on the voltage waveforms when the mechanical amplitude becomes very low.

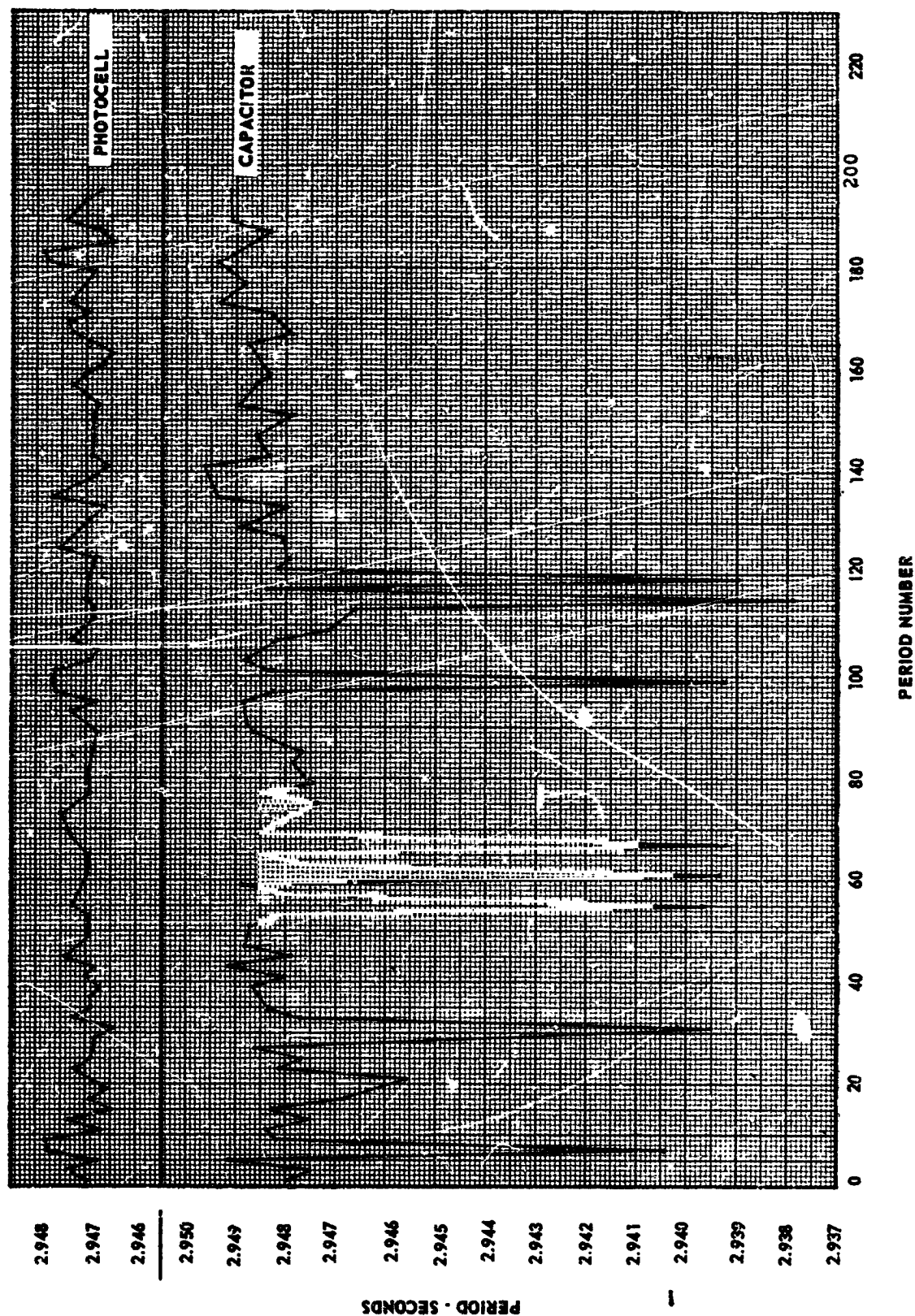


FIGURE 41 TEST NO. 8 - INITIAL AMPLITUDE 0.005 RADIAN

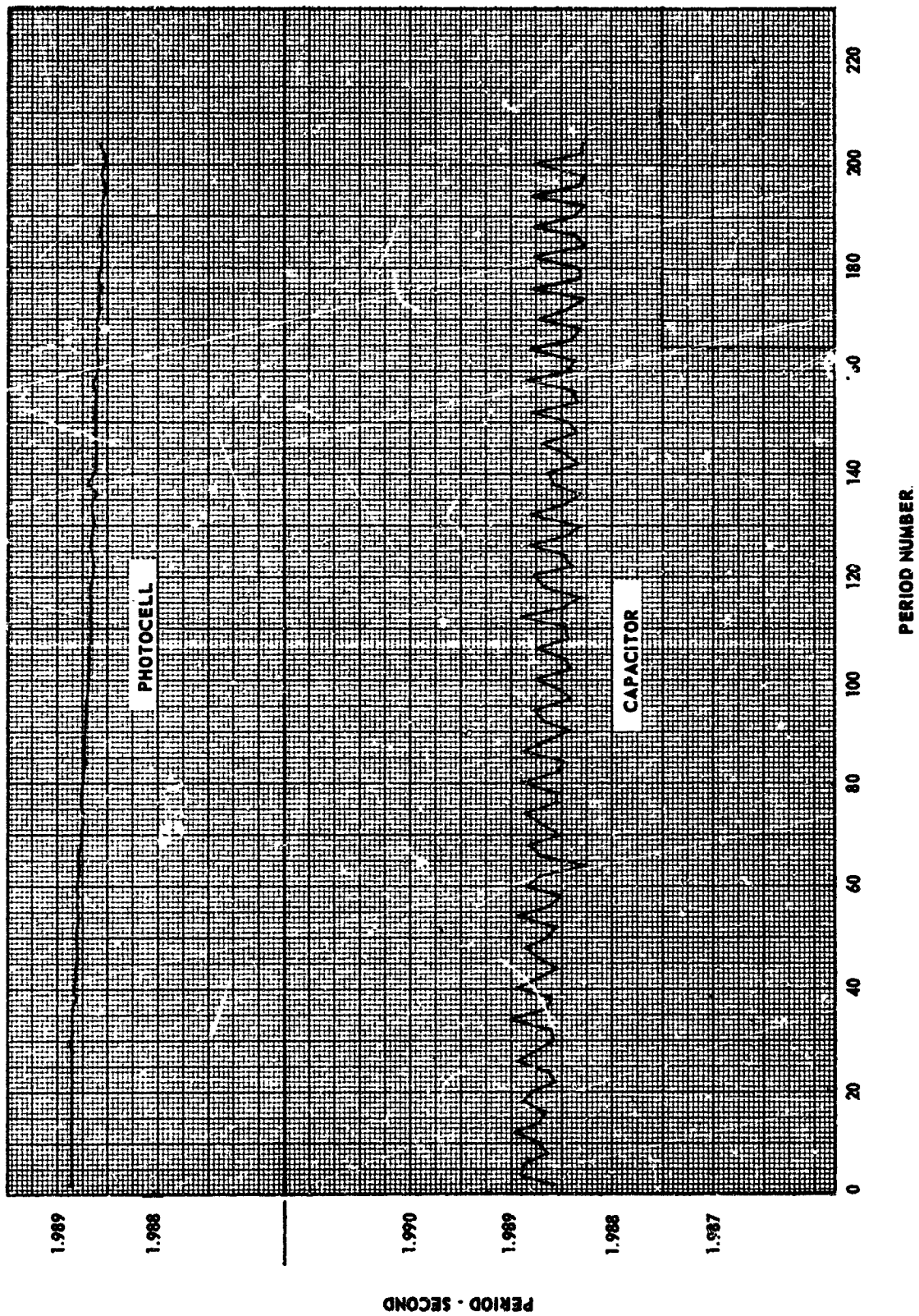


FIGURE 42 TEST NO. 7A - INITIAL AMPLITUDE 0.13 RADIAN

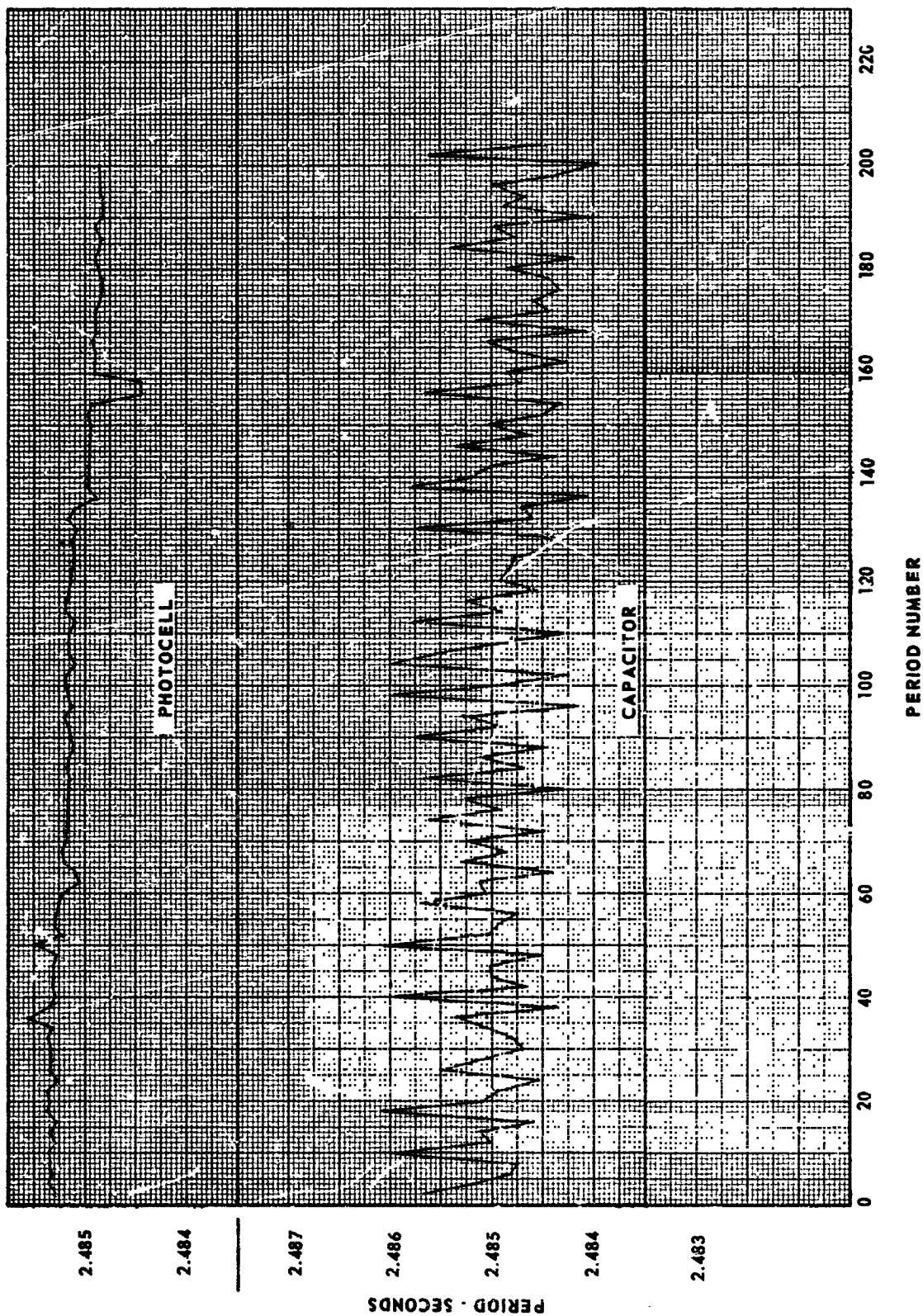


FIGURE 43 TEST NO. 1 - INITIAL AMPLITUDE 0.05 RADIAN

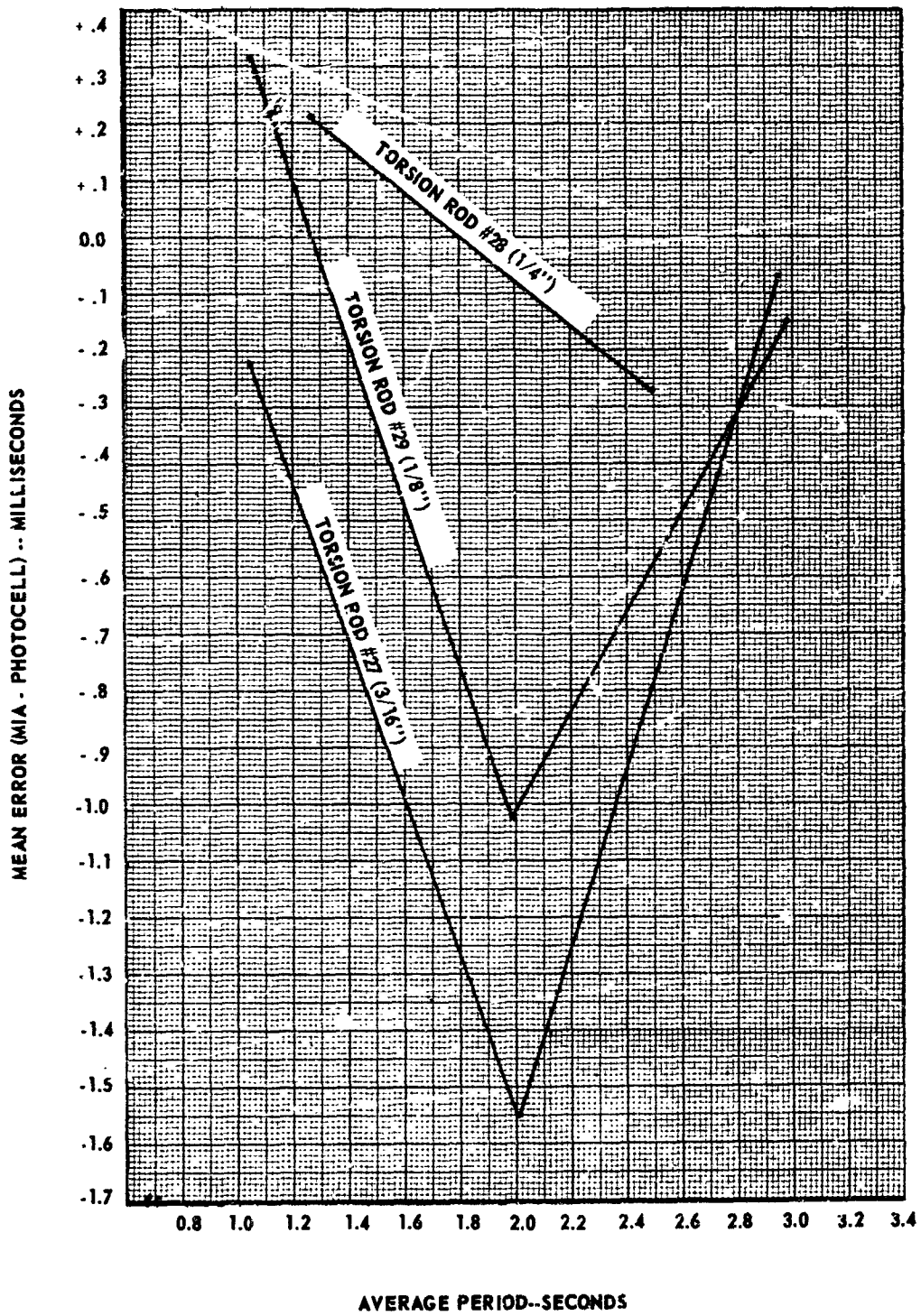


FIGURE 44 TIMING ANALYSIS

Table 16 Timing Analysis of MIA Revised System

Test No.	Torsion Rod No.	Dia. In.	Initial Displacement Rad.	Mean Period-Seconds Photocell	Mean Period-Seconds MIA	Mean Error-Seconds MIA - P.E.C.
2	29	1/8	0.003	1.05796	1.05827	+0.00051
7	29	1/8	0.004	1.98767	1.98665	-0.00102
9	29	1/8	0.005	2.98022	2.98007	-0.00015
5	27	3/16	0.003	1.04507	1.04485	-0.00022
6	27	3/16	0.003	2.00835	2.00680	-0.00155
8	27	3/16	0.005	2.94735	2.94728	-0.00007
3	28	1/4	0.003	1.26888	1.26909	+0.00021
1	28	1/4	0.05	2.48520	2.48493	-0.00027

A look at the mean error curves shows quite an increase in error near 2 cycles, the largest error being 0.08%. No explanation has been found for this effect.

2.2.4.1.4 Conclusions: In view of the results presently obtainable with the two methods, and in consideration of the relatively small amount of equipment needed with the photocell method, it appears that it has the greater promise for improvement. The capacitance method, however can be improved considerably.

2.2.4.1.5 Recommendations: The sensitivity of the capacitor transducer can be increased by reducing the plate separation. Another increase in sensitivity can be had by reducing the transducer's shunt capacitance which at present is perhaps 10 times that of the transducer. This would require relocating the oscillator into the transducer housing and using a variable tank inductance for tuning, thus eliminating the cable capacitance and padder now being used. Mechanical rigidity of all oscillator components is essential. Another increase in sensitivity can be obtained by using a narrow band F.M. detector. A limiter stage ahead of this might be desirable. Better hum filtering techniques should also be investigated such as inter-stage decoupling and D.C. heater supply, along with shielding techniques.

All of the above measures would increase the signal to noise ratio. It might also prove helpful to consider transistors rather than tubes, to reduce the likelihood of microphonics.

2.2.4.2 MIB Prototype Development

2.2.4.2.1 Problem Definition: A major objective of the contract effort is the design of a mechanical/electrical system capable of automatic and accurate determination of moment of inertia. Before a design was finalized, a feasibility study was made with an analog prototype, to ensure that the final product performs the anticipated function. In this feasibility study, new equipment design was minimized, forcing the engineer to optimize the use of available equipment in an attempt to conserve time that could be used for developing the final product.

The heart of the new design is an air-bearing table that is forced to oscillate by means of a torsional rod attached to the table and placing an initial displacement on the table (Figure 45). This equipment satisfies the basic pendulum equation. Instrumentation of the table was used to study the damped sinusoidal output for determination of the moment of inertia of the object under test.

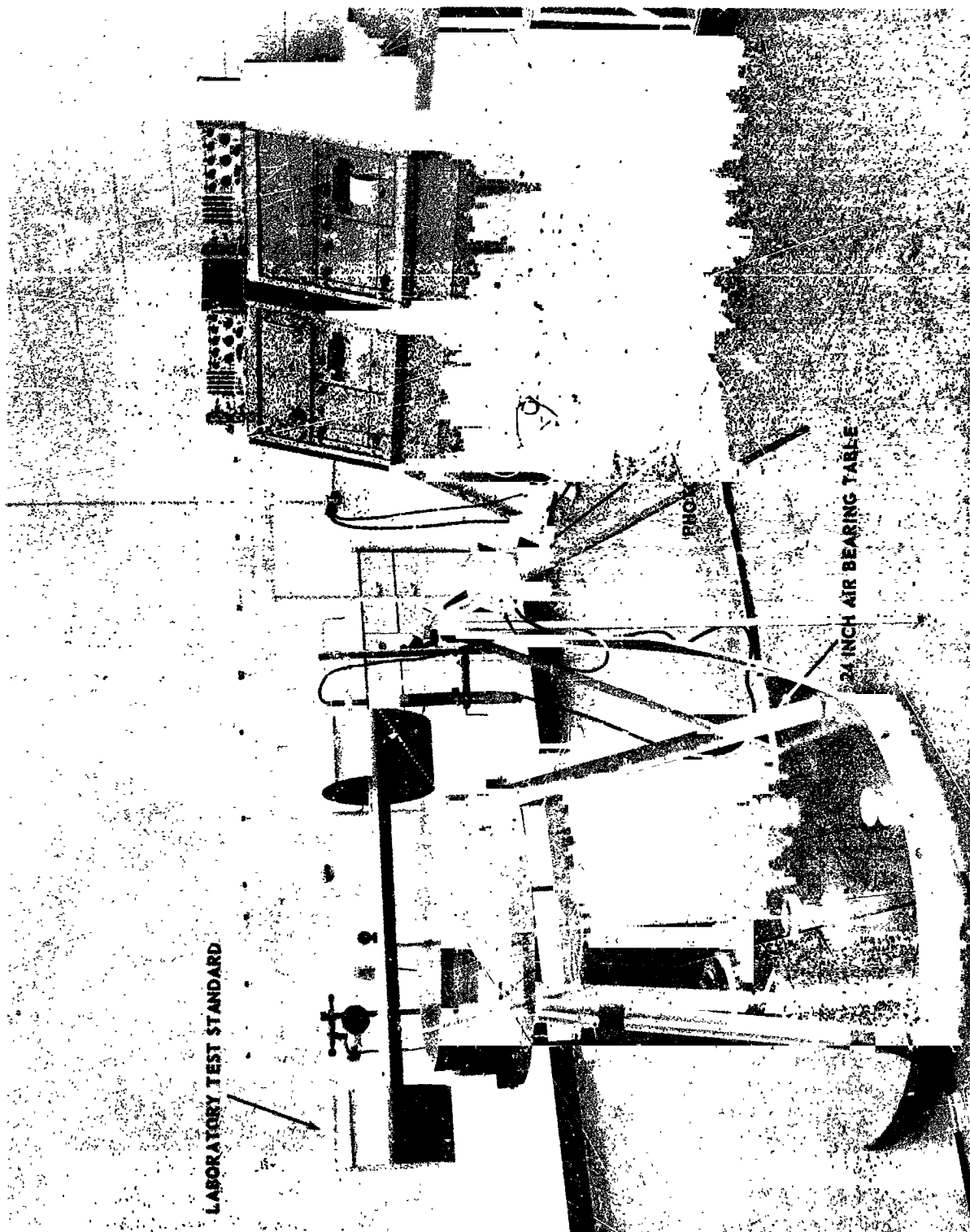


FIGURE 45 24 INCH AIR BEARING TABLE AND ASSOCIATED EQUIPMENT

The tests performed using this table were accomplished in a temperature and humidity controlled environment. The air-bearing table exhibits a minimum of frictional forces and extreme care was exercised in the manufacture of the torsion rods. These precautions ensured the accuracy and repeatability of measurements.

Laboratory determination of K (torsional rod factor) was made by using the air-bearing table with a laboratory standard for moment of inertia. Oscillatory periods of time were measured with a counter-timer unit and associated photocell detection device and collimated light source. Detection of the zero-axis-crossing of the oscillating table was made by breaking a light beam (by a wand attached to the table) that is incident to the photosensitive surface of the photocell. When the light beam is broken, a change of bias is noted in a transistorized amplifier creating a trigger, which excites a bistable multivibrator circuit; this, in turn, starts or stops the counter. This method of measuring an oscillatory or rotating period of time is well recognized as standard.

2.2.4.2.2 Problem Solution: The proper utilization of available signals and equipment permitted the computation of the moment of inertia through the equation, $I = Kt^2$. No attempt was made to determine additional mass effects, which include aerodynamic and minute drag of frictional losses encountered by the table. Compensation for the additional mass effects would have complicated this study beyond the feasibility phase but in the final design of the device, compensation will be made for mass effects.

The calculation of the moment of inertia through the equation $I = Kt^2$ was performed by an analog computer utilizing a voltage analogous to the function t . An established method of simulating a linear function of time in an analog computer is the derivation of a ramp function. A ramp function is derived by the integration of a constant. Thus, if the computer reference voltage can be controlled in regard to the beginning and the ending of the ramp, a ramp analogous to the function t can be obtained.

To switch the computer reference voltage synchronous with the period of oscillation of the air-bearing table, it was necessary to develop an electronically controlled switch. As depicted in Figure 46, a pulse is generated by the photo-electric timing device at each zero crossing of the oscillatory period. These pulses were amplified and used to trigger a multivibrator, yielding a square wave of $1/2$ period duration. If this square wave is amplified, as shown as the amplified wave, and this amplified wave is shaped by a resistance-capacitance circuit and the positive pulses are removed by diode blocking, two negative pulses are developed as shown by the multivibrator input waveform. These pulses are a direct result of photocell detection of one oscillatory period.

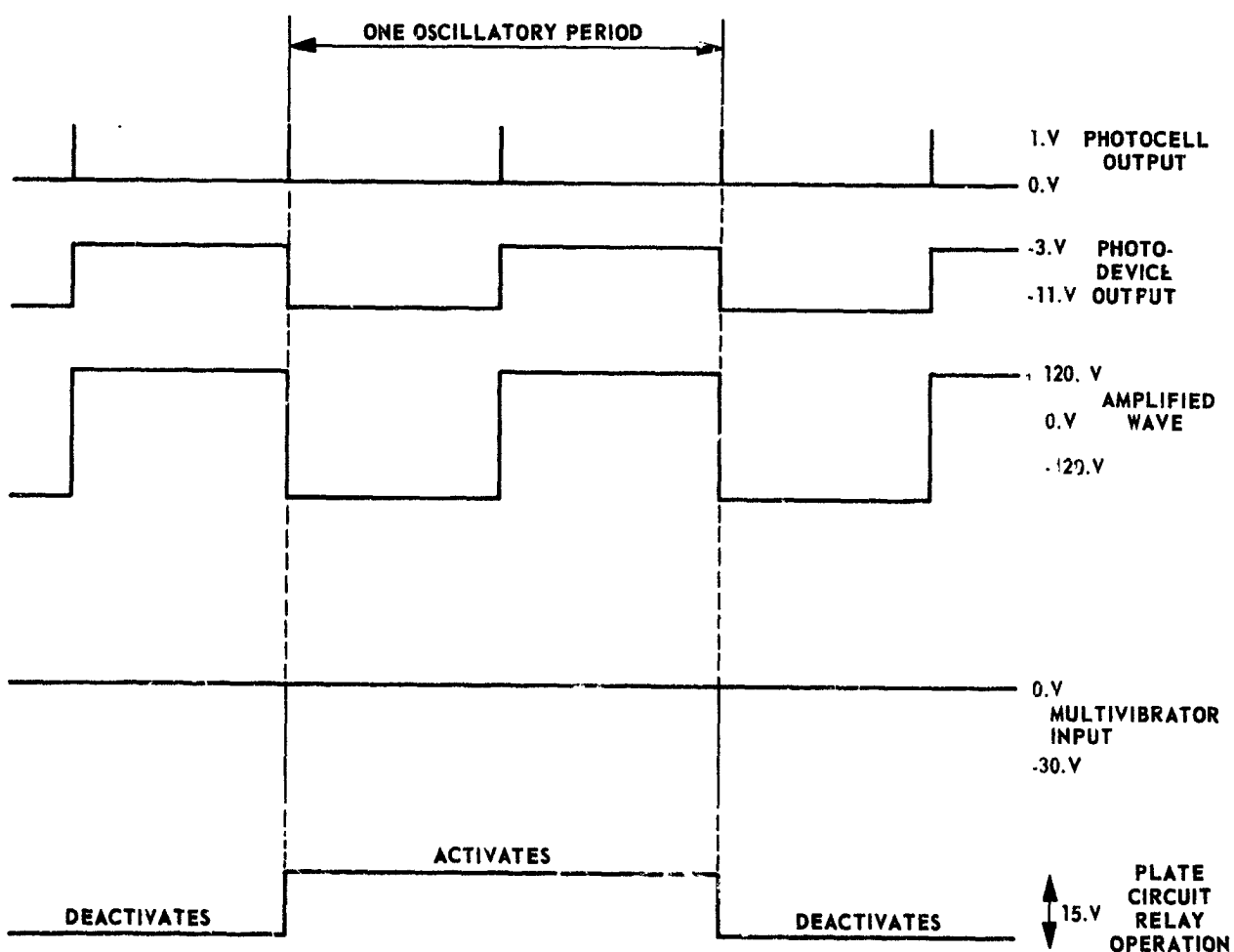


FIGURE 46 WAVEFORM CHART

These pulses were used in a conventional manner to trigger a bistable multivibrator. By substitution of a suitable plate circuit relay in one of the bistable multivibrator plate circuits (in place of a load resistance) the relay operated synchronous with one oscillatory period of the air-bearing table. Thus, the operation of an electronic switch was obtained for computer control.

2.2.4.2.2.1 Computer Solution: Figure 47 illustrates the overall functional diagram of the designed interface equipment, and analog computer patching required for the solution of the study program. Study of Figure 47 will clearly define the operation of this system. From the interface output, the opening and closing of the relay switches the computer reference voltage on the integrator input synchronous with the oscillatory period. A ramp function of sawtooth voltage is derived, whose period is also equal to the oscillatory period. This ramp function is squared and then multiplied by a constant, equivalent to the torsional rod constant. The resultant product, the gross moment of inertia (composed of the moment of inertia of the test specimen and the oscillating portion of the air-bearing table), is read from the computer digital voltmeter. Further refinement of the computer circuit may be accomplished by subtracting from the resultant product the moment of inertia of the air-bearing table. Figure 48 illustrates the developed prototype, referred to as MIB, and the completed interface equipment and analog computer are illustrated in Figure 49. Figure 50 is a working schematic of the developed prototype, MIB.

2.2.4.2.2.2 Computer Scaling: Scaling of the computer is not only essential for the quantity K , but also to prevent computer overloading. (Scaling is accomplished on the computer by the use of potentiometers for voltage division). The necessity of time scaling of the ramp function is obvious. If the potentiometer setting were selected for a ramp function analogous to an oscillatory period of one second, the computer would overload for any oscillatory period greater than one second. Scaling represents a minor problem, but for some instances of moment of inertia determination, it may be necessary to proportionally scale the readout of the digital voltmeter.

Scaling of this output can be avoided if the maximum ramp function is selected for a very large oscillatory period, for example 10 seconds. This can be done--at the expense of accuracy--in cases where the period is less than 1 second, since the constant voltage from which the ramp was derived would be very small. General computer practices discourage the use of very small voltages, since undersirable low-level signals may affect

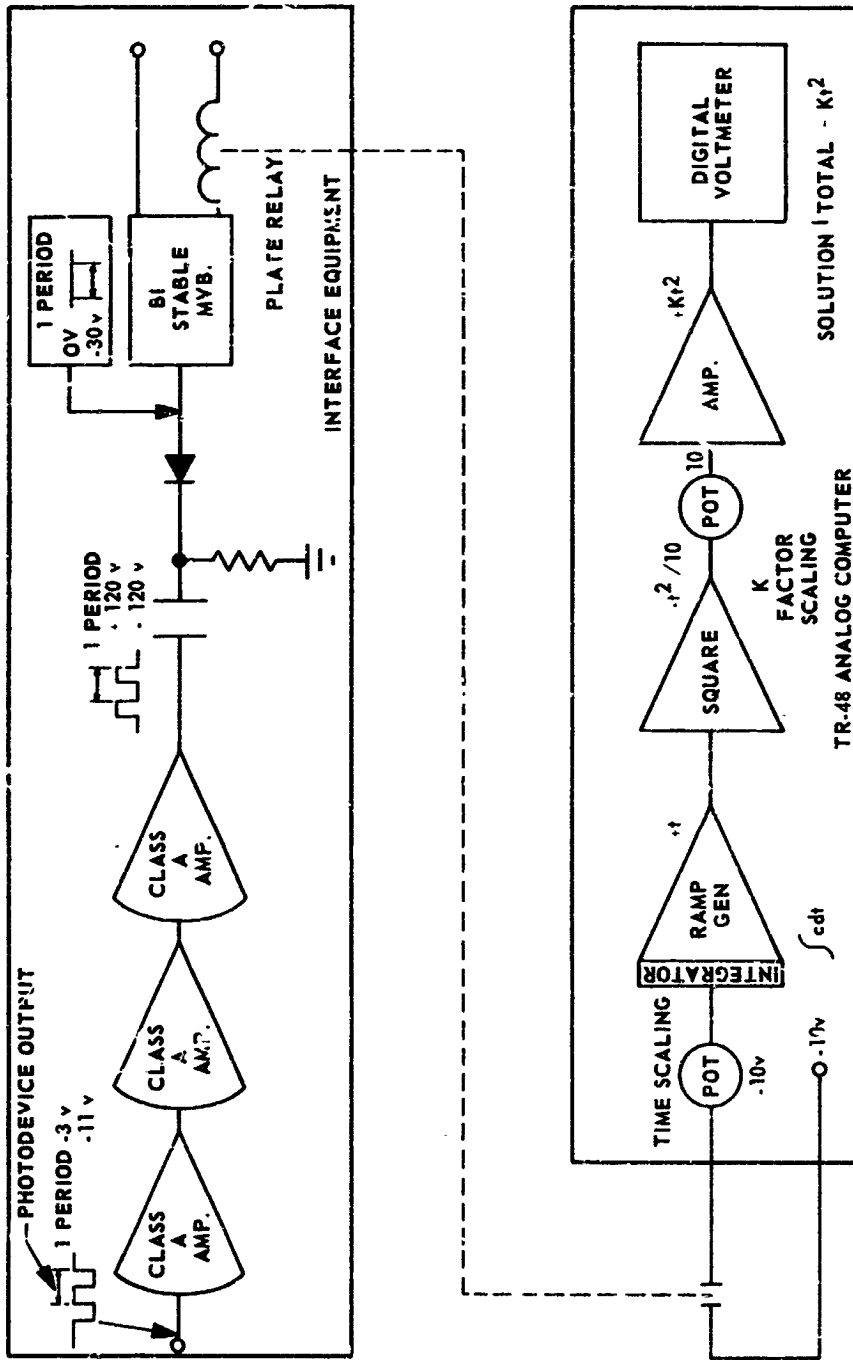


FIGURE 47 INTERFACE EQUIPMENT AND ANALOG COMPUTER FUNCTIONAL DIAGRAM

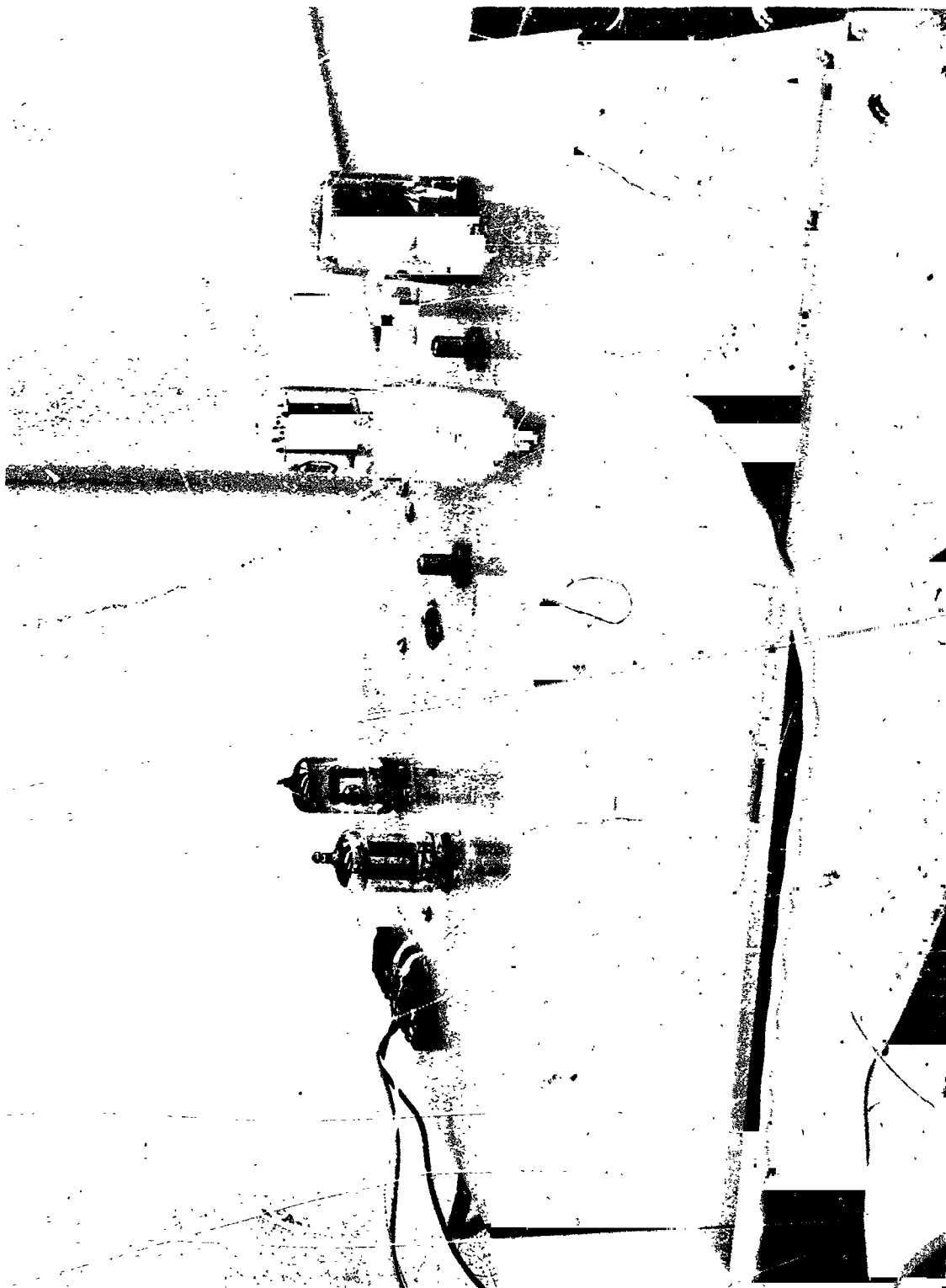


FIGURE 48 PROTOTYPE MIB

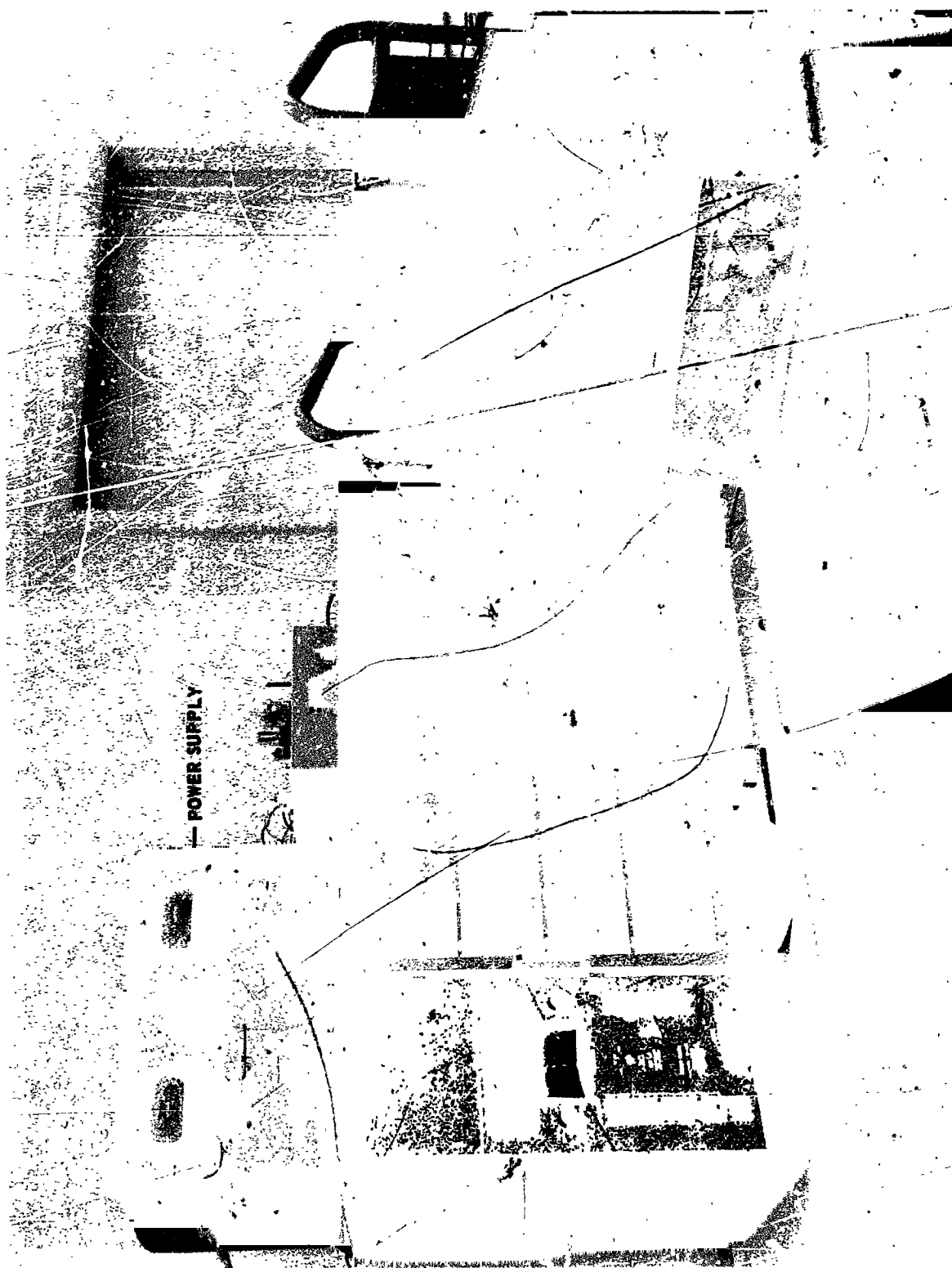
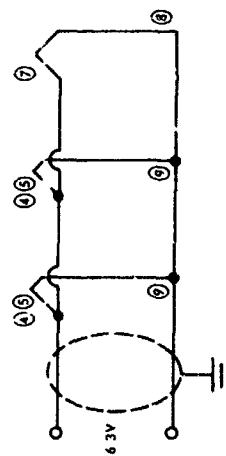


FIGURE 49 COMPLETE ANALOG SYSTEM



- FIGURE 50 MIB SCHEMATIC**

the overall result.

2.2.4.2.2.3 Accuracy Considerations: Several factors determine the overall accuracy of the determination of the moment of inertia:

- (1) The overall accuracy of the computer is published ranging from 0.1 to 1.0%.
- (2) A small, but measurable, quantity of time is lost by the interface equipment plate circuit relay. This time was measured and appeared to be constant at approximately 6 microseconds. No adjustment to the computer program could be made for such a minute error.
- (3) To reiterate, no compensation for additional mass effects was attempted in this feasibility study.

2.2.4.2.3 Testing and Analysis: Preliminary testing of the analog system and prototype unit was sufficient to prove the feasibility of design of the more accurate final product. In order that the accuracy and repeatability of the analog system be ascertained, final testing consisting of five tests was accomplished using laboratory standards of moment of inertia for comparison purposes.

Tables 17 through 21 depict the results of all final testing performed. It should be noted that both percent time and percent moment of inertia errors were determined.

2.2.4.2.3.1 Laboratory Equipment Arrangement: The equipment arrangement employed in testing consisted of the 24-inch air bearing with torsion rod and laboratory test standard, light source with photo detection unit which triggers the laboratory counter/timer units, and the analog system. Figure 51 illustrates the equipment arrangement used in testing.

Each test was conducted under as near-identical conditions as possible, in regard to temperature, humidity, table air pressure, and original table displacement. Sufficient warm-up period was allowed in all cases for the electronic equipment utilized. Scaling of the analog computer (time and amplitude) was set as accurately as possible. By controlling these variables and varying only the laboratory test standards, conditions for testing are optimized by minimization of external functions.

Testing progressed in a usual manner as described by established laboratory techniques. After the installation of the desired torsional rods and laboratory standards on the air bearing table, the table was

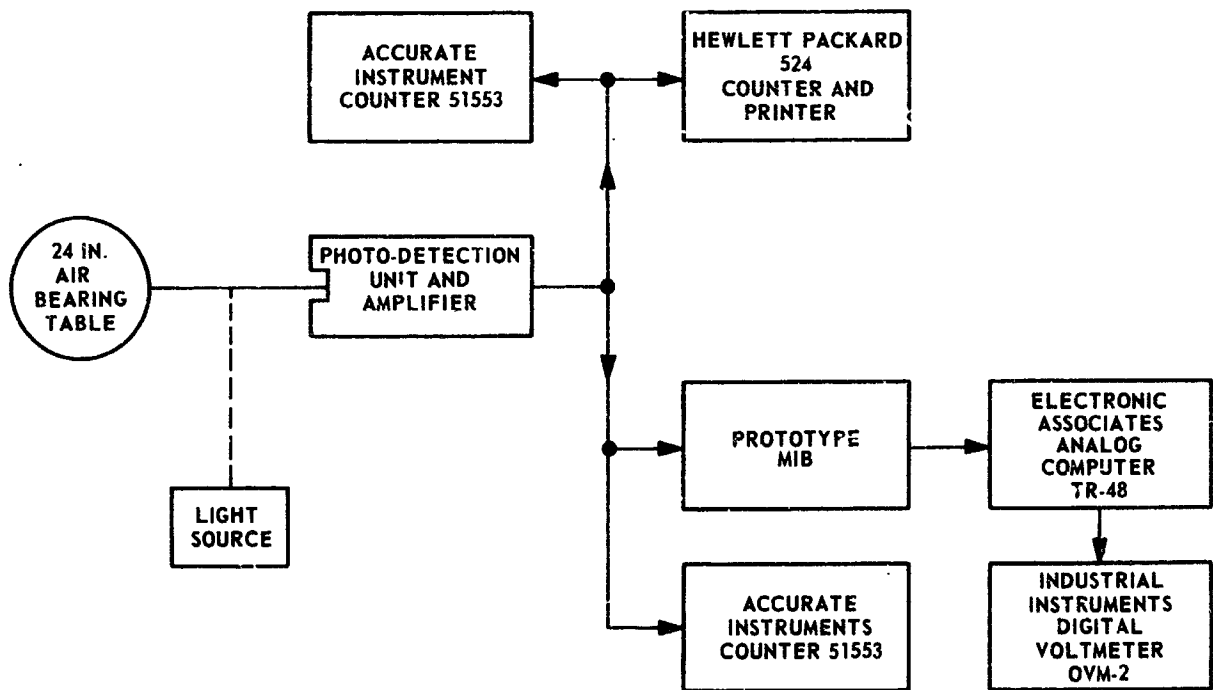


FIGURE 51 TEST EQUIPMENT ARRANGEMENT

Table 17 Prototype MIB Moment of Inertia
Determination Capability Final Test No. 1

Date: April 7, 1965

Computer Time Scaling: 10V = 10 seconds

Air Bearing Table Pressure: 25 PSI

Original Table Displacement: .035 radians

	Begin	End
Test Time	8:10 a. m.	8:35 a. m.
Temperature	70	70
Humidity	42%	44%

Torsion Rod Factor:

Testing Personnel:

A. Berisford

K. Comer

Cycle No.	Time (Computer) Seconds	Time (Actual) Seconds	% Time Error	Moment of Inertia (Measured) in-lb-sec ²	Moment of Inertia (Calculated) in-lb-sec ²	% Moment of Inertia Error
100	1.490	1.48722	0.187	10.20	9.912	2.90
200	1.490	1.48724	0.186	10.20	9.912	2.90
300	1.490	1.48718	0.190	10.20	9.912	2.90
400	1.490	1.48703	0.200	10.20	9.912	2.90
500	1.490	1.48705	0.198	10.20	9.912	2.90
600	1.490	1.48728	0.183	10.20	9.912	2.90
700	1.490	1.48685	0.212	10.20	9.912	2.90
800	1.490	1.48668	0.223	10.20	9.912	2.90
900	1.490	1.48702	0.200	10.20	9.912	2.90
1000	1.490	1.48717	0.190	10.20	9.912	2.90
Mean Value of Data	1.490	1.48707	0.197	10.20	9.912	2.90

Required Equipment

1. Prototype MIB with Hewlett Packard 712B Power Supply
2. Electronic Associates TR-48 Analog Computer
3. Hewlett Packard 524 Counter with associated Printer
4. Photocell Detection Unit and light source
5. Accurate Instruments Counter 51553
6. 24 inch Air Bearing Table with Torsion Rod Number 28
7. Laboratory Test Standard: None
8. Industrial Instruments Digital Voltmeter DVM-2

Table 18 Prototype MIB Moment of Inertia
Determination Capability Final Test No. 2

Date: April 7, 1965
Computer Time Scaling: 10V = 10 seconds

Air Bearing Table Pressure: 25 PSI
Original Table Displacement: .035 radians

	Begin	End	Torsion Rod Factor: 4.4809
Test Time	10:42 a.m.	11.31 a.m.	Testing Personnel:
Temperature	70°F	70°F	<u>A. Berisford</u>
Humidity	46%	40%	<u>K. Comer</u>

Cycle No.	Time (Computer) Seconds	Time (Actual) Seconds	% Time Error	Moment of Inertia (Measured) in-lb-sec ²	Moment of Inertia (Calculated) in-lb-sec ²	% Moment of Inertia Error
100	2.880	2.89134	0.392	37.30	37.412	0.299
200	2.880	2.89123	0.388	37.30	37.412	0.299
300	2.879	2.89121	0.422	37.30	37.412	0.299
400	2.880	2.89119	0.387	37.30	37.412	0.299
500	2.879	2.89114	0.420	37.30	37.412	0.299
600	2.880	2.89121	0.388	37.30	37.412	0.299
700	2.880	2.89100	0.380	37.30	37.412	0.299
800	2.880	2.89107	0.383	37.36	37.412	0.139
900	2.880	2.89167	0.404	37.37	37.412	0.112
1000	2.880	2.89074	0.372	37.37	37.412	0.112
Mean Value of Data	2.880	2.89118	0.394	37.32	37.412	0.246

Required Equipment

1. Prototype MIB with Hewlett Packard 7123 Power Supply
2. Electronic Associates TR-48 Analog Computer
3. Hewlett Packard 524 Counter with associated Printer
4. Photocell Detection Unit and light source
5. Accurate Instruments Counter 51553
6. 24 inch Air Bearing Table with Torsion Rod Number 28
7. Laboratory Test Standard: 30 in.-lb-sec²
8. Industrial Instruments Digital Voltmeter DVM-2

Table 19 Prototype MIB Moment of Inertia
Determination Capability Final Test No. 3

Date: April 7, 1965
Computer Time Scaling: 10V = 10 seconds

Air Bearing Table Pressure: 25 PSI
Original Table Displacement: .035 radians

	Begin	End	Torsion Rod Factor: 67.08535
Test Time	13:45 p.m.	14:05 p.m.	Testing Personnel:
Temperature	72°F	72°F	<u>A. Berisford</u>
Humidity	44%	46%	<u>L. Fretwell</u>

Cycle No.	Time (Computer) Seconds	Time (Actual) Seconds	% Time Error	Moment of Inertia (Measured) in-lb-sec ²	Moment of Inertia (Calculated) in-lb-sec ²	% Moment of Inertia Error
100	1.030	1.02776	0.218	74.49	70.843	5.15
200	1.030	1.02738	0.255	74.49	70.843	5.15
300	1.030	1.02713	0.279	74.50	70.843	5.16
400	1.030	1.02698	0.294	74.50	70.843	5.16
500	1.030	1.02687	0.305	74.49	70.843	5.15
600	1.030	1.02676	0.316	74.40	70.843	5.02
700	1.030	1.02674	0.318	74.40	70.843	5.02
800	1.030	1.02670	0.321	74.30	70.843	4.88
900	1.030	1.02662	0.329	74.30	70.843	4.88
1000	1.030	1.02669	0.322	74.30	70.843	4.88
Mean Value of Data	1.030	1.02696	0.296	74.42	70.843	5.05

Required Equipment

1. Prototype MIB with Hewlett Packard 712B Power Supply
2. Electronic Associates TR-48 Analog Computer
3. Hewlett Packard 524 Counter with associated Printer
4. Photocell Detection Unit and light source
5. Accurate Instruments Counter 51553
6. 24 inch Air Bearing Table with Torsion Rod Number 120
7. Laboratory Test Standard: 60" lb. sec²
8. Industrial Instruments Digital Voltmeter DVM-2

Table 20 Prototype MIB Moment of Inertia
Determination Capability Final Test No. 4

Date: April 7, 1965

Computer Time Scaling: 10V = 10 seconds

Air Bearing Table Pressure: 25 PSI

Original Table Displacement: .035 radians

Test Time Begin End
 15:05 p.m. 15:30 p.m.
Temperature 72°F 72°F
Humidity 46% 46%

Torsion Rod Factor: 67.08535

Testing Personnel:

A. Berisford

E. Pauli

Cycle No.	Time (Computer) Seconds	Time (Actual) Seconds	% Time Error	Moment of Inertia (Measured) in-lb-sec ²	Moment of Inertia (Calculated) in-lb-sec ²	% Moment of Inertia Error
100	1.430	1.41386	1.141	138.0	134.044	2.95
200	1.410	1.41332	0.234	138.0	134.044	2.95
300	1.410	1.41297	0.210	138.0	134.044	2.95
400	1.410	1.41276	0.195	138.0	134.044	2.95
500 1	1.410	1.41261	0.184	138.0	134.044	2.95
600	1.420	1.41241	0.537	138.0	134.044	2.95
700	1.410	1.41233	0.164	138.0	134.044	2.95
800	1.410	1.41223	0.157	138.0	134.044	2.95
900	1.420	1.41226	0.548	138.0	134.044	2.95
1000	1.410	1.41230	0.162	138.0	134.044	2.95
Mean Value of Data	1.414	1.41271	0.353	138.0	134.044	2.95

Required Equipment

1. Prototype MIB with Hewlett Packard 712B Power Supply
2. Electronic Associates TR-48 Analog Computer
3. Hewlett Packard 524 Counter with associated Printer
4. Photocell Detection Unit and light source
5. Accurate Instruments Counter 51553
6. 24 inch Air Bearing Table with Torsion Rod Number 120
7. Laboratory Test Standard: 120 in. lb-sec²
8. Industrial Instruments Digital Voltmeter DVM-2

Table 21 Prototype MIB Moment of Inertia
Determination Capability Final Test No. 5

Date: April 8, 1965

Computer Time Scaling: 10V = 10 seconds

Air Bearing Table Pressure: 25 PSI

Original Table Displacement: .035 radians

Test Time Begin End
 8:30 a. m. 9:40 a. m.
Temperature 70°F 70°F
Humidity 42% 44%

Torsion Rod Factor: 4.4809

Testing Personnel:

C. Bridges

A. Berisford

Cycle No.	Time (Computer) Seconds	Time (Actual) Seconds	% Time Error	Moment of Inertia (Measured) in-lb-sec ²	Moment of Inertia (Calculated) in-lb-sec ²	% Moment of Inertia Error
100	3.960	3.97754	0.440	70.30	70.843	0.766
200	3.960	3.97703	0.428	70.30	70.843	0.766
300	3.960	3.97670	0.419	70.30	70.843	0.766
400	3.960	3.97692	0.425	70.30	70.843	0.766
500	3.960	3.97711	0.430	70.30	70.843	0.766
600	3.960	3.97683	0.423	70.30	70.843	0.766
700	3.960	3.97645	0.415	70.30	70.843	0.766
800	3.960	3.97856	0.466	70.30	70.843	0.766
900	3.960	3.97534	0.385	70.30	70.843	0.766
1000	3.960	3.97668	0.419	70.40	70.843	0.625
Mean Value of Data	3.960	3.97692	0.425	70.31	70.843	0.752

Required Equipment

1. Prototype MIB with Hewlett Packard 712B Power Supply
2. Electronic Associates TR-48 Analog Computer
3. Hewlett Packard 524 Counter with associated Printer
4. Photocell Detection Unit and light source
5. Accurate Instruments Counter 51553
6. 24 inch Air Bearing Table with Torsion Rod Number 28
7. Laboratory Test Standard: 60 in. -lb-sec²
8. Industrial Instruments Digital Voltmeter DVM-2

displaced to 0.035 radian and released. The measurements of periods (by the laboratory counters and the analog computer) and calculation of moment of inertia (by the analog computer) were made for the hundredth through the thousandth cycle at 100-cycle intervals. This range is compatible with normal moment of inertia calculations utilizing the 24-inch air bearing table.

It should be noted that Final Test Number 1 was made without a laboratory moment of inertia standard. This test was made to determine the moment of inertia of the air bearing table. In Tests Number 2 through 5, the moment of inertia of the table is additive to that of the laboratory standard.

2.2.4.2.3.2 Time Errors: The final testing of the prototype system indicates a mean time-error ranging from 0.197 to 0.425%. This is well within the published accuracy of the computer, which should contribute the major portion of the error encountered. (The time error of the electronic switching unit was measured at 6 microseconds difference.) One point should be noted from the test data. The actual time was measured to only three significant digits beyond the decimal point. This condition was dictated by the capacity of the analog computer and digital voltmeter. Since the error is within computer accuracy, further investigation and analysis is believed to be unwarranted.

2.2.4.2.3.3 Moment of Inertia Errors: The mean of moment of inertia errors ranged from 0.246 to 5.05%. It should be reiterated that the over-all published accuracy of the computer ranges from 0.1 to 1.0%. For most operations utilizing linear function generations, the accuracy will be well within stated limitations. However, the computation performed for moment of inertia determination requires a non-linear operation; namely, squaring.

The TR-48 analog computer performs the squaring operation by diode-resistance networks. Electrical conduction through the diodes occurs at discrete levels. Thus, a squaring-curve is composed of many segments of straight line, rather than a smooth curve. It should be realized that a limitation to the number of diode resistor circuits exists. The number of circuits utilized in the squaring operation determines the accuracy of the operation.

From the data, a trend for better accuracy of moment of inertia determination is evident when relatively large period of oscillation were established. Even through the computer was utilized in recommended ranges of operation, it is apparent that better accuracies were achieved when the squaring operations were made at smaller frequencies and

consequently greater computer excitation voltages.

An improvement of accuracy in squaring can be obtained by one of the following methods:

- (1) Establish period of oscillation which will drive the analog computer to voltages just below the saturation level.
- (2) Establish time scaling which will drive the analog computer to voltages just below the saturation level.

2.2.4.2.4 Conclusions: The degree of repeatability and accuracy obtained by the analog prototype is well above the required 85% accuracy. Preliminary and final testing of the analog prototype definitely indicates the feasibility of developing a digitized system. Refinements to the digitized system for compensation for additional mass effects will be made by mathematical analysis of the air bearing table torsional rod system and electronic incorporation of the necessary refinements into the final system.

This test demonstrates the value of the analog computer in mass metrology experiments and feasibility studies, especially as an in-line computation device. This is attributed to the natural frequencies of torsional experiments and the versatility of the analog computer, both mathematically and electronically. Further versatility of the computer may be achieved by hybrid computations, where both digital and analog computations are performed simultaneously. The developed prototype utilized the computer in this manner.

2.3 PRODUCTS OF INERTIA

2.3.1 Basis for System Design: In an endeavor to develop an analog prototype system for determination of products of inertia as funded under NASA 8-11314, a literature search was made. This search revealed a method for determining products of inertia which was favorable to system fabrication, basically requiring the computation by an analog computer of an equation containing two variables and one constant.

From Figure 52, it can be ascertained that a measurement of torque exerted by a body about axis Oy as the body rotates at a constant angular velocity, ω , about Ox , will lead to the solution of product of inertia. Each particle situated at a distance r from the axis Ox will exert a radial force $m\omega^2 r$. Thus, the total torque about the axis Oy is:

$$T_y = \sum x m \omega^2 r \sin \theta = \omega^2 \sum x m r \sin \theta \quad (55)$$

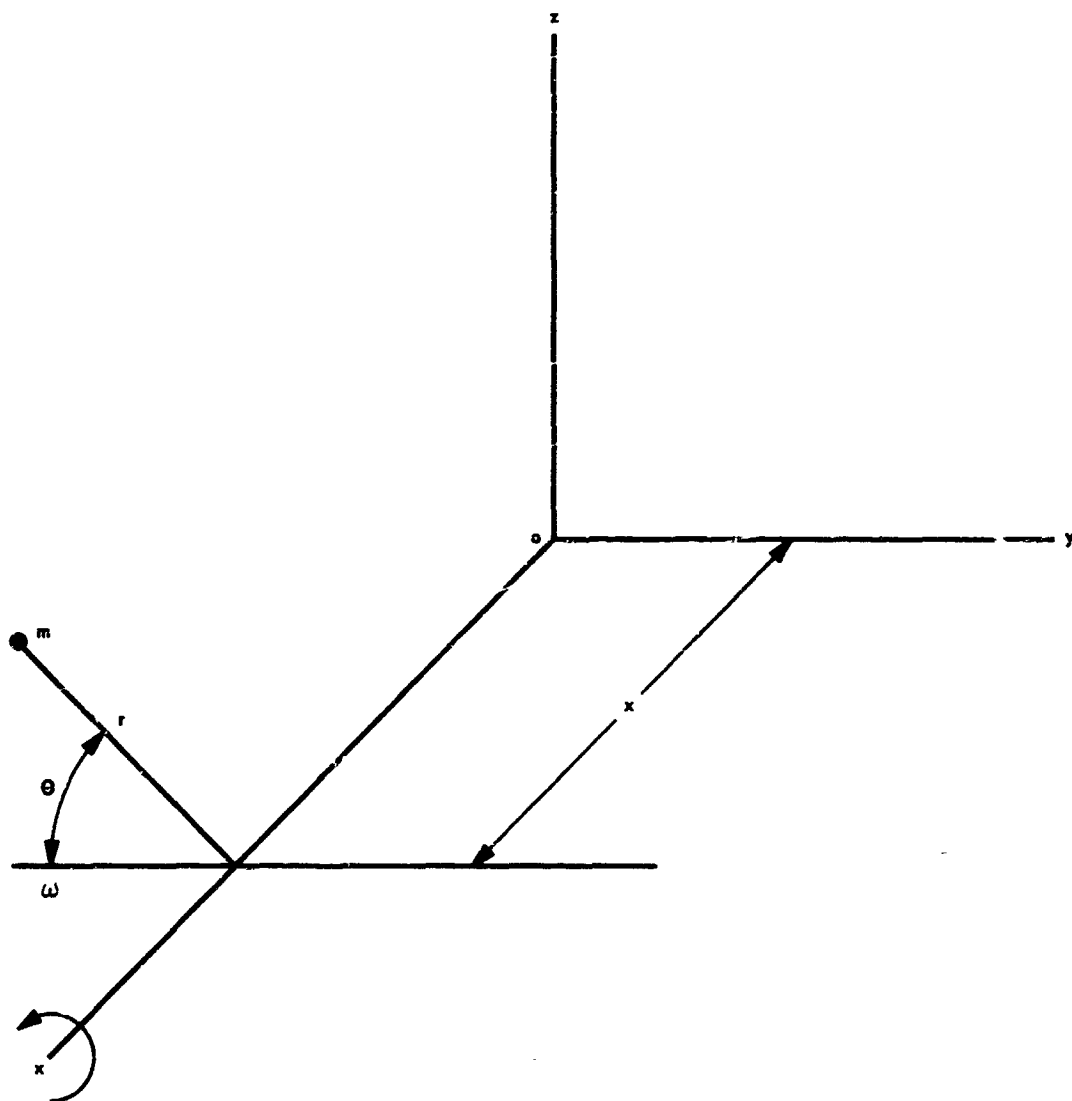


FIGURE 52 COORDINATE SYSTEM FOR PRODUCT OF INERTIA SOLUTION

But from Figure 52,

$$r \sin \theta = z \quad (56)$$

$$\therefore T_y = \omega^2 \sum mzx = \omega^2 I_{zx} \quad (57)$$

where I_{zx} is the product of inertia

$$\text{Thus, } I_{zx} = \frac{T_y}{\omega^2} \quad (58)$$

This expression may be further simplified for purposes of machine design by recalling that torque is defined as the product of force and length. Therefore,

$$I_{zx} = \frac{FL}{\omega^2} \quad (59)$$

2.3.2 Methods of System Solution: Equation 59 lends itself readily for fabrication of a desired system. From the equation, the following restrictions may be seen:

- (1) The test body must be rotated at a constant angular velocity.
- (2) The table top or surface on which the test body is rotated must have its vertical axis of rotation through the center of gravity of the test body to insure that no component of static unbalance enters the solution of equation 59.
- (3) When the body is rotated at ω , a force F at a distance L from the axis of rotation must be measured.

From these basic stipulations, three methods of system solution were proposed.

- (1) Utilize an air bearing table or other near frictionless support, rotate the table top, and for a particular revolution, determine the equation parameters. This method was eliminated since a lack of control and measurement of parameters is evident. Certainly, the angular velocity, ω , is not constant since the device is not absolutely frictionless.
- (2) Using an air bearing table or other near frictionless device or support, provide a precision drive for the device. This method is feasible, however, the cost of fabrication was believed to be prohibitive.

- (3) Procure a precision rate table, which is of sufficient quality to be used in testing precision gyros. This table would include all accessories such as servo amplifiers which would provide precise variable control, and low noise slip rings which provide transmission of electrical data from the table top to necessary interface equipment and the analog computer.

2.3.3 System Design: From the later proposed method, a precision rate table manufacturer, by Inland Controls was selected and requisitioned. A decision to requisition instead of manufacture the device was made due to cost, delivery date, and degree of precision as specified by the following manufacturer's specifications:

Inland Controls Rate Table Model 712:

Speed range:	0 to 600°/sec
Speed accuracy:	0.1% of indicated speed or 0.0001°/sec, whichever is greater
Wcw and flutter	0.1% of indicated speed or 0.0001°/sec, whichever is greater
Table acceleration:	100°/sec ²
Peak torque	5 ft lbs
Table top diameter	24 inches
Table flatness	0.001" T.R.
Table load capacity:	300 lb
Shaft runout:	0.0001"

This table, although procured for use in an analog model feasibility program, should be of sufficient quality for use in a more sophisticated and precise digital machine, which may be developed in the future.

Modifications to the rate table, and accompanying amplifier drive device were made to permit collection of the necessary data. Figure 53 indicates the rate table and the tilt top which was placed above the rate table. This tilt top rotates with the rate table and permits measurement of the variable F, which is a result of product of inertia. This variable is measured by two load cells which are 180° apart through the center of the

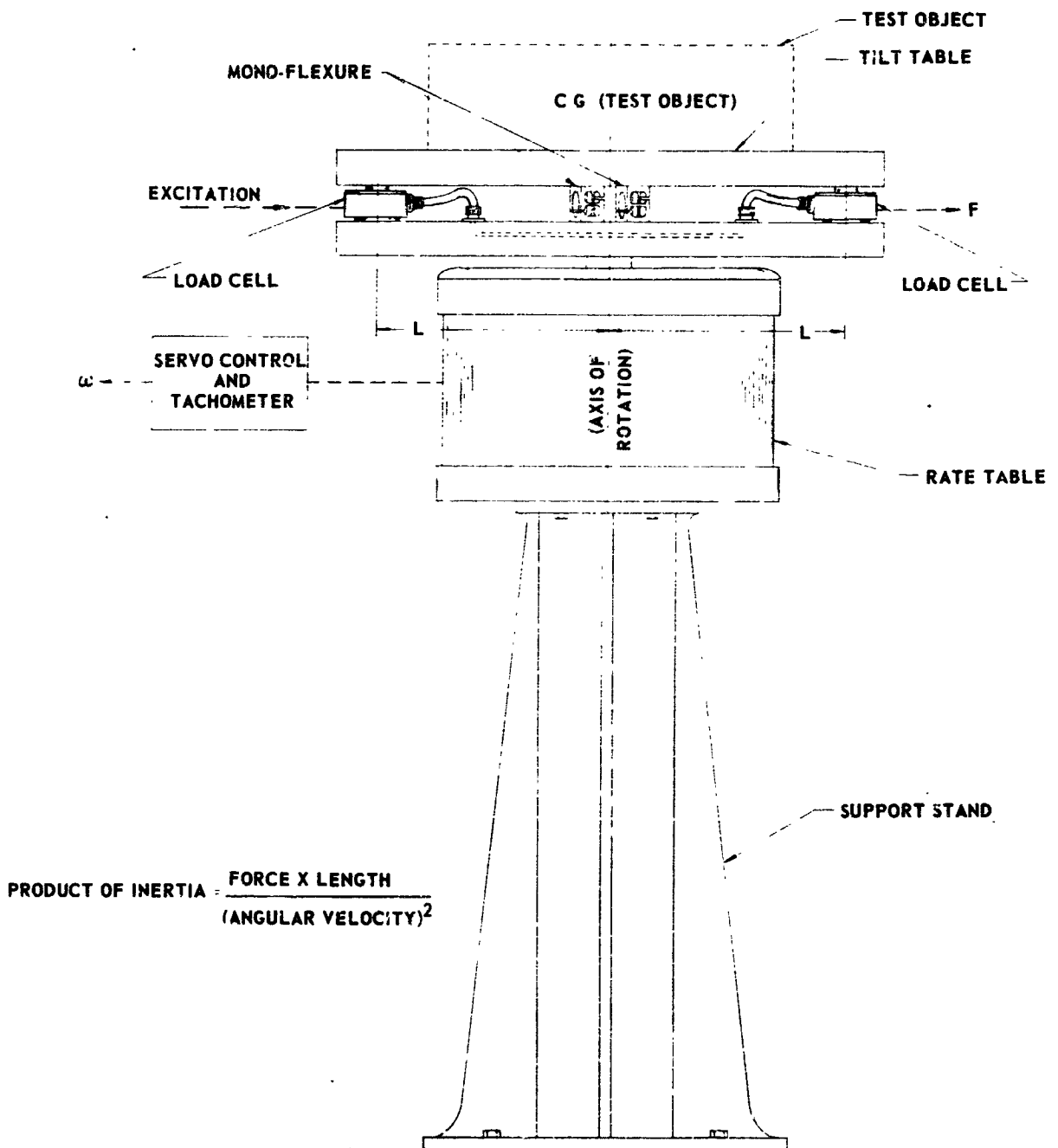


FIGURE 53 PRODUCT OF INERTIA TABLE AND ACQUISITION OF VARIABLES

tilt top. In this configuration, when a product of inertia is encountered, one cell is in compression and the other cell in tension. The load cell specifications were as follows:

Revere Super Precision Universal Load Cells:

Capacity:	25 lb
Terminal resistance:	350 \pm 1 ohm
Output:	3.000 \pm 0.1% mv/volt
Zero balance:	\pm 1% of rated output
Nonlinearity:	0.05% of rated output
Repeatability:	0.02% of rated output
Hysteresis:	0.03% of rated output

It should also be noted from the figure that monoflexures were employed. This permits the measurement of product of inertia in one axis only, since the resulting tilt (0.005 inches maximum) is through the axis of the load cells. Manufacturers monoflexure specifications are:

Ormond Mono-Flexure Type MF-8-3.0

Rated Capacity:	3000 lb
Initial stiffness:	1.8 in-lb/degree
Efficiency (load per unit of stiffness):	1670
Maximum deflection:	\pm 8°

The quantity L is a constant and was determined by a measurement from the center of the tilt top to the point at which the force, F, was measured by the load cells.

The variable, ω , was taken from the servo drive of the rate table. This quantity was obtained in a suitable d.c. form, with only scaling necessary before insertion into equation 59.

In regard to scaling, scaling of the equation variables and constant was necessary before solution of equation 59. The maximum combined load cell output was calculated to be 0.09 volts. This was amplified and scaled to include the distance L such that 250 inch pounds (maximum) was equivalent to 2.5 volts. Referring to the variable ω , a scale of 7 volts/radian/second was obtained from the servo drive. This was scaled such that 1 radian/second angular velocity was equal to 10 volts. By performing scaling in units of tens, it was necessary to place the decimal point on the voltage read from the analog computer. Thus, further mathematical manipulations were unnecessary.

2.3.3.1 Electrical Concepts and Design: Figure 54 depicts the completed electrical system in a block diagram fashion. From the diagram, the variable F data is obtained from the load cells, appropriately scaled by a factor of $-L/100$ and placed in the dividend portion of the division circuit. The variable ω is scaled to a value of $\omega/10$ and squared, thus yielding

$$\frac{\omega^2}{100} \cdot \frac{1}{10}$$

where the scale down by $1/10$ is achieved in the squaring operation. Thus, the division operation is performed, utilizing both variables and yielding

$$+ \frac{10 FXL}{\omega^2},$$

which is the desired solution.

2.3.3.2 Mechanical Concepts and Design: From the basic rate-table, a mechanical design was formulated wherein an additional table or platform was secured above the rate-table and was permitted to tilt in one plane. This was achieved and measured through the use of monoflexures and load cells which were accurately located and secured between the rate-table top and the working platform. Additional efforts were expended to insure the levelness of the table in a static condition and that the test body was accurately located with its center of gravity over the vertical axis of rotation.

STIPULATIONS:

1 RAD/SEC 10 VOLTS
250 INCH LB 2.5 VOLTS

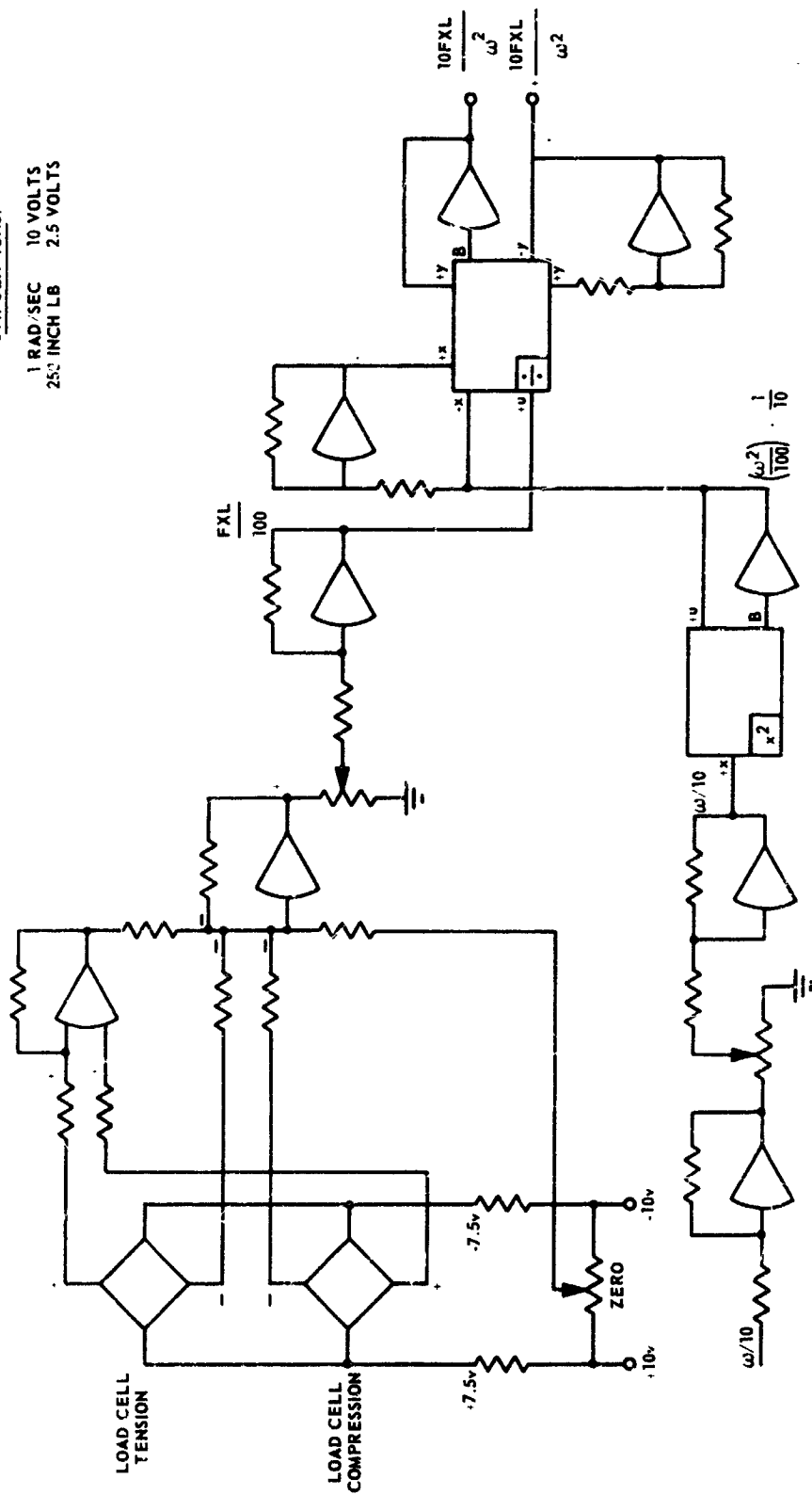


FIGURE 54 ELECTRICAL DESIGN OF ANALOG PRODUCT OF INERTIA MACHINE

2.3.4 System Evaluation

2.3.4.1 Results: After connection of the electrical circuitry according to the block diagram of Figure 54, a checkout test of the system was made, and final adjustments completed. Measurement accuracy was determined by testing a number of laboratory test standards. These standards are triangular solids for which the products of inertia about selected axes have been calculated. Table 22 illustrates the difference in readings obtained.

2.3.4.2 Analysis of Results: One of the major contributing factors to the errors shown in Table 22 would normally be the squaring operation performed by the analog computer. In this case the squaring was reasonably accurate as can be seen by comparison of the ω and ω^2 values in Table 22. Instability in the torque output (FL in Table 22) caused a shifting of the scale factor which affected the results. It has not yet been determined whether the instability is inherent in the load cells or mechanical friction in the tilt table. The latter appears more probable. Another major factor was the low voltage value used for FL in the computer, which is a result of an insufficient number of operational amplifiers in the computer. Increasing this value would probably result in improved accuracy. Other minor errors are contributed by deviation of the object support surface from a plane perpendicular to the axis of rotation, tachometer output variation, and mechanical alignment errors in the tilt table system.

From the experience obtained thus far it is concluded that the basic system concept is sound, and is capable of producing higher accuracies as refinements are made.

2.4 PRINCIPAL AXES

2.4.1 Math Basis: To specify the dynamical properties of a body in rotational motion about any point O, six inertia coefficients are necessary. These coefficients are the three moments of inertia and the three products of inertia. To define these quantities, the classical three-dimensional rotor as shown in Figure 55 will be used. The quantities needed to describe the i^{th} particle are:

mass of i^{th} particle	m_i
unit vectors	$\bar{i}, \bar{j}, \bar{k}$
position vectors	$\bar{r} = x\bar{i} + y\bar{j} + z\bar{k}$
angular velocity	$\bar{\omega} = \omega_x\bar{i} + \omega_y\bar{j} + \omega_z\bar{k}$

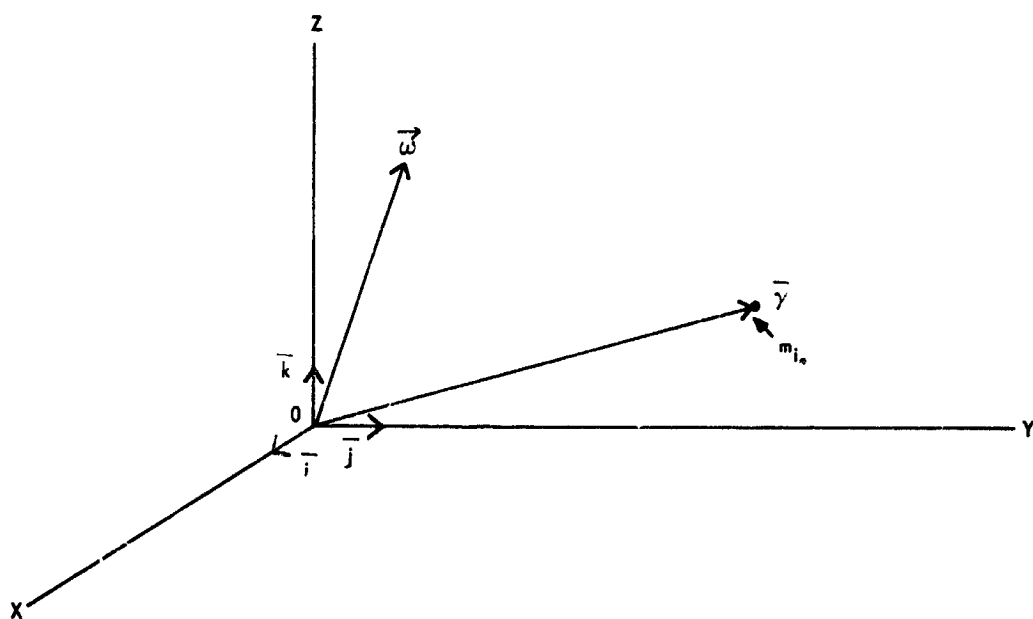


FIGURE 55 CLASSICAL THREE-DIMENSIONAL ROTOR

Table 22 Product of Inertia Machine Test Result Summary

Test No.	Specimen No.	Rate Table Speed o/sec	Analog Computer Measurements				Product of Inertia in-lb.-sec ²	Calculated Product of Inertia in-lb.-sec ²	Percent Error
			Volts	Volts	FL Volts	Volts			
1	3	160	3.93	1.60	0.322	2.11	0.103	0.104	-0.962
2	3	200	4.93	2.48	0.500	2.05	0.100	0.104	-3.84
3	3	240	5.38	3.63	0.740	2.04	0.100	0.104	-3.84
4	3	280	6.80	4.91	1.01	2.12	0.104	0.104	0.00
5	4	160	3.91	1.62	0.249	1.66	0.0814	0.0737	+10.4
6	4	200	4.90	2.48	0.390	1.58	0.0774	0.0737	+5.03
7	4	240	5.86	3.60	0.544	1.56	0.0765	0.0737	+3.80
8	4	280	6.80	4.91	0.753	1.59	0.0779	0.0737	+5.70
9	5	160	3.91	1.61	0.358	2.29	0.112	0.114	-1.75
10	5	200	4.90	2.49	0.565	2.26	0.111	0.114	-2.63
11	5	240	5.88	3.60	0.815	2.24	0.110	0.114	-3.51
12	5	280	6.80	4.91	1.22	2.32	0.114	0.114	0.00
Mean Error									3.455

Note: Each Test is a Average of Four Runs.

linear velocity	$\bar{v} = \bar{\omega} \times \bar{r}$
linear momentum	$\bar{p} = m_i \bar{v} = m_i \bar{\omega} \times \bar{r}$
angular momentum	$\bar{P} = \bar{r} \times \bar{p} = m_i \bar{r} \times [\bar{\omega} \times \bar{r}]$

The components of the angular momentum of the i^{th} particle are

$$P_x = m_i (y_i^2 + z_i^2) \omega_x - m_i (xy_i) \omega_y - m_i (xz_i) \omega_z \quad (60)$$

$$P_y = -m_i (xy_i) \omega_x + m_i (x_i^2 + z_i^2) \omega_y - m_i (yz_i) \omega_z \quad (61)$$

$$P_z = -m_i (xz_i) \omega_x - m_i (yz_i) \omega_y + m_i (x_i^2 + y_i^2) \omega_z \quad (62)$$

where the identity $\bar{r} \times (\bar{\omega} \times \bar{r}) = (\bar{r} \cdot \bar{r}) \bar{\omega} - (\bar{r} \cdot \bar{\omega}) \bar{r}$ is used. If all the particles of the object are considered, the total momentum becomes

$$P = \sum_{i=1}^n P_i = P_x \bar{i} + P_y \bar{j} + P_z \bar{k}, \quad (63)$$

and the components become

$$P_x = I_{xx} \omega_x - I_{xy} \omega_y - I_{xz} \omega_z \quad (64)$$

$$P_y = -I_{xy} \omega_x + I_{yy} \omega_y - I_{yz} \omega_z \quad (65)$$

$$P_z = -I_{xz} \omega_x - I_{yz} \omega_y + I_{zz} \omega_z \quad (66)$$

The quantities

$$I_{xx} = \sum_{i=1}^n m_i (y_i^2 + z_i^2) \quad (67)$$

$$I_{yy} = \sum_{i=1}^n m_i (x_i^2 + z_i^2) \quad (68)$$

$$I_{zz} = \sum_{i=1}^n m_i (x_i^2 + y_i^2) \quad (69)$$

are the moments of inertia, and

$$I_{xy} = \sum_{i=1}^n m_i x_i y_i \quad (70)$$

$$I_{yz} = \sum_{i=1}^n m_i y_i z_i \quad (71)$$

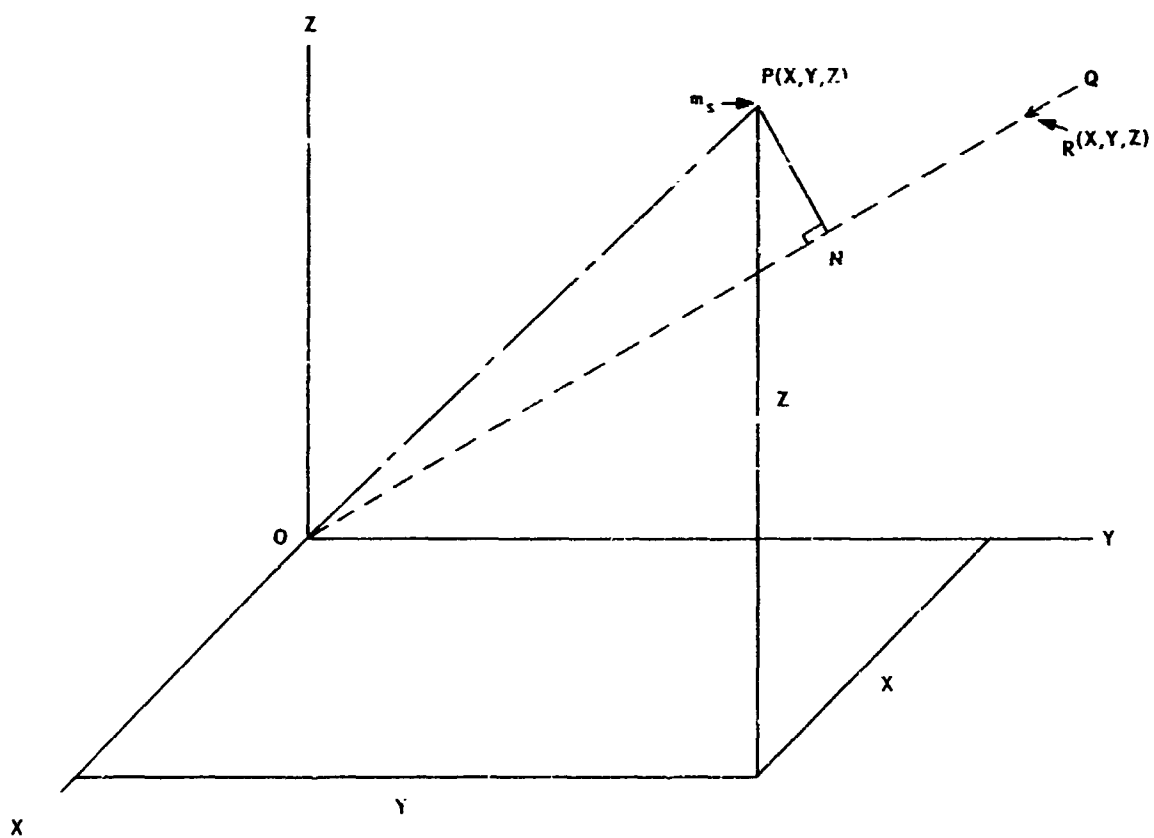


FIGURE 56 ARBITRARILY SHAPED OBJECT

$$I_{21} = \sum_{i=1}^n m_i z_i x_i \quad (72)$$

are the products of inertia with respect to the set of axes O_{xyz} . If the total mass M and center of gravity C of the body are known, the dynamical information is complete.

Knowing the six inertia coefficients I_{xx} , I_{yy} , I_{zz} and I_{xy} , I_{yz} , I_{zx} for any axes O_{xyz} and knowing the mass M and the position of G one can determine the orientation of the principal axes O'_{xyz} for any other point O' . Figure 56 shows a diagram of an arbitrarily shaped object where R is the position of a particle of mass m_s with respect to the axes O_{xyz} . The body is composed of n particles such that

$$M = \sum_{s=1}^n m_s \quad (73)$$

The position vector of OP is:

$$\vec{p} = x\vec{i} + y\vec{j} + z\vec{k} \quad (74)$$

The direction of OQ is given by

$$\vec{q} = \ell\vec{i} + m\vec{j} + n\vec{k} \quad (75)$$

The moments and products of inertia with respect to O_{xyz} are defined in Equations 67 through 72. By definition, the moment of inertia about OQ , a rotated axis, is

$$I_{OQ} = \sum m_s (PN)^2 \quad (76)$$

$$I_{OQ} = \sum m_s (OP^2 - ON^2) \quad (77)$$

$$I_{OQ} = \sum m_s [(x^2 + y^2 + z^2) - (\ell x + my + nz)^2] \quad (78)$$

$$I_{OQ} = I_{xx}\ell^2 + I_{yy}m^2 + I_{zz}n^2 - 2(I_{xy}\ell m + I_{yz}m n + I_{zx}n\ell) \quad (79)$$

Equation 79 can be rewritten as

$$I = \frac{[I_{xx}x^2 + I_{yy}y^2 + I_{zz}z^2 - 2(I_{xy}xy + I_{yz}yz + I_{zx}zx)]}{(x^2 + y^2 + z^2)} \quad (80)$$

where coordinates (x, y, z) now refer to any arbitrary point R lying along OQ and are, therefore, independent variables. If OQ is directed along a

principal axis, the value of I remains constant along that axis; therefore,

$$\frac{\partial I}{\partial x} = 0, \frac{\partial I}{\partial y} = 0, \frac{\partial I}{\partial z} = 0 \quad (81)$$

and

$$\frac{\partial I}{\partial x} = \frac{2(I_{xx}x - I_{xy}y - I_{xz}z)}{(x^2 + y^2 + z^2)} - \frac{2Ix}{(x^2 + y^2 + z^2)} \quad (82)$$

$$\frac{\partial I}{\partial y} = \frac{2(I_{yy}y - I_{xy}x - I_{yz}z)}{(x^2 + y^2 + z^2)} - \frac{2Iy}{(x^2 + y^2 + z^2)} \quad (83)$$

$$\frac{\partial I}{\partial z} = \frac{2(I_{zz}z - I_{yz}y - I_{zx}x)}{(x^2 + y^2 + z^2)} - \frac{2Iz}{(x^2 + y^2 + z^2)} \quad (84)$$

Now Equation 81 becomes

$$(I_{xx} - I)x - I_{xy}y - I_{xz}z = 0 \quad (85)$$

$$-I_{xy}x + (I_{yy} - I)y - I_{yz}z = 0 \quad (86)$$

$$-I_{xz}x - I_{yz}y + (I_{zz} - I)z = 0 \quad (87)$$

where x, y, z define the positions of the principal axes. To obtain x, y, z from equation 85 through 87, the following matrix must be solved.

$$\begin{vmatrix} (I_{xx} - I) & -I_{xy} & -I_{xz} \\ -I_{xy} & (I_{yy} - I) & -I_{yz} \\ -I_{xz} & -I_{yz} & (I_{zz} - I) \end{vmatrix} = 0. \quad (88)$$

Equation 88 leads to the cubic equation

$$\begin{aligned} I^3 - (I_{xx} + I_{yy} + I_{zz})I^2 + (I_{xx}I_{yy} + I_{xx}I_{zz} + I_{yy}I_{zz} - I_{xy}^2 - I_{yz}^2 - I_{xz}^2)I - (I_{xx}I_{yz} + I_{yy}I_{xz} + I_{zz}I_{xy} - 3I_{xy}I_{yz}I_{xz}) &= 0. \end{aligned} \quad (89)$$

The three roots of I are the principal moments of inertia. Equations 85 through 87 can now be solved using these principal inertias to determine the values of x, y, z . The values of x, y, z will in turn determine the direction of the principal axes.

As an example of the method just described, a rectangular solid as shown in Figure 57 will be used. The principal axes will be found with respect to O. The six coefficients of inertia are.

$$I_{xx} = 100, \quad I_{yy} = 136, \quad I_{zz} = 164$$

$$I_{xy} = 60, \quad I_{yz} = 36, \quad I_{zx} = 45$$

Equation 89 becomes

$$I^3 - 400I^2 + 45,383I - 1,040,600 = 0 \quad (90)$$

with roots

$$A = 30.50613, \quad B = 180.24604, \quad C = 189.24783.$$

Now Equations 85 and 86 yields

x	y	z
1	0.7531	0.5402
1	-1.1180	-0.2926
1	2.1720	-4.8793

where A, B and C are used in turn. The direction cosines relative to O_{xyz} are

l	m	n
0.7531	0.5524	0.3962
0.6544	-0.7316	-0.1915
0.1840	0.3997	-0.8980

which are derived from

$$l = \frac{x}{x^2 + y^2 + z^2} \quad (91)$$

$$m = \frac{y}{x^2 + y^2 + z^2} \quad (92)$$

$$n = \frac{z}{x^2 + y^2 + z^2} \quad (93)$$

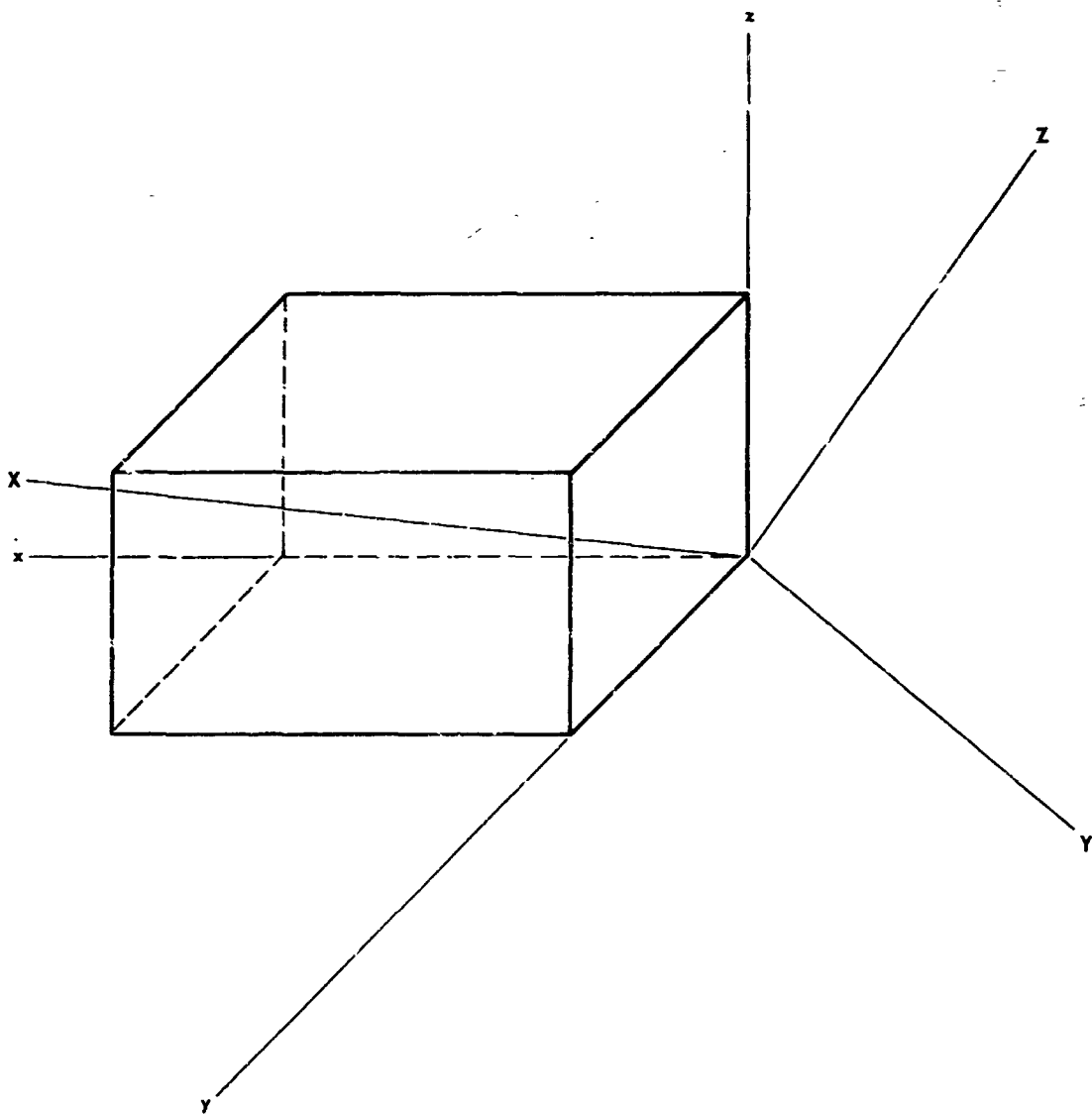


FIGURE 57 RECTANGULAR SOLID

A computer program for determining the principal axes is available and is shown in Figure 58. To use this program, the moments and products of inertia about the center of gravity must be known. The reference axis is chosen about the center of gravity because the moments and products of inertia are determined about the point in all the laboratory tests. A brief explanation of the computer program in Figure 58 will be given to show its relation to the previous theory. (All step references are in relation to Figure 58) Steps 1 through 13 tell what the program is and what variables are needed for the solution, that is, I_{xx} , I_{yy} , I_{zz} , I_{xy} , I_{xz} , I_{yz} . Steps 14 through 20 solve the coefficients of Equation 89, and then this equation is solved in steps 21 through 44. To illustrate these various steps; the cubic equation in step 21 is

$$y^3 + Py^2 + Qy + R = 0, \quad (94)$$

where

$$y = x - P/3 \quad (95)$$

$$a = 1/3 (3Q - P^2) \quad (96)$$

$$b = 1/27 (2P^3 - 9PQ + 27R). \quad (97)$$

Since the products will be less than the moments of inertia where the reference axis is taken through the center of gravity

$$\frac{b^2}{4} + \frac{a^3}{27} < 0. \quad (98)$$

The roots of Equation 94 are

$$x_k = 2 - \frac{a}{3} \cos \left(\frac{\phi}{3} + 120^\circ k \right) \quad k = 0, 1, 2 \quad (99)$$

where

$$\cos \phi = \frac{-b^2/4}{-a^3/27} \quad (100)$$

The minus sign will be used since b is positive for the problems considered. Equation 96 and 97 are solved in steps 22 and 23. Equation 100 is solved in steps 24 and 25. Steps 24 through 37 change the angle from degrees to radians after a manual input of the arc-cosine of ϕ in radians is performed. The next step is to solve the three angles in Equation 99. The three roots of Equation 94 are solved in steps 38 through 41 and are given in steps 42, 43 and 44. These roots of Equation 99 are now used in Equation 85 through 87 to solve

```

1 C Fx DIRECTION COSINES
2 C CALCULATE MOMENTS OF INERTIA ABOUT PRINCIPAL AXIS AND SOLVE
3 C READ MOMENTS (AND PRODUCTS) OF INERTIA ABOUT REF. AXIS (THROUGH C.G.)
4 100 FORMAT(14.8)
5 102 FORMAT(28HLOAD IXX,IYY,IZZ,IXY,IXZ,IYZ,1X,20HFORMAT F14.8 ON 6 CD)
6 504 PRINT 102
7 READ 100,A1XX
8 READ 100,A1YY
9 READ 100,A1ZZ
10 READ 100,A1XY
11 READ 100,A1XZ
12 READ 100,A1YZ
13 DIMENSION RT(3),X(3),Y(3),Z(3)
14 C CALCULATE COEFFICIENT (P) OF Y**2 TERM MAKE NEGATIVE
15 P=-(A1XX+A1YY+A1ZZ)
16 C CALCULATE COEFFICIENT (Q) OF Y TERM
17 Q=A1XX*A1YY+A1XX*A1ZZ+A1YY*A1ZZ-A1XY**2-A1XZ**2-A1YZ**2
18 C CALCULATE CONSTANT TERM (R)
19 R=-(A1XX*A1YY+A1ZZ)+2.*A1XY*A1XZ+A1YZ**2+A1XX*A1YZ**2
20 R=R+A1ZZ*A1XY**2
21 C SOLVE CUBIC EQ. FORM  $X^3+P*X^2+Q*X+R=0$ 
22 A=(3.*Q-P**2)/3.
23 B=(2.*P**3-Q*P*9.+27.*R)/27.
24 CONST=(-1.*A**3/27.)
25 BETA=(-B/2.)/(SQRTF(CONST))
26 200 FORMAT(9HCGS BETA=,2X,F14.8)
27 PRINT 200,BETA
28 201 FORMAT(39HTYPE BETA IN DEGREES AND MINUTES XXX,XX)
29 202 FORMAT(F3.0,F2.0)
30 PRINT 201
31 ACCEPT 202,BETA,BETA1
32 BETA1=BETA/60.
33 BETA=BETA+BETA1
34 BETA=(BETA*3.14159)/180.
35 ANGL1=BETA/3.
36 ANGL2=(BETA/3.+2.0944)
37 ANGL3=(BETA/3.+4.1888)
38 CONS=-1.*(A/3.)
39 XONE=(2.*SQRTF(CONS))*COSF(ANGL1)
40 XTWO=(2.*SQRTF(CONS))*COSF(ANGL2)
41 XTHRE=(2.*SQRTF(CONS))*COSF(ANGL3)
42 RT(1)=XONE-(P/3.)
43 RT(2)=XTWO-(P/3.)
44 RT(3)=XTHRE-(P/3.)
45 539 DO 506 I=1,3
46 CONST=A1YZ*(A1XX-RT(I))+A1XY*A1XZ
47 DONST=CONST/A.YZ*(A1YY-RT(I))+A1XY*A1YZ)
48 CONST=CONST/(A1XY*(A1ZZ-RT(I))+A1XZ*A1YZ)
49 X(I)=SQRTF(1./(1.+DONST**2+CONST**2))
50 Y(I)=DONST*X(I)
51 Z(I)=CONST*X(I)
52 OUTPUT
53 703 FORMAT(4X,6H1B-IN2,8X,9HKG-M-SEC2,9X,1HX,13X,1HY,14X,1HZ)
54 103 FORMAT(6X,17HMOment OF INERTIA,18X,17HDIrection COSINES)
55 GO TO (508,509,509),I
56 508 PRINT 103
57 PRINT 703
58 104 FORMAT(14.8,4F15.8)
59 509 CONST=RT(1)*.29841E-04
60 PRINT 104 RT(1),CONST,X(1),Y(1),Z(1)
61 506 CONTINUE
62 GO TO 504
63 END

```

FIGURE 58 COMPUTER PROGRAM FOR DETERMINING PRINCIPAL AXIS

for x, y and z. This is accomplished in steps 45 through 48. In solving for the direction cosines, the variable x is set equal to one since only the direction of the axis is needed; therefore, steps 49, 50 and 51 are

$$l = \frac{1}{1 + y^2 + z^2} \quad (101)$$

$$m = \frac{y}{1 + y^2 + z^2} \quad (102)$$

$$n = \frac{z}{1 + y^2 + z^2} \quad (103)$$

respectively. The remaining steps, 52 through 63, are the computer steps necessary to give a print-out of the principal moments of inertia and the direction cosines necessary to rotate the reference axes to the principal axes.

In summary the principal axes of an object can be easily obtained if the moment and product of inertia of the object about its center of gravity are known. The Mass Metrology Laboratory has available to it at SPACO, INC. an IBM 1520 computer which is capable of handling the principal axis determination.

2.5 MASS PROPERTIES OF LIQUIDS

2.5.1 Technical Discussion of the Problem

2.5.1.1 Background: In the past, considerable effort has been made in the theoretical and experimental study of liquids. Studies have included, sloshing, pressure, baffles, vibration, acceleration, viscosity, flow, and other studies. A literature search was made to determine the problem and to acquaint this laboratory with prior work in this area. Appendix B lists the materials accumulated by the Mass Metrology Laboratory during the literature search.

2.5.1.2 Requirements

A basic requirement for flight vehicles is to predict their reaction to applied forces, whether internal or external. One factor which greatly affects the action or reaction of a space vehicle is the fuel carried on board. Mass properties of liquids is more of a problem today than in the past because larger quantities of liquid fuel are required for extended flights. At launch more than ninety percent of the vehicle weight is contained in fuel for some

of the present rockets.

Since fuel motion in the vehicle has such an effect on the vehicle's overall stability more details must be known about liquid motion. One important aspect is to learn the effects of the moving liquid on the moment of inertia of the vehicle during oscillatory motions. These oscillatory motions can be caused by gimbaling of the engines about the pitch or yaw axis or by external forces such as wind currents. For oscillations about the yaw-pitch axis the moment of inertia about this same axis must be known to determine the behavior and trajectory of the vehicle. In light of this requirement the Mass Metrology Laboratory at SPACO, INC. has performed experimental studies and theoretical analysis into the problem of determining moments of inertia of a liquid rotating about its yaw-pitch axis.

The basic problem was to determine the moment of inertia of a partially filled cylindrical container about its yaw-pitch axis. A partially filled tank was used instead of a full tank because this closer simulates an actual fuel tank. The equipment used was all government furnished except for a few small items and modifications.

2.5.1.3 Solution: The method of solving this problem, experimentally was to oscillate the partially filled tank at various frequencies, by forcing it with different torsion rods, and using various amounts of water to determine the relationship of the moment of inertia, frequency and aspect ratio (ratio of liquid height to tank diameter.) The experimental data was used to determine the ratio of the moment of inertia of the liquid system versus the moment of inertia of the system if the liquid were solid. This ratio was compared to the aspect ratio to determine the relationship between the two. The experimental results were then compared to theoretical results to determine the validity of the theoretical approach.

2.5.2 Procedure

2.5.2.1 Equipment: The basic items of equipment used in the tests program are the plexiglass tank and stand, torsion rods, radian scale, photo-cell timing equipment and a capacitive transducer. Figure 59 shows a sketch of the equipment and Figure 60 shows the tank set-up in the laboratory. All the above equipment was government furnished except the torsion rods, radian scale, capacitive transducer, and special brackets, which were made at SPACO. The torsion rods were pre-selected and designed to produce certain frequencies of oscillation of the tank. The radian scale was used for obtaining rough measurements of angular displacement and the capacitive transducer was used to obtain precise angular displacement measurements. More information on the capacitive transducer is given in Appendix D. The photo-cell timing device with its associated counters and read out devices were used to

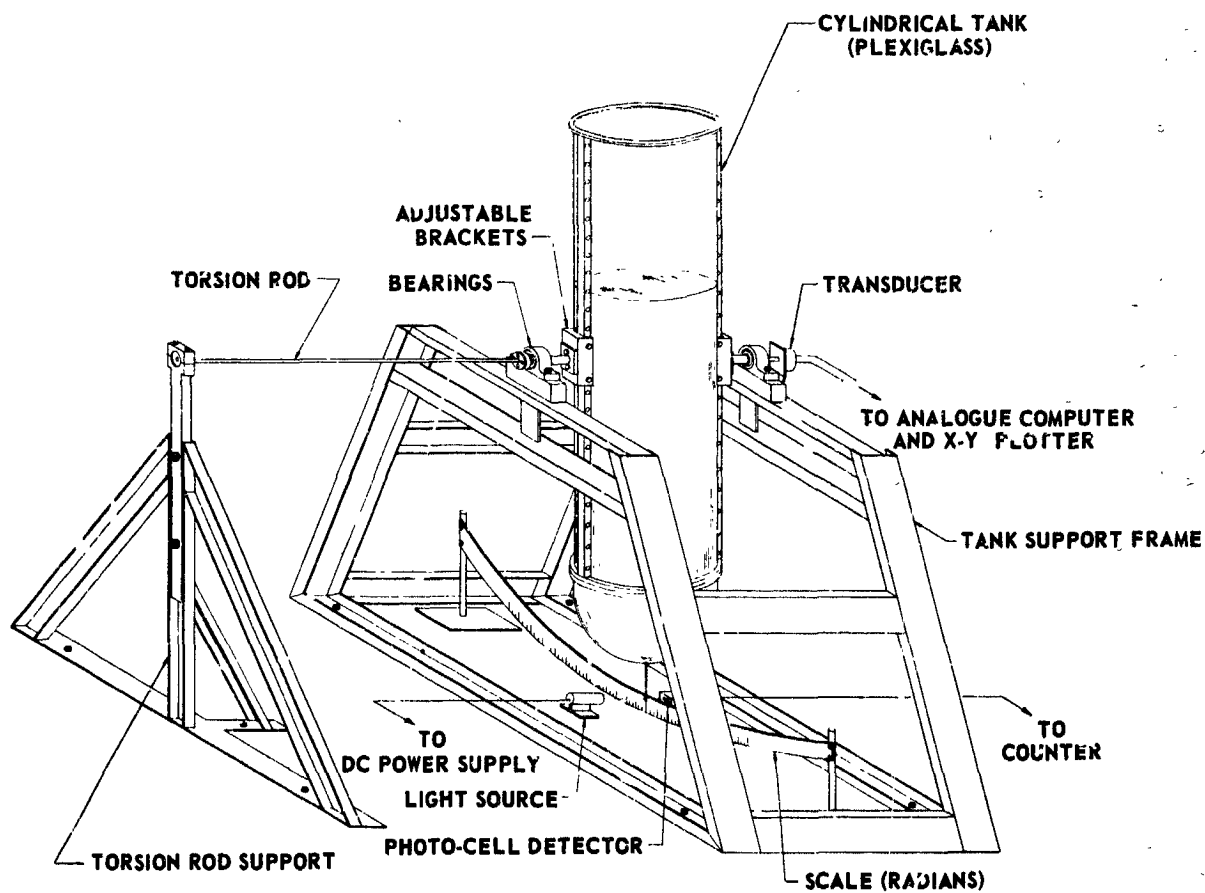


FIGURE 59 MASS PROPERTIES OF LIQUIDS (TEST SYSTEM)

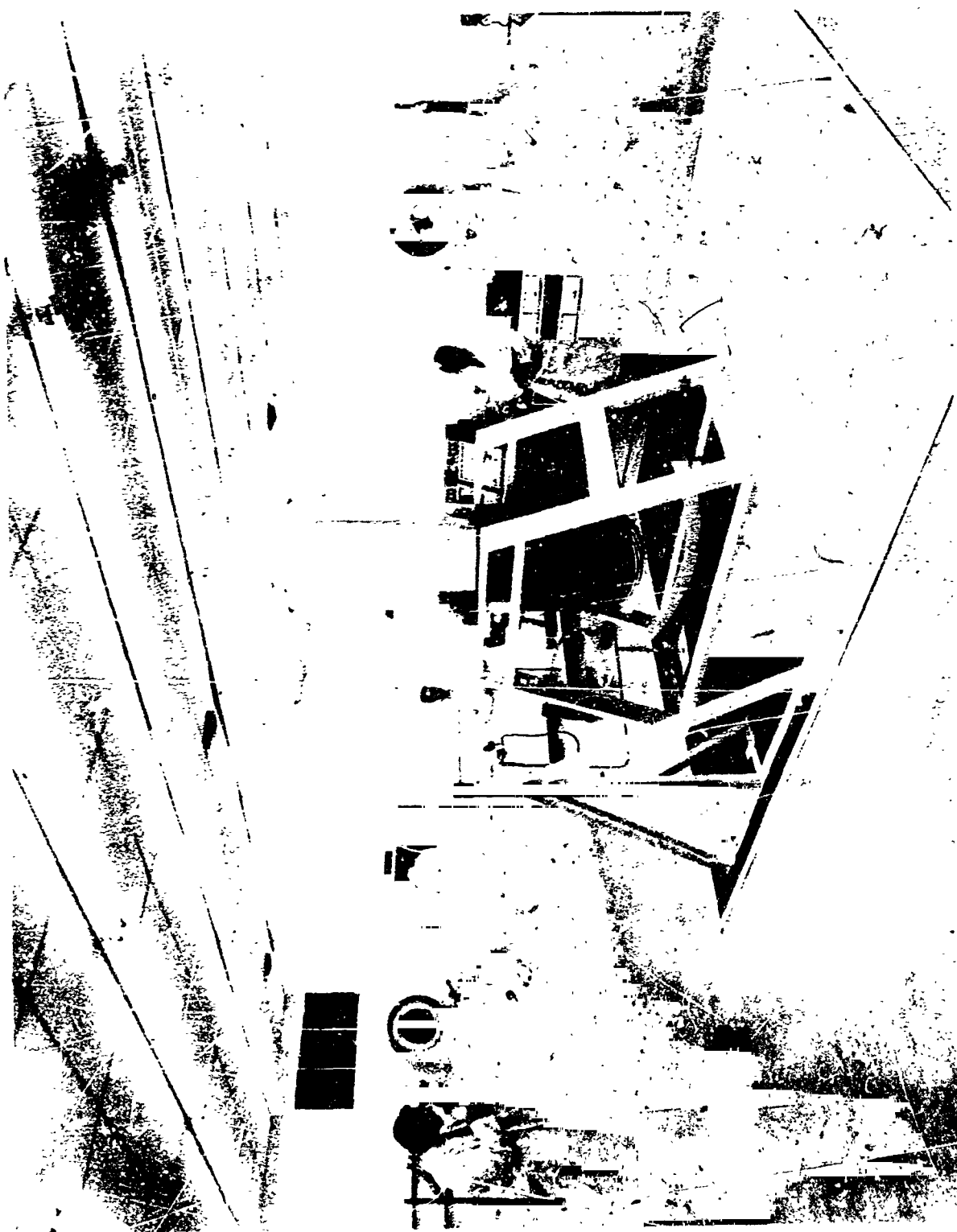


FIGURE 60 OSCILLATING TANK SYSTEM

measure the period of oscillation. Any other minor special equipment was designed and fabricated as needed.

2.5.2.2 Test Program

2.5.2.2.1 Center of Gravity and Moment of Inertia of Empty Tank: The government furnished plexiglass tank and stand were the basic elements in the experiment. The first tests consisted of determining the center of gravity and moment of inertia of the empty tank. The center of gravity was determined by using three different methods; knife edge, two point suspension and Bytrex center of gravity locator. The results of the Bytrex tests appeared to be the most accurate; therefore, this data was used. The moment of inertia of the empty tank was obtained by suspending the tank on a torsion rod from an over head "I" beam and measuring its period of oscillation to determine the moment of inertia.

2.5.2.2.2 Rod Calibration: The next testing program was the calibration of all the torsion rods to be used with the tank. The smaller rods were calibrated as described previously in paragraph 2.2 Moment of Inertia. The stiffer rods were calibrated using a static method. A sketch of the test equipment is shown in Figure 61. K was determined using,

$$T = K \theta \text{ or } K = \frac{T}{\theta} \quad (104)$$

where $t = W \times r$ is the torque produced by a weight acting at a distance r and θ is the angular displacement.

The apparatus for determining spring constants of torsion rods statically was used to calibrate the three largest rods 107, 122, and 123. The values obtained appear to be relatively inaccurate because of high friction in the calibration apparatus. To check these values, the constants were calculated using an average value of modulus of rigidity obtained from earlier tests. Differences of as much as 5% were found. Table 23 shows the measured values obtained for all of the torsion rods. For all but rods 107, 122, and 123, the constants were obtained from a suspended pendulum tests using a moment of inertia standard. The differences in the deviation from the mean value points up the relative errors in the dynamic and static methods. Table 24 shows the calculated values of rod constants, using a modulus of rigidity of 12.022×10^6 . Table 25 lists the differences between the calculated and measured values of rod constants.

The conclusions from these tests are not that the static method is in error but that the equipment is not adequate.

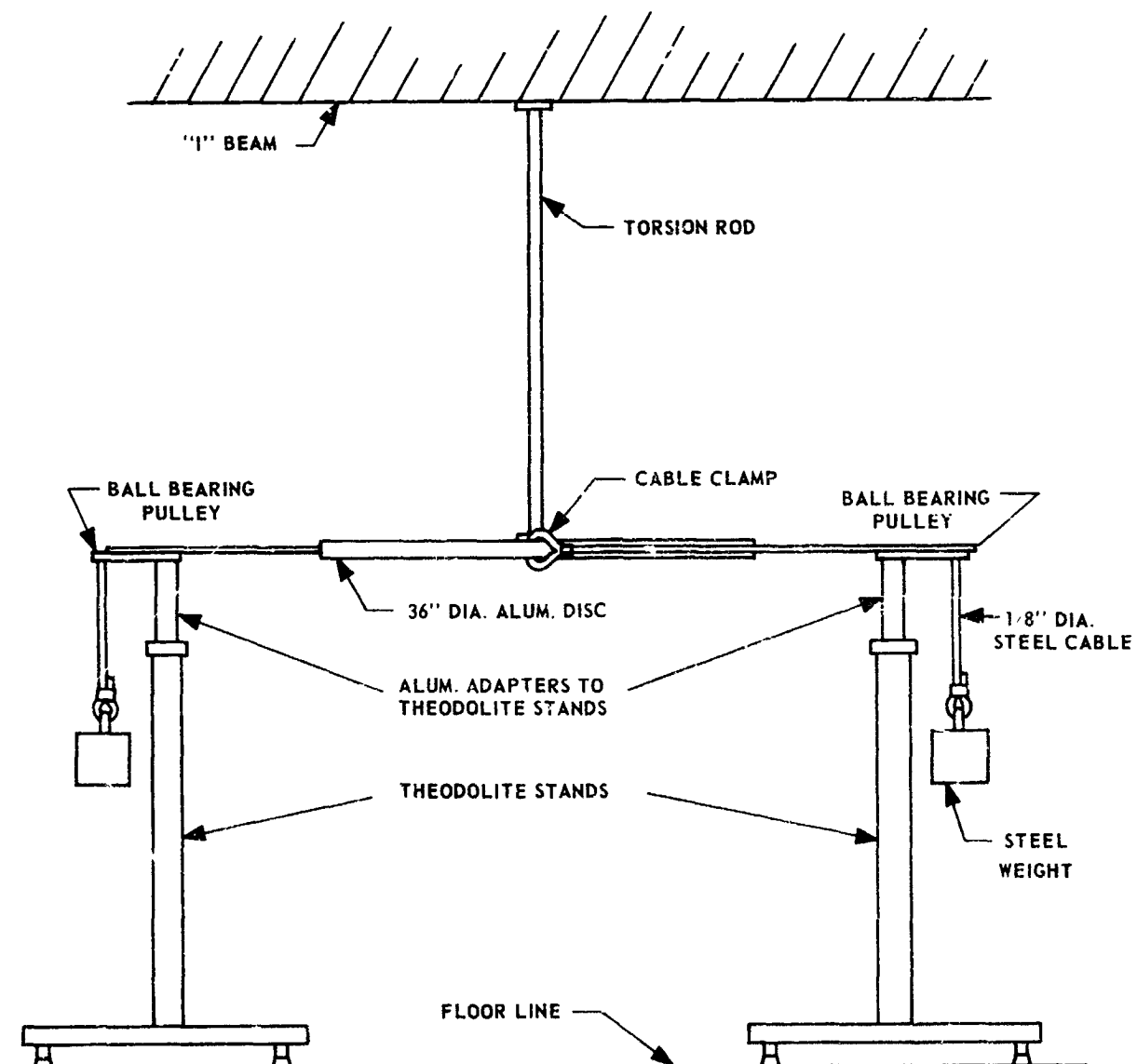


FIGURE 61 SET-UP FOR STATIC TESTING OF TORSION RODS

Table 23 Experimental Values of Torsion Rod Constants

Rod Number	Length In Inches	Diameter In Inches	"K" Value	Maximum Percentage Deviation from the Mean	Maximum θ Radians for 30,000 psi Shear Stress
100	48	0.500	1,540.68 $\frac{\text{in.} \cdot \text{in.}^3}{\text{radian}}$	0.006	0.48
102	36	0.500	2,058.52	0.029	0.36
103	24	0.500	3,077.54	0.061	0.24
104	48	0.375	482.11	0.036	0.65
105	36	0.375	645.05	0.016	0.50
106	24	0.375	975.68	0.010	0.32
107	24	0.625	7,715.02 (1)	0.81	0.19
108	36	0.625	5,008.31	0.072	0.28
109	48	0.625	3,752.66	0.043	0.38
122	24	0.750	16,262.80 (1)	1.34	0.16
123	24	1.000	51,753.63 (1)	1.09	0.12

(1) Obtained from static measurement setup

Table 24 Theoretical Values of Torsion Rod Constants

Rod Number	J	G	Theoretical K Using Avg G
101	0.006136	12.052×10^6	1,536.81
102	0.006136	12.077×10^6	2,049.08
103	0.006136	12.037×10^6	3,073.62
104	0.001941	11.922×10^6	486.13
105	0.001941	11.964×10^6	648.18
106	0.001941	12.064×10^6	972.27
107	0.014979	-	7,503.23
108	0.014979	12.037×10^6	5,022.15
109	0.014979	12.025×10^6	3,751.61
122	0.031062	-	15,559.47
123	0.098175	-	49,177.49
Avg.		12.022×10^6	
$J = \frac{\pi d^4}{32}$ $G = \frac{KL}{J}$ $K = \frac{GJ}{L}$			

Table 25 Comparison of Theoretical and Experimental Values
of Torsion Rod Constants

Rod #	Theoretical K	Experimental K	Difference	% Difference
101	1536.81	1540.68	3.87	0.251
102	2049.08	2058.52	13.31	0.649
103	3073.62	3077.54	3.92	0.127
104	486.13	482.11	4.02	0.826
105	648.18	645.05	3.13	0.482
106	972.27	975.68	3.41	0.350
107	7503.23	7715.02	211.79	2.822
108	5002.15	5008.31	6.16	0.123
109	3751.61	3752.66	1.05	0.027
122	15559.47	16262.80	703.33	4.520
123	49177.49	51753.63	2576.14	5.238

2.5.2.2.3 Moment of Inertia of Liquid System

2.5.2.2.3.1 Objective: The final test program was the determining of the moment of inertia of the tank system for various frequencies and water levels. The test objective was to conduct extensive experimentation to determine the percentage of liquid which acts as a solid in measuring the moment of inertia of a rotating liquid system.

2.5.2.2.3.2 Equipment and Equipment Function: A government furnished cylindrical plexiglass tank with a hemispherical bottom along with its supporting stand was the basic item of equipment. The tank was supported in an upright position by two (SKF SYH 100x) self-aligning ball bearings that enable the tank to rotate about its yaw-pitch axis. The tank's supporting shafts were designed so that various torsion rods could be mounted to the tank for producing forced oscillations. A capacitor transducer was mounted on one side of the tank to provide angular displacement measurements as the tank oscillates. The capacitor transducer was fed to an X-Y Plotter (Moseley 136 A) so that a complete time-displacement history would be available. A photocell-light timing device was mounted to the tank stand and provided the period of oscillation. The timing device was triggered by a wand extended from the tank. This output was fed to a Hewlett-Packard 524 D counter which provided a visual display of the period time. A Hewlett-Packard 560 A printer was used to produce a permanent record.

2.5.2.3 Test Procedure: The test apparatus was utilized as follows. The plexiglass tank and stand were firmly mounted on the isopad. The tank was suspended so that its center of gravity was on the axis of rotation. This was accomplished by using two adjustable brackets on each side of the tank. After the tank had been placed with its center of gravity on the axis of rotation, the capacitor transducer and photocell device were zeroed. The output of the photocell device was connected to the Hewlett-Packard 524 D counter which was adjusted for measuring each alternating period, then this signal went into a H-P 560 A for automatic readout. The output of the capacitive transducer was fed to the Mosely 136 A, X-Y Plotter. The torsion rod to be used in the specific test was mounted in its support stand and was accurately aligned, by using a theodolite, so that the tank was zeroed in its static position. The specific amount of water was weighed on the Shadowgraph and poured into the tank. All electrical equipment was activated and allowed to warm up. The tank was then manually oscillated so that its displacement slowly increased while maintaining a relatively steady water surface. When the tank reached a displacement of 0.18 radians the forcing motion was ceased and the tank began to decrease in amplitude. When the maximum swing decayed to 0.16 radians both the timer and X-Y Plotter were started and the period and displacement measurements were automatically recorded until the tank stopped oscillating.

The data sheet contained the following information:

Date	Time	Temperature	Humidity	Personnel
Rod Number		Water Level	X-Y Plot of Displacement	
Period Readout				

2.5.2.4 Results Analysis: The data obtained from a given test was used to determine the moment of inertia of the system at its particular frequency of oscillation. This was accomplished by plotting the period per cycle versus the displacement and determining the period as the amplitude approaches zero as shown using representative data in Figure 62. The displacement was plotted every 0.005 radians, from 0.16 to 0.005 radians. The period was plotted at the corresponding displacement to the nearest 0.0001 second. This method of determining moment of inertias is thoroughly explained in the moment of inertia section of this report.

The period at zero amplitude T_0 will be used in the formula

$$I = (WL + K) T^2 / 4\pi^2, \quad (105)$$

along with the weight of the system W , the distance from the pivot to the center of gravity of the system L , and the torsion rod constant K , in determining the moment of inertia of the system. Equation 105 is derived from the equation of motion of the tank system

$$I \ddot{\theta} + WL \sin \theta + K\theta - M_f = 0 \quad (106)$$

The term M_f is a frictional moment which includes all frictional losses. In arriving at Equation 93, M_f is assumed to be zero but it can be compensated for by using

$$I_{\text{Total System}} - I_{\text{Empty System}} = I_{\text{Effective Water (for a given frequency)}} \quad (107)$$

This equation eliminates all losses produced by air drag and bearing friction at a given frequency since these effects are subtracted out. Therefore, $I_{\text{Effective Water}}$ gives the true moment of inertia of the water. Another method of eliminating all losses in order to obtain the true effect of slosh, is by replacing the liquid with a solid that has the same density of the water. This possibility was investigated and a wax was found that would be very suitable. The wax had a specific gravity of 0.998 and had good characteristics which would allow it to be formed in the tank to simulate the water. This program was not pursued because of the cost involved, the time

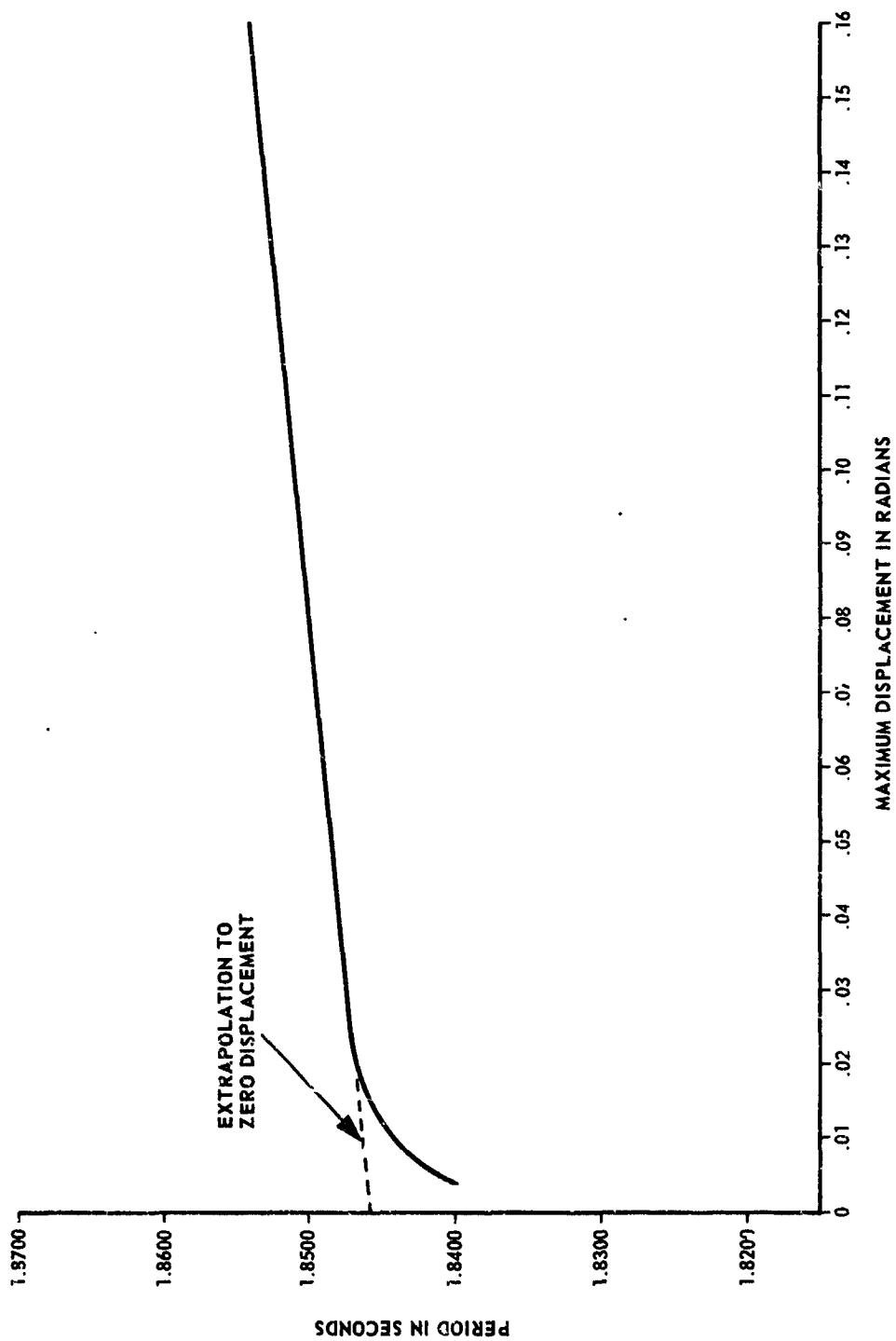


FIGURE 62 PLOT OF PERIOD VS MAXIMUM DISPLACEMENT

required and present need for this type accuracy.

The accuracy of the results can be determined by analyzing the effects of each variable on the total results. The total differential of the moment of inertia

$$I, \text{ where } I = f(W, L, K, T), \text{ is} \quad (108)$$

$$dI = \frac{1}{4\pi^2} (T^2 L dW + T^2 W dL + T^2 dK + (WL + K) 2T dT) \quad (109)$$

where I of Equation 105 is used. Equation 109 will yield the maximum error in I for a specific experiment if the maximum errors of in W , L , K and T are substituted for dW , dL , dK and dT . The following tolerances,

$$\begin{aligned} dW &= 0.1 \text{ pound} \\ dL &= 0.1 \text{ inch} \\ dK &= 0.01 \text{ inch-pounds/radians} \\ dT &= 0.001 \text{ seconds} \end{aligned}$$

along with typical test results used in Equation 108 yields

$$dI = 2.134 \text{ inch-pounds/radian,}$$

and the total error of the moment of inertia result is approximately 0.2%. This percentage error is a typical value to show the accuracy of the system.

2.5.3 Test Results

2.5.3.1 Experimental: Table 26 shows a complete listing of the results of mass properties of liquids test program. The majority of the items listed in the table are self explanatory but a few that might not be obvious will be explained in more detail.

The water weight is the amount of water in the tank measured to the nearest tenth of a pound. The aspect ratio is the ratio of the water height to the tank diameter. In a cylindrical tank the water height is considered from the tank bottom but with a hemispherical bottom a different reference level must be used. For a complete solution to the problem the water height should be taken from the bottom of the hemispherical segment. This method is very complicated and time consuming; therefore, an alternate method will be used. This method is described in Reference 1. This report states that the use of an equivalent flat bottom, where equal volumes of liquid are used, is justifiable for tanks with non-flat bottoms, except for extremely shallow fluid depths ($h/d < .25$). The conversion from the hemispherical bottom to an equivalent flat bottom cylindrical tank is shown in Figure 63

along with other tank dimensions. The various aspect ratios are taken with respect to this bottom.

The system weight, W is the weight of the empty tank plus the amount of water in it.

The system center of gravity from the pivot point, L and the moment of inertia of an equivalent solid, I_s were derived from theoretical calculations. The center of gravity of the system was determined by using the standard mass distribution formula. The moment of inertia of an equivalent solid was determined by using

$$I = I_{\text{hemi}} + M_{\text{hemi}} L_{\text{hemi}}^2 + I_{\text{cyl}} + M_{\text{cyl}} L_{\text{cyl}}^2 \quad (110)$$

where

$$I_{\text{hemi}} = 0.26 Mk^2 \quad (111)$$

and

$$I_{\text{cyl}} = M \left(\frac{d^2}{16} + \frac{h^2}{12} \right) \quad (112)$$

The quantities L_{hemi} and L_{cyl} are the distance from the center of gravity of each object to the pivot point. For the case of the empty tank the moment of inertia was determined experimentally. This was accomplished in the standard manner by oscillating the tank from the overhead "I" beam on a torsion rod and measuring the period. The moment of inertia of the empty tank was also calculated from tank measurements but due to the rough construction of the tank this method was considered inadequate. For the 100 pound load the hemisphere was not completely filled; therefore, Equation 110 could not be used and

$$I = I_{\text{seg}} + M_{\text{seg}} L_{\text{seg}}^2 \quad (113)$$

where

$$I_{\text{seg}} = \frac{\pi \rho R^5}{60} \left[\frac{9H^5}{R^5} - \frac{10H^3}{R^3} - \frac{15H}{R} + 16 \right] \quad (114)$$

had to be used. Equation 114 had to be derived because it is not included in any handbooks. The term L_{seg} is the distance between the center of gravity of the hemispherical segment and the pivot point.

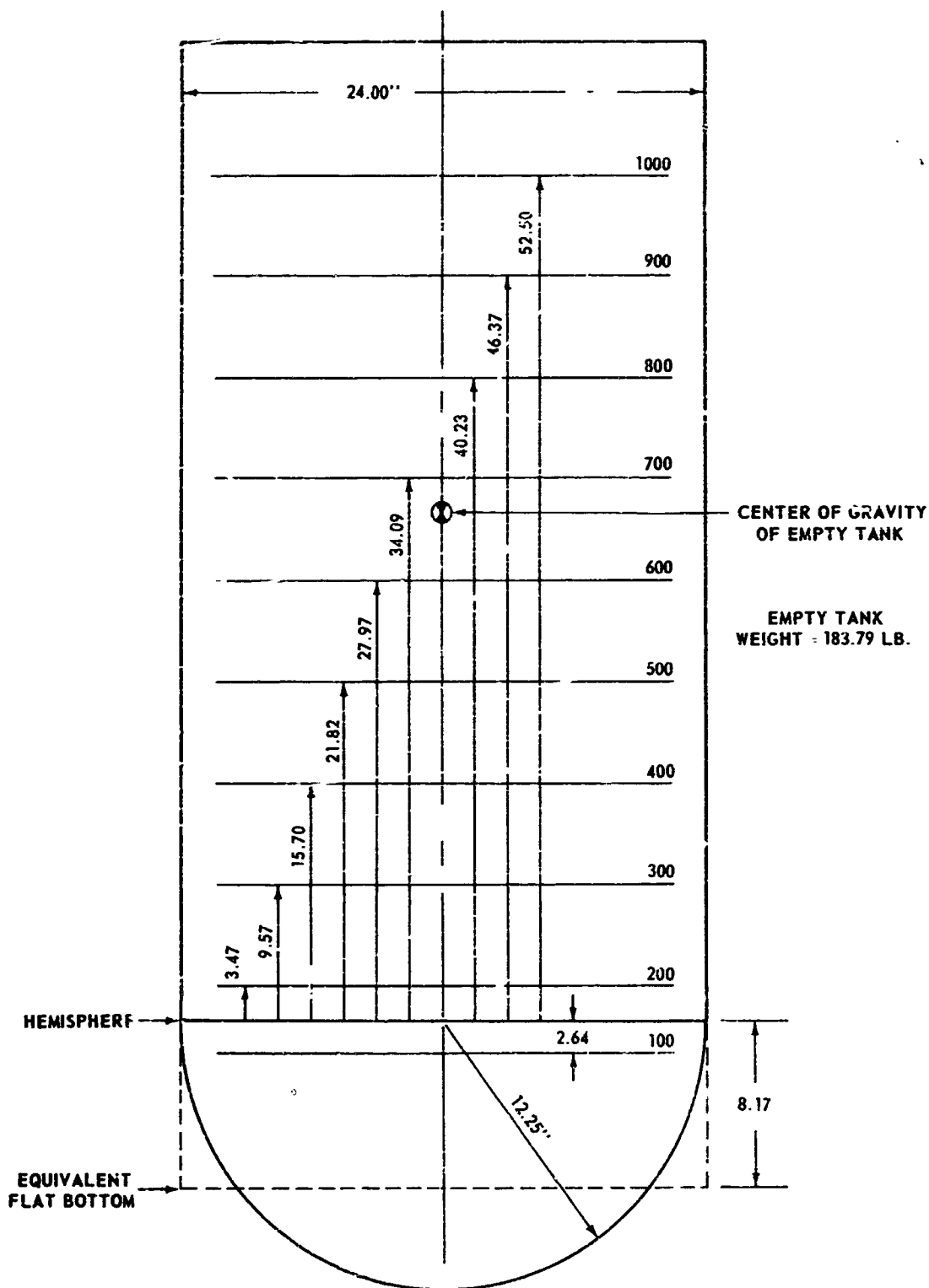


FIGURE 63 CONVERSION FROM A HEMISPHERICAL BOTTOM TANK TO AN EQUIVALENT FLAT BOTTOM CYLINDRICAL TANK

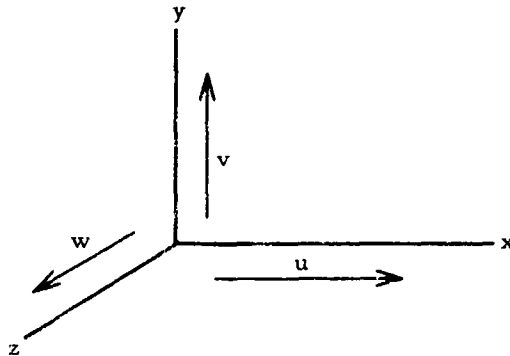
The period T is the experimental period obtained from the oscillating system. It is used in

$$I = (WL + K) \frac{T^2}{4\pi^2} \quad (115)$$

to calculate the moment of inertia, I_F of the system. W and L in Equation 115 have previously been described and K is the rod constant of the particular rod used. The ratio I_F/I_S shows the effect of using liquid instead of a solid in determining moments of inertia.

Figure 64 shows a plot of moment of inertia versus aspect ratio and Figure 65 shows the ratio of I_{liquid} to I_{solid} versus aspect ratio. The results of this test program will be discussed in more detail in the conclusion after the theoretical approach has been discussed.

2.5.3.2 Theoretical: In order to understand the basic foundation of the theoretical approach a brief review of basic hydrodynamics was undertaken. The equations of motion of a liquid can be obtained by using the method of Euler. This method investigates the knowledge of the velocity, the pressure and the density at all points of space occupied by the liquid for all instants. Let u, v, w be the velocity components of x, y, z at time t parallel to the co-ordinate axis as shown below.

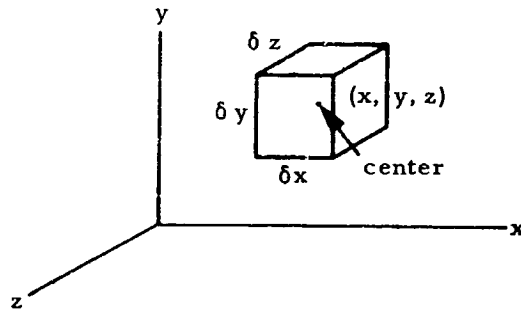


The values u, v, w are finite and continuous functions of x, y, z . The values

$$\frac{\partial u}{\partial x}, \frac{\partial v}{\partial x}, \frac{\partial w}{\partial x}, \frac{\partial u}{\partial y}, \frac{\partial v}{\partial y}, \frac{\partial w}{\partial y}, \frac{\partial u}{\partial z}, \frac{\partial v}{\partial z}, \frac{\partial w}{\partial z}$$

are assumed everywhere to be finite. Let p be the pressure, ρ the density and X, Y, Z the components of the extraneous forces per unit mass at point x, y, z at time t . The equations of motion are derived by examining an

element of liquid bound by δx , δy , δz as shown below.



The rate at which the x-component of the momentum is increasing in the x direction is given by

$$\rho \delta x \delta y \delta z \frac{du}{dt}.$$

The extra-ous forces in the x direction are given by $\rho \delta x \delta y \delta z X$. The pressure on the $\delta y \delta z$ faces are

$$\left(p - \frac{1}{2} \frac{\partial p}{\partial x} \cdot \delta x \right) \delta y \delta z$$

and

$$\left(p + \frac{1}{2} \frac{\partial p}{\partial x} \cdot \delta x \right) \delta y \delta z$$

respectively from the origin outward. Therefore the resultant pressure is their difference

$$- \frac{\partial p}{\partial x} \delta x \delta y \delta z.$$

The equation of motion for the x direction is obtained by summing all the forces, is

$$\rho \delta x \delta y \delta z \frac{du}{dt} = \rho \delta x \delta y \delta z X - \frac{\partial p}{\partial x} \delta x \delta y \delta z.$$

Substitute

$$\frac{du}{dt} = \frac{\partial u}{\partial t} + u \frac{\partial u}{\partial x} + v \frac{\partial u}{\partial y} + w \frac{\partial u}{\partial z} \quad (117)$$

the total differential of $u(x, y, z, t)$ in the above equation, now becomes

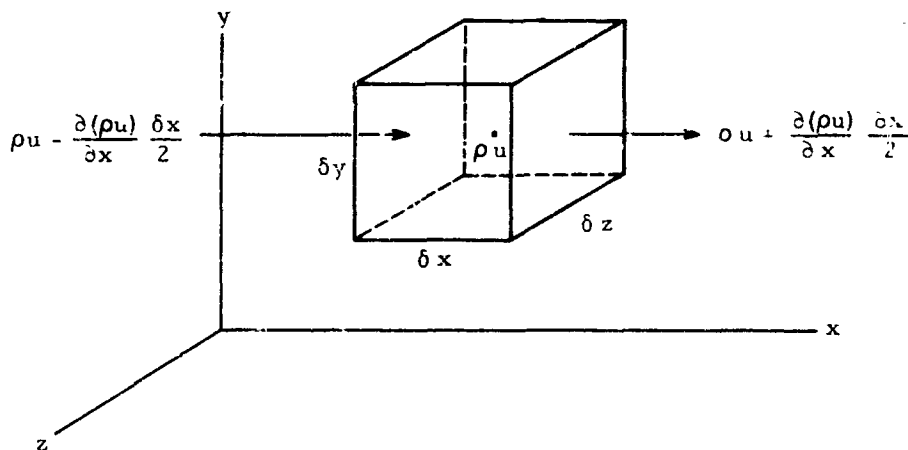
$$\frac{\partial u}{\partial t} + u \frac{\partial u}{\partial x} + v \frac{\partial u}{\partial y} + w \frac{\partial u}{\partial z} = X - \frac{1}{\rho} \frac{\partial p}{\partial x} \quad (118)$$

Likewise for the y and z directions:

$$\frac{\partial v}{\partial t} + u \frac{\partial v}{\partial x} + v \frac{\partial v}{\partial y} + w \frac{\partial v}{\partial z} = Y - \frac{1}{\rho} \frac{\partial p}{\partial y} \quad (119)$$

$$\frac{\partial w}{\partial t} + u \frac{\partial w}{\partial x} + v \frac{\partial w}{\partial y} + w \frac{\partial w}{\partial z} = Z - \frac{1}{\rho} \frac{\partial p}{\partial z} \quad (120)$$

The equations along with the conservation of mass must be satisfied for any liquid system. The conditions that must be satisfied for the conservation of mass can be described by considering an element of liquid as shown.



If the change in velocity with distance is considered, the rate of mass flux across face $\delta y \delta z$ is

$$\left(\rho u - \frac{\partial(\rho u)}{\partial x} \frac{\delta x}{2} \right) \delta y \delta z$$

and

$$(\rho u + \frac{\partial (\rho u)}{\partial x} \frac{\delta x}{2}) \delta y \delta z$$

as shown. The net rate of influx of mass into the element is their difference

$$- \frac{\partial (\rho u)}{\partial x} \delta x \delta y \delta z.$$

Likewise, for the other two faces

$$- \frac{\partial (\rho v)}{\partial y} \delta x \delta y \delta z$$

$$- \frac{\partial (\rho w)}{\partial z} \delta x \delta y \delta z.$$

The sum of these three must equal the total change of mass

$$- \frac{\partial (\rho u)}{\partial x} + \frac{\partial (\rho v)}{\partial y} + \frac{\partial (\rho w)}{\partial z} \delta x \delta y \delta z = \frac{\partial (\rho \delta x \delta y \delta z)}{\partial t} \quad (121)$$

$$\text{or} \quad \frac{\partial (\rho u)}{\partial x} + \frac{\partial (\rho v)}{\partial y} + \frac{\partial (\rho w)}{\partial z} = - \frac{\partial \rho}{\partial t} \quad (122)$$

This is the equation of continuity. For a homogenous incompressible fluid the density is independent of time and space; therefore, the above equation reduces to

$$\frac{\partial u}{\partial x} + \frac{\partial v}{\partial y} + \frac{\partial w}{\partial z} = 0. \quad (123)$$

For an incompressible, non viscous, irrotational, homogenous liquid, i. e. a perfect liquid, a function called the velocity potential can be used. This velocity potential ϕ is analogous to potentials such as that of gravitational attraction and electrostatic, forces, and satisfies the relations

$$u = \frac{-\partial \phi}{\partial x} \quad (124)$$

$$v = \frac{-\partial \phi}{\partial y} \quad (125)$$

$$w = \frac{-\partial \phi}{\partial z} \quad (126)$$

The continuity equation now becomes

$$\frac{\partial^2 \phi}{\partial x^2} + \frac{\partial^2 \phi}{\partial y^2} + \frac{\partial^2 \phi}{\partial z^2} = 0 . \quad (127)$$

This equation is also called the Laplacian and is represented by

$$\nabla^2 \phi = 0 . \quad (128)$$

These equations describing the velocity potential also yield

$$\frac{\partial v}{\partial z} = \frac{\partial w}{\partial y} , \quad (129)$$

$$\frac{\partial w}{\partial x} = \frac{\partial u}{\partial z} , \quad (130)$$

$$\frac{\partial u}{\partial y} = \frac{\partial v}{\partial x} . \quad (131)$$

which can be substituted in the three previous equations of motion to give

$$\frac{\partial^2 \phi}{\partial x \partial t} + u \frac{\partial u}{\partial x} + v \frac{\partial v}{\partial x} + w \frac{\partial w}{\partial x} = X - \frac{1}{\rho} \frac{\partial \rho}{\partial x} \quad (132)$$

$$\frac{\partial^2 \phi}{\partial y \partial t} + u \frac{\partial u}{\partial y} + v \frac{\partial v}{\partial y} + w \frac{\partial w}{\partial y} = Y - \frac{1}{\rho} \frac{\partial \rho}{\partial y} \quad (133)$$

$$\frac{\partial^2 \phi}{\partial z \partial t} + u \frac{\partial u}{\partial z} + v \frac{\partial v}{\partial z} + w \frac{\partial w}{\partial z} = Z - \frac{1}{\rho} \frac{\partial \rho}{\partial z} . \quad (134)$$

In most cases the extraneous forces X, Y, Z have a potential

$$X = - \frac{\partial \Omega}{\partial x} \quad (135)$$

$$Y = - \frac{\partial \Omega}{\partial y} \quad (136)$$

$$Z = - \frac{\partial \Omega}{\partial z} \quad (137)$$

Using this assumption and integrating the previous equations with respect to x , y , and z respectively gives

$$\frac{\partial \phi}{\partial t} + \frac{u^2}{2} + \frac{v^2}{2} + \frac{w^2}{2} = -\Omega - \frac{P}{\rho} + F_1(t) \quad (138)$$

$$\frac{\partial \phi}{\partial t} + \frac{u^2}{2} + \frac{v^2}{2} + \frac{w^2}{2} = -\Omega - \frac{P}{\rho} + F_2(t) \quad (139)$$

$$\frac{\partial \phi}{\partial t} + \frac{u^2}{2} + \frac{v^2}{2} + \frac{w^2}{2} = -\Omega - \frac{P}{\rho} + F_3(t) \quad (140)$$

Since F_1 , F_2 , and F_3 are arbitrary constants of integration, let $F_1 = F_2 = F_3 = F$; therefore, the three equations above reduce to

$$\frac{\partial \phi}{\partial t} + \frac{u^2}{2} + \frac{v^2}{2} + \frac{w^2}{2} = -\Omega - \frac{P}{\rho} + F(t) \quad (141)$$

which is Euler's equation. Euler's equation along with the continuity equation are the two basic equations necessary for solving the hydrodynamic problems of sloshing.

The two basic equations, Equations 127 and 141, will now be applied to a cylindrical tank performing rotational motion. Since the tank is a cylinder the best coordinate system to use is the cylindrical coordinate system. The Laplacian in cylindrical coordinates is

$$\frac{\partial^2 \phi}{\partial r^2} + \frac{1}{r} \frac{\partial \phi}{\partial r} + \frac{1}{r^2} \frac{\partial^2 \phi}{\partial \theta^2} + \frac{\partial^2 \phi}{\partial z^2} = 0 \quad (142)$$

where

$$x = r \cos \theta \quad (143)$$

and

$$y = r \sin \theta \quad (144)$$

has been used.

To find the velocity potential ϕ for the specific system, the Laplacian must satisfy the specific boundary condition dictated by the system. Since the liquid cannot penetrate the wall or the bottom, the liquid velocity component

normal to the tank surface must equal the velocity of the tank surface normal to itself. As the tank rotates as shown in Figure 66 about the center of gravity of the liquid the following conditions must be satisfied

$$\frac{\partial \theta}{\partial r} = -i \omega \theta_0 e^{i\omega t} z \cos \theta \quad \text{for } r = a \quad (145)$$

and

$$\frac{\partial \theta}{\partial z} = i \omega \theta_0 e^{i\omega t} r \cos \theta \quad \text{for } z = -h/2, \quad (146)$$

where θ_0 is a small angular displacement about the center of gravity.

The free liquid surface motion must also satisfy certain restrictions derived from Euler's equation, Equation 141. If the z axis is oriented vertically along the longitudinal axis of the tank the only extraneous forces acting on the tank is that of gravity; therefore,

$$\Omega = g z \quad (147)$$

Since $F(t)$ is arbitrary it can be included in

$$\frac{\partial \theta}{\partial t}.$$

The motion being considered is assumed to be small; therefore, $1/2 q^2$ can be neglected. Now Equation 141 becomes

$$P = \rho \left(\frac{\partial \theta}{\partial t} - \alpha_t z \right). \quad (148)$$

At the liquid surface

$$\frac{dP}{dt} = 0 \quad (149)$$

because the pressure variation must be zero.

But

$$\frac{dP}{dt} = \frac{\partial P}{\partial t} + u \frac{\partial P}{\partial r} + \frac{v}{r} \frac{\partial P}{\partial \theta} + w \frac{\partial P}{\partial z} = 0 \quad \text{at } z = 1/2 \quad (150)$$

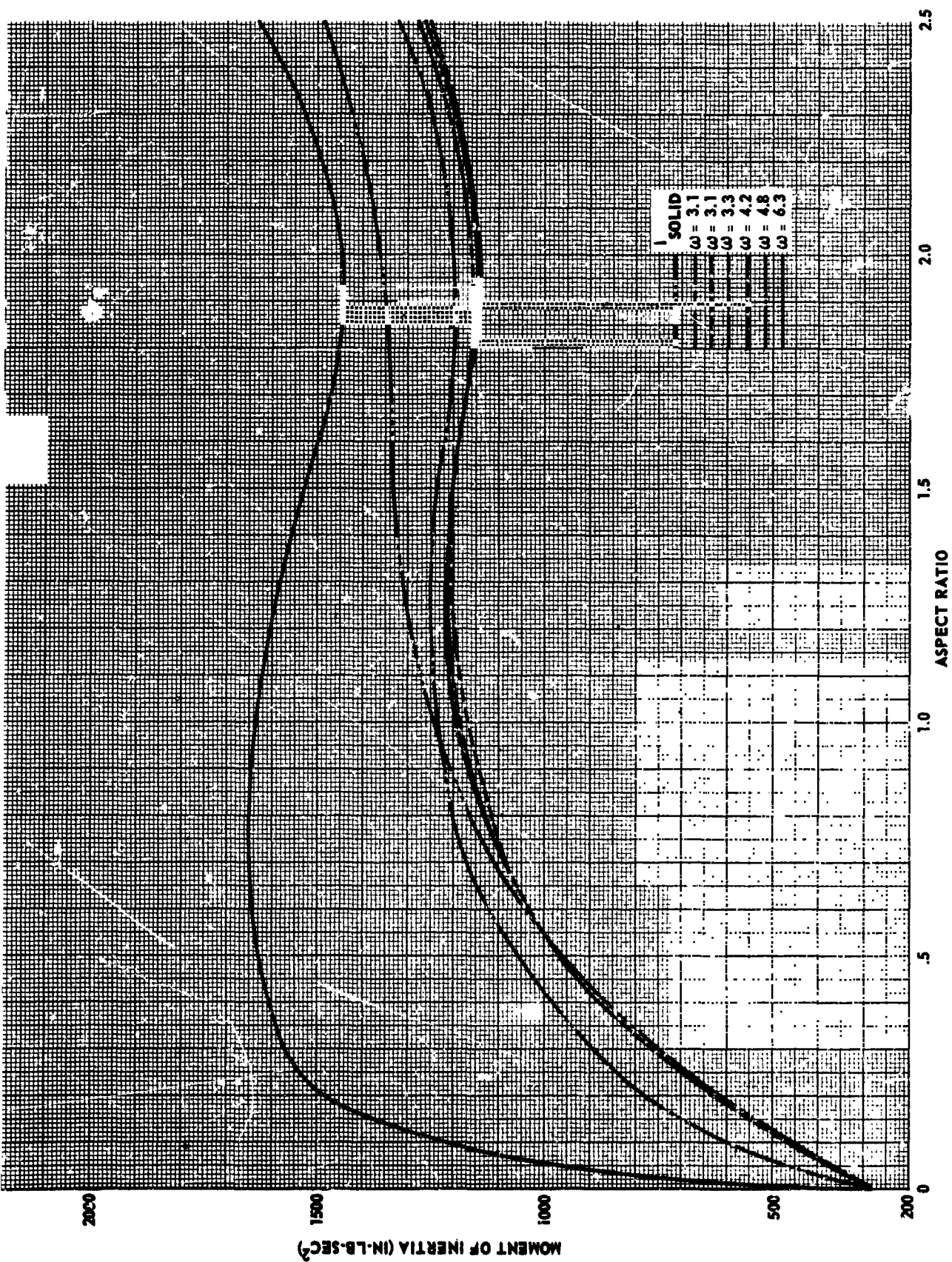


FIGURE 64 PLOT OF MOMENT OF INERTIA VS ASPECT RATIO

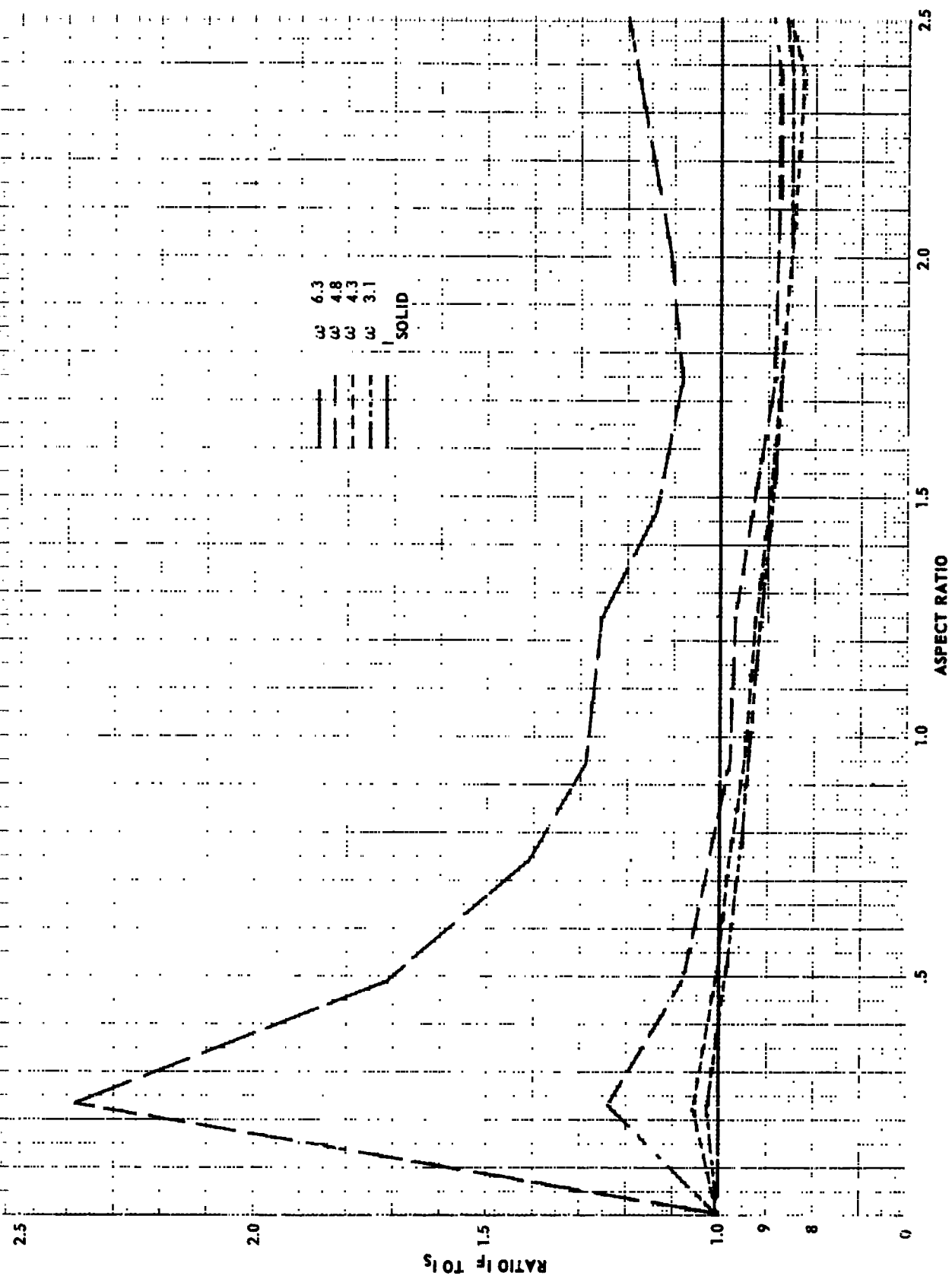


FIGURE 65 PLOT OF THE RATIO OF I_{LIQUID} TO I_{SOLID} VS ASPECT RATIO
FOR VARIOUS ANGULAR VELOCITIES

Now Equation 148, 149 and 150 yield

$$\frac{\partial P}{\partial t} = \rho \left(\frac{\partial^2 \theta}{\partial t^2} - \alpha_t \frac{\partial z}{\partial t} \right) = 0 \quad (151)$$

but

$$\frac{\partial z}{\partial t} = \omega = -\frac{\partial \theta}{\partial z} \quad (152)$$

therefore

$$\frac{\partial P}{\partial t} = \rho \left(\frac{\partial^2 \theta}{\partial t^2} + \alpha_t \frac{\partial \theta}{\partial t} \right) = 0 \quad (153)$$

or

$$\frac{\partial^2 \theta}{\partial t^2} + \alpha_t \frac{\partial \theta}{\partial z} = 0 \quad \text{at } z = \frac{h}{2} \quad (154)$$

Equation 154 along with Equation 145 and 146 are the three boundary conditions necessary to solve for the velocity potential in the Laplace equation, Equation 142.

The solution of this problem has been derived by many authors; therefore, only the results of the derivations will be listed here to save time. Dr. Helmut Bauer who was formerly with the Aeroballistics Lab of the Dynamics Analysis Branch at MSFC has done extensive research into the theoretical approach to this problem; therefore, the results of some of his works will be used.

For a pitching motion about the y axis as shown in Figure 66 the velocity potential is

$$\begin{aligned} \phi(r, \theta, z, t) = & -i\omega\theta_0 e^{i\omega t} a^2 \cos \theta \cdot \left\{ \frac{zr}{a^2} + 2 \sum_{n=1}^{\infty} \frac{1}{(E_n^2 - 1)} \cdot \right. \\ & \frac{E_n \frac{r}{a}}{E_n \frac{\omega_n^2}{\omega^2} - 1} \cosh(E_n \frac{h}{a}) \cdot \left[\frac{b}{a\omega^2} + \frac{h}{2a} \cosh \left[\frac{E_n}{a} \left(z + \frac{h}{2} \right) \right] \right. \\ & \left. \left. \left. - \frac{4b}{a\omega^2} \sinh \left(\frac{E_n h}{2a} \right) \cdot \sinh \left(\frac{E_n z}{a} \right) - \frac{2}{E_n} \sinh \left[\frac{E_n}{a} \left(\frac{h}{2} - z \right) \right] \right] \right\} \quad (155) \end{aligned}$$

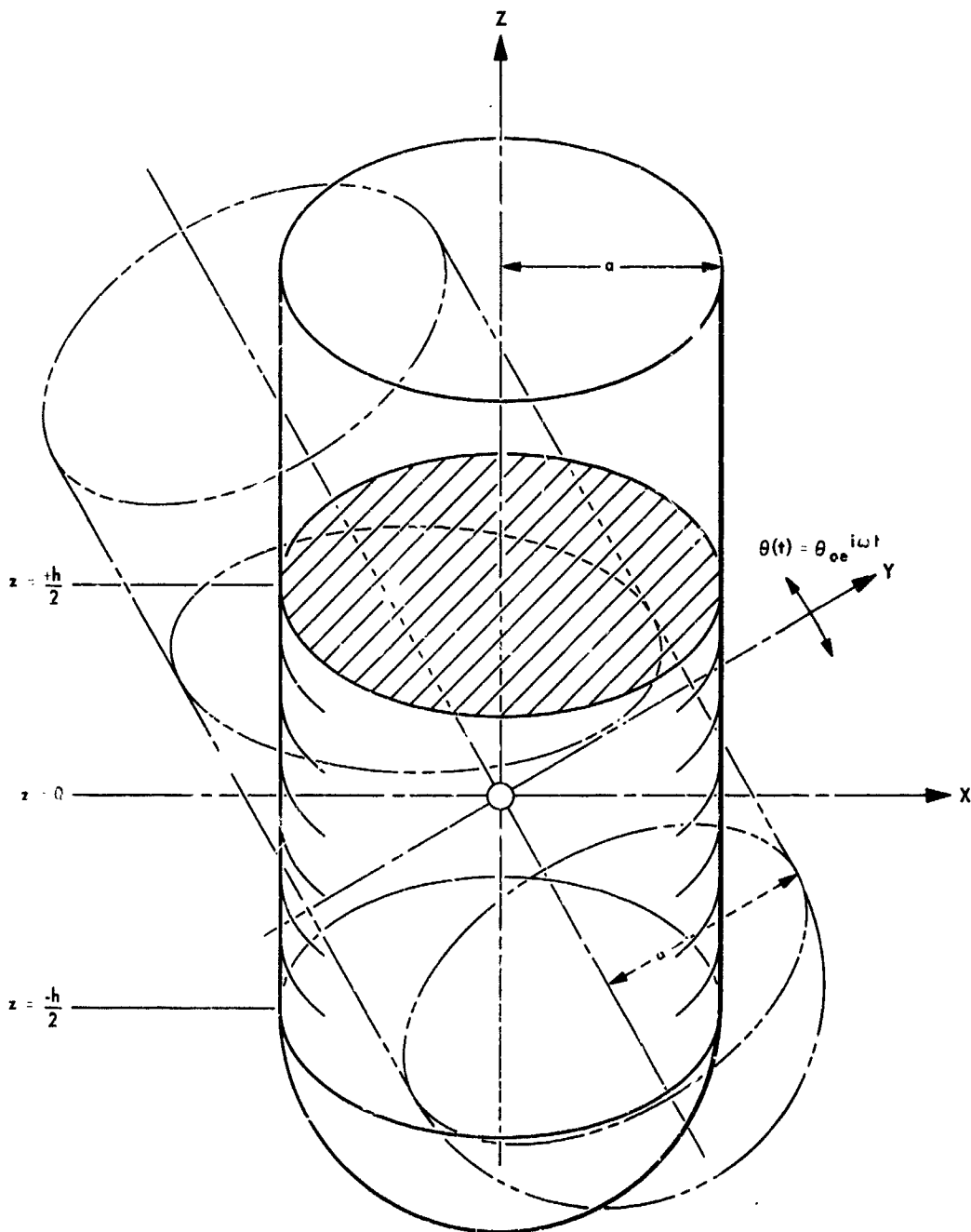


FIGURE 66 ROTATIONAL MOTION OF A PARTIALLY FILLED TANK ABOUT THE LIQUID'S CENTER OF GRAVITY

where

a = tank radius

b = acceleration in z direction

h = liquid height

ω = forced frequency

$\omega_n = \sqrt{\frac{b}{a} E_n \tanh\left(E_n \frac{h}{a}\right)}$ = natural frequency

E_n = zeros of the first derivative of the Bessel function of first order and first kind

Equation 155 is the same as Equation 59 of Reference 2. To find the moment of inertia of the system first the moment must be found. By using

$$M = I \ddot{\theta} = -\omega^2 \theta I \quad (156)$$

the moment of inertia can be found. The moment is obtained by finding the pressures at the bottom and walls of the tank, then by integrating the pressure component over the tank surfaces the fluid force on the tank wall can be obtained. The moment is obtained from the fluid force by using the moment, force, lever arm relationship. The moment becomes

$$M = -\omega^2 \theta_0 e^{i\omega t} m a^2 \left[\frac{1}{12} \left(\frac{h}{a} \right)^2 - \frac{1}{8} + \frac{b}{4\omega^2 h} + 2 \sum_{n=1}^{\infty} \frac{1}{E_n^2 (E_n^2 - 1) (\alpha^2 - 1) \cosh \beta} \cdot \left\{ \left(\frac{2}{E_n} - \frac{4b}{a\omega^2 \beta} \right) + \left(\frac{5b}{\omega^2 \beta} + \frac{1}{2E_n} \right) \cosh \beta + \left(\frac{1}{4} \frac{h}{a} - \frac{5b}{2a\omega^2} - \frac{4}{E_n \beta} \right) \sinh \beta \right\} \right] \quad (157)$$

where

$$\alpha = \frac{\omega_n}{\omega}$$

$$\beta = \frac{E_n h}{a}$$

Equation 157 is the same as Equation 66 of Reference 2. The moment of inertia is now obtained from Equation 156 and becomes

$$I = ma^2 \left[\frac{1}{12} \left(\frac{h}{a} \right)^2 + \frac{1}{4} \right] + 2ma^2 \sum_{n=1}^{\infty} \frac{1}{E_n^2 (E_n^2 - 1) (\alpha^2 - 1)} \cdot \left\{ \frac{2}{\cosh \beta} - \frac{4\alpha^2}{\beta \sinh \beta} + \frac{5\alpha^2}{\beta \tanh \beta} + 2 + \frac{\beta \tanh \beta}{4} - 3\alpha^2 - \frac{4 \tanh \beta}{\beta} \right\} \quad (158)$$

If the damping is introduced as shown in Reference 3, Equation 36b, Equation 158 above now becomes

$$I = ma^2 \left[\frac{1}{12} \left(\frac{h}{a} \right)^2 + \frac{1}{4} \right] + 2ma^2 \sum_{n=1}^{\infty} \frac{1}{E_n^2 (E_n^2 - 1) (\alpha^2 - 1 + i g \alpha)} \cdot \left\{ \frac{2}{\cosh \beta} - \frac{4\alpha^2}{\beta \sinh \beta} + \frac{5\alpha^2}{\beta \tanh \beta} + 2 + \frac{\beta \tanh \beta}{4} - 3\alpha^2 - \frac{4 \tanh \beta}{\beta} \right\} \quad (159)$$

where g is the damping factor.

Since the moment of inertia of a cylindrical solid is

$$I_1 = ma^2 \left[\frac{1}{12} \left(\frac{h}{a} \right)^2 + \frac{1}{4} \right] \quad (160)$$

Equation 159 can be written as

$$I = I_1 + I_2 \quad (161)$$

where

$$I_2 = 2ma^2 \sum_{n=1}^{\infty} \frac{1}{E_n^2 (E_n^2 - 1) (\alpha^2 - 1 + i g \alpha)} \left\{ \frac{2}{\cosh \beta} - \frac{4\alpha^2}{\beta \sinh \beta} + \frac{5\alpha^2}{\beta \tanh \beta} + 2 + \frac{\beta \tanh \beta}{4} - 3\alpha^2 - \frac{4 \tanh \beta}{\beta} \right\} \quad (162)$$

is the effective moment of inertia contributed by the liquid.

Equation 159 is the moment of inertia of a partially filled cylindrical tank about the liquids center of gravity. The experimental data was obtained for a point of rotation displaced from the center of gravity. The parallel axis theorem can be used to transfer the moment of inertia from the liquids center

of gravity to a displaced parallel axis. If the transfer axis theorem is used the moment of inertia equation becomes

$$I = I_1 + I_2 + ML^2 \quad (163)$$

where I_1 and I_2 have previously been defined and ML^2 is the transfer relationship. Table 26A shows the results of the theoretical calculations for a period of 1.5 seconds, a damping factor of 0.5 and for five aspect ratios. The damping factor of 0.5 was obtained from previous experimental work performed by the Aeroballistics Laboratory. I is the total theoretical moment of inertia of the system where the moment of inertia of the empty tank has been included. The ratios of I_{liquid} to I_{solid} for both theoretical and experimental are shown in the last two columns.

A plot of the theoretical and experimental results is shown in Figure 67.

2.5.4 Conclusions: The results of this test program verified some properties of dynamic liquid containers and also produced some new results. The fact that the moment of inertia of a liquid is frequency dependent was verified as shown in Figure 6. For angular velocities of $\omega = 3.1$ to 4.8 radians per second the moment of inertias of the liquid remain relatively constant. For an angular velocity of $\omega = 6.3$ radian per second the moment of inertia has a much larger deviation. The deviation is very large at small aspect ratios because splashing occurred. Splashing differs from sloshing in that some liquid frees itself from the liquid surface in splashing while in sloshing the liquid surface is continuous. The violent motion produced by splashing causes the effective moment of inertia to differ greatly because variable frequencies of oscillation are produced. For larger aspect ratios the curve for $\omega = 6.3$ radian per second more nearly resembles the curves for smaller angular velocities because less liquid is being splashed as compared to lower levels. Since splashing creates many problems and normally is not a factor in considering the dynamics of liquid fuel tanks this data will not be included in the remaining analysis.

Figure 68 shows the plots of experimental data for $\omega = 3.14$ and two theoretical curves. Curve I_s depicts the moment of inertia of the same liquid system if the liquid were a solid. Curve I' is obtained by subtracting the moment of inertia of a spherical segment from the moment of inertia of the theoretical solid for various aspect ratios. This approach is based on the fact that a certain amount of liquid in the center of the tank is not constrained to move; therefore, it does not contribute to the moment of inertia. This curve has the same shape as the experimental curve but not the proper magnitude, but this is understandable because none of the other sloshing factors which can change the moment of inertia have been considered.

Table 26A Results of Theoretical Calculations

h/d	I_1	I_2	ML^2	I	Theoretical I_F/I_S	Experimental I_F/I_S
0.489	24.3	+ 2.4	630.3	929.9	1.003	1.01
0.995	86.6	- 2.5	858.2	1,215.3	0.997	0.95
1.506	236.7	- 5.2	795.8	1,300.2	0.996	0.89
2.017	480.7	+ 7.8	563.7	1,325.2	1.006	0.86
2.528	890.0	- 26.5	277.1	1,466.6	1.018	0.86

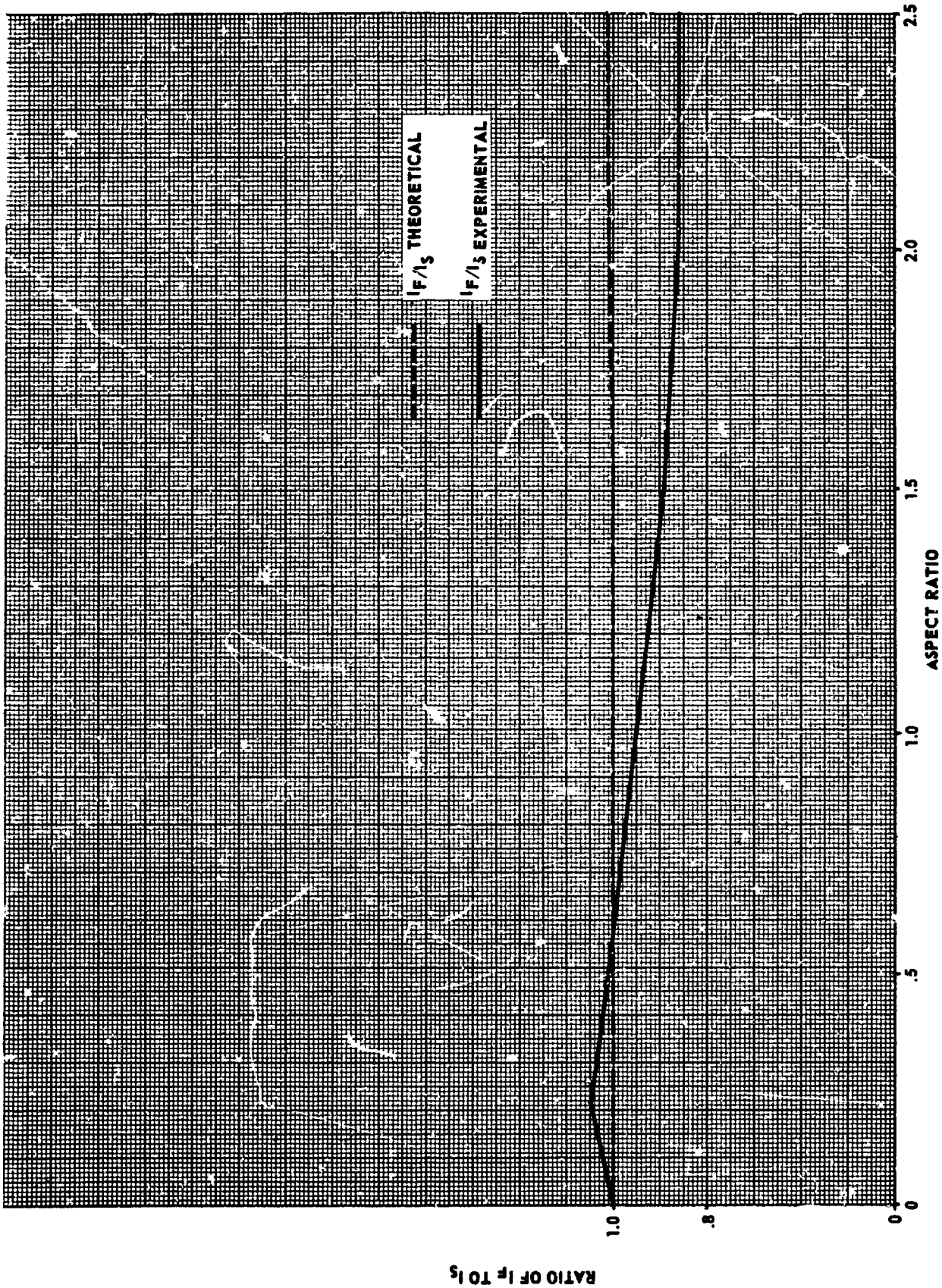


FIGURE 67 PLOT OF THE RATIO OF LIQUID VS ASPECT RATIO FOR EXPERIMENTAL RESULTS AT $\omega = 4.3$ RAD/AS PER SECOND AND THEORETICAL RESULTS

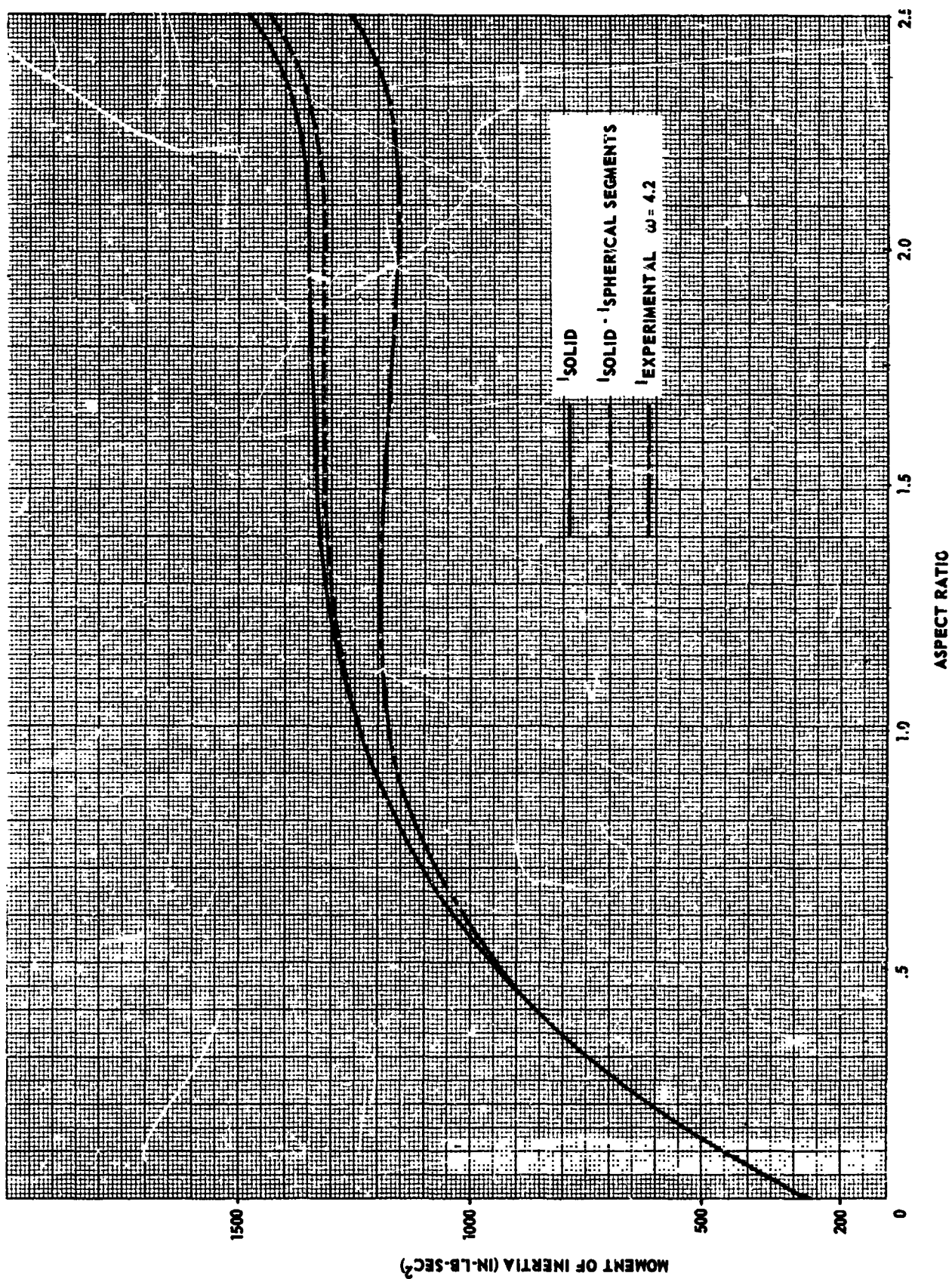


FIGURE 68. PLOT OF MOMENT OF INERTIA VS ASPECT RATIO

One new result which was obtained from the test program was the fact that the standard transfer formula for moments of inertia does not apply for liquids. A comparison of the experimental and theoretical as shown in Figure 67 reveals that the theoretical approach is not correct. This is understandable by examining Table 26. For small aspect ratios the experimental and theoretical data are relatively the same because the transfer term ML^2 is the predominant factor and is common to both. The slosh effect in this case is so small that it does not contribute much to the overall result.

As the aspect ratio increases the moment of inertia of the liquid about its center of gravity, I_1 approaches the magnitude of the transfer term ML^2 and; therefore, has a predominant effect on the total moment of inertia. For these liquid levels the slosh has an effect on the moment of inertia as shown in the experimental curve in Figure 67. The theoretical determination does not show this effect because the slosh term was calculated about the center of gravity of the liquid instead of the axis of rotation. Since liquids do not conform to the same rules as solids in moment of inertia determination the standard transfer formula is completely inadequate for use with liquids. In order to obtain the correct moment of inertia theoretically either a new transfer expression must be derived or new boundary conditions must be applied. A general transfer formula for liquids would be the best approach but it would also be the most difficult. If a liquid transfer formula could be derived it would greatly advance the state of the art in moment of inertia determination of liquids. If this approach proves too difficult, new boundary conditions that will replace Equations 145 and 146 can be used with Equations 142 and 154 to derive an expression for the moment of inertia about a displaced axis.

2.5.5 Recommendations: In view of the fact that the transfer formula does not yield accurate values for liquid moments of inertia, further research should be made into this problem. Additional experimental results can easily be obtained from the existing test equipment with possible small modification. Testing can also be performed using nine government furnished cylindrical tanks with nine different aspect ratios. These tanks can readily be adapted to fit the air bearing table at different pivot points to test the effect of transferred axes on filled containers. A rigorous theoretical investigation can then be performed to derive the correct expression for transferring liquid moments of inertia.

2.6 CENTER OF GRAVITY

2.6.1 Background: In order to assure proper mass distribution for optimum flight performance of the Saturn V, it is necessary to know the precise weight and center of gravity location for all components of the vehicle. In the past,

efforts at locating the center of gravity of objects have largely been confined to mathematical calculations, use of knife-edge balances, tension or compression of load cells by the object combined with a mathematical solution of the summation of moments, and the use of strain gage moment detectors.

Each of the above methods of center of gravity locating has limitations that introduce errors into the final result.

The mathematical method is limited in that it can become a long and laborious task subject to simplifying assumptions, such as, the uniformity of density of the materials involved. Mathematical calculations of the center of gravity can be accurate provided the object is homogeneous, and has accurately machined surfaces that are flat, parallel, and perpendicular to each other. This is seldom the case with mechanical or electronic equipment or any object that the location of its center of gravity is desired.

When the knife-edge method is used the system is almost always unstable and therefore, the object cannot be balanced on the knife-edge. It then becomes a matter of an intelligent guess as to when the knife edge is as close to the center of gravity plane of the object as desired for a particular allowable tolerance. The test object may also be large, heavy and difficult to handle for this method to be used. Friction between the radius edge of the knife-edge and the test object or supporting fixture can cause error in the final results.

Load cells and strain gage moment detectors are limited in their accuracy. Most manufacturers will not specify more than 0.1% of capacity. This accuracy limitation is due largely to energy loss in the form of heat and hysteresis effects.

The SPACO Mass Metrology Laboratory, on contract NAS8-11314, has developed a method of center of gravity location that utilizes a spherical segment air bearing and optical measuring equipment.

This system is limited only by the accuracy of levels and the optical measuring equipment. A small error is introduced by the air friction against the spherical ball segment of the air bearing. This friction error is not expected to be significant except when testing very light objects. The accuracy of the levels, which are mounted to the object support surface, is ± 2 seconds and the optical equipment is capable of measurements of ± 0.001 inch.

This laboratory also uses a moment detector system, in conjunction with the optical system for center of gravity locations, where an accuracy beyond 0.01 inch is not required.

2.6.2 System Description: The center of gravity program consists of three subprograms. These subprograms are referred to as the Optical System, Bytrex System and Spherical-Segment Air Bearing System.

This section is composed of a discussion of each subprogram with the purpose of revealing the progress that has been made on the Center of Gravity program

2.6.2.1 Optical System: Due to the need for a measuring system that could conveniently be used to locate the distance of the center of gravity of objects, of varying shapes and sizes, with respect to any reference point on the object itself, the following optical equipment was purchased from Brunson Instrument Co., Kansas City, Mo.

(1) #76 Optical telescope transit square assembly with a two inch minimum focusing range, a hollow vertical spindle, #190 optical micrometer, #195-T coincidence leveling vial, #191 projection reticle and fixed elbow eyepiece.

(2) #200-10-AM tooling bar assembly with two special support stands having 19 inches travel and a height of 35 inches, and telescope carriage.

(3) Miscellaneous equipment: #187 box level, #185 stellite mirror, three bulls eye leveling vials, #197-H mounting ring, #235-5 theodolite adapter, #708 Bi-filar target, #721 decal target, #717 plug type end view target, #706 side view target and a #709 bulls-eye target.

The system consists basically of a 10 ft tooling bar extrusion mounted on two mobile tooling bar stands, a master index bar, a scale and vernier, a telescope carriage, a telescopic transit square, and a collimation mirror. (See Figure 69.)

The main telescope is provided with a special short focus (1 inch from micrometer to infinity), so that full advantage can be made of the angular resolution when making measurements.

A cross telescope is used, in conjunction with a collimation mirror, for establishing the sighting plane of the main telescope perpendicular to the tooling bar. Special brackets were designed and built for mounting the mirror to the tooling bar.

The transit has a hollow vertical spindle which will allow vertical sightings from the tooling bar if the transit is mounted to a special offset bracket.

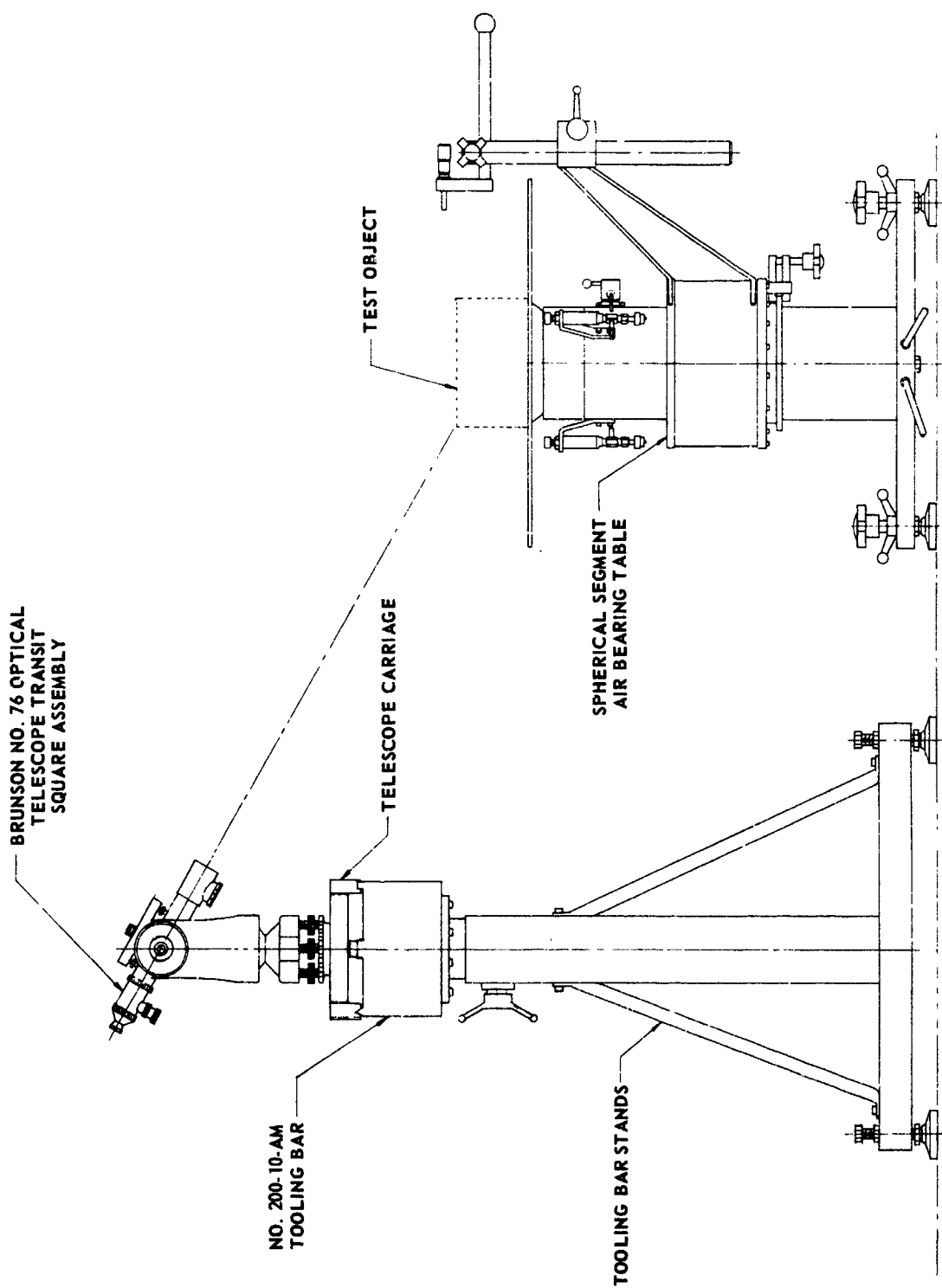


FIGURE 69 CENTER OF GRAVITY LOCATING SYSTEM USING A SPHERICAL
SEGMENT AIR BEARING AND OPTICAL TELESCOPE

An optical micrometer is provided in the main telescope and is used for bucking in the transit when a set up is made.

Tests were conducted, using a Brunson Line Scope (#1172) for collimation, to determine the accuracy of measurement taken with this system. The tests were completed on February 15, 1965. The test procedure is located in Appendix C1, and the data is recorded in Table 27.

The results of these tests indicate that a distance, between clearly defined points, can be measured to within ± 0.001 inch with the present optical system.

A new alignment system, which includes a mirror mounted on one end of the tooling bar positioned such that the face of the mirror is perpendicular to the line of sight of the cross telescope was installed to replace the line telescope. Testing similar to that conducted in the Optical System Program was performed for comparison of accuracy of the new alignment system against the original method of using the line telescope. This test was completed on February 19, 1965. The test procedure is located in Appendix C2, and the data recorded is in Table 28.

The results of these tests indicate that the accuracy of the system was not affected by the change in the method of collimating the telescope.

This method of collimation was selected because it was the least expensive, easier to set up, and requires less floor space for operation.

The present optical system has an accuracy of ± 0.001 inch using extreme care when operating. If an accuracy of ± 0.001 inch is to be obtained in locating the center of gravity of objects, the measuring system must have an accuracy better than ± 0.001 inch if any other errors are introduced into the test. Therefore, development of a more accurate dimension measuring system is needed to allow taking advantage of improvements in the state of the art in other parts of the center of gravity determination system.

2.6.2.2 Moment Detection (Bytrex) System for Location of Center of Gravity:

It was desirable to develop a system that could be used for rapidly locating the center of gravity of large and heavy objects where extreme accuracy would not be required.

A moment detection system was considered to be the least expensive as the major components of such a system could be purchased and would not have to be developed by the laboratory.

Table 27 Accuracy Test Results Using the Brunson Line Scope (No. 1172)

Specimen	Carriage Position		Difference (B-A)	Error		
	Initial (A)	Final (B)		Individual	Average	Maximum
Brass Block (5,000 Side)	1.717	6.718	5.001	0.001	0.001	0.002
	1.718	6.718	5.000	0.000		
	1.717	6.718	5.001	0.001		
	1.718	6.720	5.002	0.002		
	1.717	6.718	5.001	0.001		
	1.717	6.719	5.002	0.002		
Stainless Steel Block (5,000 Side)	3.095	8.096	5.001	0.001	0.001	0.002
	3.096	8.095	4.999	0.001		
	3.096	8.096	5.000	0.000		
	3.097	8.095	4.998	0.002		
	3.097	8.096	4.999	0.001		
	3.094	8.096	5.002	0.002		
Graduated Scale Reading of 5,000 Increment	4.916	9.916	5.000	0.000	0.0003	0.001
	4.916	9.916	5.000	0.000		
	4.916	9.915	4.999	0.001		
	4.916	9.916	5.000	0.000		
	4.917	9.917	5.000	0.000		
	4.916	9.917	5.001	0.001		

Table 28 Comparison of New Alignment System Against Original Method

Specimen	Carriage Position		Difference (B-A)	Error		
	Initial (A)	Final (B)		Individual	Average	Maximum
Graduated Scale (5.000 Increment)	6.914	1.913	5.001	0.001	0.0005	0.001
	6.913	1.913	5.000	0.000		
	6.913	1.913	5.000	0.000		
	6.914	1.913	5.001	0.001		
	6.913	1.913	5.000	0.000		
	6.913	1.914	4.999	0.001		
Brass Block (5.000 Side)	6.148	1.146	5.002	0.002	0.001	0.002
	6.149	1.148	5.001	0.001		
	6.148	1.148	5.000	0.000		
	6.146	1.148	4.998	0.002		
	6.147	1.147	5.000	0.000		
	6.147	1.148	4.999	0.001		
Stainless Steel Block (5.000 Side)	7.197	2.199	4.998	0.002	0.0013	0.002
	7.197	2.199	4.999	0.001		
	7.198	2.200	5.002	0.002		
	7.199	2.198	5.001	0.001		
	7.198	2.200	5.002	0.002		
	7.198	2.198	5.000	0.000		

The equipment that was purchased consists of a 25 in. -lb and a 250 in. -lb Moment Detection Unit and an Instrumentation and Power Supply Unit. These items were manufactured by the Bytrex Corporation, Newton, Massachusetts. The moment detector produces an electrical signal directly proportional to any unbalance moment about its center. It has two perpendicular axes of sensitivity and resolves unbalance moments into two components. The portable instrumentation and power supply unit amplifies the electrical signals to a level high enough to drive a meter movement. A zero suppression arrangement extends the effective range of the meter. The related equipment furnished by the Mass Metrology Laboratory includes two new test object support surfaces and a support and leveling stand that incorporates four overload protection arms.

With this system, the center of gravity of an object can be located by:

- (1) placing object on the moment detector support surface
- (2) reading the unbalance moment
- (3) dividing the unbalance moment by the weight of the object.

The moment detector indicates the unbalance moment in two perpendicular axes. The test object must be repositioned to locate the center of gravity relative to a third axis.

Figure 70 is provided to show the Moment Detection System component relation. The system as shown was completed on December 3, 1964. The following is a description of each component of the present system.

2.6.2.2.1 Test Object Support Surface: The test object support surface is an 18 inch square, 1/2-inch thick, hard anodized aluminum plate. It is inscribed with perpendicular positioning lines which run from +x to -x and from +y to -y.

2.6.2.2.2 Support and Leveling Stand: A stand to support and level the moment detector was added to the system. The moment detector must be leveled before reliable results can be obtained. The support surface is positioned at a convenient height for testing large and heavy test specimens.

2.6.2.2.3 Overload Protection Supports: Four protection supports protect the moment detector against overload damage. These support arms are designed to take-over when an object weighing more than 250 in. -lb is placed on the test object support surface.

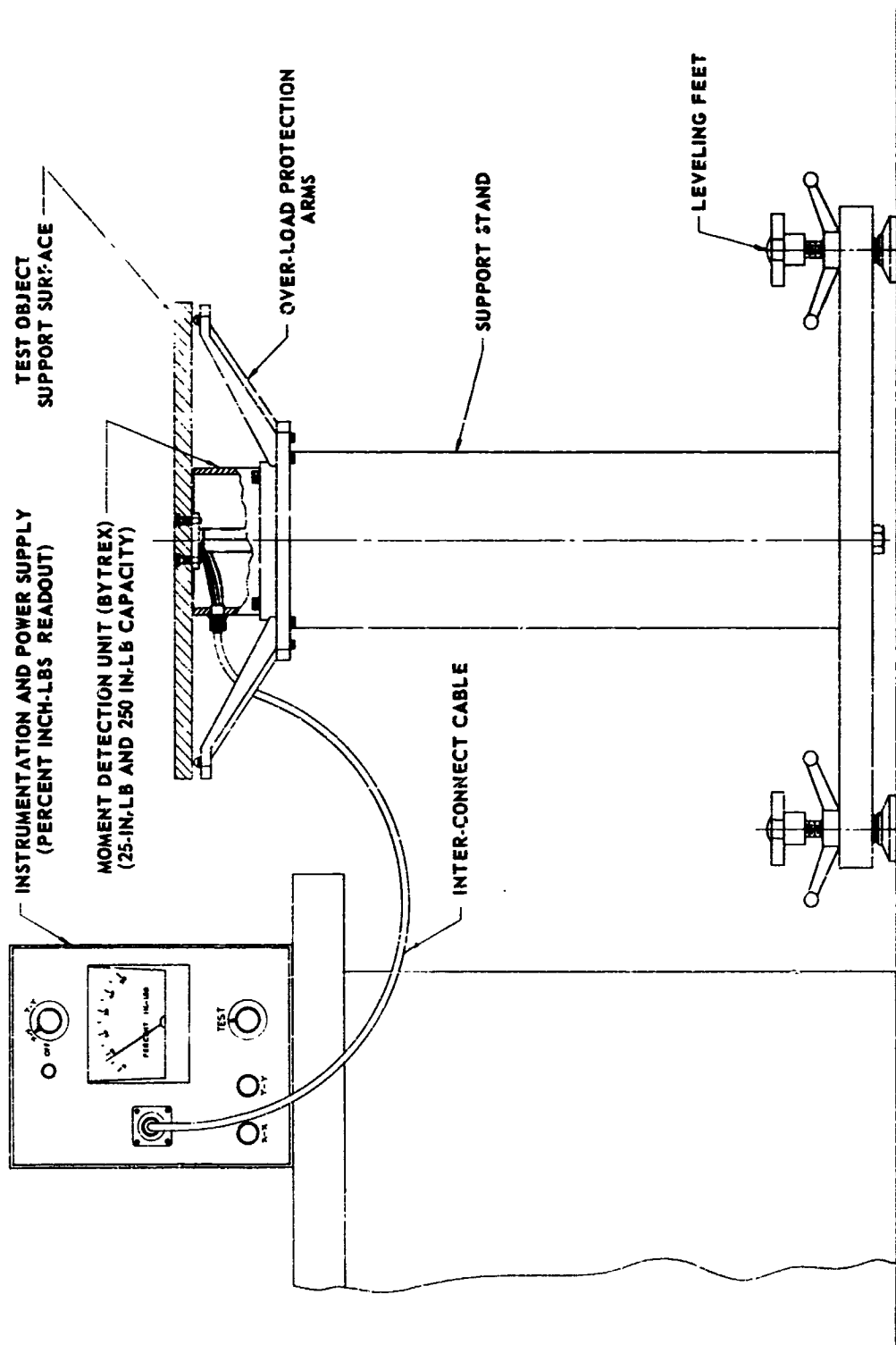


FIGURE 70 MOMENT DETECTION SYSTEM FOR CENTER OF GRAVITY DETERMINATION

2.6.2.2.4 Moment Detector Unit: The moment detector consists essentially of a vertical bending element bolted to two horizontal plates. The bending element has eight bonded wire strain gages cemented to it to sense bending strains. These gages are mounted into two separate Wheatstone Bridges, each composed of four gages mounted two and two on opposite sides of the neutral bending axis. These gages change their electrical resistances proportional to strain, and electrically unbalance the Wheatstone bridge. When voltage is applied across two corners of the Wheatstone bridge, an output voltage directly proportional to bridge unbalance appears across the output connections.

The object support surface, fastened to the top of the bending element, is machined and positioned so that its edges are precisely located with respect to the centerline of the moment detector. The bottom plate is drilled so that the detector may be bolted down. A rugged cylindrical cover encircles the bending element.

These detectors can withstand a vertical load ten times their moment rating. The accuracy of the unbalance moment reading is not affected by the vertical load.

2.6.2.2.5 Instrumentation and Power Supply Unit: This unit operates on four flashlight batteries which give about 100 hours of service. Its basic components are an oscillator which supplies voltage to the strain gage bridge, a detector, an amplifier, and a meter. Feedback circuits are used to achieve maximum stability. The principal operating controls of the unbalance indicator are an operation selector switch; an add-to reading switch, which is used to increase the range of the meter and select proper polarity; a meter adjust control, which is used to set the amplifier gain; two zero sets, one each for the x-x and y-y axis to bring the meter to zero with no applied unbalance; and two span controls, one each for the x-x and y-y axis used to set the calibration of the system.

The indicator and moment detector are connected by a 20 foot cable with connectors at each end.

The indicator reads in percent of in.-lb of full range of the detector. For example, an 80 percent reading with the 25 in.-lb detector indicates an unbalance of 20 in.-lb about the center line of the detector.

2.6.2.2.6 System Accuracy: The accuracy of the Moment Detection System is affected by the weight of the test specimen. As the weight of the specimen decreases, the absolute value of the unbalance moment that must be indicated for a given accuracy of the center of gravity location also decreases. For example, on a 4000 pound test specimen, the unbalance moment must be

determined to 4 in. -lb to locate the center of gravity to 0.001 inch. If the test specimen weighs 1000 pounds the unbalance moment must be known to 1 in. -lb for the same 0.001 inch, center of gravity location.

The manufacturer states that the unbalance readings are accurate to ± 1 percent of indication or ± 0.25 in. -lb on the 25 in. -lb unit and 2.50 in. -lb for the 250 in. -lb unit.

Error analyses tests were run on the two "Bytrex" units. Out of fifteen (15) readings the average error in the 25 in. -lb unit was 0.007 in. From nine (9) readings, the average error of the 250 in. -lb unit was 0.003 in. Each unit was first calibrated above 95% of scale reading.

It will be possible to measure the center of gravity to the nearest 0.01 inch on the 250 in. -lb unit with care. However, it will require great care to obtain this accuracy on the 25 in. -lb unit.

The test procedure is located in Appendix C3, and the data is recorded in Table 29 and 30. Figure 71 presents a graph depicting indicated moment versus actual moment 25 in. -lb detector, while Figure 72 presents a graph using the 250 in.-lb detector.

A test was also conducted on February 25, 1965, to determine the accuracy of locating the center of gravity of a test specimen using the optical system with the Bytrex system. The same test specimen, a brass block, was used as in a previous test where depth gages were used for measurements or dimensions.

In the previous test, measurements were taken from the edge of the brass block to the center of the Bytrex unit. The block had to be positioned parallel to a plane through the center of the moment detector for this measurement to be of any value in locating the center of gravity of the specimen. Locating the center of gravity of the specimen, by measuring from scribed cross-marks, eliminates the necessity of the block being in this parallel position, thus removing a source of error. This can be easily done when using the optical telescope.

Eleven readings were taken, ten representing approximately 10% intervals of unbalance moment and the last reading at 5% of unbalance moment.

These readings produced an average error of 0.003 inch in locating center of gravity as compared to an average error of 0.009 inch in the test using depth gages. This represents an increase in accuracy of better than 60%. The tests were made using the same moment detector (25 in. -lb), the same specimen (brass block), and at the same room temperature of 70°F.

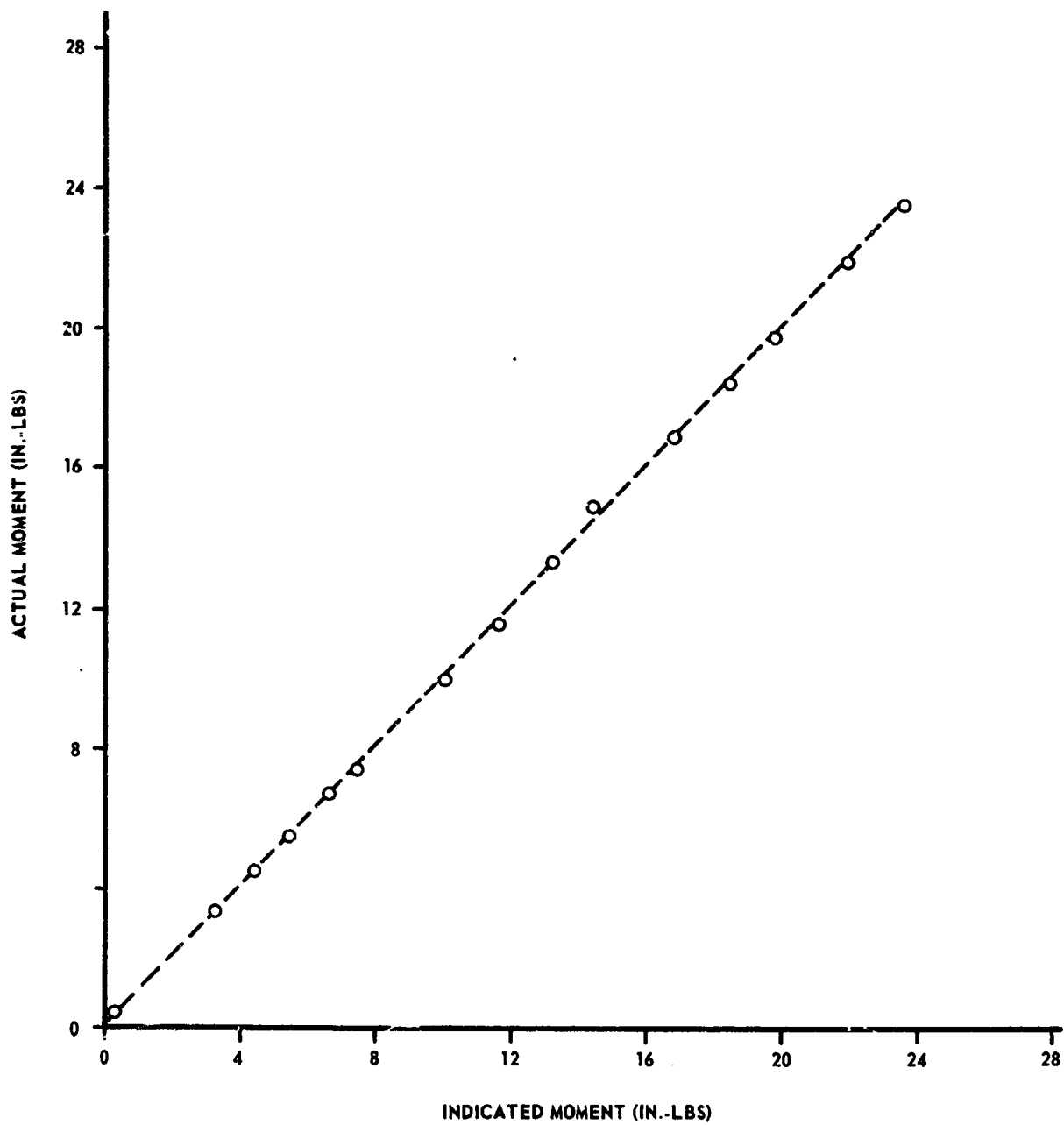


FIGURE 71 INDICATED MOMENT VS ACTUAL MOMENT 25 IN.-LB DETECTOR

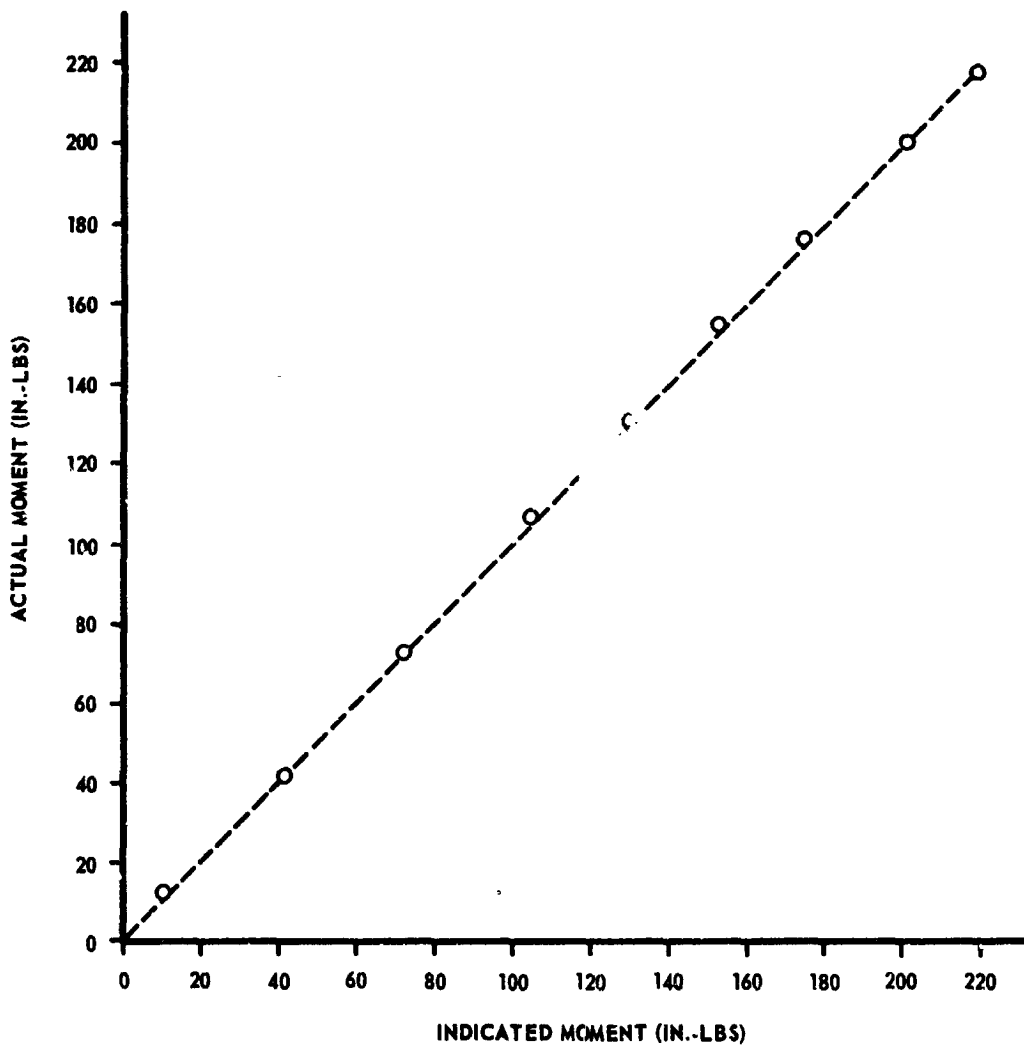


FIGURE 72 INDICATED MOMENT VS ACTUAL MOMENT 250 IN.-LB DETECTOR

Table 29 Tests Using the 25 in. -lb Moment Detection Unit

TEMP <u>70° F</u>		TEST OBJECT		DIM. <u>1.500 x 3.000 x 5.000</u>		WT. <u>6.8122 LBS</u>			
REL. HUMIDITY <u>40%</u>		TESTS USING THE 25 IN-LB MOMENT DETECTION UNIT							
TEST DATE <u>12-10-64</u>									
RUN NO.	ACTUAL C. G. (INCHES)	C. G. INDICATED BY SYSTEM (INCHES)	ERROR (INCHES)	ACTUAL MOMENT (IN-LB)	MOMENT INDICATED BY SYSTEM (IN-LB)	ERROR (IN-LB)	INSTRUMENT READING (% IN-LBS)	ACTUAL VALUE (% IN-LBS)	ERROR (% IN-LBS)
1	3.453	3.461	0.008	23.52	23.57	0.05	94.3	94.1	0.20
2	3.205	3.215	0.010	21.83	21.90	0.07	87.6	87.3	0.30
3	2.897	2.903	0.006	19.73	19.78	0.05	79.1	78.9	0.20
4	2.703	2.705	0.002	18.41	18.42	0.01	73.7	73.6	0.10
5	2.472	2.470	0.002	16.84	16.82	0.02	67.3	67.4	0.10
6	2.127	2.121	0.006	14.49	14.45	0.04	57.8	58.0	0.20
7	1.963	1.952	0.011	13.37	13.30	0.07	53.2	53.5	0.30
8	1.696	1.706	0.010	11.55	11.62	0.07	46.5	46.2	0.30
9	1.459	1.479	0.020	9.94	10.08	0.14	40.3	39.8	0.50
10	1.084	1.101	0.017	7.38	7.50	0.12	30.0	29.5	0.50
11	0.976	0.985	0.009	6.65	6.71	0.06	26.8	26.6	0.20
12	0.800	0.815	0.015	5.45	5.55	0.10	22.2	21.8	0.40
13	0.650	0.660	0.010	4.43	4.50	0.07	18.0	17.7	0.30
14	0.483	0.490	0.007	3.29	3.34	0.05	13.4	13.2	0.20
15	0.048	0.051	0.003	0.33	0.35	0.02	1.4	1.3	0.10
		AVG. ERROR		AVG. ERROR		AVG. ERROR		AVG. ERROR	
		0.009		0.009		0.06		0.26	
		MAX. ERROR		MAX. ERROR		MAX. ERROR		MAX. ERROR	
		0.020		0.14		0.14		0.50	

Table 30 Tests Using the 250 in. -lb Moment Detection Unit

TEMP <u>70° F</u>			TESTS USING THE 250 IN-LB					TEST OBJECT		
REL. HUMIDITY <u>40%</u>			MOMENT DETECTION UNIT					DIM. 10.00 DIA. x 4.50 Thick		
TEST DATE <u>12-10-64</u>								WT. <u>98.71 lbs.</u>		
RUN NO.	ACTUAL C.G. (INCHES)	C.G. INDICATED BY SYSTEM (INCHES)	ERROR (INCHES)	ACTUAL MOMENT (IN-LB)	MOMENT INDICATED BY SYSTEM (IN-LB)	ERROR (IN-LB)	INSTRUMENT READING (% IN-LBS)	ACTUAL VALUE (% IN-LBS)	ERROR (% IN-LBS)	
1	2.225	2.224	0.001	219.63	219.50	0.13	87.80	87.80	0	
2	2.041	2.036	0.005	201.47	201.00	0.47	80.60	80.40	0.20	
3	1.779	1.773	0.006	175.60	175.00	0.60	70.20	70.00	0.20	
4	1.563	1.558	0.005	154.28	153.00	1.28	61.70	61.20	0.50	
5	1.327	1.320	0.007	130.99	130.25	0.74	52.40	52.10	0.30	
6	1.068	1.069	0.001	105.42	105.50	0.08	42.20	42.20	0	
7	0.732	0.734	0.002	72.26	72.50	0.24	28.90	29.00	0.10	
8	0.424	0.420	0.004	41.85	41.50	0.35	16.70	16.50	0.20	
9	0.109	0.104	0.005	10.76	10.25	0.51	4.30	4.10	0.20	
					AVG. ERROR				AVG. ERROR	
					MAX. ERROR				MAX. ERROR	
					0.004				0.49	
					0.007				1.28	
									0.19	
									0.50	

The test procedure is located in Appendix C4, and the test data is recorded in Table 31.

Table 31 Bytrex Test

Date: 2-25-65		PRELIMINARY BYTREX TEST USING OPTICAL MEASURING		Temp 70°
				R H 36%
Run No.	Indicated Unbalance % in.-lb	Actual C G From Bytrex Center (in.)	Indicated C G From Bytrex Center (in.)	Error (in.)
1	94.5	3.469	3.468	0.001
2	85.5	3.137	3.138	0.001
3	75.3	2.764	2.763	0.001
4	65.7	2.415	2.411	0.004
5	55.1	2.020	2.022	0.002
6	45.1	1.652	1.655	0.003
7	34.7	1.275	1.273	0.002
8	25.0	0.910	0.917	0.007
9	15.2	0.550	0.558	0.008
10	10.1	0.366	0.371	0.005
11	5.0	0.184	0.183	0.001
AVG. ERROR				0.003
MAX. ERROR				0.008

Based on the results of the above tests, it is recommended that the Bytrex stand be modified to allow 90° rotation of the Bytrex unit. This will permit measurement in two axes using the optical equipment, without disturbing the position of the test specimen relative to the support surface. The design and fabrication drawings for this modification have been completed.

Another modification is suggested that would involve the addition of a weight sensing device at the base of the moment detection unit to measure the test object weight at the same time the unbalance moment is being recorded. The major advantage of such a system is that it readily lends itself to a system for automatic read-out of the center of gravity locations from a constant reference point on the object support surface.

This automatic system will require only an electronic circuit that would perform the following mathematical operation:

$$\frac{\text{Unbalance Moment Indication} \times \text{Detector Capacity}}{\text{Test Object Weight}} = \text{Distance from Detector Center To Reference Point}$$

A prototype system could be developed and evaluated, using the company owned PACE analog computer.

Performance tests of the system would also be performed to establish the system accuracy and develop a set of performance curves. These performance curves would consist of plots of accuracy vs weight of test object and accuracy vs center of gravity elevation of test object. The objective of this modification is to perfect a system which will be relatively immune to human errors in operation of the test equipment.

2.6.2.3 Air Bearing Table for Location of Center of Gravity: The air bearing table consist of: (See Figure 73.)

- (1) A test object support surface
- (2) A spherical-segment air bearing
- (3) Three staolizing air cylinders
- (4) An air cylinder control valve.
- (5) A support and leveling stand
- (6) A test object positioner

With this system, the center of gravity of an object can be located by placing the test object on the support surface and positioning the object until the support surface becomes and remains level.

The support surface, attached to a segment of a hard-anodized, aluminum, sphere, is supported by air pressure.

The air bearing can be safely operated using 10 psi to 60 psi of air pressure.

When a test specimen is being supported in a level position, the center of gravity of the specimen is then coincident with the pre-determined center of gravity of the system.

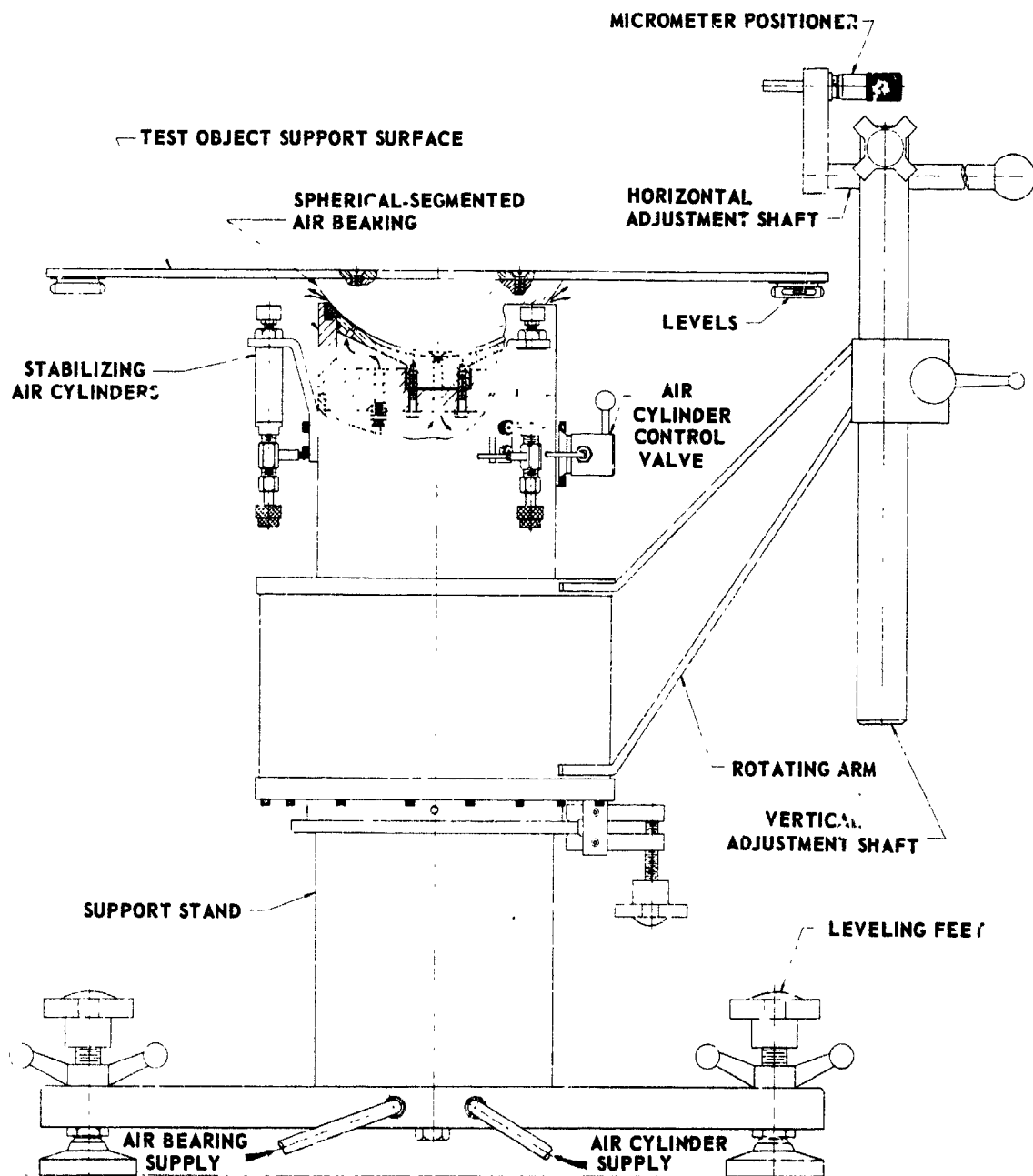


FIGURE 73 SPHERICAL AIR BEARING TABLE FOR CENTER OF GRAVITY DETERMINATION

2.6.2.3.1 Equipment Description

2.6.2.3.1.1 Test Object Support Surface: Two support surfaces are used. One is a 24 inch diameter x 1/2 inch thick hard-anodized aluminum plate, which is lapped to a flatness of 0.0005 inch and the other a 24 inch diameter x 1 inch thick surface composed of two 1/16 inch thick hard-anodized aluminum sheets bonded to each side of a honeycomb core and lapped to 0.0005 inch flatness. The aluminum support surface is for use with heavy test objects. This aluminum support surface is used to prevent objects having feet, pads, or other small supports from rupturing the honeycomb core. A light-weight support surface is needed to increase the sensitivity of the system when small or light objects are to be tested.

These object support surfaces fasten to the spherical segments of hard-anodized aluminum by means of four 1/4 diameter flat head stainless steel screws.

2.6.2.3.1.2 Spherical-Segment Air Bearing: The air bearing consists of a segment of a 5 inch nominal radius, hard-anodized, aluminum cup. The cup is fastened into a stainless steel air chamber. The cup and ball are lapped to a roundness of 4 millionths of an inch.

The air for operation of the bearing is filtered to 7 microns and supplied to the air chamber of the bearing through 1/8 inch O.D. nylon tubing. The air then passes through a series of very small holes in the cup and forces the ball to ride on a layer of air with no metal contact. A 1/4 diameter hole in the center of the cup allows air to enter a sealed air chamber below the bearing.

This chamber of air dampens vibrations of the ball caused by air flow.

A teflon ring around the edge of the cup prevents contact between the ball and cup when the air supply is off.

2.6.2.3.1.3 Stabilizing Air Cylinders: Three air cylinders are mounted, 120° apart, below the object support surface. These cylinders have a 1/2 inch diameter bore and a 1 inch stroke and are used to stabilize the object support surface while a test object is being repositioned. Each cylinder has an individual needle valve used to control the rate of plunger travel. It is necessary that the three cylinders make contact with the support surface at approximately the same time. This is necessary to prevent tipping of the support surface and causing unwanted movements of the test object.

2.6.2.3.1.4 Air Cylinder Control Valve: The air cylinder control valve is used to control air flow to the three air cylinders. This three-way valve has ports for air input, air extraction and system bleeding.

2.6.2.3.1.5 Support and Leveling Stand: The object support surface is held 28 inches above the floor by this support stand and a floor area of 5 sq. ft. is needed for proper operation of the equipment.

The stand consist of a 7.25 inch O.D aluminum tube welded to a three legged base. The base is 1.25 inch thick steel, machined such that three arms protrude 8 inches from an 8 inch diameter center section. The three arms are 120° apart and each contains a leveling pad. Attached to the steel tube is a bearing-supported rotating arm, referred to as the test object positioner.

2.6.2.3.1.6 Test Object Positioner: The test object positioner consists of a micrometer, mounted on a $3/4$ inch diameter shaft that is movable in a horizontal direction. The horizontal shaft is held by an adjustable, 1.50 inch diameter, vertical shaft. A rotating arm supports the vertical shaft. This arm extends approximately 16 inches from the center of the stand and is mounted to the 7.25 diameter aluminum tube. The arm is mounted on a ball bearing and rotates freely through 360° and may be locked in any position. A micrometer positioner is used to obtain very small movements of the test objects in order to secure a level condition of the support surface.

2.6.2.4 Operation: When a test object is positioned on the support surface such that a level condition exists, the center of gravity of the test object is then known to act through the pre-determined, center of gravity of the system. It is then necessary to locate this plane of action to a reference point on the test object. Rotation of the test object and support surface through an angle of 90° allows the location of a second plane to the same reference point. It is then necessary to reposition the test object so that it rests on a surface or side that is 90° from the initial plane of rest. The third plane of action can then be located from the reference point.

2.6.2.5 Evaluation: Final assembly of the present system was completed on May 19, 1965 and testing was started immediately. The test procedure is located in Appendix C5.

The results of the tests are summarized in Table 32. The maximum location error is the greatest displacement of the center of gravity mark on the specimen from the table center, at any point of table rotation. The repeatability error is the maximum spread between location errors. It is apparent from Table 32 that large errors in location of center of gravity exist, but the causes cannot be determined from this test. The location

Table 32 Evaluation of Spherical Segment Air Bearing Table Test Results

Specimen Description	Room Temp	Relative Humidity	Date of Test	Run No.	Maximum Location Error	Maximum Repeatability Error
Brass Cylinder 2.785 dia x 5.250 high wt - 9.69 lb.	72°	48%	5-26-65	1	0.012	0.000
				2	0.012	
				3	0.012	
Triangular Solid 3.385 x 3.385 x 6.051 in. wt - 9.05 lbs.	69°	48%	5-27-65	1	0.005	0.001
				2	0.006	
				3	0.006	
Brass Rectangular Solid 3.000 x 5.000 x 1.500 in. wt - 6.815 lbs.	69°	48%	5-27-65	1	0.003	0.001
				2	0.0025	
				3	0.002	
Triangular Solid 5.339 x 5.355 x 6.022 in. wt. - 22.56 lbs.	70°	46%	5-28-65	1	0.010	0.0025
				2	0.0075	
				3	0.008	

error is in effect a summation of all errors, whether in the system or in the specimens. Probably the largest component is the error in the marks on the specimens.

Of greater significance is the repeatability of the error readings, which is in the range of 0.001 to 0.002 inch. A standard deviation of the six repeatability values was computed, using the equation:

$$s = \frac{\sum_{i=1}^n (x_i - \bar{x})^2}{n - 1} \quad (164)$$

where:

s = standard deviation

i = test number

n = total number of tests

x_i = individual error readings

\bar{x} = mean error, = $\frac{\sum_{i=1}^n x_i}{n}$

Substituting the repeatability errors from this test into Equation 164 produces a standard error of 0.0013 inch, which is an indication of the random error in the spherical air bearing table and optical system. When standards with more accurate center of gravity location marks are available, tests should indicate errors approaching the standard error.

Attempts were made to correlate the test error with other parameters such as specimen weight, elevation of the specimen center of gravity, location of the suspended system center of gravity with respect to the center of rotation of the spherical bearing, air pressure in the bearing, room temperature, etc. No clear-cut trends could be detected.

2.6.2.6 Recommendations: From the tests it is concluded that the system has an ultimate accuracy capability approaching ± 0.001 inch. The errors in location of the center of gravity marks on the specimens obscured much of the remaining system errors. A large number of additional tests are needed before a meaningful evaluation of the system can be made.

It is recommended that the following modifications be made to the air bearing center of gravity system.

(1) Larger capacity air cylinders are to be added to the air bearing table. When the present cylinders are adjusted for slow travel the rate of travel cannot be controlled accurately. It is necessary that all three cylinders arrive at maximum travel at the same time to prevent tipping of the object support surface and therefore displacing the test object. The present cylinders also do not have the capacity to lift objects in excess of 300 lbs while adjusted for slow travel. Slow travel is necessary to prevent large vibrations from disturbing the test object position. Three air cylinders are needed to support the test object while it is being positioned on the air bearing table.

(2) A new suspended counter-weight system will be added to the air bearing table. This system is necessary to correct unstable conditions of the system created by test objects whose center of gravity and weight are such that the total center of gravity of the system (test object included) is no longer within the area of the spherical ball segment of the air bearing. The present counter-weight system consists of three 3/8 inch diameter rods attached to the test object support surface from which various sizes of weights may be suspended. When large weights are suspended from the rods and the test object causes the support surface to tilt, permanent deflections of these rods may occur, resulting in erroneous center of gravity location.

(3) The optical system is to be combined with the air bearing table on a common base. This design will result in a center of gravity system that is complete within itself and would require only an air supply for operation. (See Figure 74)

Tests are to be conducted to determine the accuracy of the modified equipment and to develop system performance curves. The curves are to represent the tests made with various air pressures supplied to the air bearing, accuracy vs weight, and accuracy vs vertical elevation of the center of gravity of the test object.

2.7 FACILITIES AND EQUIPMENT

2.7.1 Description of Laboratory: Because of the strict specialized requirements of the contract work, it was necessary to construct a new facility expressly for the effort. Construction of the laboratory was started in June, 1964, and completed in October, 1964. The facility contains 4,200 square feet of floor area, including a 144 square foot isolation pad. The pad was built with a separate deep foundation to isolate it from the building structure. The entire area is kept at a constant temperature and humidity by a special heating-air conditioning system.

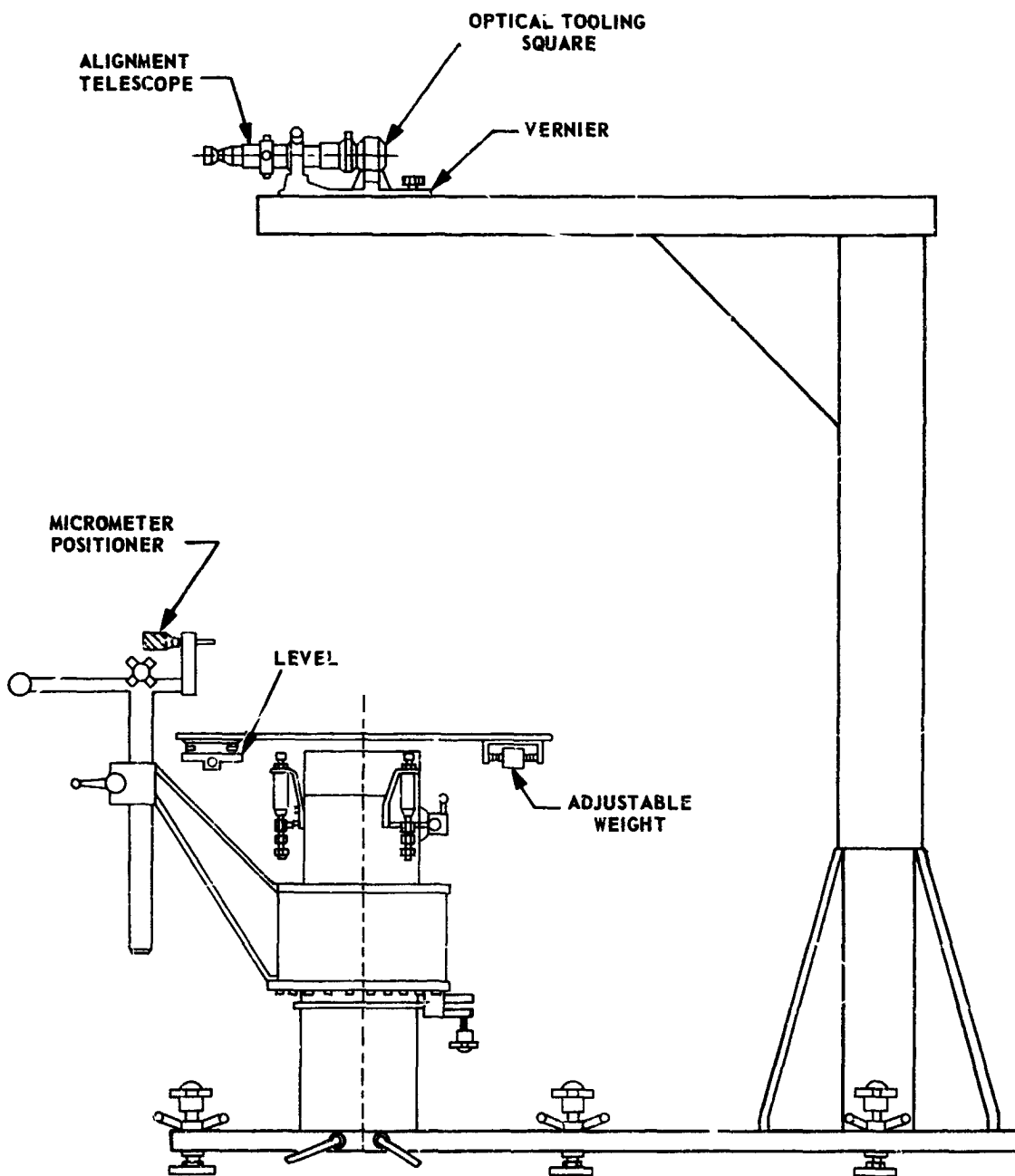


FIGURE 74 CENTER OF GRAVITY TEST FIXTURE

Access to the laboratory is via one of two air locks which prevent dilution of the controlled atmosphere. The main entrance air lock doors are secured by solenoid operated latches which are electrically interlocked to prevent simultaneous opening of both doors. The service air lock contains large overhead doors for oversize objects.

2.7.2 General Laboratory Improvements: During the course of laboratory activities on the major tasks, numerous other support projects were accomplished. Most of these were design and fabrication of equipment to improve laboratory operations. Some of the major efforts are discussed below.

2.7.2.1 Photocell Timing Device: The government-furnished photo electric period timing device was improved considerably, but further improvement in the accuracy of the device are required. In order to improve timing accuracy, the velocity of the light intensity change on the face of the photocell must be such that the time required for a significant intensity change is small compared to the time being measured. A study of possible methods was made, and decision was made to pursue the technique of velocity magnification by an optical lever arm. The intent was to project the rotating light source to a photocell some distance away.

An experimental light source was constructed using an inexpensive Zirconium arc lamp having an arc diameter of 0.005 inch, and a short focal length high speed lens. This light source proved to be effective up to about 25 feet with the photo-diode as a detector. The system proved to be inferior in timing accuracy, however, because of a large amount of instability of the arc. The amount of transverse wander of the arc was in fact larger than the total arc width. In view of these poor results, the project was abandoned.

The arc instability problem could be solved by using a larger lamp in conjunction with a suitable aperture to control the size, which would in turn require a high speed long focal length optical system. Considering the high equipment cost of such a system, it was decided that efforts would be better expended along other approaches to the problem. Two proposed methods which have not yet been evaluated are a laser light source and a high magnification lens system for increasing light source deflection.

2.7.2.2 Capacitive Motion Transducer: In the mass properties of liquids test program, many of the measurement requirements are identical to those for the moment of inertia program. Both require measurement of the length of the oscillation period, and a photoelectric counter was used for both projects. For amplitude measurement, a device is needed which will indicate the value of peak angular displacement of the oscillating object, from which an envelope can be constructed. The capacitive transducer was selected for use both on the moment of inertia and the mass properties of liquids program. The

application to the moment of inertia program has been previously described in paragraph 2.2.4.1. The application to the mass properties of liquids program was accomplished in a somewhat different manner, both mechanically and electrically. Flat capacitor plates rather than cylindrical were used here and are in a "twin T" circuit arrangement rather than a modulated oscillator. The performance of the unit proved to be very satisfactory, fully justifying the effort expended in development.

A complete technical report of the design and testing of the unit is presented in Appendix D.

2.7.2.3 Analog Computer: Upon the decision to purchase a PACE TR-48 analog computer for the Mass Metrology Laboratory, SPACO embarked on a program to familiarize the laboratory personnel with operation of the unit. Two of the laboratory engineers attended a short course in analog computer fundamentals given by the manufacturer. Following this, a paper was prepared by one of the engineers, outlining the computer fundamentals for use by others in the laboratory. This paper is included in this report as Appendix E.

2.7.2.4 General Laboratory Improvements: Numerous other improvements were made in the conduct of the laboratory, by virtue of improvements in facilities, some of which are listed below:

1. Leveling plates were installed on the overhead ceiling beam to improve the accuracy of torsion rod calibration tests.
2. Two air filter regulator units were designed and constructed for the air bearing units.
3. An air line pressure drop warning system was designed and installed.
4. An electrical ground bus was installed for electronic instruments.
5. A hydraulic lift for handling dumbbell standards was procured and modified.
6. A portable cart was designed and built for transporting and leveling the laboratory surface plate.
7. Two new moment of inertia standards were built, and the others were refinished to precision tolerances.
8. Several additional torsion rods were fabricated.

9. Test standards for the center of gravity and product of inertia program were designed and built.

APPENDIX A
MOMENT OF INERTIA

APPENDIX A1

Torsional Pendulum System

The equation of motion of the torsion system shown in Figure A1-1 about axis $O - O'$ is

$$I \ddot{\theta} = T \text{ (moment or torque).} \quad (A1-1)$$

The torque is proportional to the angle of twist

$$T = -K \theta \text{ (the minus sign shows an opposing force)} \quad (A1-2)$$

Therefore

$$I \ddot{\theta} + K \theta = 0. \quad (A1-3)$$

A standard solution gives

$$\theta = \theta_0 \cos \sqrt{\frac{K}{I}} t \quad (A1-4)$$

where

$$\theta_0 = \text{initial angle.}$$

now

$$\omega = \sqrt{\frac{K}{I}} \quad (A1-5)$$

since

$$\omega = 2\pi f = \frac{2\pi}{T},$$

then

$$I = \frac{KT^2}{4\pi^2} \quad (A1-6)$$

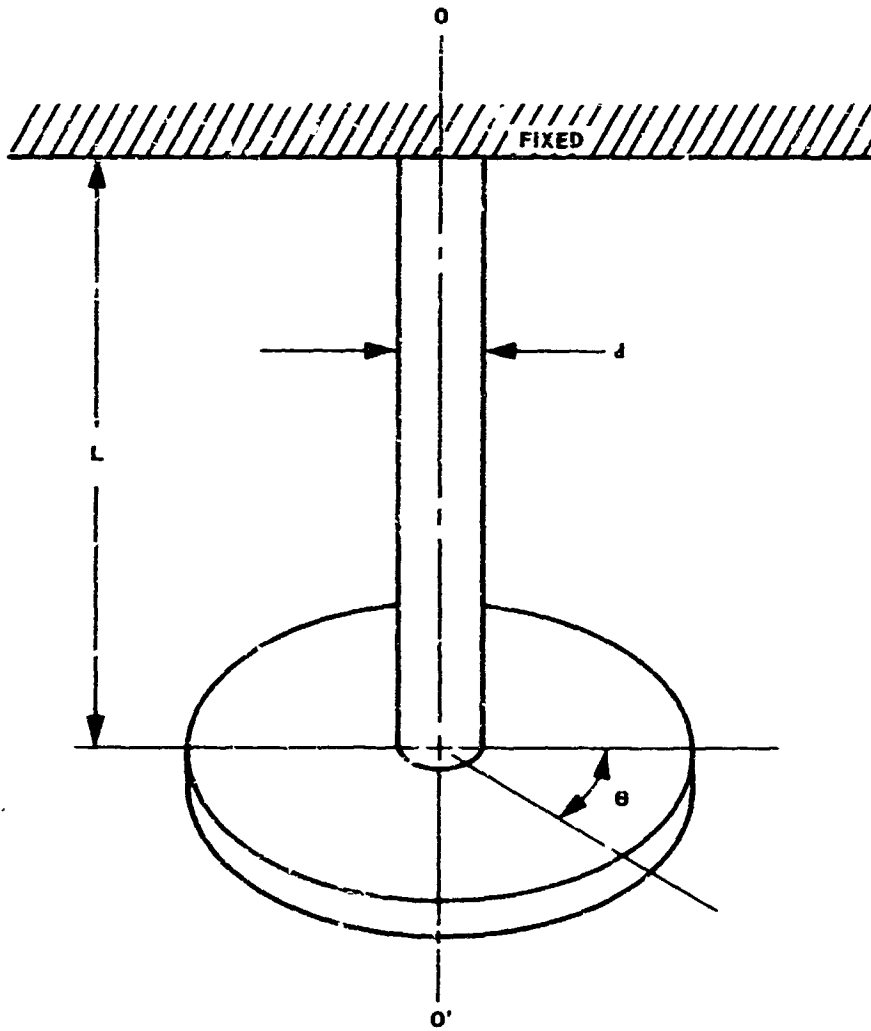


FIGURE A1-1

The development of the expression for the torque and the value of K is obtained from Figure A1-2. The shearing strain is the elongation divided by the length, or $\frac{r\theta}{L}$. For small angles $\phi = \frac{r\theta}{L}$ approximately. Therefore, the strain is approximately equal to ϕ . The torque associated with the force acting over the area of the cylinder of radius r and thickness dr is

$$\begin{aligned} dT &= (\text{Area}) (\text{Stress}) (\text{Distance Arm}) \\ &= (2\pi r dr) \left(\frac{n r \theta}{L} \right) (r) \end{aligned} \quad (\text{A1-7})$$

where the stress is $2n\phi$, and n is the modulus of rigidity.

Therefore,

$$T = \int_0^R 2\pi n \theta \frac{r^3}{L} dr \quad (\text{A1-8})$$

and

$$T = \frac{\pi n \theta R^4}{2L} \quad (\text{A1-9})$$

Let

$$J = \frac{\pi R^4}{2}, \text{ the polar moment of inertia.} \quad (\text{A1-10})$$

Then

$$T = \frac{J n \theta}{L} \quad (\text{A1-11})$$

or

$$T = K \theta \text{ where } K = \frac{J n}{L} \quad (\text{A1-12})$$

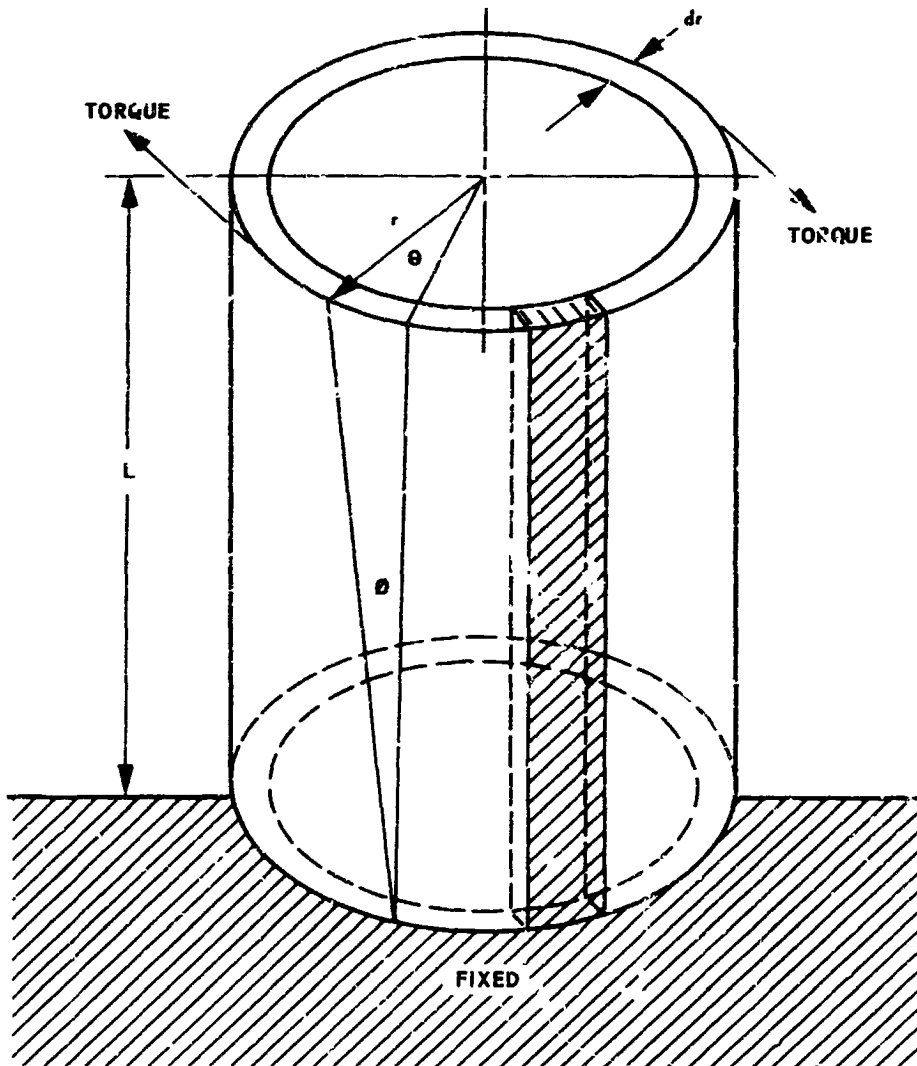


FIGURE A1-2

The equation of motion of a damped torsional pendulum system is

$$I \ddot{\theta} + C \dot{\theta} + K\theta = 0 \quad (A1-13)$$

In solving this equation assume a solution $\theta = e^{bt}$. Now Equation A1-13 becomes

$$(Ib^2 + Cb + K) e^{bt} = 0, \quad (A1-14)$$

and

$$b_{1,2} = \frac{-C}{2I} \pm \sqrt{\left(\frac{C}{2I}\right)^2 - \frac{K}{I}} \quad (A1-15)$$

Now $e^{b_1 t}$ and $e^{b_2 t}$ are both solutions to Equation A1-13. The general solution is

$$\theta = C_1 e^{b_1 t} + C_2 e^{b_2 t}, \quad (A1-16)$$

where C_1 and C_2 are arbitrary constants. Two solutions, real or complex, are possible--depending on the value of $\left(\frac{C}{2I}\right)^2$. If $\left(\frac{C}{2I}\right)^2 > K/I$,

both values of b are real and it can be shown that this solution yields no oscillation but merely a return to equilibrium. For $\left(\frac{C}{2I}\right)^2 = \frac{K}{I}$,

the damping is called "critical damping". For damping less than critical or, $\left(\frac{C}{2I}\right)^2 < \frac{K}{I}$ Equation A1-15 can be rewritten as

$$b_{1,2} = \frac{-C}{2I} \pm j \sqrt{\frac{K}{I} - \left(\frac{C}{2I}\right)^2} \quad (A1-17)$$

Now Equation A1-16 becomes

$$\theta = C_1 e^{\left(\frac{-C}{2I} + jq\right)t} + C_2 e^{\left(\frac{-C}{2I} - jq\right)t} \quad (A1-18)$$

where

$$q = \sqrt{\frac{K}{I} - \left(\frac{C}{2I}\right)^2} \quad (A1-19)$$

Then Equation A1-18 becomes

$$\theta = e^{-\frac{Ct}{2I}} (C_1 e^{jqt} + C_2 e^{-jqt}) . \quad (A1-20)$$

Equation A1-19 can be written as

$$\begin{aligned} \theta &= e^{-\frac{Ct}{2I}} [C_1 (\cos qt + i \sin qt) + C_2 (\cos qt - i \sin qt)] \\ \theta &= e^{-\frac{Ct}{2I}} [(C_1 + C_2) \cos qt + (i C_1 - i C_2) \sin qt] \\ \theta &= e^{-\frac{Ct}{2I}} [C_1' \cos qt + C_2' \sin qt] \end{aligned} \quad (A1-21)$$

where q is defined in A1-19. Using the relationship

$$\sqrt{a^2 + b^2} \sin(\omega t + \phi) = a \cos \omega t + b \sin \omega t$$

Equation A1-21 becomes

$$\theta = A e^{-\frac{Ct}{2I}} \sin(qt + \phi) \quad (A1-22)$$

where

$$A = \sqrt{C_1'^2 + C_2'^2} , \quad (A1-23)$$

is arbitrary and ϕ is arbitrary.

REFERENCES

1. Carpenter, G. T. and Meredith, D. T. : Determining Inertias by Using the Amplitude Decay Rate of a Mechanical Oscillating System. N.A.S.A. T.N. No. D-1114, May 1962.
2. Carpenter, G. T. and Meredith, D. T. : The Derivation of an Efficiency Factor and Its Application to a Torsional System for Determining Mass Moments of Inertia. S. A. W. E. Technical Paper No. 296, May 1961.
3. Den Hartog, J. P. : Mechanical Vibrations, 4th Edition, McGraw Hill, 1956.
4. Gracey, William: The Additional Mass Effect of Plates as Determined by Experimental. N. A. C. A. Rep. No. 707, 1941.
5. Malvestuto, F. and Gale, J. L. : Formulas For Additional Mass Corrections to the Moments of Inertia of Airplanes. N. A. C. A. T.N. No. 1187, 1947.

APPENDIX A2

Torsion Rod Calibration Test Procedure

- PURPOSE:** To determine the spring constants of various torsion rods.
- EQUIPMENT:**
- (1) Overhead "I" beam with leveling plates
 - (2) Photocell timing device
 - (3) Hewlett-Packard 524 D Electronic Counter
 - (4) Hewlett-Packard 560 A Digital Recorder
 - (5) Radian scale, light and mirror arrangement.
 - (6) Dumbbell Standards
 - (7) Torsion Rod
- SET UP:**
- (1) Turn on electronic equipment for warm up.
 - (2) Level leveling plates on "I" beam.
 - (3) Mount rod number ____ to the leveling plates.
 - (4) Attach dumbbell to rod so that the center of the dumbbell is on the vertical axis of the rod.
 - (5) Place the teflon bearing against the rod with minimum of pressure.
 - (6) Place the wand on the dumbbell and align the photocell and light.
 - (7) Place radian scale 140 inches from the center of the air bearing table.
 - (8) With the rod aligned, table leveled, and specimens mounted, zero the wand and photocell device and zero the light source on the radian scale.
- TEST PROCEDURE:**
- (1) Set test up as described in set up.
 - (2) Gradually displace the dumbbell, increasing its amplitude until it reaches 0.05 radians then release the dumbbell and let it decay to 0.035 radians. At 0.035 radians start recording data. Record data until the displacement reaches 0.001 radians.
- DATA:**
- (1) Test No. -
 - (2) Date -
 - (3) Personnel -
 - (4) Temperature -
 - (5) Humidity -
 - (6) Torsion Rod -
 - (7) Dumbbell -
 - (8) Total cycles -
 - (9) Period read out with displacements -

NUMBER OF TESTS:

- (1) Run each test 3 times.
- (2) Record the period every 20 cycles for a 10 period average.
- (3) Record displacement every 0.001 radians.

SPECIAL WORK:

- (1) Plot period vs total cycles for every period recorded. Average the periods between 0.002 and 0.001 radians and record _____.
- (2) Plot period vs displacement at every 0.001 radians.

Written By: _____

Approved By: _____

Date: _____

APPENDIX 43

Moment of Inertia Test Procedure

- PURPOSE:** To determine the moment of inertia of an object by using the air bearing table.
- EQUIPMENT:**
- (1) Government furnished 24 inch air bearing table.
 - (2) Photocell timing device
 - (3) Hewlett-Packard 524 D Counter
 - (4) Hewlett-Packard 560 A Digital Recorder
 - (5) Radian scale, light and mirror arrangement
 - (6) Torsion Rod
 - (7) Test Object
- SET UP:**
- (1) Turn on electronic equipment for warm up.
 - (2) Place the test object on the air bearing table such that its center of gravity is over the center of the table.
 - (3) Set air pressure at 25 psi.
 - (4) Level air bearing table on the iso-pad.
 - (5) Mount torsion rod and align it vertically.
 - (6) Place wand on air bearing table.
 - (7) Place radian scale at 140 inches from the center of the air bearing table.
 - (8) With rod aligned, table leveled, and specimens mounted, zero the wand and photocell device and zero the light source on the radian scale.
- TEST PROCEDURE:**
- (1) Set test up as described in set up.
 - (2) Gradually displace the table, increasing its amplitude until it reaches 0.05 radians then release the table and let it decay to 0.035 radians. At 0.035 radians start recording data. Record data until the displacement reaches 0.001 radian.
- DATA:**
- (1) Test No. -
 - (2) Date -
 - (3) Personnel -
 - (4) Temperature -
 - (5) Humidity -
 - (6) Torsion Rod -
 - (7) Test Object -
 - (8) Total cycles -
 - (9) Period read out with displacements -

NUMBER OF TESTS:

- (1) Run each test _____ times.
- (2) Record period every 20 cycles for a 10 period average.
- (3) Record displacement every 0.001 radians.
- (4) Record total cycles

SPECIAL WORK:

- (1) Plot displacement every 0.001 radians vs period every 0.001 radians to the nearest 0.00001 second.
- (2) Plot period vs total cycles for every period recorded. Average period between 0.002 and 0.001 radians and record _____.
- (3) Plot the \log_{10} of displacement vs total cycles.

Written By: _____

Approved By: _____

Date: _____

APPENDIX A4

Table Load and Air Bearing Pressure Test Procedure

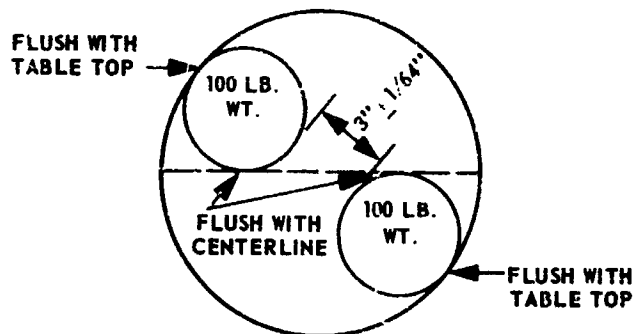
PURPOSE: To determine the effect of various air pressures in the table and various loads on the table.

EQUIPMENT:

- (1) Government furnished 24 inch air bearing table
- (2) Photocell timing device
- (3) Hewlett-Packard 524 D Electronic Counter
- (4) Hewlett-Packard 560 A Digital Recorder
- (5) Radian scale, light and mirror arrangement
- (6) _____ 100 pound cylindrical weights
- (7) Special drag adapter

SET UP:

- (1) Turn on electronic equipment for warm up.
- (2) Insert Rod Number 120, level rod and table on iso-pad. Set air pressure at _____ psi.
- (3) Mount _____ 100 pounds weights on table as shown.



- (4) Place special drag adapter over weights and fasten to table top.
- (5) Place radian scale 140 inches from the center of the air bearing table.
- (6) With the rod aligned, table leveled, and specimens mounted, zero the wand and photocell device and zero the light source on the radian scale.

TEST PROCEDURE:

- (1) Set test up as described in Set Up.
- (2) Gradually displace the table, increasing its amplitude until it reaches _____ radians then release the table and let it decay to _____ radian. At _____ radians start recording data. Record data until the displacement reaches _____ radians.

DATA:

- (1) Test No. -
- (2) Date -
- (3) Personnel -
- (4) Temperature -
- (5) Humidity -
- (6) No. of 100 pound cylindrical weights -
- (7) Total cycles -
- (8) Period read out with displacements -

NUMBER OF TESTS:

- (1) Run each test _____ times.
- (2) Record the period every 20 cycles for a 10 period average.
- (3) Record displacement every _____ radians.

SPECIAL WORK:

- (1) Plot period vs total cycles for every period recorded. Average the periods between 0.002 and 0.001 radians and record _____.
- (2) Plot the \log_{10} of displacement vs total cycles.

Written By:

Approved By:

Date:

APPENDIX A5

Air Drag Test Procedure

- PURPOSE:** To determine the effect of three different drag plates on the decay rate of the air bearing table.
- EQUIPMENT:**
- (1) Government furnished 24 inch air bearing table
 - (2) Photocell timing device
 - (3) Hewlett-Packard 524 D Electronic Counter
 - (4) Hewlett-Packard 560 A Digital Recorder
 - (5) Radian scale, light and mirror arrangement
 - (6) Drag plate number _____
 - (7) _____ 100 pound cylindrical weights
- SET UP:**
- (1) Turn on electronic equipment for warm up.
 - (2) Insert Rod No. 120, level rod and table on iso-pad. Set air pressure at 25 psi.
 - (3) Mount drag plate number _____ on table. Place _____ 100 pound weights on table as shown.

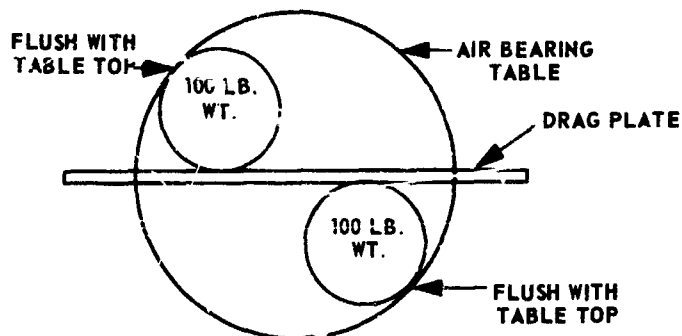


FIGURE A5-1 WEIGHT LOCATION

- (4) Place radian scale 140 inches from the center of the air bearing table.
 - (5) With the rod aligned, table leveled, and specimens mounted, zero the wand and photocell device and zero the light source on the radian scale.
- TEST PROCEDURE:**
- (1) With the test set up as described above the testing is ready to begin.
 - (2) Gradually displace the table, increasing its amplitude until it reaches 0.16 radians then release the table and let it decay to 0.15 radians. At 0.15 radians start recording data. Record data until the displacement reaches 0.001 radian.

DATA:

- (1) Test No. -
- (2) Date -
- (3) Personnel -
- (4) Temperature -
- (5) Humidity -
- (6) Drag Plate No. -
- (7) Number of 100 pound cylindrical weights -
- (8) Total cycles -
- (9) Period read out -

NUMBER OF TESTS:

- (1) Run each test _____ times.
- (2) Record period every 20 cycles for a 10 period average.
- (3) Record displacement every _____ radians.
- (4) Record total cycles

SPECIAL WORK:

- (1) Plot displacement every _____ radians vs period every _____ radians to the nearest _____ second.
- (2) Plot period vs total cycles for every period recorded. Average period between 0.002 and 0.001 radians and record _____.
- (3) Plot the \log_{10} of displacement vs total cycles.

Written By:

Approved By:

Date:

APPENDIX A6

Temperature Effect Test Procedure

- PURPOSE:** To determine the effect of temperature change on moment of inertia determination.
- EQUIPMENT:**
- (1) Government furnished 24 inch air bearing table.
 - (2) Photocell timing device
 - (3) Hewlett-Packard 524 D Electronic Counter
 - (4) Hewlett-Packard 560 A Digital Recorder
 - (5) Radian scale, light and mirror arrangement
 - (6) Dumbbell B-60, 9308 in. -lb-sec²
- SET UP:**
- (1) Set thermostat to desired level and let temperature stabilize over night.
 - (2) Turn on electronic equipment for warm up.
 - (3) Mount dumbbell B on the table top as shown below with its center of gravity located directly over the air bearing tables center point.

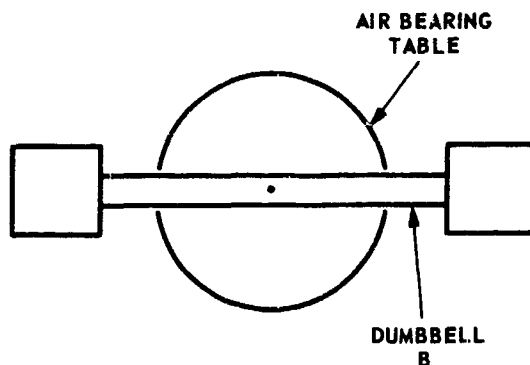


FIGURE A6-1 DUMBBELL LOCATION

- (4) Set air pressure at 25 psi. Insert rod No. 120 level rod and table on iso pad.
- (5) Place radian scale 140 inches from the center of the air bearing table.
- (6) With the rod aligned, table leveled, and specimens mounted. zero the light source on the radian scale.

TEST PROCEDURE:

- (1) With the test set up as described above the testing is ready to begin.
- (2) Gradually displace the table, increasing its amplitude until it reaches 0.05 radians then release the table and let it decay to 0.035 radians. At 0.035 radians start recording data. Record data until the displacement reaches 0.001 radian.

DATA:

- (1) Test No. -
- (2) Date -
- (3) Personnel -
- (4) Temperature -
- (5) Humidity -
- (6) Total cycles -
- (7) Period readout -

NUMBER OF TESTS:

- (1) Repeat each test 3 times.
- (2) Record period every 20 cycles for a 10 period average.
- (3) Record displacement every 0.001 radians.
- (4) Record total cycles.

SPECIAL WORK:

- (1) Plot displacement every 0.001 radians vs period every 0.001 radians to the nearest 0.00001 second.
- (2) Plot period vs total cycles for every period recorded. Average period between 0.002 and 0.001 radians and record _____.

Written By:

Approved By:

Date:

APPENDIX A7
MIA SCHEMATIC DIAGRAMS

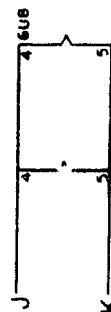


**FIGURE A7-1 MIA 100 KC OSCILLATOR
SHAPE CIRCUITRY**



204

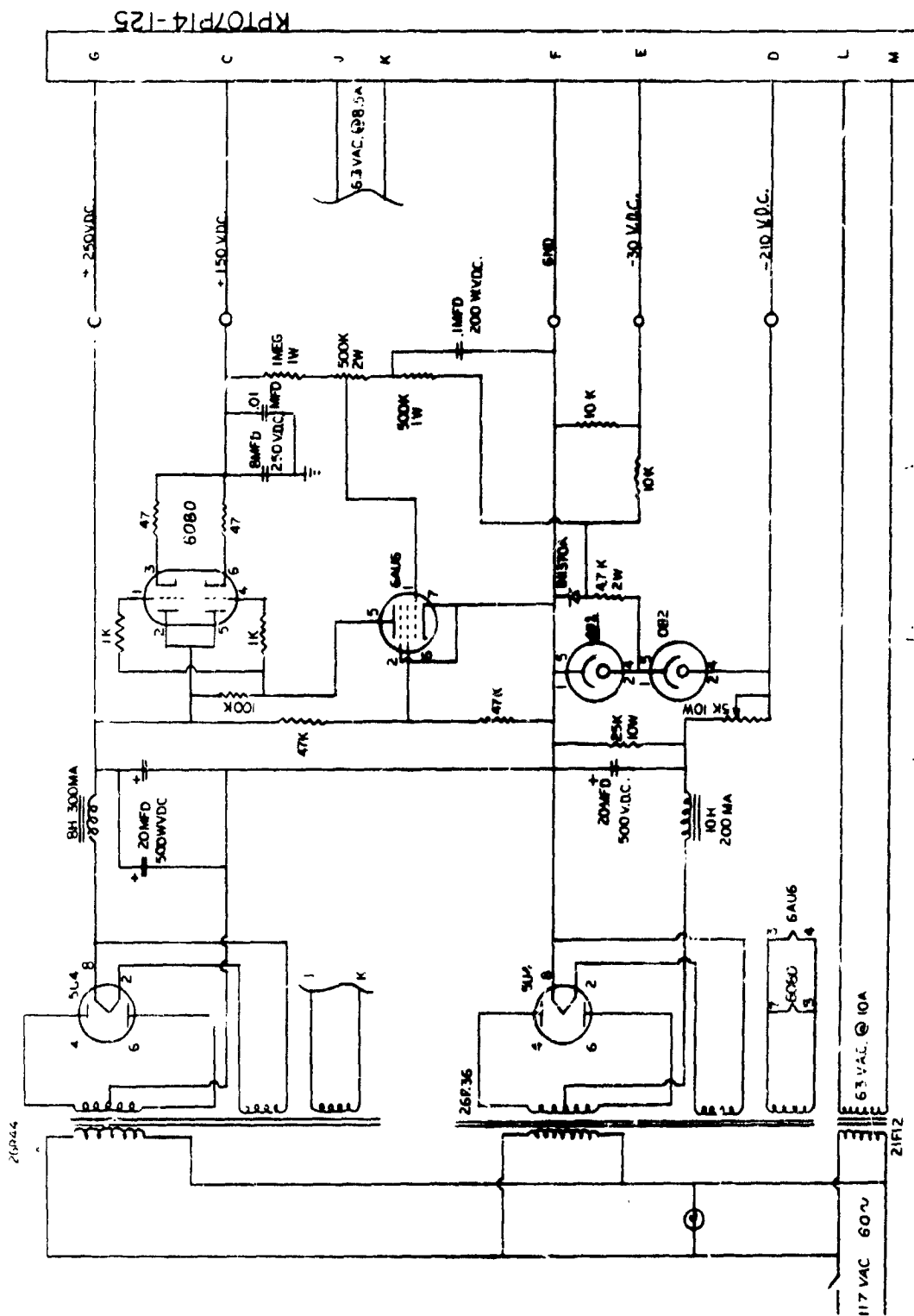
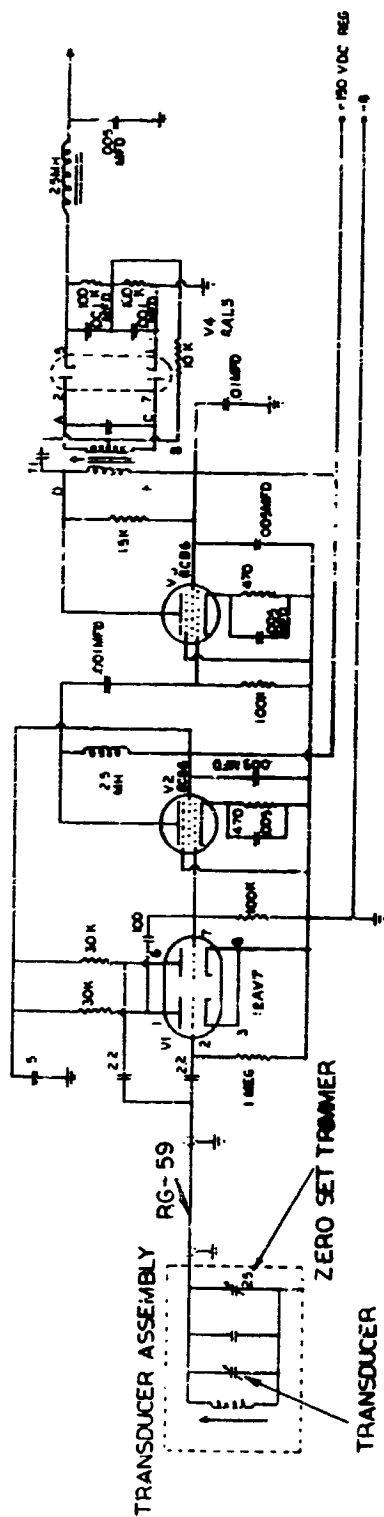


FIGURE A7-3 MIA POWER SUPPLY



TI 45 MC DISCR. XFMR.
MERIT TV 109

ALL CAPACITANCE VALUES IN MICRO-MICRO FARAD EXCEPT WHERE NOTED.

FIGURE A7-4 OSCILLATOR-DISCRIMINATOR CIRCUITRY

APPENDIX A8

Test Procedure for Determining Time Measurement Abilities of Prototype MIA

PURPOSE:

The purpose of this test is to ascertain the time measurement ability of the developed prototype which will be used for determining moments of inertia.

DESCRIPTION OF DEVELOPED PROTOTYPE:

The prototype consists of a capacitive transducer and associated oscillator/discriminator circuitry with amplifiers, which are used to derive a pulse at zero crossing of the oscillating table and thus, start and stop decimal counting units for period time measurement.

LABORATORY ARRANGEMENT FOR TEST EQUIPMENT:

The developed prototype, which has been developed for use with the 6 inch Air Bearing Table, is adjusted so that when the table is at rest, with a torsion rod installed, the output voltage is zero. (This adjustment may be made with a Tripplet 630 Volt-ohm meter or equivalent). The air pressure and particular choice of torsion rods are depicted by the sample data sheet. Other ambient and initial conditions are depicted by the sample data sheet. Other ambient and initial conditions are depicted by this data sheet, including all requirements for data collection.

The existing laboratory photo-electric system, with associated counters, counter-timers, and printers will be utilized to measure the oscillatory period for comparison to the time measured by the prototype. In this arrangement, the time measured by the counters shall be construed as a standard.

As an aid and further explanation as to the equipment arrangement, see Figure A8-1.

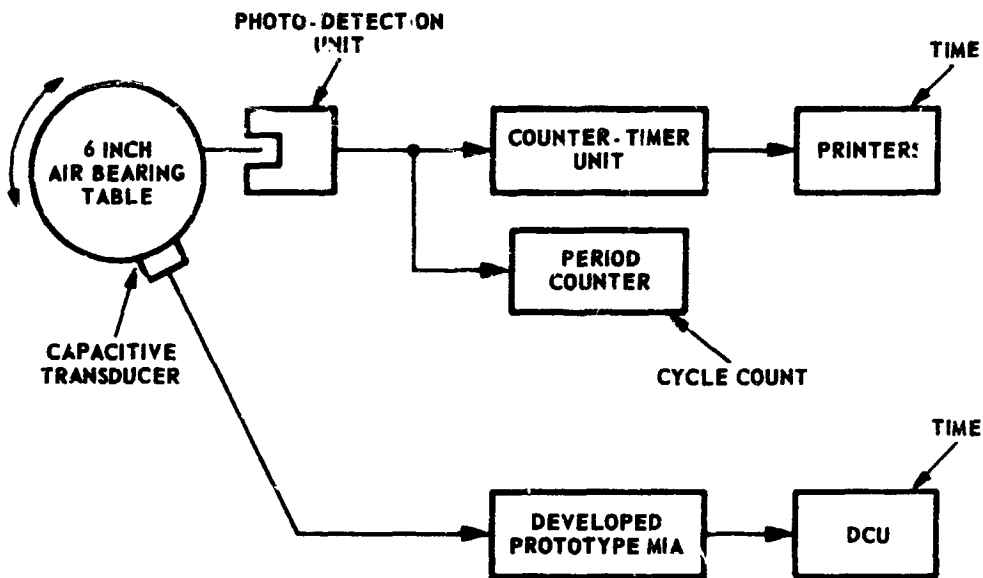


FIGURE A8-1 TEST EQUIPMENT SETUP

REQUIRED EQUIPMENT:

The list of equipment required for accomplishing the described test are included on the test data sheet. Substitutions may be made, but must be recorded, in all cases, except for the prescribed device to be tested. Substitutions should be made with equivalent equipment.

All modifications to the procedure established herein should be recorded in attached sheets, dated, and signed.

Written By: _____

Approved By: _____

Date: _____

APPENDIX B
MASS PROPERTIES OF LIQUIDS

APPENDIX B

MASS PROPERTIES OF LIQUIDS PROGRAM LIST OF REFERENCES AVAILABLE IN THE MASS METROLOGY LABORATORY 24 May 1965

1. Abramson, H. N. & Ransleben, G. E., Some Comparison of Sloshing Behavior in Cylindrical Tanks with Flat and Conical Bottoms, SRI Project 43-768-2, Report No. 4, May, 1959.
2. Abramson, H. N. & Ransleben, G. E., A Note on the Effectiveness of Two Types of Slosh Suppression Devices, SRI Project 43-768-2, Report No. 6, June, 1959.
3. Abramson, H. N. & Ransleben, G. E., A Note on Wall Pressure Distributions During Sloshing in Rigid Tanks, SRI TR-5, SWRI Report 43-768-2, June, 1959.
4. Abramson, H. N. & Ransleben, G. E., A Theoretical & Experimental Study of Fuel Sloshing, SWRI 1251-QPR-7, February 1, 1960.
5. Abramson, H. N., Ransleben, G. E., Chu, Wen-Hwa, & Squire, W., A Theoretical & Experimental Study of Fuel Sloshing, SWRI 1251-QPR-8, May, 1960.
6. Abramson, H. N. & Ransleben, G. E., Simulation of Fuel Sloshing Characteristics in Missile Tanks by Use of Small Models, ARS Journal, July, 1960.
7. Abramson, H. N., Garza, L. R. & Kana, D. D., Liquid Sloshing in Compartmented Cylindrical Tanks, ARS Journal, June, 1962.
8. Abramson, H. N., Chu, Wen-Hwa & Garza, L. R., Liquid Sloshing in Spherical Tanks, AIAA Journal Vol. 1 No. 2 P. 384, February, 1963.
9. Abramson, H. N., Lindholm, W. S., Kana, D. D. and Chu, Wen-Hwa, Research on Liquid Dynamics in Missile Fuel Tanks, TR No. 6, SWRI, Proj. No. 4-961-2, 1961.
10. Baer, H. W., An Approximate Approach to the Prevention of Sloshing of an Incompressible Fluid by Introduction of Mechanical Damping, Ramo-Wooldridge, GM-TM-83, May, 1956.
11. Baron, M. L. & Bleich, H. H., The Dynamics Analysis of Empty and Partially Full Cylindrical Tanks, Part I. Frequencies and Modes of Free Vibration and Transient Response by Modes Analysis, Paul Weidlinger, Consulting Engineer, New York, New York, DASA Contract DA-29-044-X2-557 DASA, No. 1123A, May, 1959.
12. Baron, M. L. & Skalak, R., Free Vibrations of Fluid-Filled Cylindrical Shells, Jour. Eng. Mech. Div., June, 1962.
13. Bauer, H. F., Propellant Behavior in the Tanks of Large Space Vehicles, MTP-AERO-61-81, NASA, MSFC, 1961.
14. Bauer, H. F., The Effect of Propellant Sloshing on the Stability of an

Accelerometer Controlled Rigid Space Vehicle, NASA TN-D-1831, Marshall, October, 1963.

15. Bauer, H. F., Approximate Effect of Ring Stiffener on the Pressure Distribution in an Oscillating Cylindrical Tank Partly Filled with Liquid, ABMA, DA-M-114, Sept., 1957.

16. Bauer, H. F., Fuel Oscillations in a Circular Cylindrical Tank, DA-TR-1-58, April 18, 1958.

17. Bauer, H. F., Fluid Oscillations of a Circular Cylindrical Tank Performing Lissajous-Oscillations, DA-TR-2-58, April, 1958.

18. Bauer, H. F., Fluid Oscillations in a Circular Cylindrical Tank Due to Bending of Tank Wall, ABMA, TR-3-58, April 18, 1958.

19. Bauer, H. F., Fluid Oscillations in a Cylindrical Tank with Damping, DA-TR-4-58, April 23, 1958.

20. Bauer, H. F., The Moment of Inertia of a Liquid in a Circular Cylindrical Tank, DA-TR-5-58, April, 1958.

21. Bauer, H. F., Determination of Approximate First Natural Frequencies of a Fluid in a Spherical Tank, DA-TN-75-58, Oct. 1958.

22. Bauer, H. F., The Effective Moment of Inertia in Roll of Propellant and Roll Damping, DA-TM-67-59, May 26, 1959.

23. Bauer, H. F., Theory of the Fluid Oscillations in a Circular Cylindrical Ring Tank Partially Filled with Liquid, NASA, TN D-557, Dec. 1960.

24. Bauer, H. F., Mechanical Analogy of Fluid Oscillations in Cylindrical Tanks with Circular and Annular Cross Section, MSFC, MTP-Aero-61-1, Jan. 12, 61.

25. Bauer, H. F., Mechanical Analogy of Fluid Oscillations in Cylindrical Tanks with Circular and Annular Cross Section, NASA, MTP Aero 61-4, Jan., 1961.

26. Bauer, H. F., Parametric Study of the Influence of Propellant Sloshing on the Stability of Space Craft, Jour. Aerospace Sc., Oct., 1961.

27. Bauer, H. F., Theory of Liquid Sloshing in Compartmented Cylindrical Tanks Due to Bending Excitation, NASA, MTP-Aero-62-61, July, 1962.

28. Bauer, H. F., The Damping Factor Provided by Flat Annular Ring Baffles for Free Fluid Surface Oscillations, NASA, MTP-Aero-62-81, Nov., 1962.

29. Bauer, H. F., Theory of Liquid Sloshing in Compartmented Cylindrical Tanks Due to Bending Excitation, AIAA Jour. Vol. 1 No. 7, July, 1963.

30. Bauer, H. F., Liquid Sloshing in a Cylindrical Quarter Tank, AIAA Jour. Vol. 1 No. 11, Nov. 1963.

31. Bauer, H. F., Fluid Oscillations in the Containers of a Space Vehicle and Their Influence Upon Stability, NASA, TR R-187, Feb., 1964.
32. Benedikt, E. F., Scale of Separation Phenomena in Liquids Under Conditions of Nearly Free Fall, ARS Journal of February, 1959.
33. Berlot, R. R., Production of Rotation in a Confined Liquid Through Translational Motion of the Boundaries, Jour. App. Mech., Dec., 1959.
34. Bhuta, P. G. & Koval, L. R., Coupled Oscillations of a Liquid with a Free Surface in a Tank Having a Flexible Bottom, Vol. 15, 1964.
35. Brooks, J. E., Dynamics of Fluids in Moving Containers, TRW Space Tech. Labs., GM04.4-26, Feb., 1959.
36. Brooks, J. A., Generalized Missile Dynamic Analysis, VII Programming, STL, GM-TR-0165-00431, April, 1958.
37. Brown, K. M., Laboratory Test of Fuel Sloshing, Douglas Testing Division, Report No. Dev-783, March, 1954.
38. Budiansky, B., Sloshing of Liquids in Circular Canals and Spherical Tanks, Jour. Aero/Space Sciences Vol 27 No. 3, March, 1960.
39. Chobotov, V. & Fowler, J. R., Experimental Investigations of the Moment of Inertia in a Cylindrical Tank, Ramo Wooldridge, Feb., 1957.
40. Chu, Wen-Hwa, Sloshing of Liquids in Cylindrical Tanks of Elliptic Cross Section, SRI, ARS Journal, April, 1960.
41. Chu, Wen-Hwa, Liquid Sloshing in a Spherical Tank Filled to an Arbitrary Depth, SWRI, Report 4, December, 1962.
42. Cole, H. A. & B. J. Gambucci, Measured Two-Dimensional Damping Effectiveness of Fuel-Sloshing Baffles Applied to Ring Baffles in Cylindrical Tanks, NASA, TN D-694, Ames Research Center, Moffett Field, Calif., Feb., 1961.
43. Cooper, R. M., Dynamics of Liquids in Moving Containers, STL, ARS Journal Aug. 1960.
44. Dodge, F. T., A Review of Research Studies on Bubbles Motion in Liquids Contained in Vertically Vibrating Tanks, TR No. 1, SWRI, Proj. No. 1-1391-2, 1963.
45. Dodge, F. T., Kana, D. D. & Abramson, H. N., Liquid Surface Oscillations in Longitudinally Excited Rigid Cylindrical Containers, SRWI, TR-2, NAS-11045, April, 1964.
46. Eulitz, W. R., Theoretical Discussion of the Sloshing Phenomena and Proposed Method for Depressing of Sloshing in Fuel Containers of Missiles, ETC. ABMA, ORD AB DSM-45, Jan, 1957.

47. Eulitz, W. R., Discrepancies with Δp Sensors for Monitoring Liquid Propellant Sloshing Driving Rocket Flight, MT P-P&VE-P-62-6, NASA, MSFC, 1962.
48. Eulitz, W. R., The Sloshing Phenomenon and the Mechanism of a Liquid in Motion in an Oscillating Missile Container, ABMA, DS-R-31, Oct. 30, 1957.
49. Gaza, L. R., A Brief Comparison of Ring and Asymmetrical Baffle Characteristics, SWRI, TR-6, NAS8-1535, April, 1963.
50. Gleghorn, G. J., Motion of Fluid in a Cylindrical Tank, Ramo-Wooldridge Memo, Feb. 7, 1956.
51. Gnaya, T. R. & Abramson, H. N., Measurements of Liquids Damping Provided by Ring Baffles in Cylindrical Tanks, TR No. 5, SWRI, Proj. No. 6-1072-2, 1963.
52. Gray, S. P., Properties of Spheres, Spheroids & Elliptical Lenses Used as Propellant Tanks, MTP-P&VE-F-61-16, Dec. 5, 1961.
53. Gray, S. P. & Burns, R. E., Properties of Toroids with Circular Cross Sections Used as Propellant Tanks, MTP-P&VE-F-62-9, Aug. 1, 1962.
54. Graham, E. W. & Rodriguez, A. M., The Characteristics of Fuel Motion which Affect Airplane Dynamics, Jour. App. Mech., Sept. 1952.
55. Harlow, F. H. and Fromm, J. E., Computer Experiments in Fluid Dynamics, Scientific American, March, 1965.
56. Harvey, T. J., Moment of Inertia of Liquids in Cylindrical Tanks, LMSD-56263, SAWE Tech. P-184, May 19, 1958.
57. Hays, P. J., Stability Analysis of Saturn Block II, S-IV Stage Flight, NASA, MSFC, MTP-Aero-63-27, April, 1963.
58. Hays, P. J., & Sumrall, J. P. Stability Analysis of Saturn SA-5 with Live S-IV Stage, NASA, MSFC, TM X-53017, March, 1964.
59. Heist, E. K., Equations of Motion of Missile with Sloshing, Ramo-Wooldridge, GM-TM-146, Feb., 8, 56.
60. Hieatt, J. L. & Riley, J. D., Digital Program for Fluid Sloshing in Tanks with Axial Symmetry, STL TM-59-0000-000389, Sept. 30, 1959.
61. Holmstrom, J. S., Effect of Dynamic Imbalance on the Motion of a Spinning Vehicle in Free Flight, Chrysler Missile Division, SAE-TN-12-62, April, 1962.
62. Kachigan, K., Forced Oscillations of a Fluid in a Cylindrical Tank, Convair ZU-6-046, Oct., 1955.
63. Kana, D. D., A Resistive Wheatstone Bridge Liquid Wave Height Transducer, SWRI-TR-3, NAS8-11045, May, 1964.

64. Kana, D.D. and Dodge, F.T. Bubble Behavior in Liquid Contained in Vertically Vibrated Tanks, TR No. 4, SWRI, Proj. No. 02-1391, 1964.
65. Karpov, B.G., Experimental Observations of the Dynamic Behavior of Liquid Filled Shell, Report No. 1171, Ballistic Research Labs, Aberdeen, Maryland, August, 1962.
66. Knopp, M., Centrifugal Sloshing, TRW Space Tech. Labs. PA-2297-0212 June, 1959.
67. Kribetsky, Bauer, W.H., Locus, Padlog, Robinson & Walters, Final Report, Report on Zero-Gravity Expulsion Techniques, Bell Aerosystems, Report 7129-733003, NAS r-44, March, 1962.
68. Langer, C.G., A Preliminary Analysis of Optimum Design of Ring & Partition Antislosh Bubbles, RTR No. 4, SWRI, Proj. No. 6-1072-2, 1963.
69. Lawrence, H.R., Wang, C.J. & Reddy, P.B., Variational Solution of Fuel Sloshing Modes, R-W Corp. Jet Propulsion, Nov., 1958.
70. Longuet-Higgins, Mass Transport in the Boundary Layer at a Free Oscillating Surface, Nat. Inst. Oceanography, 1959.
71. Lorell, Jack, Forces Produced by Fuel Oscillations, Jet Propulsion Lab, Progress Report No. 20-149, October 1951.
72. Luskin, H. & Lapin, E., An Analytical Approach to the Fuel Sloshing and Buffeting Problems of Aircraft, Douglas, J. Aero. Sc. Vol. 19 No. 4 April, 1952.
73. Martin, D.G., Control System Equations, Report No. EM 8-14 Space Technology Labs, April, 1958.
74. McCarty, J. L. & Stephens, D.G., Investigation of the Natural Frequencies of Fluids in Spherical and Cylindrical Tanks (Langley) NASA, TN D 252 May, 1960.
75. McKenna, K.J., Palmer, J.L. & Wakamiya, Y., Final Report of Saturn V Control Systems Studies, TRW for NASA, MSFC under NAS8-2635, Feb., 1964.
76. Miles, J. W. & Young, D., Generalized Missile Dynamics Analysis, IV Sloshing, Space Tech. Labs, GM TR-0165-00361, April, 1958.
77. Miles, J. W., Free Surface Oscillations in a Rotating Liquid, Vol. 2 No. 3, The Physics of Fluids, May - June, 1959.
78. Miles, J. W., On the Sloshing of Liquid in a Flexible Tank, Jour. of Applied Mechanics, June, 1958.
79. Miles, J. W., Ring Damping of Free Surface Oscillations in a Circular Tank, Jour. of Applied Mechanics, June, 1958.
80. Moiseev, N.N., On the Theory of Non-Linear Vibrations of a Liquid of Finite Volume, (Moscow) PMM Vol. 22, No. 5, 1958.

81. O'Neill, J. P., Final Report on an Experimental Investigation of Sloshing, Space Technology Labs, STL/TR-59-0000-09960, March 4, 1960.
82. Reissner, E., Complementary Energy Procedure for Vibrations of Liquid Filled Circular Cylindrical Tanks, Ramo-Wool, GM-TR-203, June 19, 1957.
83. Reissner, E., Notes on Forced and Free Vibrations of Pressurized Cylindrical Shells Which Contain a Heavy Liquid with a Free Surface, Ramo-Woolridge, GM-TR-87, November, 1956.
84. Reynolds, W. C., Behavior of Liquids in Free Fall, Journal of the Aero/Space Sciences, Dec., 1959.
85. Sbornik, Statey, Mekhanika, Moskva, 1961.
86. Schmitt, A. F., Forced Oscillations of a Fluid in a Cylindrical Tank Undergoing Both Translation and Rotation, Convair ZU-7-069, Oct., 1956.
87. Schmitt, A. F., Forced Oscillations of a Fluid in a Cylindrical Tank Oscillating in a Carried Acceleration Field- A Correction, Convair, ZU-7-074, Feb., 1957.
88. Schy, A. A., Theoretical Analysis of the Effects of Fuel Motion on Airplanes Dynamics, Report 1080, National Advisory Committee for Aeronautics, Langley Field, Nov. 21, 1950.
89. Sewall, J. L., An Experimental and Theoretical Study of the Effect of Fuel on Pitching Translation Flutter, NACA TN-4166, Dec., 1957.
90. Silveira, M. A., Stephens, D. G. & Leonard, H. W., An Experimental Investigation of the Damping of Liquid Oscillations in Cylindrical Tanks with Various Baffles, NASA, TN D-715, Langley Field, VA. May, 1961.
91. Sloane, M. N., The Dynamics of the Sloshing Phenomenon, STL GM-60-5111-2 Conf.
92. Smith, C. C., The Effects of Fuel Sloshing on the Lateral Stability of a Free-Flying Airplane Model, NACA, RM L8C16, June, 48.
93. Smoot, L. D., Modern Transport Phenomena Can, Chemical Eng., Aug. 21, 1961.
94. Summer, I. E., & Stofan, A. J., An Experimental Investigation of the Viscous Damping of Liquid Sloshing in Spherical Tanks, NASA, Washington, TN D-1991, Dec., 1961.
95. Stephens, D. G., Leonard, H. W. & Silverira, M. A., An Experimental Investigation of the Damping of Liquid Oscillations in a Oblate Spheroidal Tank with and Without Baffles, NASA TN D-808, Langley Field, Va, June, 1961.
96. Stofan, A. J. and Armstead, A. L., Analytical & Experimental Investigation of Forces & Frequencies Resulting from Liquid Sloshing in a Spherical Tank, TN D-1281, NASA, Lewis, 1962.

97. Stofur, A. J., and Pauli, A. J., Experimental Damping of Liquid Oscillations in a Spherical Tank by Positive - Expulsion Bags & Diaphragms, NASA, Lewis, TN D-1311, July, 1962.

98. Townsend, A. A., The Development of Turbulent Boundary Layers with Negligible Wall Stress, Fluid Mech., 1959.

99. Townsend, D., Saturn V Wind Response Studies, MTP AERO 63-63, Sept. 63.

100. Trembath, N. W. Fluid Sloshing in Tanks of Arbitrary Shape, Ramo-Woolridge Corp., G.M. 45 3-378, 28 August 1957.

101. Troesch, B. A., Some New Exact Sloshing Solutions, TRW Space Tech. Labs., STL NN-132, March, 1959.

102. Troesch, B. A., Free Oscillations of a Fluid in a Container, Boundary Problems in Differential Equations, Editor, Langer, R. E., University of Wisconsin Press, Pages 279-299, 1960

103. Warner, R. W. & Caldwell, J. T., Experimental Evaluation of Analytical Models for the Inertias and Natural Frequencies of Fuel Sloshing in Circular Cylindrical Tanks, NASA TN D-856, Moffett, 1961.

104. Wilmayer, E., & Reese, J. R., Moment of Inertia and Damping of Fluid in Tanks Undergoing Pitching Oscillations, Langley, RML53E01a, June, 1953.

105. Young, D., Generalized Missile Dynamic Analysis II - Equations of Motion, STL, GM-TR-0165-00359, April, 1958.

APPENDIX C
CENTER OF GRAVITY

APPENDIX C1

OPTICAL EQUIPMENT TEST Test Procedure I

TEST OBJECTIVE:

To determine the reliable accuracy that can be expected when measuring objects with the optical equipment.

TEST EQUIPMENT:

CALIBRATION DATE:

1. Brunson #76 Optical Telescope and Tooling Bar.

2. Brunson Line Scope (Ser. No. 1172)

3. Surface plate

Level before starting test

4. Accurate specimens to measure

Check dimensions with a micrometer

5. Micrometer

ALIGNMENT PROCEDURE:

A line parallel to the tooling bar is established by adjusting the horizontal rotation of the telescope until two sight-points, on opposite ends of the tooling bar, can be viewed through the main telescope. The sight points must be viewed without further horizontal rotation of the telescope. Viewing the two points on opposite end of the tooling bar is accomplished by vertical rotation of the main telescope. (See Figure C1-1). The horizontal rotation axis is then locked and the main telescope is directed toward the position of the line scope and leveled in this position. (See Figure C1-2.)

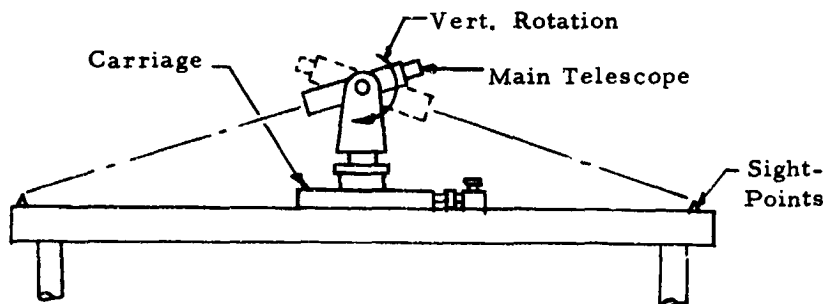


Figure C1-1 Horizontal Alignment Diagram

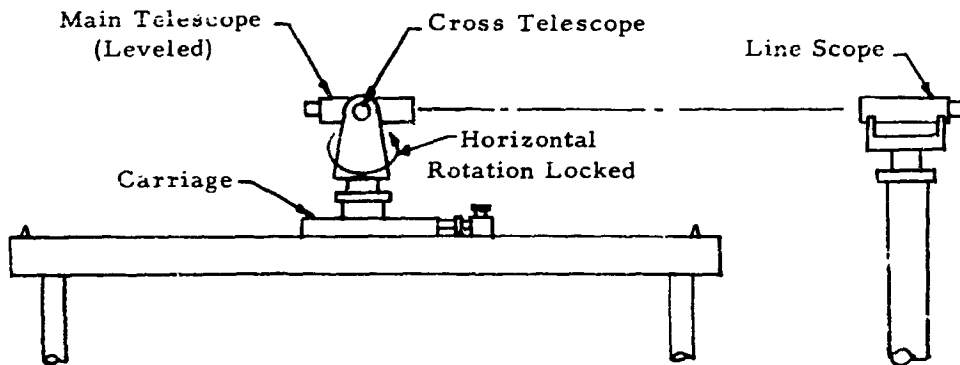


Figure C1-2 Line Scope Alignment

The line scope is then positioned such that its cross hairs of the main telescope. The line scope is now in a position that its line of sight is directed parallel to the tooling bar.

The telescope is then rotated until the cross hairs of the cross telescope are aligned with those of the line scope. The measuring telescope is now viewing perpendicular to the line of travel of the carriage.

When the telescope carriage is re-positioned on the tooling bar, the cross telescope must be re-aligned with the line scope. This procedure insures that the movement of the carriage is done in a parallel line to the tooling bar and that the measuring telescope has been moved in a line perpendicular to parallel planes passing through the two points that are to be measured.

CHECKOUT PROCEDURE:

An accurately graduated scale is placed on the surface plate, leveled, and aligned parallel to the established line of sight of the line scope. Six readings are taken of the carriage position that constituted readings of the 5.000 inch distance.

Other distances, and specimens of accurately known dimensions, should be measured as needed to better establish a system accuracy.

ALLOWABLE ERRORS:

0.0005 inch in telescope position

QUANTITY OF TESTS:

A minimum of six measurements per specimen should be taken.

RESULTS ANALYSIS:

Examination of the error in measuring specimens of known dimensions will show the accuracy to be expected from the optical equipment in measuring objects for center of gravity determination.

Written By:

Approved By:

Date:

APPENDIX C1

OPTICAL EQUIPMENT TEST PROCEDURE II

TEST OBJECTIVE:	To determine the reliable accuracy that can be expected when measuring objects with the optical equipment.
TEST EQUIPMENT:	CALIBRATION DATE:
1. Brunson #76 Optical Telescope and Tooling Bar.	1-22-65 by SPACO Calibration Lab
2. Brunson Line Scope (Ser. No. 1172)	1-12-65 by R-QUAL-OTM
3. Surface plate	Leveled at time of test
4. Brass and Stainless Steel Blocks (ground and polished to 1.500 x 3.000 x 5.000 inches)	Checked with Micrometer at time of test
5. Graduated scale	2-15-65 (MML)
6. Micrometer (4 to 5 inch range)	2-15-65 by SPACO inspection
ALLOWABLE ERROR:	0.0005 inch in reading telescope position on tooling bar
NUMBER OF TESTS:	Six measurements per specimen were taken and recorded
RESULTS ANALYSIS:	<p>Examination of the error column shows that the accuracy of reading the graduated scale is to ± 0.001 inch, where the accuracy in reading the block sizes is only ± 0.002 inch.</p> <p>The process for measuring the blocks was re-examined and the conclusion reached that the additional error introduced was due to the edges of the blocks being more difficult to determine, with the telescope, than the thin, black markings on the graduated scale.</p>
REFERENCE:	Test Procedure I

APPENDIX C2

MIRROR ALIGNMENT SYSTEM TEST PROCEDURE II

TEST OBJECTIVE: To determine the accuracy of the optical equipment in taking measurements when a mirror is used to align the telescope.

TEST EQUIPMENT: CALIBRATION DATE:

1. Brunson #76 Optical Telescope and Tooling Bar
2. Brunson Stellite Mirror (mounted to one end of the tooling bar.) Aligned before test
3. Surface plate for support of test specimens. Level at start of test
4. A brass and stainless steel block. (ground and polished to 1.500 x 3.000 x 5.000 inches) Check with micrometer
5. A graduated scale
6. A micrometer (4 to 5 inch range)

TEST SET UP: Same as in test procedure C2-II, except the Stellite Mirror is used in place of the Brunson #1172 Line Scope.

ALLOWABLE ERROR: 0.0005 inch in reading telescope position.

NUMBER OF TEST: Six measurements per specimen should be taken.

RESULT ANALYSIS: Examination of the error column will show if any additional error is introduced by using the mirror alignment system.

Written By _____

Approved By _____

Date _____

APPENDIX C3

BYTREX SYSTEM PRELIMINARY TESTS IV

TEST OBJECTIVE: To determine the accuracy of locating the center of gravity of objects using the moment detection system. To determine the accuracy of the unbalance moment readings of the instrumentation unit.

EQUIPMENT AND ITS FUNCTION: (1) Moment detection units are used to detect the unbalance of an object placed on a level surface attached to the top of these units. Two separate units were used, a 25 in.-lb and a 250 in.-lb.

(2) The detectors are used in conjunction with an instrumentation and power supply unit. This equipment was manufactured by the Bytrex Corporation.

(3) Depth gages were used to locate the object positions on the moment detectors.

(4) Accurate scales were used to determine the weight of the test objects.

(5) Two test objects of known dimensions and weight were used.

ALLOWABLE ERROR: ± 0.0005 inch in locating the position of test objects on the moment detector heads.

NUMBER OF TESTS: Nine sets of readings were taken using the 250 in.-lb unit. Each reading was taken with the object at a different location on the moment detector.

Fifteen sets of readings were taken using the 25 in.-lb moment detector. More readings were taken with this unit because of its increased sensitivity over the larger detector.

LIST OF EQUIPMENT:	CALIBRATION DATE
CG-25 Moment Detector	8-64
CG-250 Moment Detector	8-64

LIST OF EQUIPMENT: (Con't)

CALIBRATION DATE:

CG-1 Instrumentation Unit	3-64
Mfg. By: Bytrex Corp., Newton, Mass	
Depth Gages	9-64
Scales (Shadowgraph Mod 4173)	9-64

TEST PROCEDURE: Each moment detector must be calibrated with the instrumentation unit before tests are made. The calibration is accomplished by placing a known weight at a known distance from the center of the moment detector.

The instrumentation unit is then adjusted to read this unbalance moment.

The test object is then repositioned a desired number of times to cover the range of the detector. The unbalance reading and the position of the object are then recorded.

Test were made along only one axis. This was sufficient to determine the accuracy of the equipment.

DATA: The data sheets indicate measured and calculated values used in the error analysis.

Included are curves on each moment detector test showing the recorded unbalance moment plotted against the actual unbalance moment.

RESULTS ANALYSIS: The average error of the center of gravity location is 0.009 inch for the 25 in. -lb. detector with an object weight of 6.8122 lbs. and 0.004 inch for the 250 in. -lb. detector with an object weight of 98.71 lbs.

This data indicate, that the center of gravity locations for these objects measured with their respective detector sizes are accurate only to 0.010 inch.

The maximum accuracy of the unbalance moment readings is 0.50% of indication. This compares favorably with the manufacturers value of 1% of indication.

Based on the manufacturers unbalance accuracy of 1%, the object weight would have to be equal to the vertical load capacity of the detector in order to obtain an accuracy of 0.001 inch.

The test results indicate that the respective object weights could be as small as 50% of the detector capacity for this same 0.001 inch accuracy.

SUMMARY: Additional tests are to be conducted to verify the accuracy of center of gravity location for weights approaching the detector capacities and to develop a curve of % error vs object weight.

The manufacturers value of unbalance error should be used in the general application because it will present more reliable results for the average center of gravity locating problem. The data obtained in this test was obtained with unusual care and such care may not be practical in normal applications.

It is suggested that a modification be made to the support stand to allow 90° rotation of the moment detection unit. This will allow the use of an optical measuring system instead of depth gages for location of reference points on the object. This could then be done in two axes without disturbing the position of the test object with respect to the moment detector.

The optical system is desirable because of the capability of measuring accurately to ± 0.001 inch and its versatility for use with irregular shaped objects.

Written By: _____

Approved By: _____

Date: _____

Revision Symbol

Revision Date

Approved By

APPENDIX C4

PROGRAM V

TEST III

Preliminary Test of Bytrex System Using The Optical Equipment for Measurements

TEST OBJECTIVE: To compare the error involved in locating the center of gravity of test objects using the optical equipment for measurements rather than depth gages.

TEST EQUIPMENT: CALIBRATION DATE:

1. C.G. - 25 Bytrex Unit 8-64
C.G. - 1 Instrumentation Unit
2. Brunson #76 Optical Telescope 1-22-65
and Tooling Bar.
3. Brass block 1.500 x 3.000 x . Check with Micrometer
5.000 inches weighing 6.8122 lbs.
(test object.)
4. Micrometer 2-15-65

TEST PROCEDURE: The test object was placed at the desired location on the detector surface that produced an unbalance moment, by calculation, of 80% of detector capacity. The instrumentation unit was adjusted to read this unbalance. One axis was sufficient for the purpose of this test. The test object was repositioned to give unbalance readings at approximately 10% intervals of unbalance from 90% to 10% of the full range of the detector. The unbalance readings and the actual center of gravity of the test object was recorded.

ALLOWABLE ERROR: ± 0.0005 inch in reading the telescope position.

ERROR ANALYSIS:

The data from this test indicates the accuracy when using the optical equipment was 60% better than the accuracy obtained using depth gages.

WRITTEN BY: Ted Williams
Ted Williams, Project Engr.

DATE: 2-28-65

APPROVED BY: Ed Booker
Ed Booker, Director

DATE: 3-1-65

Revision Symbol	Revision Date	Approved By

APPENDIX C5

SPHERICAL AIR BEARING TABLE TEST PROCEDURE

- TEST OBJECTIVE:** To determine the accuracy of the system in location of centers of gravity of test objects.
- TEST EQUIPMENT:**
1. Spherical segment air bearing table.
 2. Brunson #76 Optical Telescope and Tooling Bar.
 3. Test specimen with center of gravity location marks.
- TEST PROCEDURE:**
1. Level the object support surface with no load.
 2. Locate center of rotation of unloaded table and zero telescope at this point.
 3. Place test specimen on surface and move with micrometer positioner until surface is again level.
 4. Read displacement of center of gravity mark from telescope zero point, and record.
 5. Repeat procedure a minimum of three times.

APPENDIX D

NONLINEAR TWIN-T NETWORK CAPACITIVE TRANSDUCER EMPLOYING PRINTED CIRCUIT BOARD CAPACITORS

SUMMARY

This paper presents the derivation and development of a capacitive transducer which is utilized for instantaneous measurements of angular displacements. The transducer is a part of a laboratory test program which employs a tank that oscillates about a horizontal axis.

The transducer employs a twin-T network which converts R. F. energy to direct current energy. The direct current energy is suitable for driving plotters or other analog devices. The entire transducer, including the active capacitor, was fabricated on printed circuit boards, which greatly reduced the effort of developing, installing, and cost of the device.

The transducer produced satisfactory results when its linearity and repeatability was tested. The development of more precise units, utilizing a similar circuit, has been proven.

TABLE OF CONTENTS

Purpose	Page 243
Introduction	243
Electronic Description	243
Mechanical Description	250
Testing Procedure	251
Testing Results	252
Conclusions and Recommendations	252
Bibliography	259
Appendix D-1	261
 <u>Figures and Illustrations</u>	
Figure 1	244
Figure 2	244
Figure 3	245
Figure 4	251
Figure 5	255
Figure 6	256
Figure 7	257

"THE NONLINEAR TWIN-T NETWORK CAPACITIVE TRANSDUCER EMPLOYING PRINTED CIRCUIT BOARD CAPACITORS"

PURPOSE

The purpose of this paper is to illustrate the application and practicality of the capacitive transducer for measuring angular displacement, and to introduce a novel approach for transducer fabrication. The developed unit utilized the nonlinear twin-T network, developed by Tibor L. Foldvari and Kurt S. Lion for conversion of radio frequency energy to direct currents analogous to the amount of angular displacement encountered. A unique method of fabricating capacitor plates for the device is disclosed, as well as a rigorous mathematical derivation of the network employed.

INTRODUCTION

The capacitive transducer offers measurement of displacements of an object without physical contact, and thus resulting friction. The device consists of two or more plates, one of which is movable with the displacement of the object. For angular displacements, it can easily be seen that pie shaped plates, similar to the shape of plates utilized by commercial variable capacitors, would offer a suitable configuration for a capacitance transducer. Other configurations may just as easily be used, but the pie shaped plates offer a simplicity of design, construction, and adjustment which is unsurpassed.

In regard to electrical concepts, the capacitor acts as the active part of the entire transducer. It should be capable of yielding a repeatable electrical signal analogous to a ΔC (change of capacitance) experienced by the capacitor.

Listed below are several methods which utilize the capacitive transducer for displacement measurements:

1. AC voltage division
2. Resonance Methods
3. Frequency Modulation
4. Methods employing voltage rise and fall time in regard to charging
5. Twin-T diode networks.

It is the author's belief that the Twin-T diode circuitry is one of the more electronically stable and simple devices, offering a desirable high output impedance.

ELECTRONIC DESCRIPTION

The network of the capacitive transducer is shown as:

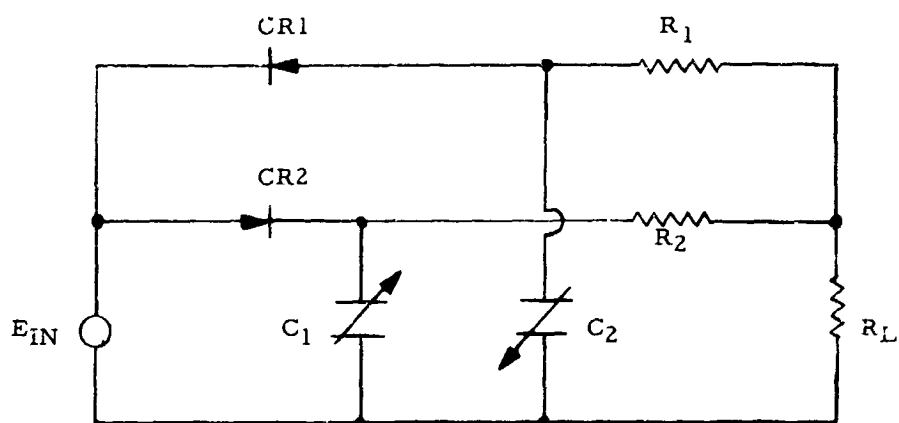


FIGURE 1

where E_{IN} is a chosen radio frequency signal (in this case a square wave generator), CR1 and CR2 are diodes possessing low forward and high reverse resistance, R_1 and R_2 are precision resistors, and R_L is the load resistance of the devices which are used for measuring displacement. The capacitances C_1 and C_2 were designed especially for the selection of other circuit parameters and the angular displacement to be measured. Actually C_1 and C_2 were designed as a differential capacitance device. The unit may be illustrated as:

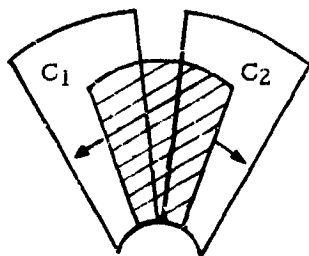


FIGURE 2

where C_1 and C_2 are separate plates of the same area and the shaded plate, which is the common rotating plate to C_1 and C_2 and whose area is the same as C_1 or C_2 plus the area of the air gap between C_1 and C_2 . Thus, the shaded plate exactly covers C_1 or C_2 at maximum displacement, and the plate opposite to the covered plate is completely uncovered.

The advantages of the differential capacitance are:

- (1) A deflection of the shaded plate in the direction of C_1 tends to add capacitance to that portion of the unit by ΔC and subtract the same amount of capacitance, ΔC , from C_2 . Thus, in a balanced

network as the twin-T circuitry, a change of $2 \Delta C$ is acquired, yielding a more sensitive device.

(2) Changes in ambient temperature and humidity do not affect the overall performance of the device, since the change is noted and balanced by the differential capacitance.

(3) By choosing a suitable layout for the capacitors and accompanying circuit, symmetry can be obtained, optimizing the effect of stray capacitance.

(4) Since the capacitors C_1 and C_2 are identical, the effect of fringe capacitance on either circuit should be equal, if all mechanical gapping and spacing of the capacitors are equal.

The network of Figure 1 may be reduced to the following equivalent circuits₂:

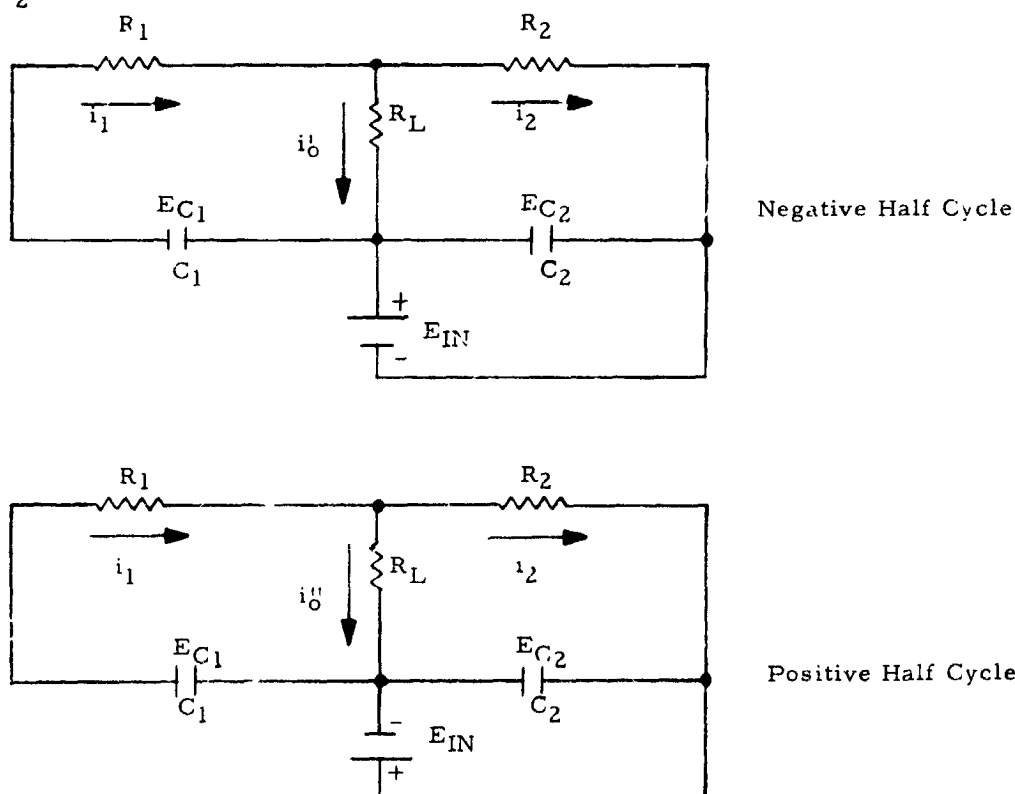


FIGURE 3

These equivalent circuits were constructed from the following assumptions:

(1) The output of the square wave generator is positive during the positive half cycle and negative during the negative half cycle. (In construction of the capacitive transducer system, d.c. restoration to a negative square wave was essential to meet these requirements.)

(2) Diodes CR_1 and CR_2 are ideal diodes, exhibiting zero forward resistance and infinite reverse resistance. (The diodes selected, 1N903A, exhibit a forward resistance of approximately 50 ohms and a reverse resistance of approximately 400 megohms. These diodes were especially selected for these specifications and their capacity to pass radio frequency signals.)

(3) The internal impedance of the square wave generator is negligible. (A Hewlett-Packard Model 211A Square Wave Generator was used to drive the device. The impedance of the generator, as used in the system, was 600 ohms.)

(4) The load of measuring devices on the transducer network is represented by R_L .

From these stipulations and Figure 3, the following expressions are derived:

For the negative half cycle, the following loop equations are derived:

$$E_{C_2} = E_{IN} - i_2 R_2 - i_o' R_L \quad (1)$$

$$E_{C_1} = -\frac{1}{C_1} \int_0^t i_1 dt = i_1 R_1 + i_o' R_L \quad (2)$$

$$\text{but } i_o' = i_1 - i_2, \text{ or } i_1 = i_o' + i_2 \quad (3)$$

$$E_{C_1} = -\frac{1}{C_1} \int_0^t (i_o' + i_2) dt = (i_o' + i_2) R_1 + i_o' R_L$$

$$\text{but: } i_2 = \frac{E_{IN} + i_o' R_L}{R_2}$$

$$\text{Then: } -\frac{1}{C_1} \int_0^t \left(i_o' + \frac{E_{IN} + i_o' R_L}{R_2} \right) dt = \left(i_o' + \frac{E_{IN} + i_o' R_L}{R_2} \right) R_1 + i_o' R_L$$

Simplifying:

$$-\frac{1}{C_1} \int_0^t \left[i_o' + \frac{E_{IN} + i_o' R_L}{R_2} \right] dt = i_o' (R_1 + R_L) + \frac{(E_{IN} + i_o' R_L) R_1}{R_2}$$

$$-\frac{1}{C_1} \int_0^t \left[i_o' + \frac{E_{IN} + i_o' R_L}{R_2} \right] dt = i_o' (R_1 + R_L) + \frac{(E_{IN} + i_o' R_L) R_1}{R_2}$$

Differentiating both sides of equation yields,

$$-\frac{1}{C_1} \left[i_o' + \frac{E_{IN} + i_o' R_L}{R_2} \right] \frac{dt}{dt} = (R_1 + R_L) \frac{di_o'}{dt} + R_L \frac{R_1}{R_2} \frac{di_o'}{dt}$$

Let $R_1 = R_2 = R$

$$-\frac{1}{C_1} \left[i_o' + \frac{E_{IN} + i_o' R_L}{R} \right] dt = [R + 2R_L] di_o'$$

$$-\frac{dt}{C_1} = \frac{(R_1 + 2R_L) R di_o'}{R i_o' + E_{IN} + i_o' R_L}$$

$$\frac{-dt}{RC_1 (R_1 + 2R_L)} = \frac{di_o'}{E_{IN} + R i_o' + R_L i_o'}$$

Multiplying both sides of the equation by $(R + R_L)$

$$\frac{-(R + R_L) dt}{RC_1 (R + 2R_L)} = \frac{(R + R_L) di_o'}{E_{IN} + (R + R_L) i_o'}$$

which is the form $\frac{du}{u}$, where $u = E_{IN} + (R + R_L) i_o'$

Integrating both sides with respect to t ,

$$\frac{-(R + R_L)}{RC_1 (R + 2R_L)} t = \ln \left[\frac{E_{IN} + (R + R_L) i_o'}{E_{IN}} \right] \quad i_o' (t)$$

Evaluating

$$\frac{-(R + R_L) t}{RC_1 (R + 2R_L)} = \ln \left[\frac{E_{IN} + (R + R_L) i_o'}{E_{IN}} \right] - \ln E_{IN}$$

$$\frac{-(R + R_L) t}{RC_1 (R + 2R_L)} = \ln \frac{E_{IN} + (R + R_L) i_o' (t)}{E_{IN}}$$

$$\frac{-(R + R_L) t}{RC_1 (R + 2R_L)} = \ln \left[1 + \frac{(R + R_L) i_o' (t)}{E_{IN}} \right]$$

$$1 + \frac{(R + R_L) i_o' (t)}{E_{IN}} = e^{\frac{-(R + R_L) t}{RC_1 (R + 2R_L)}}$$

$$i_o'(t) = \frac{E_{IN}}{R + R_L} \left[e^{\frac{-(R + R_L)t}{RC_1(R + 2R_L)}} - 1 \right] \quad (4)$$

This equation depicts the instantaneous load current in the negative half cycle.

Using Figure 3 and the stated stipulations leads to a similar solution where

$$i_o''(t) = \frac{E_{IN}}{R + R_L} \left[1 - e^{\frac{-(R + R_L)t}{RC_2(R + 2R_L)}} \right] \quad (5)$$

Since the output current, I_o , is the time average of the instantaneous currents $i_o'(t)$ and $i_o''(t)$

$$I_o = \frac{1}{T} \int_0^T [i_o'(t) + i_o''(t)] dt \quad (6)$$

At this point, it should be clarified that a continuous function does not exist due to the switching performed by the diodes. Thus, the integral should be rewritten as

$$I_o = \frac{1}{T} \int_0^{T/2} i_o'(t) dt + \frac{1}{T} \int_0^{T/2} i_o''(t) dt, \quad (7)$$

where each half cycle is considered as standing alone.

Substituting for $i_o'(t)$ and $i_o''(t)$

$$\begin{aligned} I_o &= \frac{1}{T} \int_0^{T/2} \frac{E_{IN}}{R + R_L} \left[e^{\frac{-(R + R_L)t}{RC_1(R + 2R_L)}} - 1 \right] dt \\ &\quad + \frac{1}{T} \int_0^{T/2} \frac{E_{IN}}{R + R_L} \left[1 - e^{\frac{-(R + R_L)t}{RC_2(R + 2R_L)}} \right] dt \\ &= \frac{1}{T} \left[\frac{E_{IN}}{R + R_L} \right] \left[\left[\frac{-RC_1(R + 2R_L)}{R + R_L} e^{\frac{-(R + R_L)t}{RC_1(R + 2R_L)}} - t \right]_0^{T/2} \right. \\ &\quad \left. + \left[t + \frac{RC_2(R + 2R_L)}{R + R_L} e^{\frac{-(R + R_L)t}{RC_2(R + 2R_L)}} \right]_0^{T/2} \right] \end{aligned}$$

Simplifying and using $T = 1/f$

$$\begin{aligned}
 I_0 = \frac{E_{IN} R_f (R + 2R_L)}{(R + R_L)^2} & \left[-C_1 e^{\frac{-(R + R_L) t}{RC_1 (R + 2R_L)}} \right]_{t=0}^{t = \frac{1}{2f}} \\
 & + \left[t + C_2 e^{\frac{-(R + R_L) t}{RC_2 (R + 2R_L)}} \right]_{t=0}^{t = \frac{1}{2f}} \\
 = \frac{E_{IN} R_f (R + 2R_L)}{(R + R_L)^2} & \left[-C_1 e^{\frac{-(R + R_L)}{2RfC_1 (R + 2R_L)}} - \frac{1}{2f} + C_1 + \frac{1}{2f} \right. \\
 & \left. + C_2 e^{\frac{-(R + R_L)}{2RfC_2 (R + 2R_L)}} - C_2 \right]
 \end{aligned}$$

Further Simplifying

$$I_0 = \frac{E_{IN} R_f (R + 2R_L)}{(R + R_L)^2} \left(C_1 - C_2 - C_1 e^{\frac{-(R + R_L)}{2RfC_1 (R + 2R_L)}} + C_2 e^{\frac{-(R + R_L)}{2RfC_2 (R + 2R_L)}} \right) \quad (8)$$

Equation 8 defines the current flowing through the load for any capacitance value C_1 and C_2 . The voltage across the load may be readily found by the product of I_0 and R_L . The response of the circuit is dependent upon the driving source frequency, in this case 1 megacycle.

Thus, rapid changes of displacement may be measured with such a circuitry.

In the development of this transducer, sensitivity maximization from the transducer was desired. Sensitivity may be defined as

$$S = \frac{\Delta E_0}{\Delta C} \quad (9)$$

where the sensitivity, S , is defined as the increment of voltage measured across R_L divided by the change of capacitance, ΔC , which results. Since E_0 is proportional to I_0 , the following equation results.

$$S_I = \frac{\Delta E_0}{\Delta C} \quad (10)$$

performing this differentiation

$$S_1 = E_{IN} R_f \frac{(R + 2R_L)}{(R + R_L)^2} (1 - e^{-K} - Ke^{-K}) \quad (11)$$

$$\text{where } K = \frac{R + R_L}{2RfC_1 (R + 2R_L)} \quad \text{or} \quad K = \frac{R + R_L}{2RfC_2 (R + 2R_L)} \quad (12)$$

By performing the first derivative test₄, it was found that optimum sensitivity occurs when

$$1/K = .57_5 \quad \text{or } K = 1.75_5$$

It should be noted that at the maximum sensitivity point, frequency source variations of $\pm 10\%$ changes I_0 less than 1%. Hence, frequency stabilization of the generator is not critical, however, amplitude stabilization would naturally be required.

It should also be noted that optimum linearity does not occur at optimum sensitivity. Examination of equation 8 will reveal this fact. Optimum linearity will occur when the exponential terms approach zero. Selection of circuit components and the generator frequency such that this condition exists may be performed at the expense of sensitivity loss. However, the differential capacitance, as utilized has an added advantage that linearity deviations of less than 1% exist when both plates exhibit the same capacitance at balance, or $\Delta C_1 = -\Delta C_2$ of the partial capacitance does not exceed $.5C_1$ or $.5C_2$. (This is to say that each capacitor plate is always at least 1/2 covered, resulting in a loss of sensitivity.)

Appendix A illustrates the solution of the equations for development of the utilized transducer.

MECHANICAL DESCRIPTION

In the mass properties of liquids program, which is currently under study, a record of instantaneous displacement of the oscillating tank used in this program was desired. Since the tank is forced to oscillate about a horizontal axis, a shaft was available for connection of the moving plate of the capacitor as illustrated in Figure 2.

Fabrication of the capacitor was performed in a rather novel manner. The completed circuit was etched on a printed circuit board, thus enabling a neat symmetrical layout with all components mounted to the board. This portion of the transducer was spring floated from a wall of a steel box which completely encapsulates the entire transducer. By spring floating the plates C_1 and C_2 , gapping between C_1 or C_2 and the shaded plate was performed by simple screw adjustments.

The "shaded" plate was attached to the movable shaft of the tank, and precision bearings were utilized on each end of the shaft to provide further mechanical stability, which is a prime requirement.

The entire printed circuit board was gold plated to prevent corrosion. One-eighth inch phenolic board stock was used in fabrication, as an additional aid to mechanical and electrical stability.

It should be noted that the mechanical and electrical parts, including the printed circuit boards, for this device cost less than \$100.00. At an increase in cost, this device could be greatly stabilized, but the accuracy achieved is adequate and the unit was fabricated as a prototype.

TESTING PROCEDURE

After the completion of the unit, the device was attached to the subject tank. A Hewlett-Packard 211A square wave generator was used to excite the transducer and a Moseley 136A X-Y plotter, as the recording device. A block diagram of the equipment arrangement may be illustrated as,

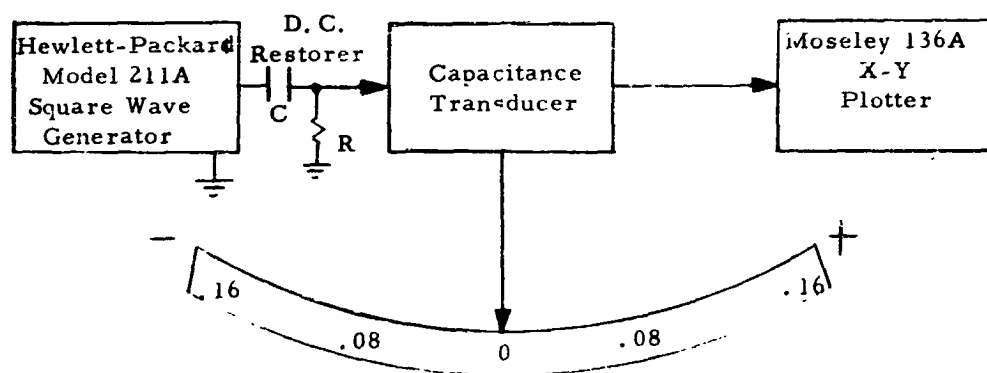


FIGURE 4

This figure illustrates two points which are worthy of mention:

- (1) A radian scale, with pointer attached to the oscillating tank was used as a visual readout of angular displacement.
- (2) A D.C. restorer, of approximately 600 ohms termination impedance was necessary to establish the excitation of the transducer symmetrically about the zero axis, and to provide maximum power transfer from the square wave generator.

An oscilloscope was used to establish the symmetry and frequency of the square wave generator, with a peak-to-peak output of approximately 13.5 volts. The plotter was set-up such that a swing from + .16 radians to - .16 radians covered approximately 6 1/2 inches of an 8 1/2 x 11 graph. This represented a transducer output of approximately ± 1.5 volts from + .16 radians to - .16 radians.

TESTING RESULTS

At definite increments, as shown on Figure 5 and observed visually on the radian scale, lines were drawn by the X-Y plotter which was excited by the transducer device. This figure depicts the linearity of the developed device. Adjustments to the capacitive plates were necessary to obtain the degree of linearity illustrated, which is approximately optimum. Figure 6 depicts "Ideal Vs Measured Linearity", indicating the degree of linearity achieved. Before leaving linearity, one point should be made. Perfect linearity is not essential to a precise measuring system. Certainly it is a desirable attribute; however, calibration charts or curves may be established, as indicated by Figure 5, and the displacements measured to a high degree of precision.

This condition is contingent upon the ability of the device to repeat itself. The repeatability was found to be excellent. With the rather crude visual radian scale employed, no error could be ascertained when attempting to repeat measurements. Actually, there are very few, but sensible reasons, for repeatability deviations:

- (1) A mechanical slippage or change in the capacitive device.
- (2) A change of diode or resistor characteristics.
- (3) A small change of source output voltage, or a large change of source frequency.
- (4) A change of the recording instrument sensitivity.

In a well designed system, all of the above characteristics are unlikely to occur. Certainly long-term changes will occur, but these may be countered by establishing calibration charts periodically.

CONCLUSIONS AND RECOMMENDATIONS

The developed device, which is a very simple electrical system, (See Figure 1) will prove very useful in further evaluation of mass properties of liquids. In practice, the tank illustrated in Figure 7 was filled with a liquid and forced to oscillate. This method is currently being used by this laboratory in evaluating mass properties of liquids. Figure 8 illustrates an actual test

run utilizing the oscillating tank and the capacitive transducer with associated electronic equipment

Other uses of the capacitive transducer are evident. Angular and linear displacements and pressure are currently being measured by capacitive devices. Commercial units are available, one of which has a published ability of measuring $1/2 \times 10^{-6}$ inches. To reiterate, these devices lend themselves readily to dynamic measurements. Configurations may be developed where the subject to be measured acts as an active part of the transducer.

The developed device has generally proven itself on the system employed, and has yielded overall satisfaction. Improvements can be made, however, which would result in overall improved linearity and stability. (It should be emphasized that this device was developed as a prototype unit.) The following is a list of possible improvements which may be incorporated:

- (1) Additional mechanical stability. This is especially applicable to rigidity, which may be achieved by developing a more rigid enclosure, using a precision mechanical couple between the oscillating tank and the capacitive device so as to avoid transmission of horizontal tank motion to the capacitance device, and removing the device from the tank frame. This last operation would avoid the detection of vibrations and oscillations inherent in the tank framework.
- (2) The incorporation of more precision yet rigid capacitor plates. The plates presently used were fabricated as a simple printed circuit board. This board has definite disadvantages, such as deviations in flatness and the "hills and valleys" which must result in the plating process. Such conditions may easily create non-linearity problems. Further, the movable portion of the capacitor could certainly be stabilized in regard to side motions and gapping.
- (3) Side motions of the movable plate, or rotor, may be countered to a degree by the addition of two stator plates which are in parallel, electrically, to C_1 and C_2 . This would nullify the side motion of the rotor plate, since an increase of gapping or spacing between one plate and the rotor would be seen as a decrease of gapping or spacing between the opposite plate, thus, resulting in zero capacitance change for the side motion encountered. The addition of the two parallel plates would greatly complicate the mechanical fabrication.
- (4) Incorporation of a crystal controlled, amplitude regulated square wave generator especially developed for use with a particular capacitance transducer. Even though no detrimental effects have been noted with the Hewlett Packard square wave generator, a more sound engineering approach would be the development of a specialized generator.

(5) Addition of a provision for zero balancing the device with the oscillating tank. Presently, a set-screw- couple arrangement is being used. Due to the sensitivity of the device, this zero adjustment to .001 volts is impossible. A vernier arrangement could be incorporated, which should result in a linearity improvement.

TWIN-T CAPACITIVE TRANSDUCER TEST
FOR LINEARITY & REPEATABILITY
4-14-65

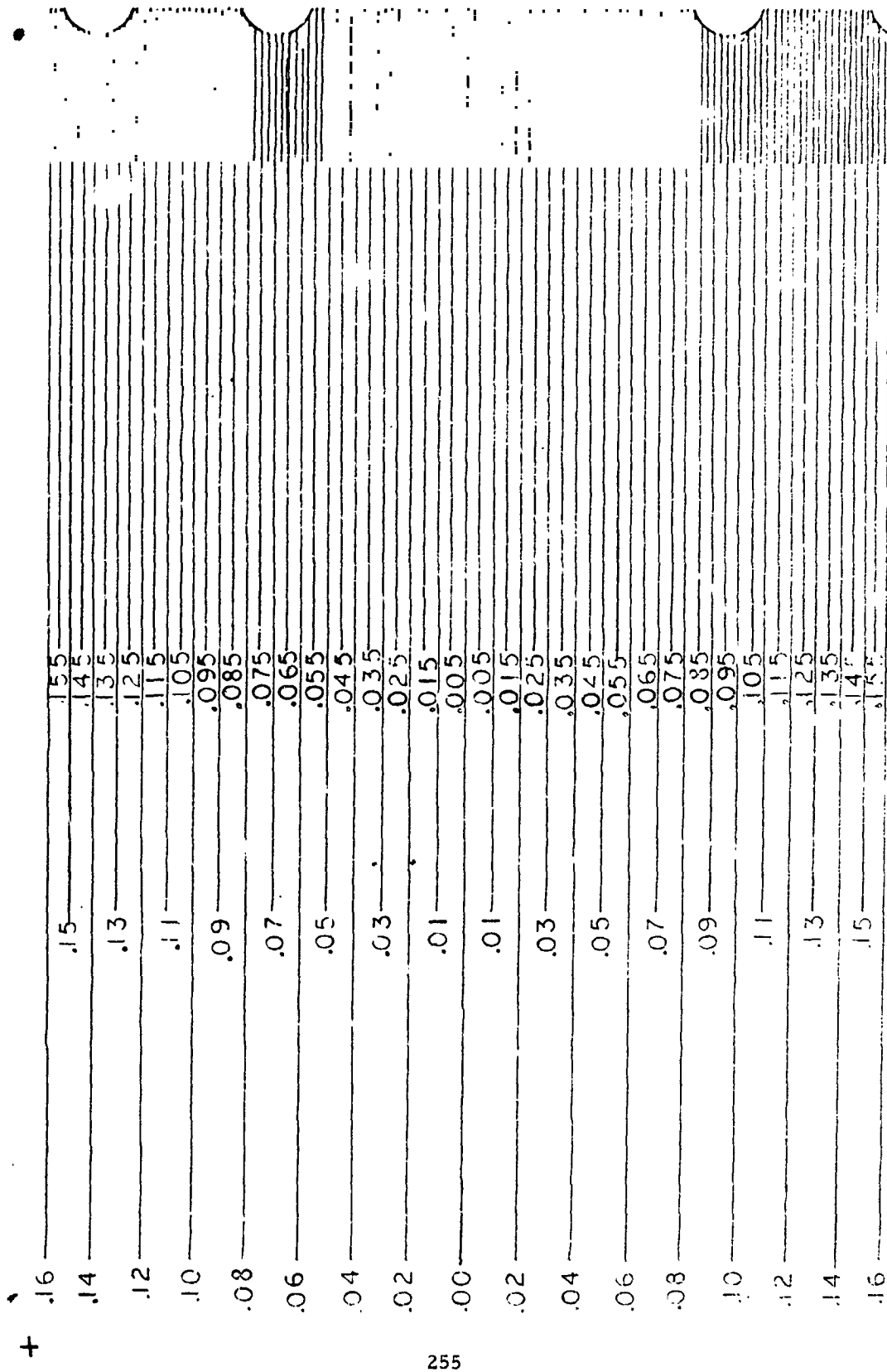


FIGURE 5

Equipment Utilized:
Phototype Capacitive Transducer (SPACO Design)
Hewlett Packard Square Wave Generator 211A (@1MC.)
Moseley X-Y Plotter 136A

SHEET NO. 1 OF 1

JOB NO. NAS 8-11314

NAS 8-11314

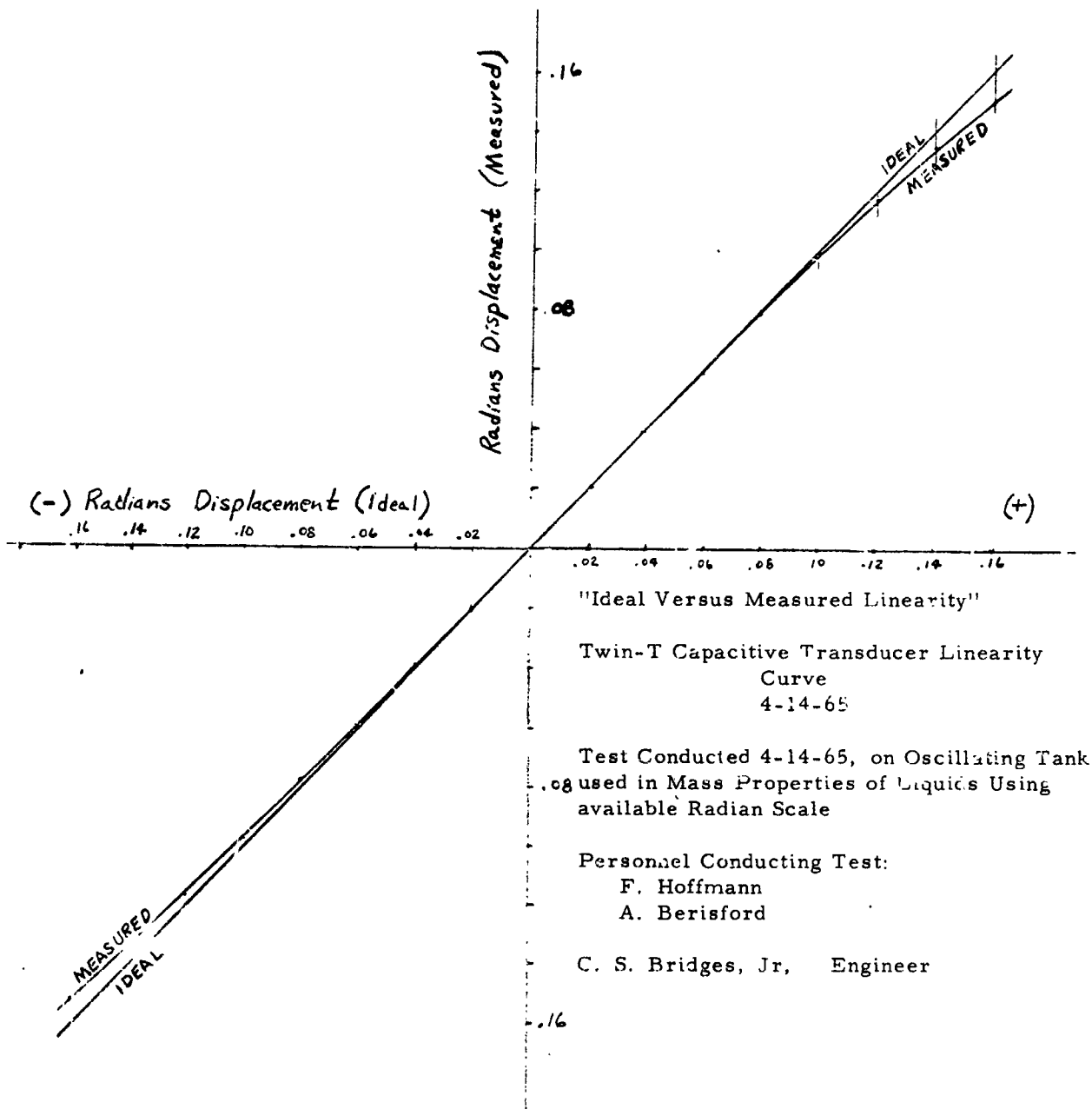


FIGURE 6

IDEAL VERSUS MEASURED LINEARITY

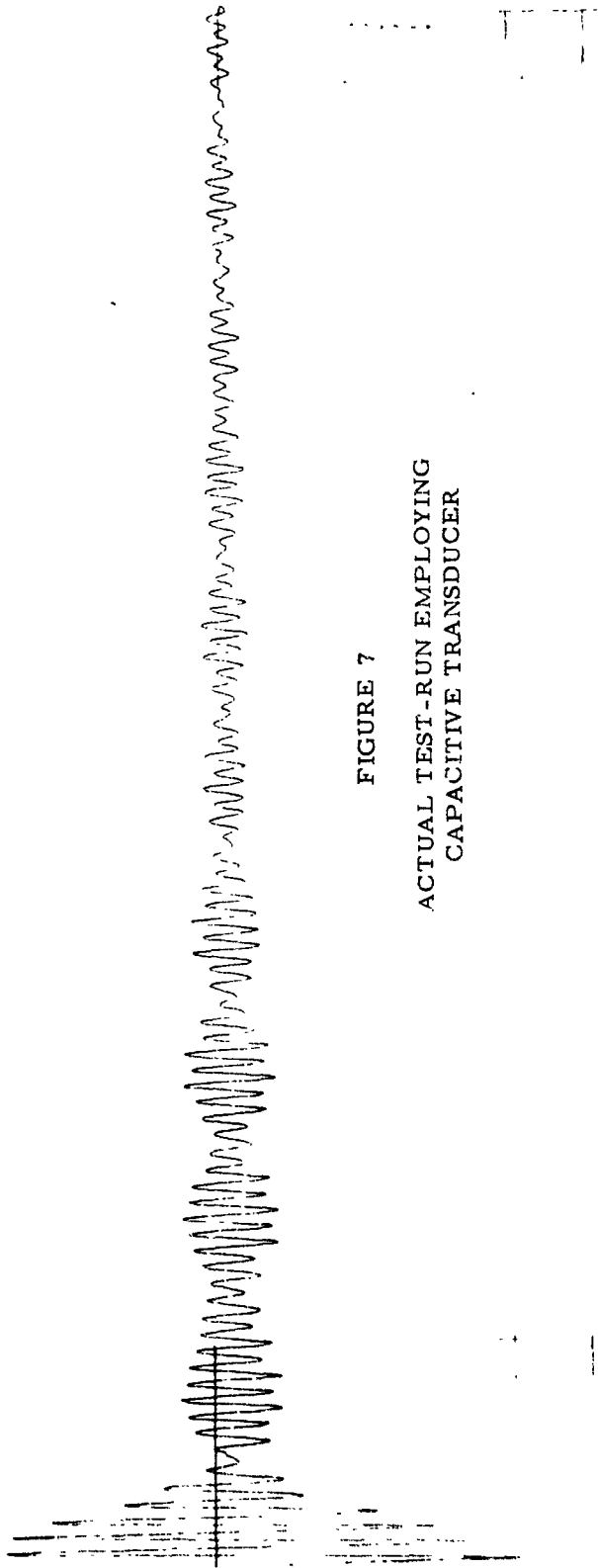


FIGURE 7

ACTUAL TEST-RUN EMPLOYING
CAPACITIVE TRANSDUCER

BIBLIOGRAPHY

1. Tibor L. Foldvari and Kurt S. Lion, Instruments & Control Systems, Vol. 37, Number 11, Page 79, May, 1964
2. Kurt S. Lion, The Review of Scientific Instruments, Vol. 35, Number 3, Page 353, March, 1964.
3. Ibid, Reference 2, page 354.
4. Lloyd L. Smail, Analytic Geometry and Calculus. Pages 133-135. Appleton-Century-Crofts, Inc., New York, 1953.
5. Ibid, Reference 2, page 354.

APPENDIX D-1

Capacitive Transducer Calculations

The following calculations are given as a record of calculations which were necessary in the design of the previously described capacitance device:

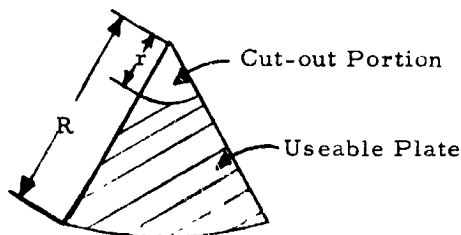
After an evaluation of various loads to the capacitance transducer, an equivalent load, R_L , was computed to be 90.393 ohms.

Further the capacitance of the device as shown in Figure 2 is,

$$C = \frac{(.001963) (\phi) (R^2 - r^2)}{d} \quad (1)$$

where C = the capacitance in pico farad
 ϕ = the angular displacement of the rotor over the stator in degrees
 d = the separation of the rotor and stator in inches

and R and r are length in inches, as shown by the figure,



Equation 1 is derived from the familiar expression,

$$C = .224 \frac{A}{d} \quad (2)$$

where .224 is the dielectric constant,

A = the area of one plate in inch^2
 d = the separation in inches
 and C = the capacitance in farad

Maximum sensitivity was desired. Thus,

$$K_1 = I_2 = K = \frac{R + R_L}{2RfC_1 (R + 2R_L)} \quad \text{Equation 12} \quad (3)$$

where $K = 1.755$

$$\text{or } C_1 = \frac{R + R_L}{2Rf(R + 2R_L)(K)} \quad (4)$$

where $R_L = 90,393$ ohms
 $f = 1$ megacycle, as chosen
 $K = 1.755$
 and C_1 and R are unknowns

By trial and error solution between equations 1 and 4, it was found that when $R = 5,000$ ohms, a practicle capacitance size resulted.

$$\text{so, } C_1 = \frac{(5000 + 90,393) \text{ ohms}}{2(5000 \text{ ohms})(1 \text{ megacycle/second})(1.755)(185,786 \text{ ohms})}$$

$$C_1 = C_2 = 29.26711 \text{ pf} \quad (5)$$

($C_1 = C_2$ since a differential capacitance was used.)

Then from equation 1, letting $d = .025$ inches to minimize fringe capacitance effect, $\phi = 20^\circ$, since the capacitor is half covered (10°) at rest and was designed for a tank swing of 10° , and r was set equal to 1 inch for practicality purposes,

$$C = \frac{(.001963)(20^\circ)}{.025 \text{ inches}} (R^2 - 1) \quad (6)$$

$$R^2 - 1 = \frac{29.26711}{1.5704} \text{ inches}^2$$

$$R^2 = 19.636721 \text{ inches}^2$$

$$R = 4.4313 \text{ inches} \quad (7)$$

Thus, the design of the transducer for the dictated conditions was complete. To complete the calculations and ascertain the output vostage of the device at different angular displacements, the following equations were solved.

$$V_o = E_{IN} \frac{(R + 2R_L)}{(R + R_L)^2} Rf(C_1 - C_2 - C_1 e^{-K_1} + C_2 e^{-K_2}) \quad (8)$$

Equation 8

@ $.1^\circ$ displacement, $C_1 : 10.1^\circ$ and $C_2 : 9.9^\circ$ and deleting units

$$C_1 = \frac{(.001963)(10.1)(18.63672)}{.025} = 14.7799 \text{ pf} \quad (9)$$

$$\text{Similarly, } C_2 = 14.4871 \text{ pf} \quad (10)$$

Then $C_1 - C_2 = .2928$ pf and since

$$1 - e^{-K} = 1 - e^{-1.755} = .8262$$

$$I_o = E_{IN} (10.20821 \times 10^4) (C_1 - C_2) (1 - e^{-K}) \quad (11)$$

Since $E_{IN} = 6.75$ volts,

$$I_o = 16.6895 \times 10^{-8} \text{ amps}$$

Then $I_o R_L = (16.6895 \times 10^{-8}) (90,393) \text{ volt ohms}$

$$I_o R_L = .91523 \text{ volts} \quad (12)$$

Similarly at 10^0 displacement,

$$I_o R_L = 1.5061 \text{ volts} \quad (13)$$

The non-linearity which results from the exponential terms may be observed in equations 12 and 13. By calculation, the maximum linearity deviation is, $100\% - \frac{1.5061}{1.5250} = 1.24\%$.

APPENDIX E

**ELECTRONIC CONCEPTS AND THEORY
EMPLOYED IN BASIC ANALOG COMPUTATION**

PURPOSE

The purpose of this paper is to provide the reader with sufficient information, concerning the analog computer, that he would be able to set up and solve problems with a degree of confidence in understanding the operation and capabilities of the device. This paper will not endeavor to tell the reader how to "patch" a computer. The mechanics of patching or wiring a computer, although differing from one to another, is straightforward and may be best illustrated by an instructor after this paper has been studied.

DESCRIPTION & USE

The analog computer is a simulator. It is not an equation solving machine, whereby numbers are inserted in an equation and the answer is read. Rather, equations are simulated by an analogous electrical circuit, wherein the operator is required to wire or patch the computer in order that the equations may be simulated by the circuits.

Here is where the importance of the analog computer appears.

After the circuit is wired, the engineer now has a mathematical model for original equations. These equations may be concerned with chemistry, mechanical or electrical system, in short, any system which may be described by differential or algebraic equations. Thus, the computer is simulating the real system. The primary value of the computer is realized by simulating and evaluating a system before the system is built.

COMPUTER FUNCTIONS AND COMPUTATIONAL COMPONENTS

The basis of the analog computer is the operational amplifier. This amplifier is capable of summing, multiplying by a constant, multiplying two variables, integration with respect to time, and generation of functions either of dependent or independent variables. In order that the reader may thoroughly understand how the computer operates, and understand what he is doing when he is patching a problem, the following explanations are given.

OPERATIONAL AMPLIFIER

The operational amplifier is a closed loop (current feed-back) electronic amplifier (tube or solid-state) with the following characteristics:

1. Very high open-loop gain (10^7 - 10^8) in D.C. operation
2. High input impedance (Negligible input current drain)
3. Linear over operating range.
4. 180° phase inversion of output versus input signal.

The block-diagram schematic of the amplifier is illustrated in Figure 1.

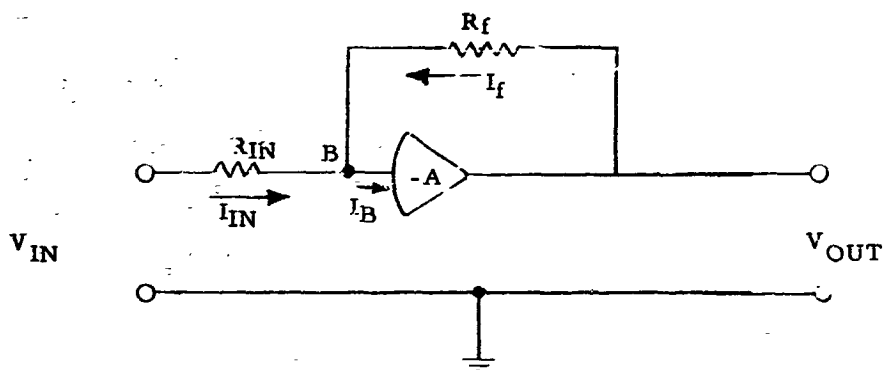


FIGURE 1
BASIC OPERATIONAL AMPLIFIER

From this figure, the current at node B is equal to the sum of the currents entering the node.

$$I_B = \frac{V_{IN} - V_B}{R_{IN}} + \frac{V_{OUT} - V_B}{R_F} \quad (1)$$

But from characteristic (2), $I_B = 0$; and if $I_B = 0$, $V_B = 0$, or the node B is essentially at ground potential.

Therefore Equation 1 reduces to:

$$\frac{V_{IN}}{R_{IN}} = - \frac{V_{OUT}}{R_F}$$

or

$$V_{OUT} = - \frac{R_F}{R_{IN}} V_{IN} \quad (2)$$

This is the equation upon which the entire operation of the amplifier and consequently the computer is dependent. The use of this equation in solution of problems and the simulation of equations will be evident in this paper.

ATTENUATORS

From equation 2, it is apparent that the output voltage of the amplifier may be varied by changing the ratio of the feedback resistance to the amplifier input resistance (R_F/R_{IN}). However, in most computers the selection of R_F and R_{IN} is limited. Therefore, potentiometers are made available in order that the input voltage to the amplifier may be attenuated. This may be illustrated by the following example:

The amplifier illustrated in Figure 2 has a gain of 10.

$$\left[\frac{V_{OUT}}{V_{IN}} = \text{Gain} \right]$$

$$\frac{V_{OUT}}{V_{IN}} = - \frac{R_F}{R_{IN}} = - \frac{100K}{10K} = - 10$$

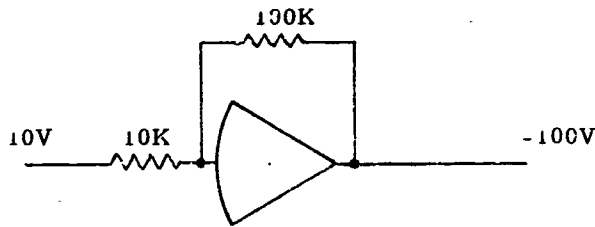


FIGURE 2
SIMPLIFIED OPERATIONAL AMPLIFIER

Thus, with an input of 10V to the amplifier the output voltage equals - 100V. The amplitude of this voltage, in the case of most solid state computers, is too high. So "scaling down" or attenuation of the input voltage must be performed through a potentiometer. For this example, the attenuation of the input signal will be sufficient that the output voltage will equal 5 volts, as shown in Figure 3.

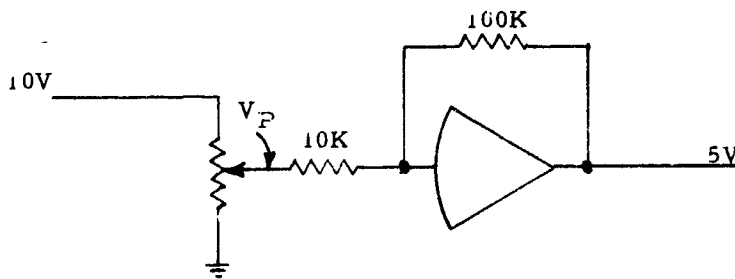


FIGURE 3
ATTENUATION OPERATION

From this circuit, the voltage at point V_P must equal .5 volts, since the gain of the amplifier is 10. The potentiometer circuit is illustrated in Figure 4.

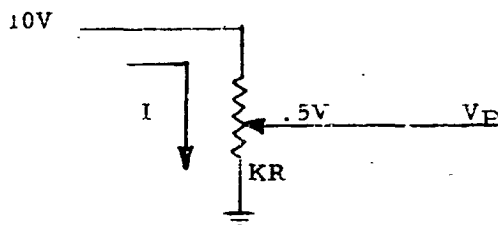


FIGURE 4
POTENTIOMETER VOLTAGE REDUCTION

If the current flowing through the slider to V_P is neglected, $I = \frac{V_{IN}}{R}$, where R is the entire resistance of the potentiometer. Also $V_P = KIR$, where K is the ratio of the resistance from the slider to ground to the total resistance. Thus, K is always less than unity and for analog computer potentiometers, greater than zero. Substituting $I = \frac{V_{IN}}{R}$ into the equation for V_P yields

$$V_P = KV_{IN} \quad (3)$$

It should be noted from the last two figures that the input voltage is referenced to ground. Since all incoming signals are referenced to ground, the ground wire will not be shown in future figures as it was in Figure 1.

From the last example, K , or the pot (potentiometer) setting is $K = .5/10 = .05$. This setting is not exact, since the current flowing through the slider is neglected, but a "ball-park" setting is achieved.

INVERTERS

The operational amplifier, by its own design, is an inverter. From equation 2, the output voltage always has an opposite polarity to the input voltage. Hence, when a sign inversion is desired it is only necessary to make $R_F = R_{IN}$ and a gain of -1 is obtained through the amplifier.

SUMMING

When working with analog computers, many times it is desirable to add or sum several inputs. This manipulation is explained by the following figure and equations:

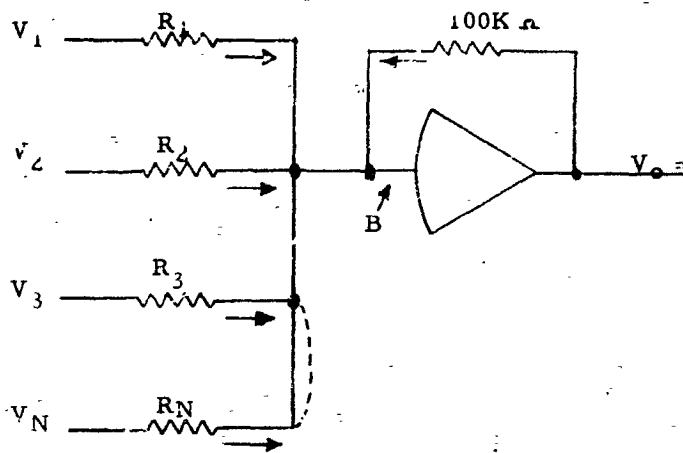


FIGURE 5
SUMMATION FUNCTION

Summing the currents flowing into Node B:

$$\frac{V_1}{R_1} + \frac{V_2}{R_2} + \frac{V_3}{R_3} + \frac{V_N}{R_N} + \frac{V_O}{100K} = 0 \quad (4)$$

Note that there is no current flowing from Node B into the amplifier. This is due to the high input impedance of the amplifier, as previously mentioned.

Simplifying equation 4 in terms of the output voltage V_O yields

$$V_O = - (100K) \left[\frac{V_1}{R_1} + \frac{V_2}{R_2} + \frac{V_3}{R_3} + \dots + \frac{V_N}{R_N} \right] \quad (5)$$

Thus, the amplifier is capable of summing any number of inputs as may be seen from the latter equation.

INTEGRATION

If the feedback resistor ($R_F = 100K$) in Figure 2 is replaced by a capacitor, the circuit shown in Figure 6 evolves.

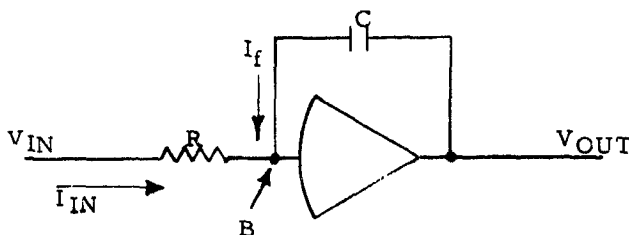


FIGURE 6
INTEGRATION FUNCTION

Again, since the point B is at virtual ground,

$$I_{IN} + I_F = 0$$

then

since

$$\frac{V_{IN}}{R} + C \frac{DV_{OUT}}{DT} = 0$$

$$I_F = C \frac{DV}{DT}$$

$$V_{OUT} = -\frac{1}{RC} \int V_{IN} DT \quad (6)$$

where

$$\text{Gain} = \frac{1}{RC} \quad (7)$$

From equation 6, it may be seen that this circuit functions as an integrator, where the gain of the integrating amplifier is controlled by the choice of R and C, as illustrated in equation 7.

If we assume values of $R = 100K$ ohms and $C = 10 \mu\text{fd}$ or 10×10^{-6} farad, it may be readily seen that the gain of the integrator is equal to unity.

From equation 6, it may be seen that integration is performed as a function of time. Since the only independent variable is time, all dependent variables must be changed to a function of time. Consider the circuit as shown in Figure 7.

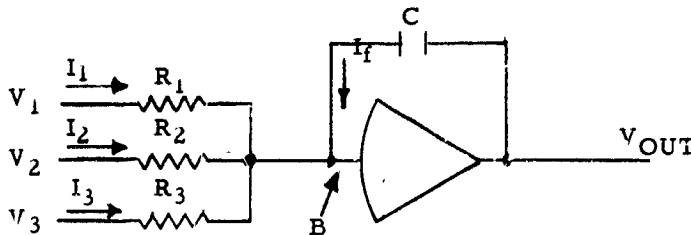


FIGURE 7
INTEGRATION OF SUMMATION

Summing the currents into point B,

$$I_1 + I_2 + I_3 + I_F = 0$$

Substituting,

$$\begin{aligned}\frac{V_1}{R_1} + \frac{V_2}{R_2} + \frac{V_3}{R_3} + C \frac{DV_{OUT}}{DT} &= 0 \\ -DV_{OUT} &= \frac{V_1 DT}{R_1 C} + \frac{V_2 DT}{R_2 C} + \frac{V_3 DT}{R_3 C} \\ V_{OUT} &= - \int \left[\frac{V_1}{R_1 C} + \frac{V_2}{R_2 C} + \frac{V_3}{R_3 C} \right] DT \quad (8)\end{aligned}$$

From this equation, several inputs may be summed and integrated, thus using the amplifier in a dual role.

At this point, the reader may anticipate substitution of a capacitor (or capacitors) in the input circuit and a resistor in the feedback circuit of the amplifier in order that the reverse of integration or differentiation may be performed. This process is not usually performed, since the differentiator is essentially a high pass filter. In other words, the differentiator circuit is capable of passing and differentiating noise and thus, yields an invalid solution.

On the other hand, the integrator is essentially a low pass filter, capable of filtering noise and unwanted signals, thus lending itself nicely to analog computer solutions.

MULTIPLICATION

From the previous sections, it is obvious that multiplication of a quantity or voltage by a constant may be performed by utilizing the gain of the amplifiers and the selection of potentiometer settings.

The analog computer is also capable of multiplication of time varying voltages. This is accomplished through a non-linear circuit by a method known as quarter square multiplication. The identity for quarter square multiplication is:

$$XY = 1/4 \left[(X + Y)^2 - (X - Y)^2 \right] \quad (9)$$

The circuitry for the manipulation of this equation is a gated-resistor application. The circuitry shown in Figure 8 illustrates the quarter square multiplier, which contains four diode/resistor cards.

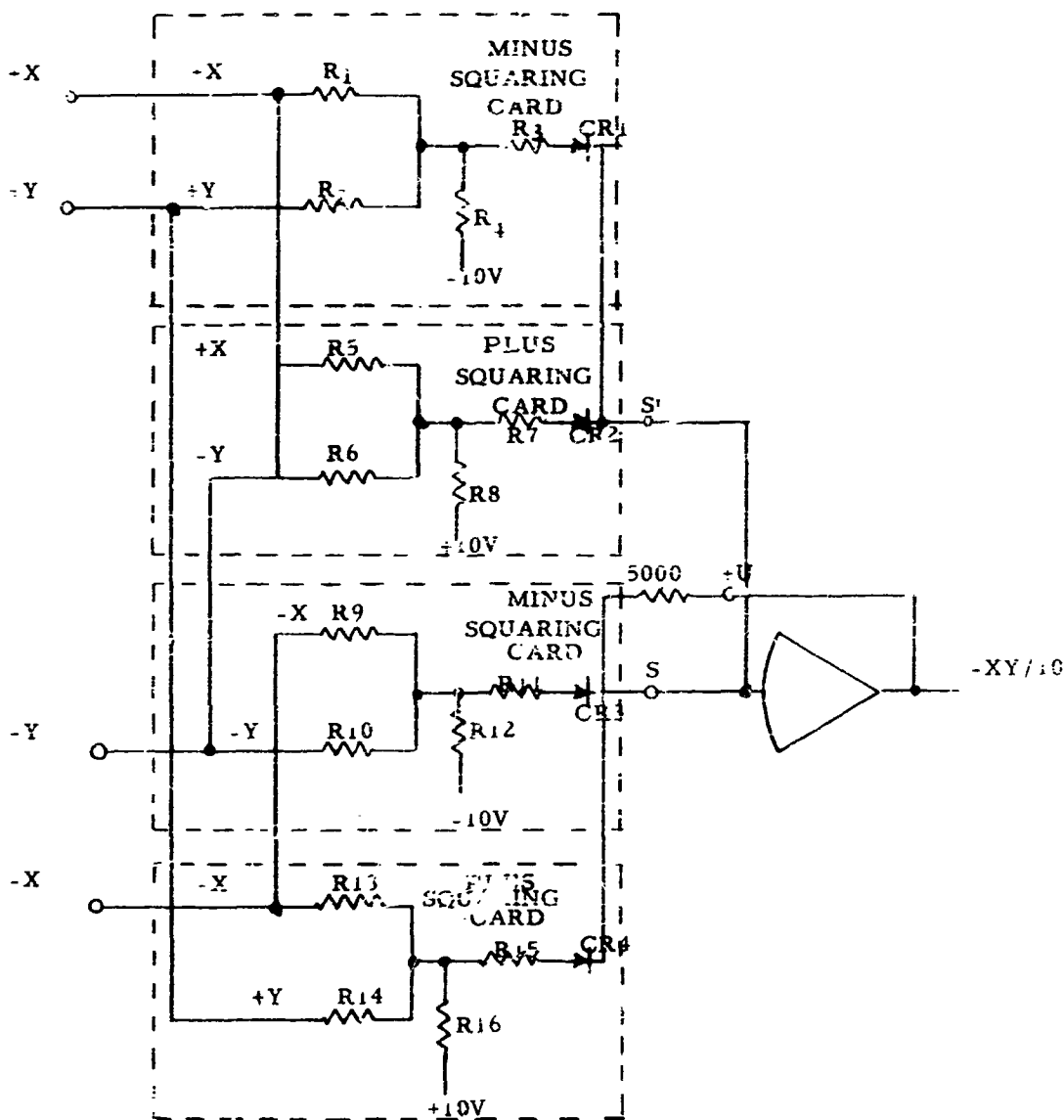


FIGURE 8
SIMPLIFIED QUARTER SQUARE MULTIPLIER

From the figure, each diode is reverse-biased to cutoff at a potential determined by $R3 - R4$, $R7 - R8$, $R11 - R12$, and $R15 - R16$. For any diode to begin conducting, the applied voltages, through the resistance legs $R1 - R2$, $R5 - R6$, $R9 - R10$, and/or $R13 - R14$ must exceed the cutoff voltage of the

diode (s), or the diode breakpoint. By proper selection of the resistors shown in Figure 8, the diodes will conduct at pre-determined values of X and Y thus controlling the output of the amplifier by the quantity of the input voltage.

It may be seen that a sign inversion takes place in this circuit and the resultant product is scaled down by a factor of 10. Therefore,

$$X(Y) = -XY/10 \quad (10)$$

Since the multiplier circuitry has +X, +Y, -X, -Y, inputs, multiplication in all four quadrants may be performed readily. Also by proper selection of the polarity in patching the multiplier, the sign inversion can be nullified, simply by placing +X on the -X input or +Y on the -Y input, or vice versa.

It should be noted that all four inputs (+X, -X, +Y, and -Y) are used in performing multiplication, even though no sign change is experienced during the operation of multiplication.

The identity for the quarter square multiplier was stated to be $XY = 1/4 [(X + Y)^2 - (X - Y)^2]$. In order that the correlation of this equation to the multiplication circuitry may be shown, Figure 8 is further simplified to Figure 9 as,

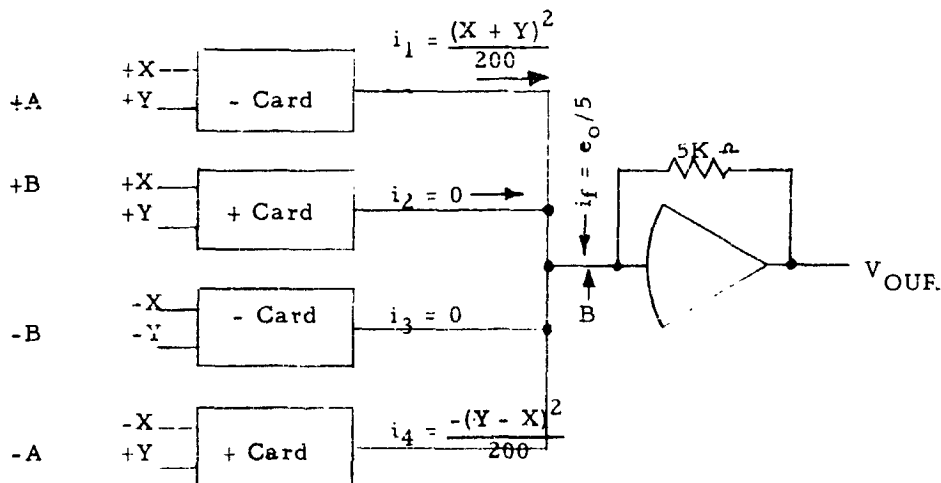


FIGURE 9
MULTIPLICATION FUNCTION

It will be assumed that inputs have been placed on the +A and -A cards. (The +B and -B cards are wired internally to the +A and -A cards, but will not yield a current, due to the assumption of the polarity of the input signals in reference to the card diodes.) It will also be assumed that the resultant current from each driven card is directly proportional to the sum of the inputs squared and inversely proportional to the resultant value of resistance in each card or 200K ohms.

From Figure 9, the summation of currents entering point B is.

$$I_1 + I_2 + I_3 + I_4 + I_F = 0 \quad (11)$$

$$\frac{(X + Y)^2}{200} - \frac{(Y - X)^2}{200} + \frac{V_{OUT}}{5} = 0 \quad (12)$$

$$\frac{X^2 + Y^2 + 2XY - Y^2 - X^2 + 2XY}{200} = - \frac{V_{OUT}}{5}$$

$$\frac{5(4XY)}{200} = - V_{OUT}$$

$$V_{OUT} = - XY/10 \quad (13)$$

This equation substantiates the quarter square multiplication, the inversion of sign, and the scale reduction by a factor of 10.

One precaution must be observed when using the quarter square multiplier. The circuitry must never be fed from a potentiometer. If the circuitry was fed from a potentiometer, an unbalance or change to the resultant card resistances would occur due to the potentiometer resistance, thus, upsetting the circuitry and causing erroneous multiplications.

DIVISION

From the last section of the report, it was seen how the input to an amplifier was controlled by a diode/resistor circuit and the process of multiplication was performed. The reverse of multiplication (division) can be performed by placing this same diode/resistor configuration in the feedback loop of an operational amplifier. The division circuitry is shown in a simplified form in Figure 10.

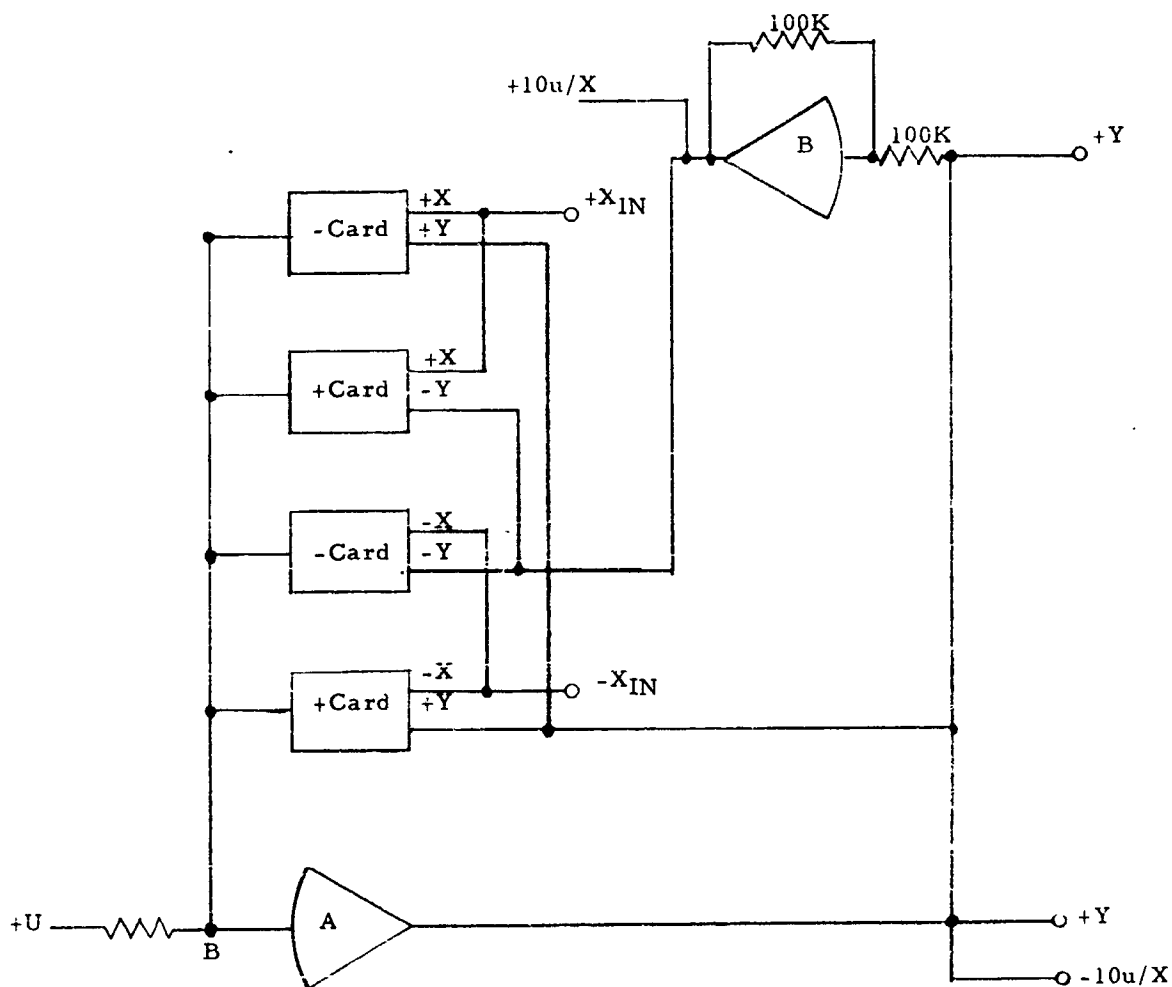


FIGURE 10
SIMPLIFIED DIVISION CIRCUITRY

Recalling the gain equation for the analog computer's operational amplifier is

$$V_{OUT} = -\frac{R_F}{R_{IN}} V_{IN}, \quad (2)$$

the division process may be shown in a system fashion based upon the proof of the quarter square multiplier operation. First the quarter square multiplier

circuit is shown in a block diagram in Figure 11

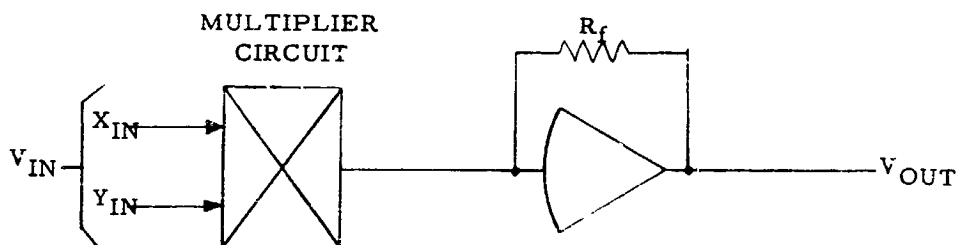


FIGURE 11
MULTIPLICATION DIAGRAM

Now, Figure 10 is further simplified to Figure 12.

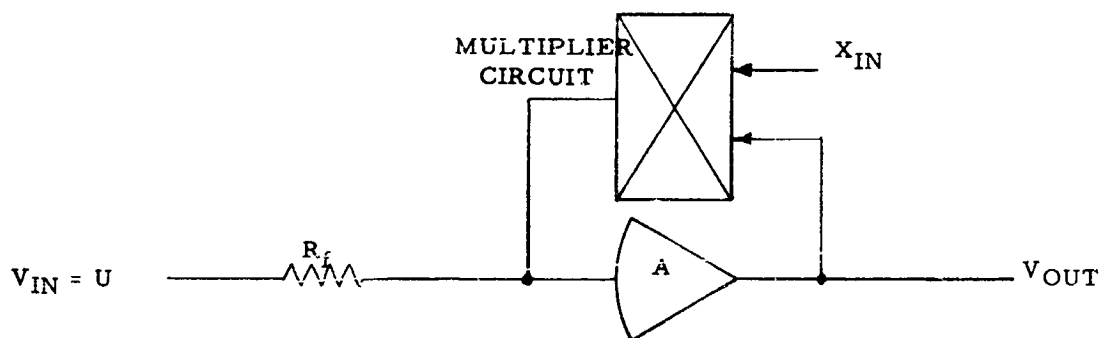


FIGURE 12
SIMPLIFIED DIVISION DIAGRAM

Note that amplifier B, has been omitted in Figure 12, to enable the reader to clearly envision that Figure 12 is the inverse of Figure 11. This may be further shown from the equations,

$$V_{OUT} = V_{IN} \frac{R_F}{R_M} \quad (\text{Multiplier, Figure 11}) \quad (14)$$

$$V_{OUT} = V_{IN} \frac{R_M}{R_F} \quad (\text{Divider, Figure 12}) \quad (15)$$

Thus, R_M/R_F is the inverse of R_F/R_M , proving in a system manner the operation of the division circuitry.

Three rules must be followed in using the division circuitry, as shown in Figure 12, to eliminate saturation of amplifier A.

(1) The divisor $X \geq V_{IN}$. Therefore $V_{OUT} \leq V_{IN}$.

(2) $X \neq 0$

(3) X must be positive. If X is negative, the $+X$ and $-X$ connections must be interchanged.

SQUARING A VARIABLE THAT DOES NOT CHANGE SIGN

The quarter square multiplier circuit may be used to perform the operation of squaring, when the variable to be squared does not change sign. Referring back to Figure 11, if both the X and Y inputs were changed to a single input, X , then the reader may readily understand that X multiplied by X is equal to X^2 . Figure 13 is a simplified version of the squaring circuitry.

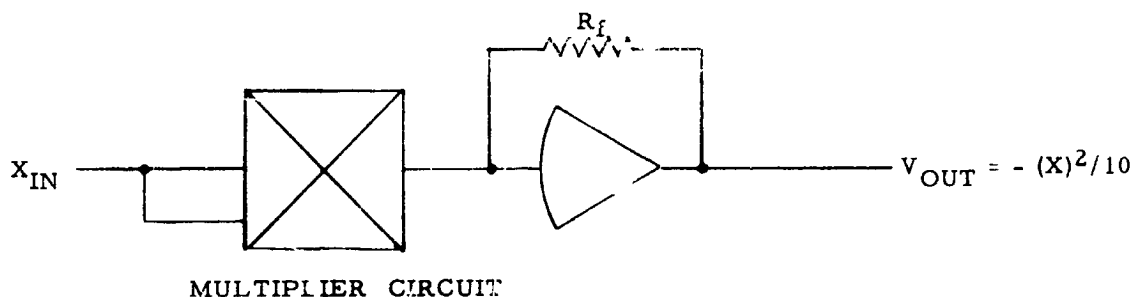
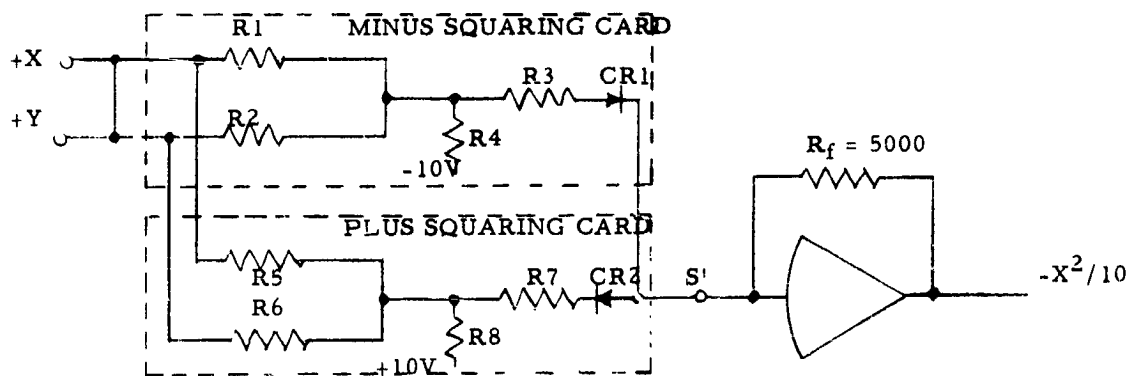


FIGURE 13
SQUARING FUNCTION

As was the case of straight multiplication, an inversion of the sign occurs and the resultant product or square is scaled down by a factor of 10.

Figure 14 illustrates the squaring circuit in more detail.



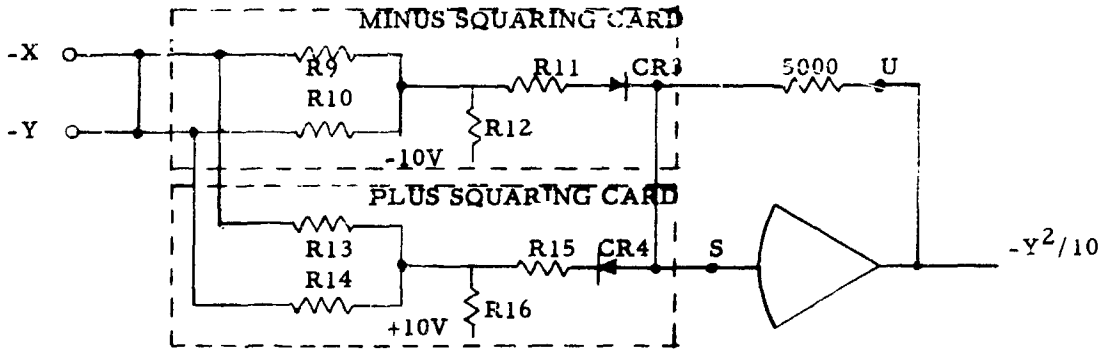


FIGURE 14
SIMPLIFIED SQUARING CIRCUIT

Note from the figure that two operations of squaring may be performed from four cards.

To further illustrate the squaring operation, assume that a +X input is placed on the multiplier +X input. Figure 14 reduces to Figure 15 as,

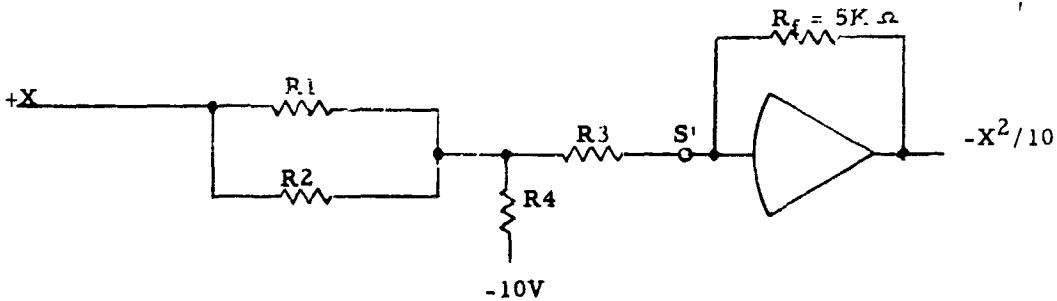


FIGURE 15
REDUCED SQUARING CIRCUIT

Note that a short has been placed across the +X and the +Y input in Figure 14, this short is used in coupling one variable to both the X and Y inputs. (This shorting is done in external computer patching.) Only one card is used for the squaring of the positive quantity X, since the diode CR2 will not pass a current with a positive polarity measured from the +X input to S'. Therefore, a summation of the currents entering S' is, from Equation 12,

$$\frac{(X + X)^2}{200} = -V_{OUT}/5 \quad (16)$$

$$V_{OUT} = \frac{-5(4X^2)}{200} = -X^2/10 = -X|X|/10 \quad (17)$$

proving the operation of the squaring or $X \times X$ capability of this circuit.

The squaring circuit cannot be patched to nullify the sign inversion, since each input (+X and +Y or -X and -Y) is redundant, with only a reversal of the diodes. This enables patching either +X or -X to the +X input and receiving the same absolute value for the square of either input.

SQUARE ROOT

The quarter square multiplier circuit may also be used to obtain the square root. Figure 12 must be modified to perform this operation to,

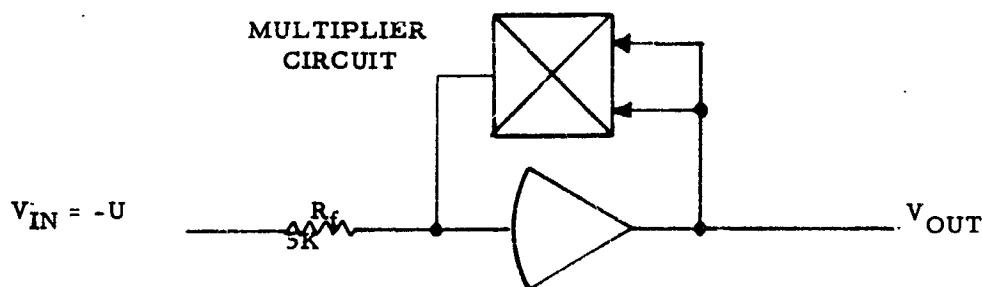


FIGURE 16
SQUARE ROOT EXTRACTION

In this configuration, the multiplier circuitry is connected in exactly the same manner as squaring, except the multiplier is placed in the amplifier feedback loop and the feedback resistance, R_F , is placed in the amplifier input circuitry. Thus, the following equations closely resemble Equations 16 and 17.

Summing the currents into the amplifier,

$$\frac{(V_{OUT} + V_{OUT})^2}{200} - \frac{U}{R_F} = 0 \quad (18)$$

$$\frac{(4 V_{OUT}^2)}{200} = + \frac{U}{5}$$

$$V_{OUT}^2 = U \quad (19)$$

$$V_{OUT} = \sqrt{10U} \quad (19)$$

If the input V_{IN} had been +U,

$$V_{OUT} = -\sqrt{10U} \quad (20)$$

These equations show the operation of square rooting, and the close electrical correlation to squaring. Since the multiplier circuit in patching and operation is not changed, a more detailed schematic of the square rooter will not be shown.

The square root circuitry, like the square circuitry, is redundant, so that the input sign is always the opposite of the output sign. Like the square operation, each multiplier unit is capable of handling two different square root extractions simultaneously, since only two cards are needed for each operation, and four cards are available in each multiplier unit.

OTHER NON-LINEAR COMPUTER CIRCUITS

The analog computer may be equipped with other diode function generators. These diode function generators are all similar to the quarter square multiplier; in that, diode gates are reverse biased so that the input voltage must be a discrete level before the diodes will begin conduction. This conduction causes the feedback impedance to input impedance ratio of the operational amplifier to change, varying the gain of the amplifier.

Three of the available fixed function type generators are:

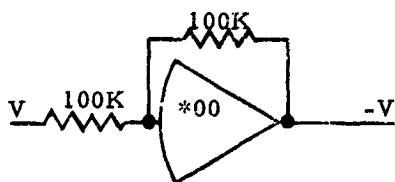
- (1) X^2
- (2) $\text{Log } X$
- (3) $1/2 \text{ Log } X$

A variable function type generator is also available. This generator utilizes the same Z_F/Z_{IN} relationship of the fixed function generator to approximate a curve with straight line-segments. The variable diode function generator provides a means, with a single quantity possibly obtained from experimental data, of generating variables which are a function of this data.

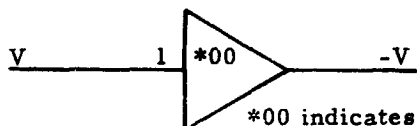
COMPUTER SCHEMATICS AND SYMBOLS

Computer diagrams are used in patching the analog computer. These computer diagrams use computer "symbols" which are abbreviated forms of the previously illustrated schematics. The computer diagrams and symbols are a history or an explanation of the patching for a particular problem. The engineer should never attempt to solve a problem on the analog computer without first making a diagram of the problem. For this reason, the following symbols are explained -

①.



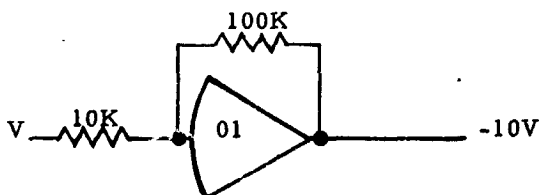
Inverter
Schematic



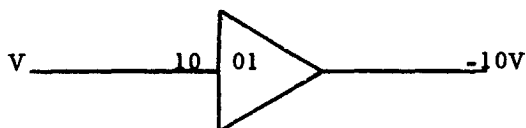
Inverter
Symbol

*00 indicates Amplifier Number

②.

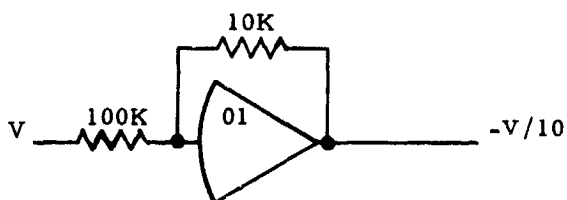


Multiplication
by -10
Schematic

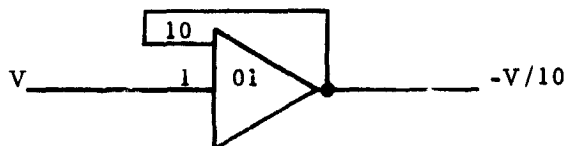


Multiplication
by -10
Symbol

③.

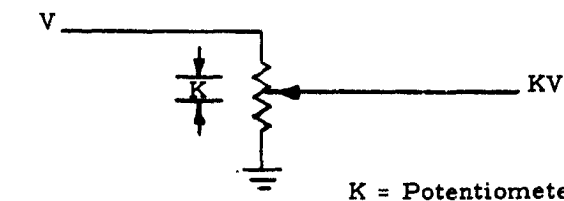


Multiplication
by -1/10
Schematic



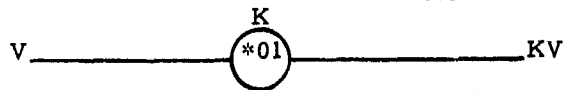
Multiplication
by -1/10
Symbol

④.



Grounded
Potentiometer
Schematic

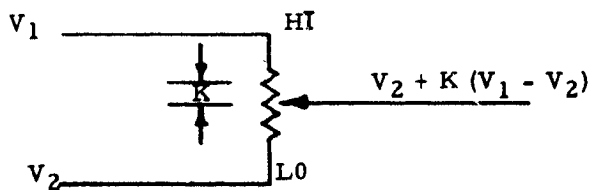
K = Potentiometer Setting



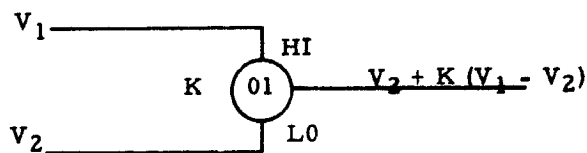
Grounded Potentiometer
Symbol

*01 indicates Potentiometer Number

5.

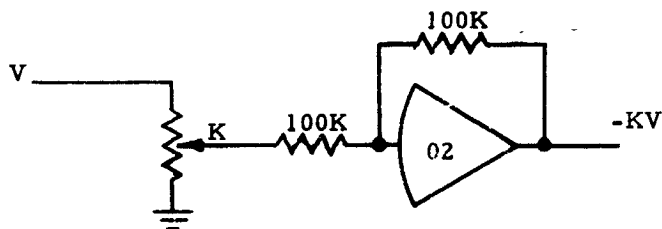


Ungrounded
Potentiometer
Schematic



Ungrounded
Potentiometer
Symbol

6.

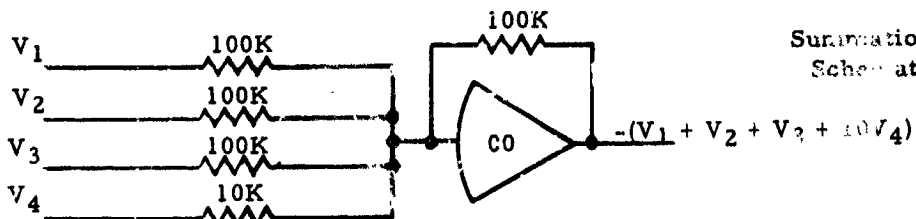


Multiplication
by -K
Schematic

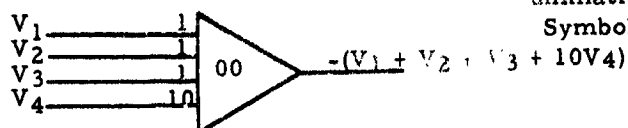


Multiplication
by -K
Symbol

7.

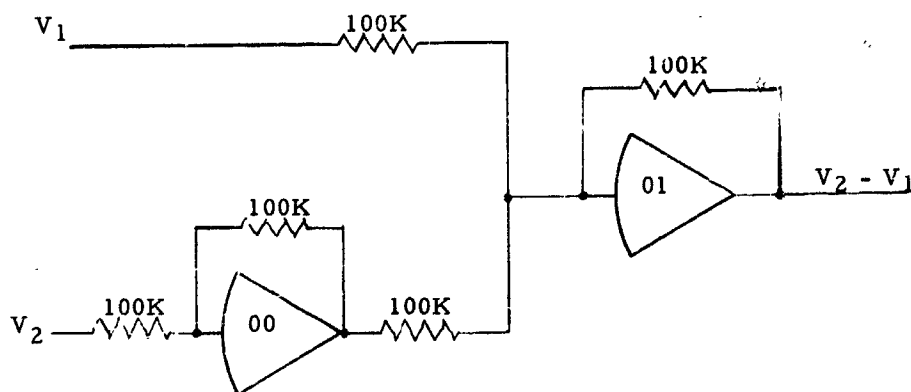


Summation
Schematic

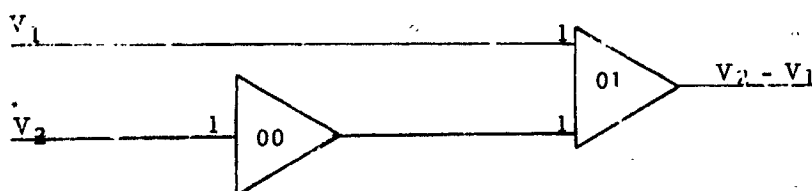


Summation
Symbol

⑧.

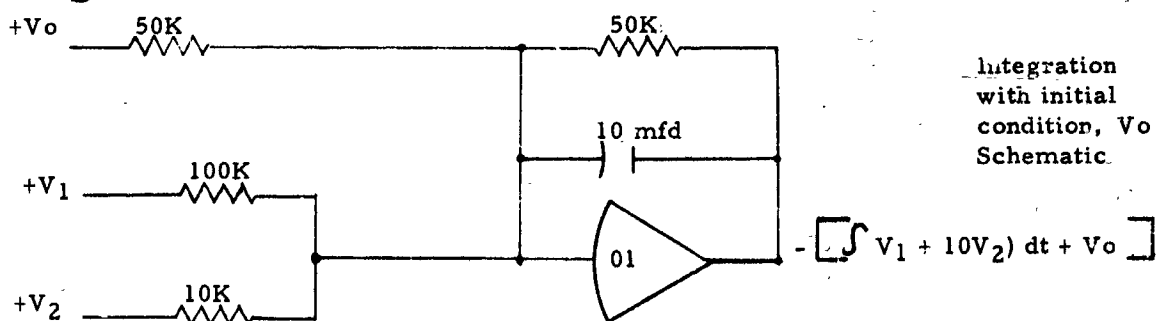


Subtraction
Schematic

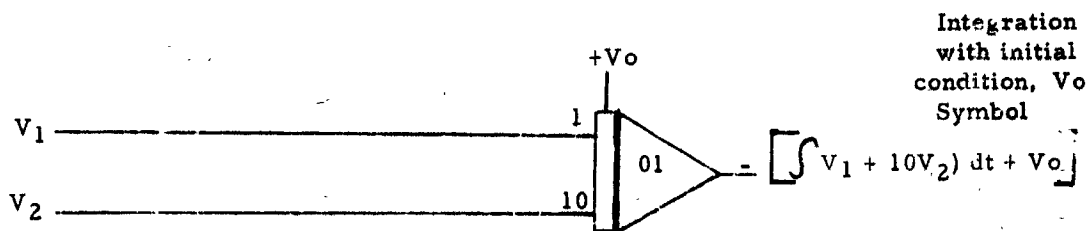


Subtraction
Symbol

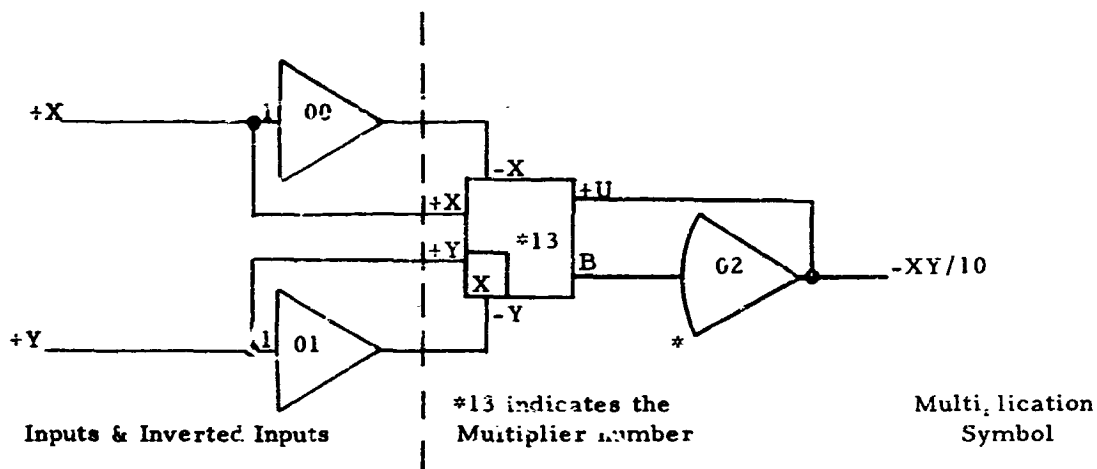
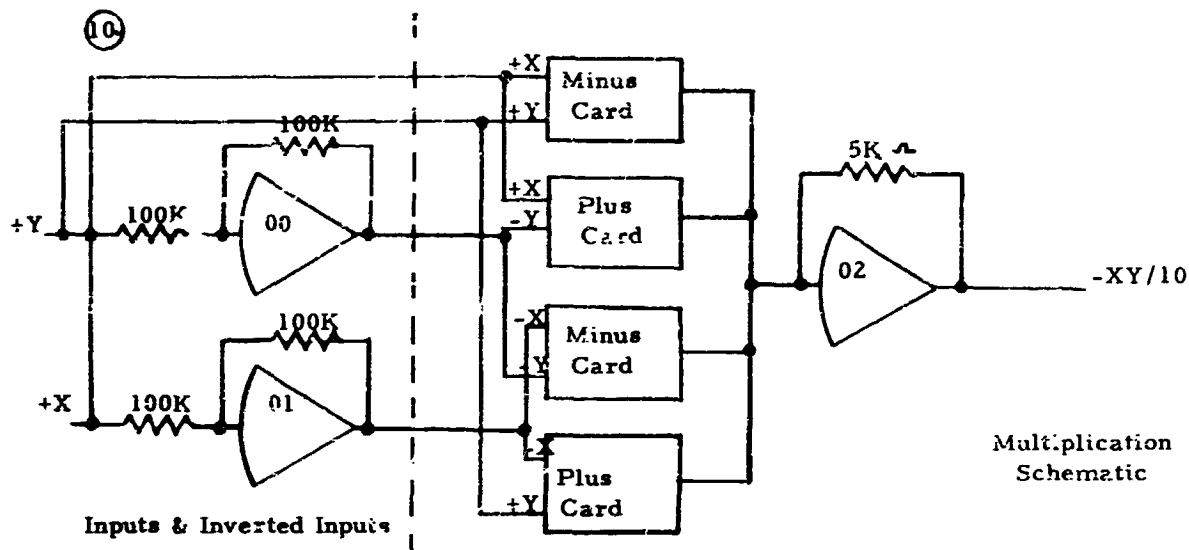
⑨.







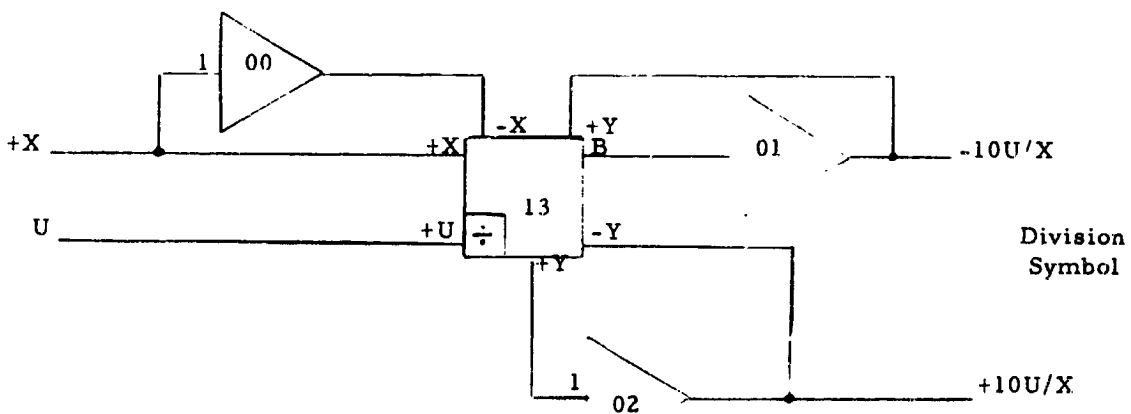
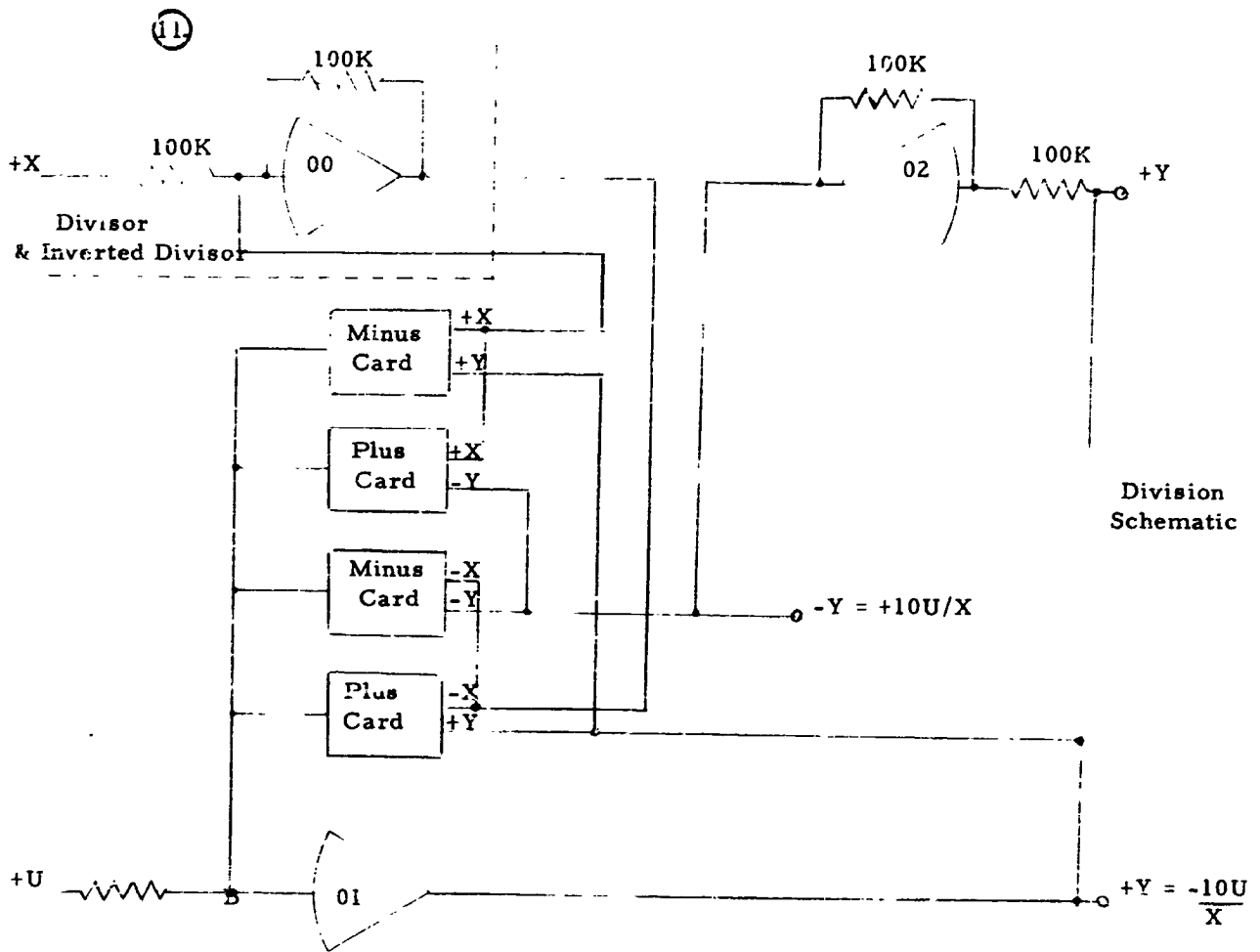
Integration
with initial
condition, V_o
Schematic



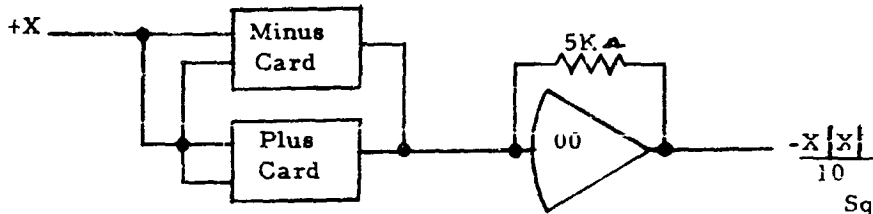
Integration
with initial
condition, V_o
Symbol



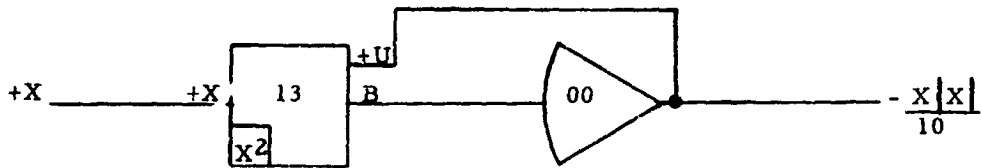
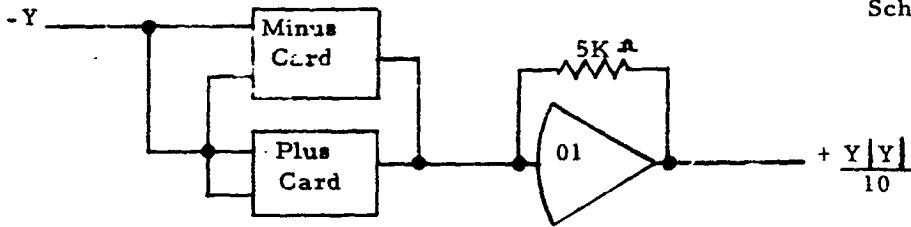
*Note: The output amplifier is drawn as  not as . The symbol  denotes a high gain amplifier without a feedback loop. The feedback loop must be furnished, and in the above case, is furnished in the multiplier circuitry. The symbol  denotes an operational amplifier with a fixed gain, which as previously illustrated, is shown at the input of the amplifier.



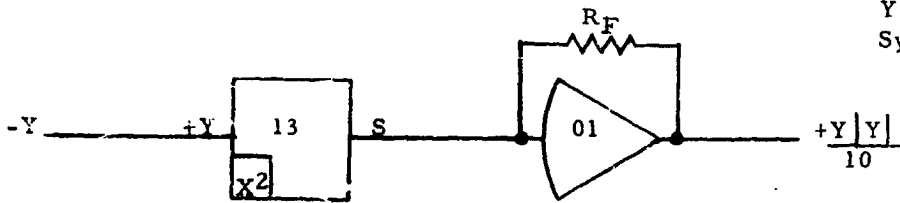
②



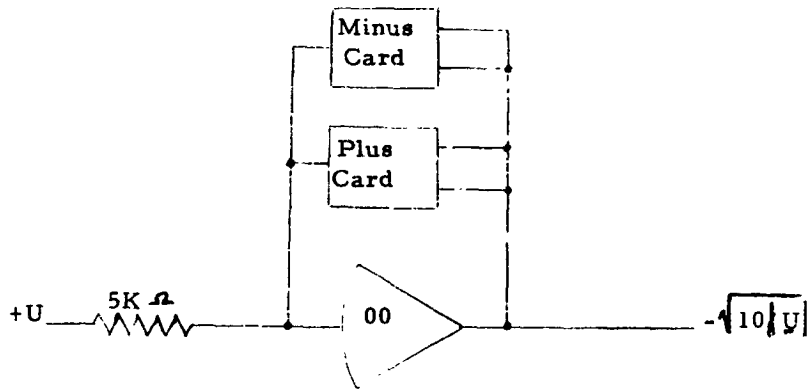
Squaring
 $X|X|$ &
 $Y|Y|$
 Schematics



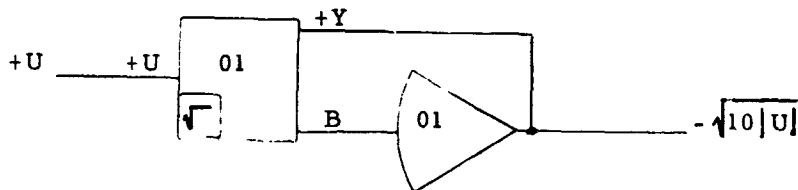
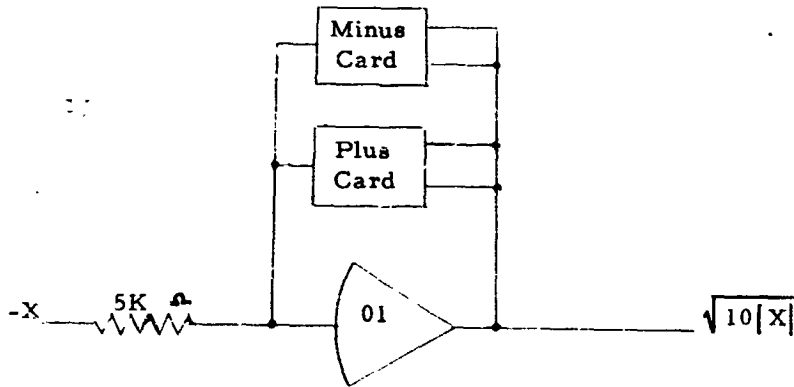
Squaring
 $X|X|$ &
 $Y|Y|$
 Symbols



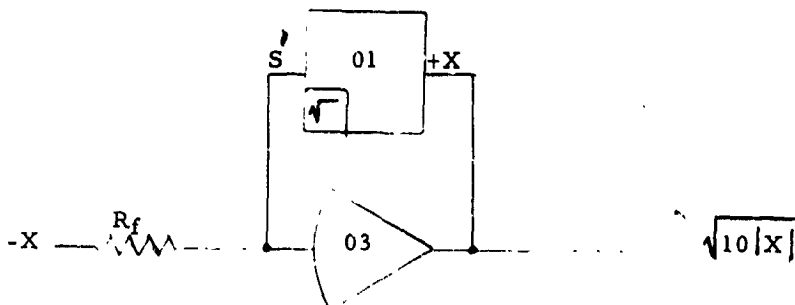
13



Square
Root
Schematics



Square
Root
Symbols



CONCLUSIONS

This paper has endeavored to illustrate some of the electronic principles involved in analog computation. The paper has been "written around" the PACE TR-48 computer employed by the Mass Metrology Laboratory. It is true that some of the techniques used in computation may differ from computer to computer; however, the major amount of techniques and components are functionally identical. In order that the reader may prepare himself for using an analog computer, it is recommended that he (1) familiarize himself with available operation manuals and (2) become familiar with the computer by practicing patching, scaling, and investigation of problem parameters by the solution of example problems.